THE APPLICATION OF ULTRASONIC NEBULIZATION TO ICP-AES ANALYSIS OF METALLURGICAL AND GEOLOGICAL SAMPLES.

BY

C.A. BARNARDT

Thesis presented in partial fulfilment of the requirements for the degree of Master of Science at the University of Stellenbosch.
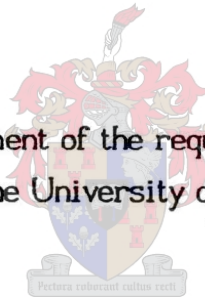
SUPERVISOR: DOCTOR D.H CORNELL
CO-SUPERVISOR: PROFESSOR P.E. WALTERS   JANUARY 1987

Dedicated to Sonette and Mia

ABSTRACT

The purpose of this project was to investigate the application of ultrasonic nebulization (with and without desolvation) to inductively coupled plasma atomic emission spectroscopy (ICP-AES) for the detection of low concentration elements in metallurgical and geological samples. The investigation included a study on the droplet sizes, the influence of desolvation on the plasma parameters and the determination of the detection limits.

Many promising results were obtained in this project. The ultrasonic nebulizer has proved to be a very efficient component in ICP-AES. The results have shown the ultrasonic nebulizer is especially suited for elements at low concentration levels as the superior power of detection produced by the ultrasonic nebulizer cannot be matched by pneumatic nebulizers. It was found that desolvation is not essential for analyses, although the results have shown that even better sensitivity and therefore better powers of detection are obtainable with the use of desolvation. An important and hitherto unknown result of the desolvation investigation is the existence of an optimum desolvation temperature where the analyte emission intensity displays a maximum. A complete Simplex optimization of the whole instrument and procedure was therefore vital for optimum results. A knowledge of the influence of the solvent on the plasma parameters proved to be essential for a better understanding of the applicability of the ultrasonic nebulizer for analyses. However the ultrasonic nebulizer system developed in this project is unfortunately not quite suitable for quick routine analysis due to slow sample changeover, but certain modifications is proposed to improve the speed of analysis.

OPSOMMING

Die doel van hierdie projek was om die toepassing van die ultrasoniese verstuiwer (met en sonder desolvasie) in induktiefgekoppelde plasma-atoomemissiespektroskopie (IGP-AES) vir die bepaling van lae konsentrasie elemente in metallurgiese en geologiese monsters te ondersoek. Die ondersoek het 'n studie van druppelgrootte, die invloed van desolvasie op plasmaparamaters en die bepaling van bepalingsgrense behels.

Baie positiewe resultate is gedurende hierdie projek verkry. Die ultrasoniese verstuiwer het homself as 'n baie effektiewe komponent in die IGP-AES bewys. Die resultate het getoon dat die uitstekende gevoeligheid, en dus lae bepalingsgrense, wat deur die ultrasoniese verstuiwer verkry is, nie deur die kommersiele pneumatiese verstuiwers geewenaar kan word nie. Die resultate het verder getoon dat die ultrasoniese verstuiwer baie geskik is vir elemente met lae konsentrasievlakke. Alhoewel desolvasie nie noodsaaklik is nie, het die resultate getoon dat 'n beter gevoeligheid met behulp van desolvasie verkry kan word. 'n Belangrike en tot dusver onbekende resultaat wat verkry is tydens die desolvasieondersoek, is die bestaan van 'n optimum desolvasietemperatuur waarby die emissie-intensiteit 'n maksimum is. 'n Volledige Simplex-optimering van die hele instrument en prosedure is gevolglik noodsaaklik vir optimum resultate. Daar is bewys dat 'n kennis van die invloed van die oplosmiddel op die plasmaparameters noodsaaklik is vir 'n beter begrip van die toepasbaarheid van die ultrasoniese verstuiwer vir analises. Ongelukkig is die ultrasoniese verstuiwer wat in hierdie projek ontwikkel is, nie heeltemal geskik vir roetine analises nie, as gevolg van die lang tydsverloop tussen monsteromruilings. Hierdie tekortkomings kan egter met sekere veranderings aan die apparaat oorbrug word om sodoende vinniger analise van monsters te verseker.

INDEX

CHAPTER 1

1. GENERAL

1.1 Introduction

It is truly said that "a sensible man judges the present on the basis of past events". Judged on the basis of acceptance by the analytical community, by the growth in usage and the increase in the number of publications (Figure 1.1) the inductively coupled plasma has so far had the greatest impact of all "flame-like" plasmas. Barnes[9] envisaged the seven ages of a new physical analytical method. Table 1.1

TABLE 1.1

The seven ages of a new physical method

1. Conception of the idea.

2. Design and construction of first operating apparatus to verify scientific principles.

3. Successful demonstration of the idea; publication of initial papers.

4. Design and construction of finely tuned facility to identify experimental parameters that lead to useful analytical figures of merit, e.g. sensitivity, selectivity, accuracy and precision.

5. Attainment of maturity as represented by general acceptance by the analytical community and by the development of standardized operating conditions and procedures; automation of operations and computer management of data.

6. Improved understanding of scientific principles

7. Old age and senescence.

PUBLICATIONS ON ICP-AES FROM 1960 TO 1983
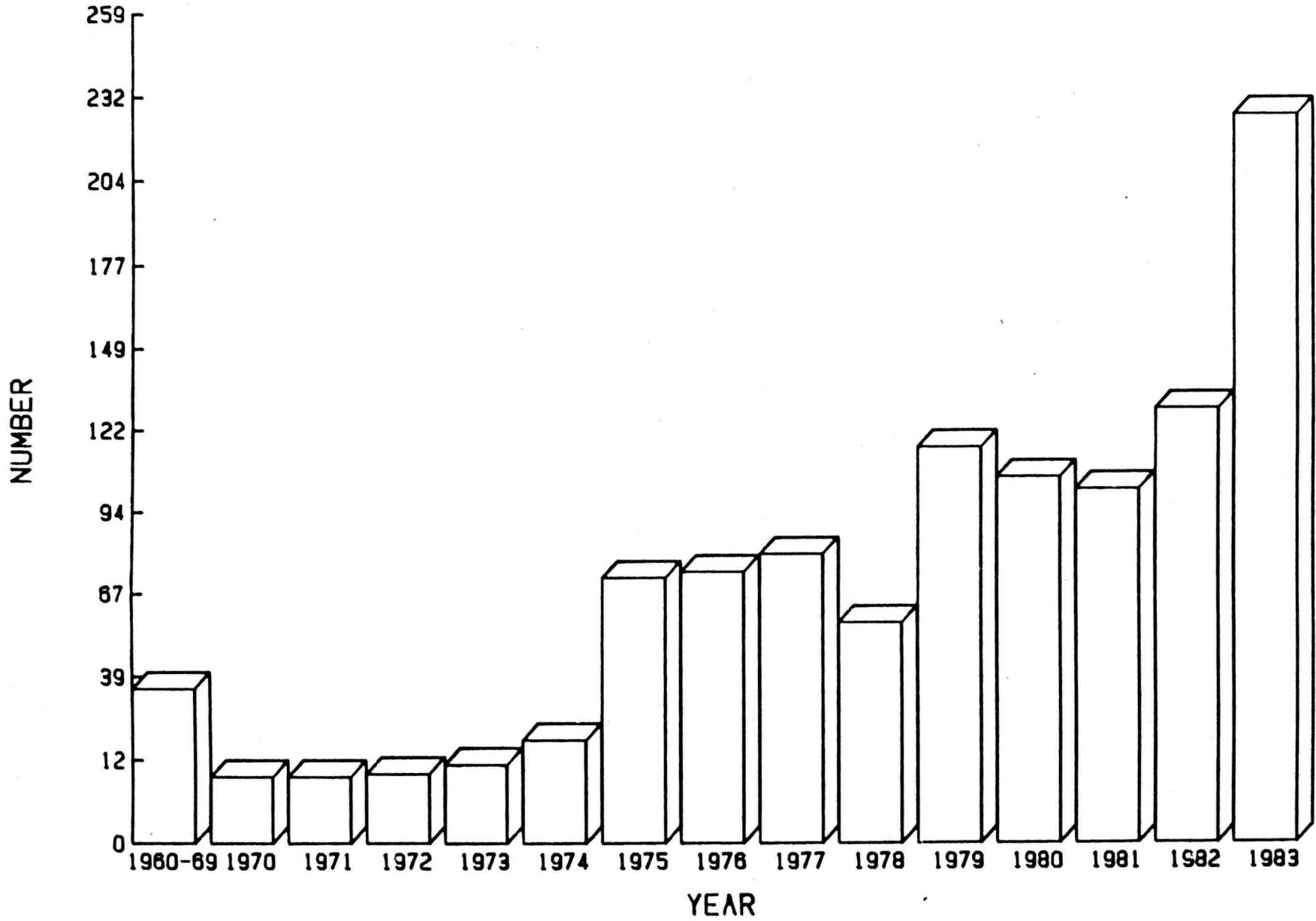
Figure 1.1

To explain the acceptance of the ICP-Atomic Emission Spectroscopy (AES) by the analytical world we need only to look at the statistics. When the first ICP-AES instruments were delivered in 1975, there were perhaps 15 facilities scattered around the world. Now, 11 years later, there are many commercial vendors, the number of facilities now total about 5 000, and the total is increasing at a rate of ~400/year.

It is clear that ICP-AES, ICP-AFS and ICP-MS have passed through the first four ages of a new analytical method[9] shown in Table 1.1, and the 5th age has now been attained, and we are moving into the 6th. The 7th age is not in sight yet because a new method that is superior to ICP has not yet emerged.

At present the ICP-AES is widely used for elemental determinations in production laboratories. But this does not mean that we have reached such a mature stage that no challenging problems remain. We therefore still expect improvements in the understanding of the complex structure and dynamics of the ICP, with the following goals in mind :

(1) achievement of even better sensitivities

(2) attainment of better accuracy and precision

(3) streamlining of analytical procedures

(4) broadening of the application base.

1.2 *Aims of this study*

The project aims mainly to achieve greater sensitivity. For various practical reasons, many analysts require even higher powers of detection than the excellent values that are presently achieved. The evolutionary improvement of the ICP-AES limits of detection during the first 12 years of its existence is clearly illustrated in Table 1.2. Typical improvement factors are from 100 000 to 500 000. The superior powers of detection represented by the data in the last column of Table 1.2

TABLE 1.2

EVOLUTION OF ICP-AES DETECTION LIMITS (μg/ml)

	1965 Wendt and Fassel[141]	1975 - 76 Boumans and de Boer[20]; Olson et al[113]	
Al	3	0,0004	(113)
As	25	0,002	(113)
Ca	0,2	0,000001	(20)
Cd	20	0,00006	(113)
Co	-	0,0001	(113)
Cr	0,3	0,00008	(113)
Cu	0,2	0,00004	(113)
Fe	3	0,00009	(20)
La	50	0,0001	(20)
Mg	2	0,000003	(20)
Mn	1	0,00001	(20)
Ni	1	0,0002	(20)
P	10	0,015	(20)
Pb	-	0,001	(113)
Si	3	-	
Sn	50	0,003	(113)
Sr	0,09	0,000003	(113)
Ta	16	-	
Th	40	-	
V	-	0,00006	(113)
W	3	0,0008	(113)
Zn	30	0,0001	(20)
Zr	15	0,06	(113)

was obtained with an ultrasonic nebulizer with aerosol desolvation, compared with the data obtained with a standard pneumatic nebulizer in 1965.

It is widely recognized that the nebulizer plays the most important part in achieving higher powers of detection. Therefore the aim of this study was to investigate the characteristics of the ultrasonic nebulizer in comparison with the standard pneumatic nebulizers in the analysis of metallurgical and geological samples. For better detection limits one needs a more efficient sample mass transfer to the plasma. This is possible with the ultrasonic nebulizer due to the effective generation of aerosol by ultrasonic waves. Effective aerosol generation also gives rise to small and uniform droplets. Measurement of the droplet sizes obtained with the ultrasonic nebulizer was done in comparison with standard pneumatic nebulizers. Unfortunately the more efficient mass transfer of sample also lead to more solvent being present in the plasma. The excess solvent greatly influences the operating conditions and excitation mechanisms of the plasma. Desolvation had therefore to be used to limit the amount of solvent present in the plasma. Ultimately the performance of the nebulizer, with and without desolvation, was compared with standard pneumatic nebulizers by determining detection limits for relevant elements. The influence of the excess solvent produced by the ultrasonic nebulizer, on the plasma excitation temperature, electron number density and the emission profile was also studied.

For the achievement of the best detection limits one needs to work at the optimum instrumental settings and the instrument was therefore optimized. Another aim of this study was to investigate the possibilities of using the ultrasonic nebulizer in a service laboratory. A few instrumental modifications were introduced for rapid and convenient sample changes.

CHAPTER 2

2. GENERAL DESCRIPTION OF THE ICP

The analytical possibilities of the ICP were noticed not long after Reed (1961) successfully introduced the ICP. From the outset it has been noted as an analytical method with extraordinary capability. It is an effective source of atomic emission which can, in principle, be used for the determination of all elements except for argon. The development of the ICP as a commercially competitive instrument took only a few years and today it is accepted as an alternative method to atomic absorption, atomic fluorescence and x-ray fluorescence.

The term "plasma" is used for a gas of which most of the atoms (more than 1%) are in the ionized state. The ionized part of the plasma is constantly diminished by recombination of the ionized atoms with electrons. This process is accompanied by a loss of energy through emission of radiation. Ionization occurs when energy is constantly fed into the plasma, and a high temperature is associated with the plasma. This high temperature assures effective dissociation of practically all molecules. Complete atomization is necessary for maximum analytical sensitivity at low concentrations. All solids or fluids become vapours above 5 000 K and no molecules can exist above 1 500 K. This is why the plasma is such an ideal source for atomic emission spectrometry.

Energy loss occurs through radiation and conduction to the edge of the plasma. Due to this loss it is necessary to add energy from outside to maintain it. This addition of energy occurs through inductive coupling between the radio frequency coil and the plasma itself.

2.1 Hardware and Functioning of the ICP

The ICP consists of a power supply that generates output levels of 1 - 15 kW and supplies it to a radio frequency (rf) oscillator. A quartz tube torch is placed inside a water-cooled conducting coil and the plasma is formed inside the quartz tube. The rf-coil consists of 2 - 5 windings and the inductance in series with a capacitor forms

part of the LC (inductance-capacitance) network of the rf-oscillator.   As mentioned before, the plasma is formed and supported by energy fed via inductive coupling to the plasma. The principle of energy transmission is essentially that of a transformer, in which the primary winding is the high frequency coil and the secondary the ionized gas or plasma.   By changing the current inside the coil an electromotive force is electromagnetically induced in the secondary circuit. Secondary currents are induced in the ionized gas when an alternating current (1 - 100 MHz) flows in the primary coil.   The alternating current flowing in the inductor coil produces a magnetic field with lines of force which are axially orientated inside the quartz tube and follow elliptical closed paths outside the coil. (Figure 2.1.) The electrons, and to a lesser extent the heavier ions, are accelerated by the concentric electric field associared with the fluctuating magnetic field. The kinetic energy which the electrons gain from the field is transferred to the gas atoms. Due to the large amount of particles per unit volume at atmospheric pressure the particle collision rate is high and leads to effective exchange of energy, as well as broadening of the spectral lines.

Nothing will happen when the generator is turned on because a gas is not a good conductor until it is ionized. A supply of electrons of sufficient energy to ionize the gas is required to initiate the plasma.   The plasma can be "ignited" by generating sparks in the argon stream with a Tesla coil. The sparks cause some argon ions and electrons to be formed which are then accelerated by the alternating field, leading to further ionization by collisions with the gas atoms.

In the region where the eddy currents are concentrated, gas temperatures are
> 4 000 K. At these temperatures it becomes necessary to thermally isolate the plasma from the walls of the quartz tube (melting point of quartz is 2000 K). This gas flow lifts the plasma partially above the rf-coil and gives it a tear drop shape. The gas flow must be sufficient to isolate the plasma but not to much as to blow the plasma out of the coil.

The quartz torch usually consists of three concentric quartz tubes which are placed inside the rf-coil (Figure 2.1). The coolant gas (usually argon, nitrogen or air) flows along the outer tube. The tangential or vortex methods are currently used both to stabilize and to thermally isolate the plasma. In addition to this outer "plasma" or
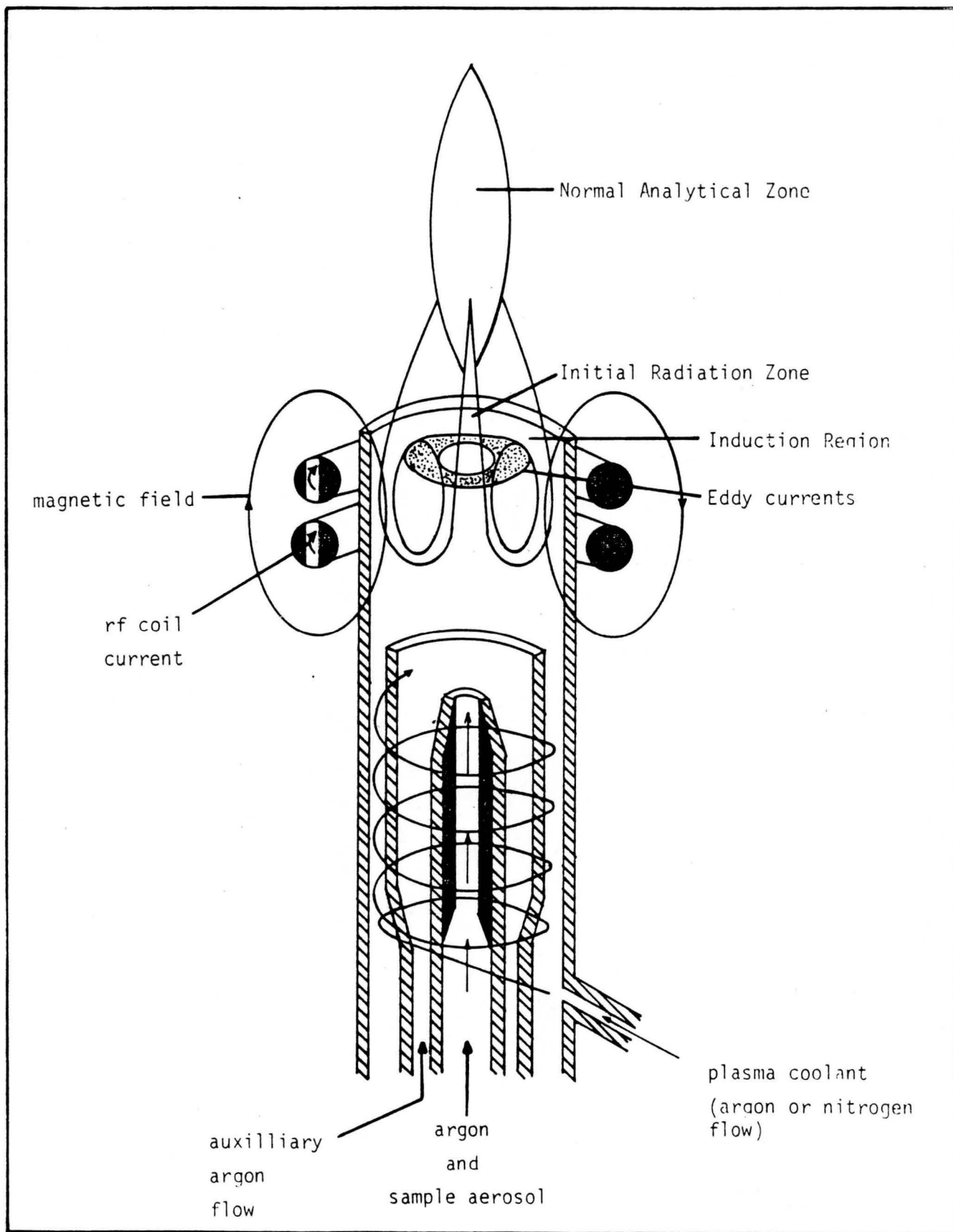
Figure 2.1 Schematic diagram of an ICP

"coolant" gas which flows spirally up the outer tube, use is also made of the intermediate or "auxiliary" gas when the plasma is operated at higher powers. The sample is introduced by means of the inner "aerosol carrier" shown in Figure 2.1. The shape of the plasma is mainly determined by the design of the torch, the gas flow conditions and the frequency of the electromagnetic field. The frequency influences the plasma via the so called "skin effect". The skin effect is characterized by the distance necessary to reduce the induced magnetic field to 1/e (e = 2.72) of its value at the outer surface of the plasma. The higher the frequency the smaller the skin depth. (Figure 2.2).

The plasma consists of a bright white non-transparent corona with a flamelike tail. The corona is situated inside the rf-coil. The radiation consist of an intense continuum with a completely developed line spectrum of neutral Ar atoms. The continuum is the zone with the highest temperature and is probably caused by recombination and bremstrahlung emission which makes it unsuitable for analytical purposes. Above the corona is another bright zone which is more transparent than the corona. This is the zone with the best signal to background ratios and the radiation from this zone is used for optical observations. The low continuum background, high radiation power, and the high excitation possibility makes this the ideal spectroscopic zone.

The third zone is the tail which is invisible to the eye when distilled water is aspirated. It becomes visible when elements with characteristic colours are aspirated. Turbulence is common in this zone due to mixing of hot plasma gases with the cold atmosphere. The spectra from this region are comparable to the spectra of chemical flames and consist mainly of radiation from low energy levels. This property makes it less applicable for analytical measurements, although it is the only useful zone for the alkali elements due to the low ionization potential and high excitation energy of these elements.

2.2 *Sample Introduction*

The third quartz tube in the torch is the inner concentric capillary tube. The carrier gas with the sample flows through this inner tube. When the nebulized sample enters

Low Frequency
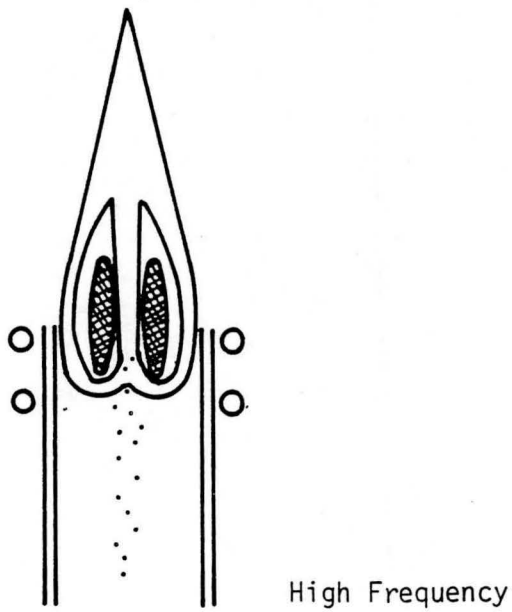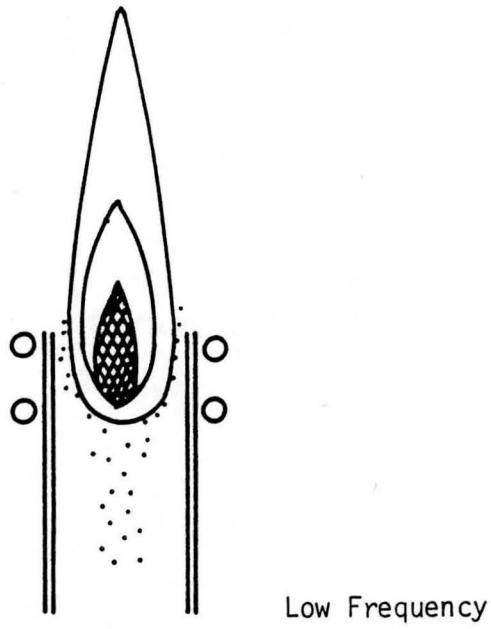
High Frequency

Figure 2.2 Operating frequency's influence on plasma shape

the plasma a few processes occur. The solvent evaporates, dissociates and the analyte must be atomized before excitation. These are all endothermic processes which are most efficient at high temperature. For the optimal sample introduction a low carrier gas flow is needed to lengthen the residence time and minimise the cooling effect, while penetrating the center of the plasma. Earlier it was mentioned that the skin depth is smaller with higher frequency, and therefore the greater the diameter of the tunnel which the carrier gas blows into the plasma, the easier it is to inject the aerosol into the plasma. (Figure 2.2). Thus the sample is concentrated along the central axial channel. It will become clear later that water vapour plays an important role in the dissociation and excitation of the sample. The finer the droplet size of the aerosol spray, the more rapidly the particle stage and subsequent atomization is reached.

The advantage of using argon as a plasma gas is the fact that it forms a chemically inactive environment in which the free atoms are distributed. Therefore interaction between analyte elements and combustion products, present in ordinary flames, is eliminated in this case. Due to the temperature gradient one can expect a change in excitation of atom and ion lines with the vertical height and lateral position in the plasma. Electrode contamination which is important in arc and spark excitation, is absent from ICP "flames".

The inductively coupled plasma has been firmly established as a reliable and efficient excitation source for spectrochemical analysis, but in ICP techniques the problem is getting the sample into the plasma. Therefore, the ICP-system will never be better than this weak link. The sample introduction process conditions the sample as it passes into the plasma, and so largely determines the accuracy of the analysis. An increasing demand for improved nebulizer systems led to an increase in research on sample introduction (Figure 2.3). Most previous workers have understood the problems of sample introduction but what has been lacking is suitable means to overcome them.

The main goal of sample introduction is the reproducible transfer of a representative part of the sample to the plasma. A high efficiency and no interferences are further goals for sample introduction. In principle the sample can be in the solid, liquid or

SAMPLE INTRODUCTION

1979   80   81   82   83
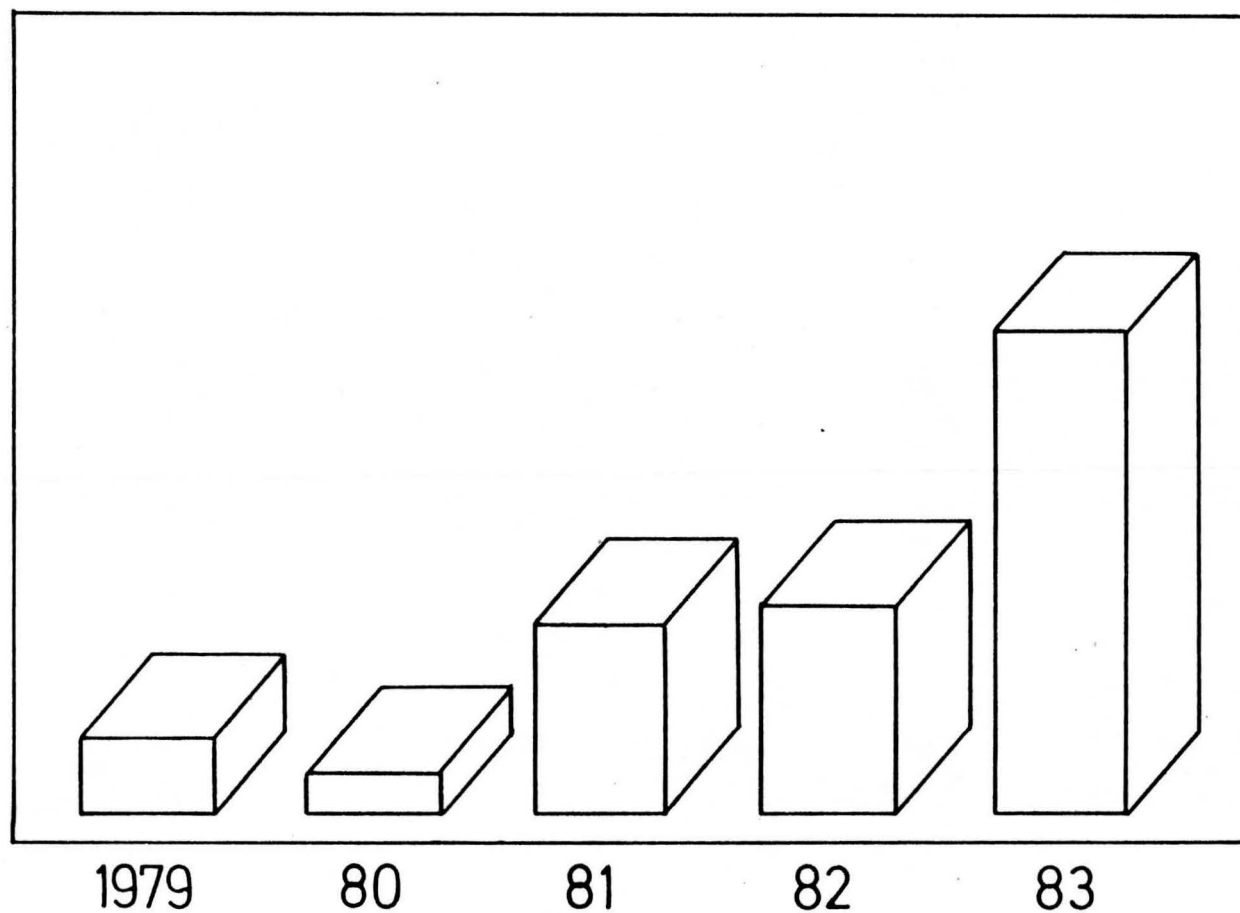
Figure 2.3 Publication trends in atomic spectroscopy, 1979 - 1983
(Browner and Boorn   )

gaseous state.

2.2.1 *Gas Phase Sample Injection*

This is an ideal technique for the ICP because no nebulizer is necessary. A 100% efficiency of injection is obtained compared to a maximum of about 2% - 5% with pneumatic nebulizers. It would be most convenient if all samples could be volatilized in a convenient manner which is compatible with ICP instrumentation.

2.2.2 *Sample Injection of Solid Samples*

The advantage of a solid sample is the fact that it is not necessary to dissolve it. Clogging of nebulizers is not a problem with solid samples. Muller[105] discussed a few methods of solid sample introduction, including the swirlcup[79], the fluidised bed chamber, the aerosol generator, and the sample elevator technique. A detailed discussion on solid samples is also given by Thomson and Walsh.[133] In their list electrothermal vaporization and laser volatilization of solid samples are also included. The introduction of slurries is also an important field of research. The problem with solids is to achieve continuous introduction of the sample. Most methods are discrete methods. The nebulization of slurries by means of the Babington nebulizer so far seems most likely the best for continuous introduction of solids.[63,141]

2.2.3 *Liquid Sample Introduction*

Simplicity and reliability are the most attractive features of liquid sample introduction. The need for improvement is realised if we look at the low transport efficiency, interferences and time wasted between the introduction of successive samples. Droplet size plays an important role in the transport efficiency and will be discussed in Chapter 5.

2.2.4 *Nebulizer Systems*

Among the various nebulizer types available, the ones most frequently used with the

ICP are the pneumatic and the ultrasonic nebulizers. Several comparative studies on pneumatic nebulizers[62,95,147] and nebulization-spray chamber arrangements[76] have been made. Inherent nebulizer characteristics are always related to a specific analytical system which is a drawback of comparative investigations.

The evaluation and selection of nebulizers for analysis requires consideration of a number of aspects. The type of sample, accuracy, precision required, the amount of material available and the levels and ranges for the elements to be determined are all important. Comparitive studies usually cover these aspects.[76,77,88,95,102]

The pneumatic nebulizers are the most widely used. One of these is the Meinhard concentric nebulizer (Figure 2.4) which is a masterpiece of glasswork and probably the most widely used ICP nebulizer.[6,88,95,102,103] Clogging of the nebulizer tip when aspirating high solid content samples is one of the main drawbacks of this nebulizer. Cross-flow nebulizers are also widely used.[95,102,110,133] A horizontal jet of gas passes across the top of a vertical narrow tube and the reduced pressure so generated draws liquid up the vertical tube where it is disrupted into fine droplets at the top. (Figure 4.6). Not all designs are self priming and a peristaltic pump is often required. Adjustable cross-flow nebulizers are also available and it is possible to optimize their performance. However the major problems with these systems are long-term stability and reproducibility. Another type of nebulizer is the Babington-design. (Figure 4.7) Water or slurries pass down a V-groove. Air is forced through a small hole in the bottom of the V-groove under pressure. The sample film is then ruptured to form a fine aerosol. Another nebulizer design utilizing a fritted disk has recently been described.[130]

 (Figure 2.5) Solution is pumped on to the face of a fine glass frit through which the injector gas passes. It offers a stable and reproducible generation of aerosol from solutions with a high salt content. The ultrasonic nebulizer is also frequently used and will be discussed in Chapter 3.
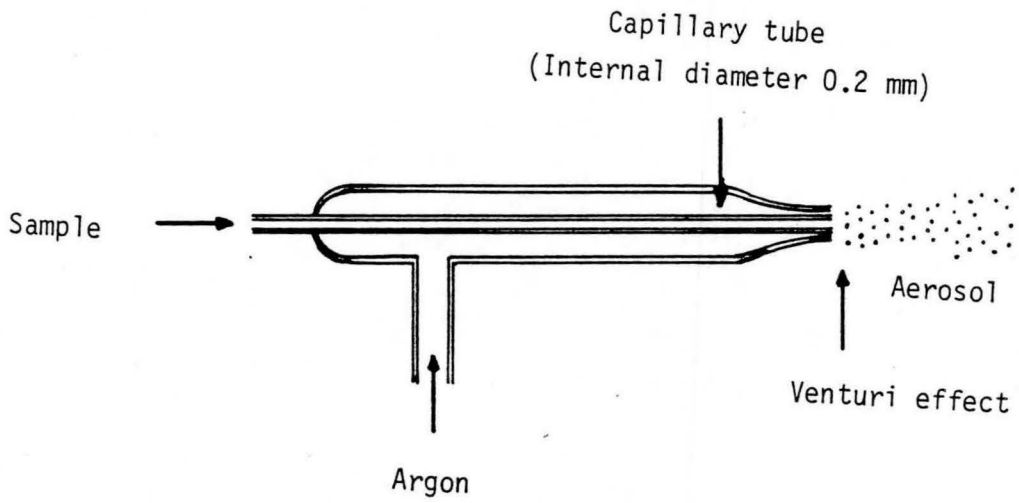
Figure 2.4 The Meinhard concentric nebulizer
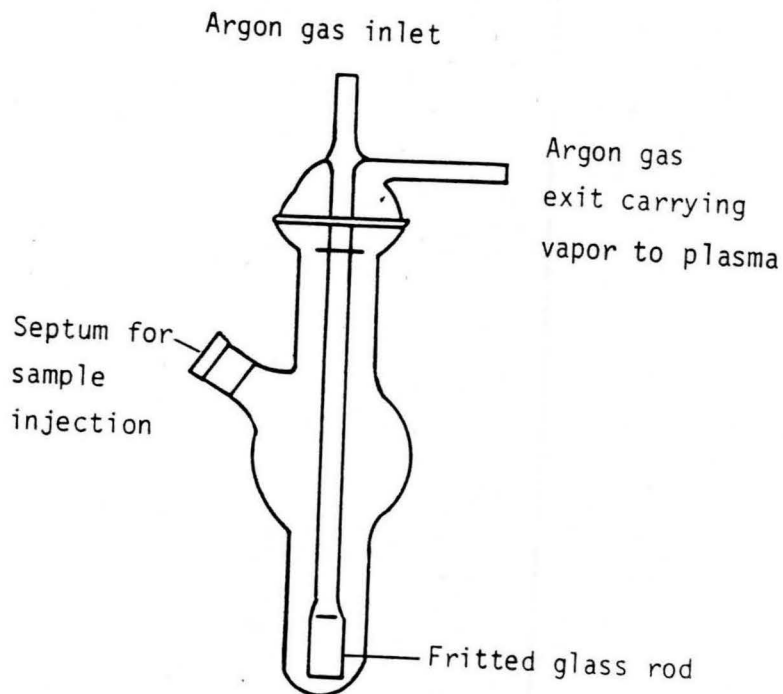
Figure 2.5 The Frit Nebulizer

CHAPTER 3

3. SOME ASPECTS OF ULTRASONIC NEBULIZATION

Ultrasonic waves are wave vibrations with a frequency above the normal audible region of the ear. This includes all waves above 20 000 cycles per second. The wavelength of ultrasonic waves in the minimum frequency region are about 0,8 m in solids, 0,24 m in fluids and 0,063 m in air. In the maximum frequency region they are about as follows, 0,0032 mm in solids, 0,01 mm in fluids and 0,025 mm in gases.

The propagation of an acoustic wave in a continuous medium is described by the general rules of wave mechanics. Two kinds of waves are involved in the propagation of the ultrasonic waves in a liquid or a gas.

(a) Longitudinal waves: the particle motion in the medium takes place along the direction of the axis of propagation.

(b) Surface waves: they appear at the liquid-gas interface or at the interface of two non-miscible liquids.

A medium may be characterized by the wave propagation velocity and by the characteristic impedance, Z, where

$$Z = p_o c$$

with p_o the specific weight and c the velocity of a plane wave in the medium. At the interface of two different media 1 and 2 under normal incidence we have an energy reflection coefficient α_r.

Under oblique incidence, reflection and refraction phenomena are observed similar to optics. From figure 3.1,

$$\frac{\text{Sin } i_1}{\text{Sin } i_2} = \frac{C_1}{C_2} = n_{12}$$

At the water-air interface, the longitudinal wave being propagated perpendicularly to the surface, produces a pressure linked to the particle motion. It is the origin of the "geyser" observed with an ultrasonic nebulizer. The wavelength, λ of the surface wave is given by

$$\lambda = (\frac{8\pi\sigma}{\rho f^2})^{1/3}$$

with σ = surface tension

ρ = density

f = wave frequency

The break of the continuity in the surface is the origin of the aerosol, provided the wave intensity is sufficient.

Although there are numerous crystalline substances which have the basic requirements of a reference element, quartz, due to its many desirable characteristics, has become the most widely accepted. Other materials that are piezoelectrically active include Rochelle-salt, tourmaline and lithium-sulphate. The application for the quartz resonator is to connect it in such a manner that the mechanical vibrations stabilize the oscillator's frequency. This is possible since the crystal acts like a tuned circuit when placed in an amplified feedback arrangement. The electrical equivalent of the quartz plate is shown in figure 3.2. When connected in an amplifying circuit, (Figure 3.3) a small amount of energy is fed back to the crystal which causes it to vibrate. These vibrations act to stablize the generated frequency at the resonance value.

It was shown in 1880, by the brothers Curie, that when some crystals are stressed along certain directions they acquire an electric field. The one surface of the
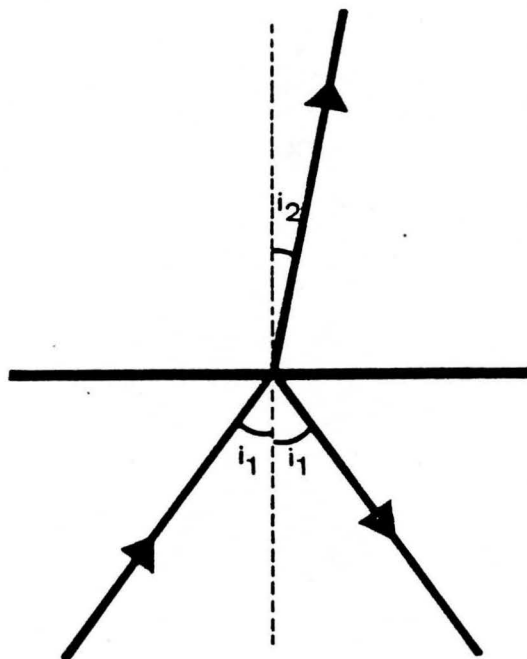
Figure 3.1 Reflection and refraction of an oblique incident
wave
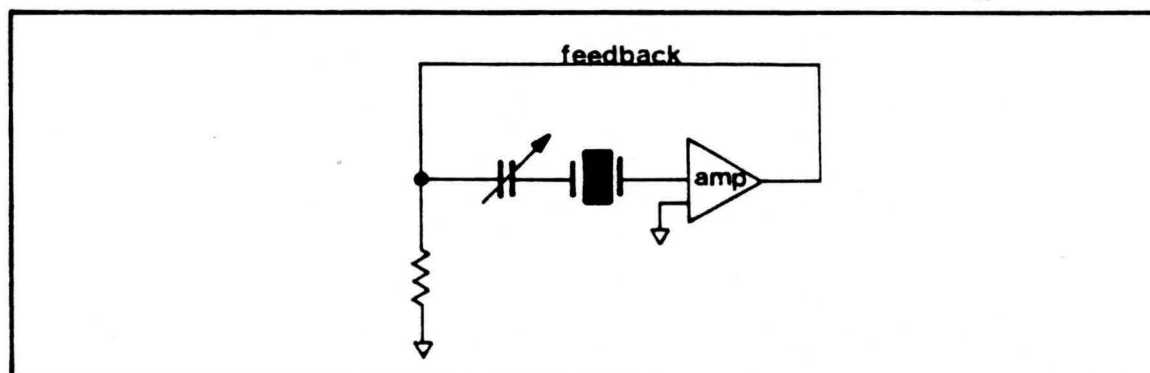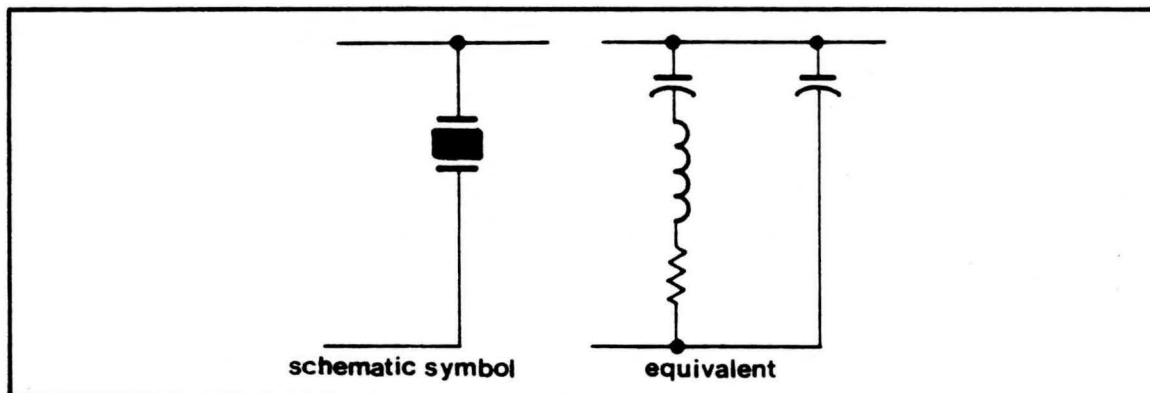
Figure 3.2 Equivalent circuit of a crystal includes the capacitances
contributed by the wire leads

Figure 3.3 Simplified amplifier feedback (oscillator) circuit using a
crystal resonator

crystal becomes positively charged and the opposite surface negative. This is called the direct piezoelectric effect. The polarized charge per unit area is given by

$$P = d\sigma$$

where σ is the stress and d a constant called the piezoelectric modulus.

Conversely, when an electric field is applied to a piezoelectric crystal its dimensions change slightly and this is known as the converse piezoelectric effect. The piezoelectric effect is a vector property, varying with the direction of applied stress. The charges produced in piezoelectric crystals originate in the disturbance and unbalancing of the electrostatic bonding forces between the atoms in the crystal. The electric polarization can be produced by strain such as bending, shear, tension and compression. The electric polarization provides a source of electromotive force (voltage). Lippman introduced the converse piezoelectric effect in 1881 and stated that if an electric field is applied across a crystal, mechanical vibrations will occur on the crystal. (Figure 3.4).

3.1 Vibration Modes

When a piece of crystal is subjected to a voltage, a stress is produced. If the voltage is caused to alternate at the proper rate, the crystal will begin vibrating and produce a steady signal. The mode of vibration depends upon the way the crystal was cut, i.e., an X cut exhibits an extensional vibration mode whereas a cut at 35 degrees off the Y axis, vibrates in the thickness shear mode. An illustration of the various vibration modes is given in Figure 3.5. The vibration set-up in the quartz crystal may produce both harmonic and nonharmonic signals and overtones.[58] The harmonic overtones are desirable since they allow the production of higher frequency crystal resonators using essentially the same cut. Nonharmonic overtones, on the other hand, are undesirable as they may lead to the generation of unwanted signals at frequencies spaced close to the one desired. When unwanted signals occur, they could also change with environmental influences. The various vibrations may then cancel, causing the crystal to stop resonating. The phenomenon is termed an "activity dip" since the crystal activity stops and starts due

Applied pressure generates
voltage

Applied voltage causes contraction
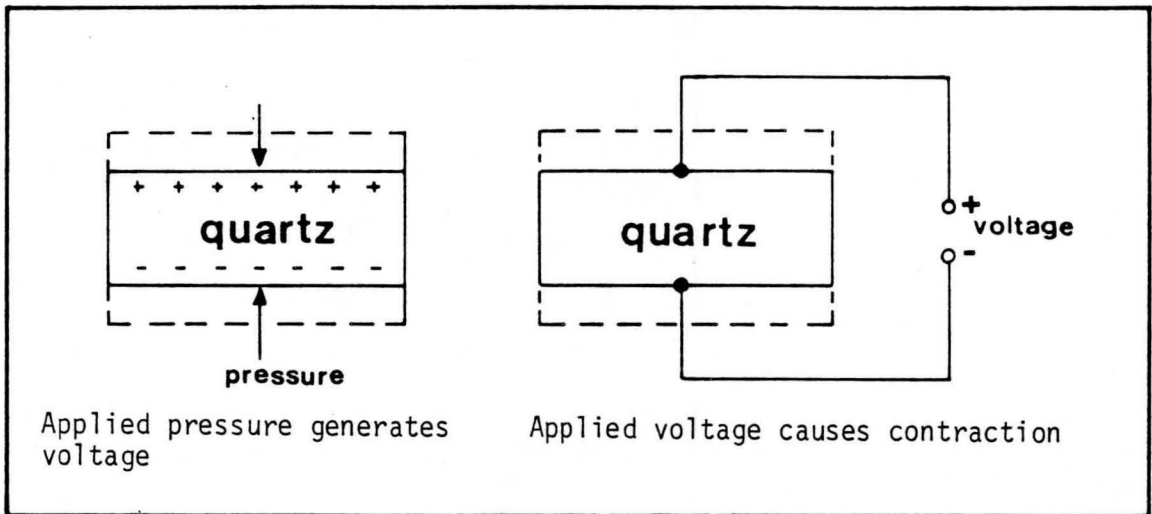
Figure 3.4 Piezoelectricity principles

Thickness Shear

Face Shear

Extensional
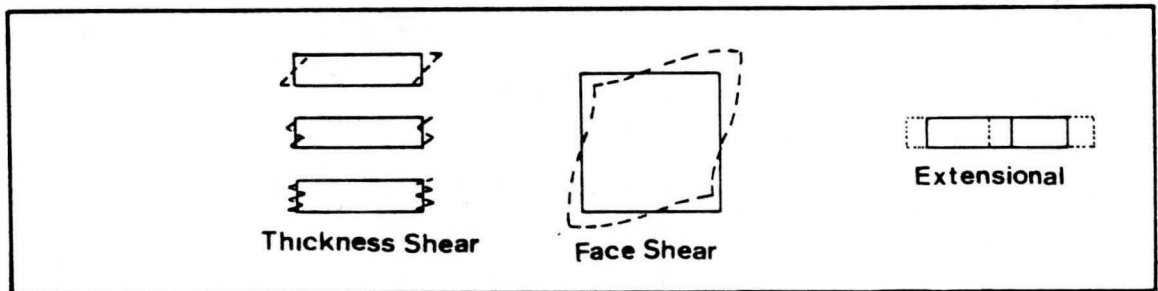
Figure 3.5 Vibration modes of various crystal cuts and the thickness
shear overtone

to a changing environment. Crystals having unwanted signals could also shift from one resonance point to another producing a frequency jump which would be an undesirable effect.

3.2 *Frequency Determination*

The frequency, or rate of vibration, is determined by the cut, size, and shape of the resonator, e.g., a 10 MHz 5th overtone unit is only 1,2 centimeters in diameter and about 1,06 mm thick. The precision with which the thickness is controlled determines the variation from crystal to crystal from a nominal center frequency. Final adjustment of the center frequency is sometimes accomplished by plating small amounts of gold on to the quartz. A monolayer (one atom thick) of gold can change the frequency by 2 parts in 10^7. Circular crystals of the thickness shear vibrating mode, when designed with the proper radius of curvature at the center, will produce "clean" frequencies with no spurious tones. It is for this reason that high performance crystal oscillators will typically utilize highly polished and properly shaped quartz resonators. In fact, these crystals are honed to a surface finish which is 10 times finer than that used for prescription eye glasses.

Resonance occurs when the distance between two adjacent nodes of the standing wave, that is excited in the crystal, is equal to the thickness of the crystal. Thus for resonance

$$t = \frac{\lambda}{2} = \frac{c}{2\nu} = \frac{1}{2\nu}\left\{\frac{E}{\rho}\right\}^{1/2}$$

where t = thickness
 λ = wavelength
 ν = frequency
 c = velocity of light
 E = elasticity modulus
 ρ = density

A crystal is therefore cut for a specific frequency, but the frequency can be doubled by working at one of the over tones.

3.3 *The Ultrasonic Nebulizer, Spray Chamber and Desolvation Apparatus*

Many researchers have done some work on ultrasonic nebulizers[20, 71,82,87,128,137]. We can divide ultrasonic nebulization into two categories, the batch type nebulizer[43,44,45,46,75,81,99,102,135,142,143,144] and the constant feed type ultrasonic nebulizer[38,64,109,113,132]. The ultrasonic nebulizer used in this study was a custom built nebulizer based on the design of Mermet et al.[99] and West and Hume [144]. (See figure 3.6). The quartz crystal (manufactured by Steeg and Reuter)* is ground concavely according to Gruetzmacher[67] with a diameter of 40 mm and a thickness of 1,4 mm. The ultrasonic energy is focussed at a distance 50 mm away from the concave crystal surface. The nebulizer consists of a radio frequency source (Figure 3.7 (a) + (b)) capable of delivering power between 0 and 80 watt. If one accepts that the conversion factor of the input energy of the oscillator to the output energy of the crystal is about 20%, then the output energy of the crystal can be varied between 0 and 16 watt. The crystal has a oscillation frequency of 2 MHz and the corresponding sound wave has a wavelength of approximately 0,7 mm in water, according to

$$\lambda = \frac{v_{H_2O}}{\nu} = \frac{1,497\times10^6}{2,0\times10^6}$$

$$\therefore 0,74$$

where λ = wavelength

ν = frequency

v_{H_2O} = velocity of sound in water

The sample container is placed in such a position that the surface of the sample coincides with the point where the ultrasonic energy is focussed by the concave crystal. The bottom of the sample container is made of a polyethylene membrane with a thickness of about 10 microns. Water serves as a transmission medium for the energy between the crystal and the sample. For good

---

* Steeg and Reuter, Bad Homburg v.d.H. Germany
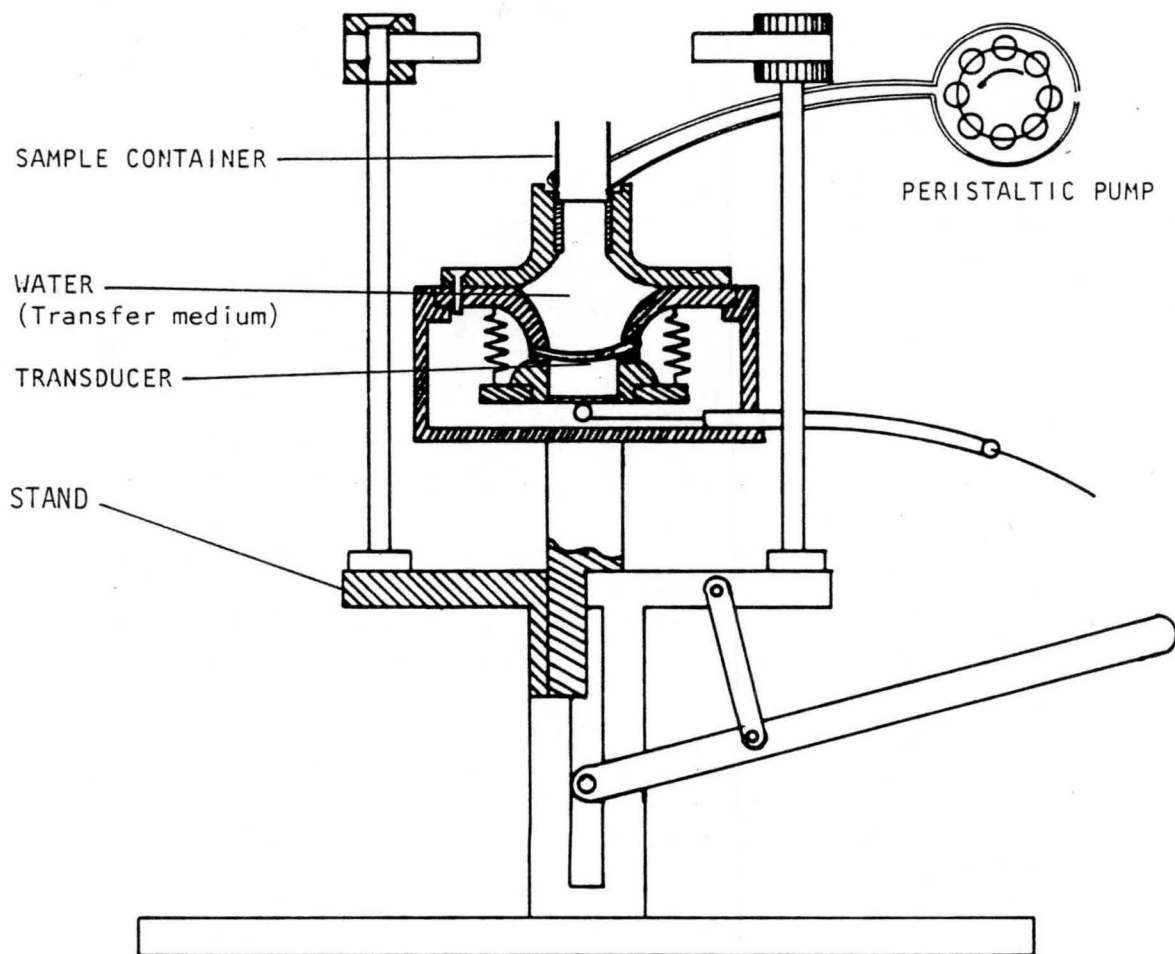
Figure 3.6 The ultrasonic nebulizer used
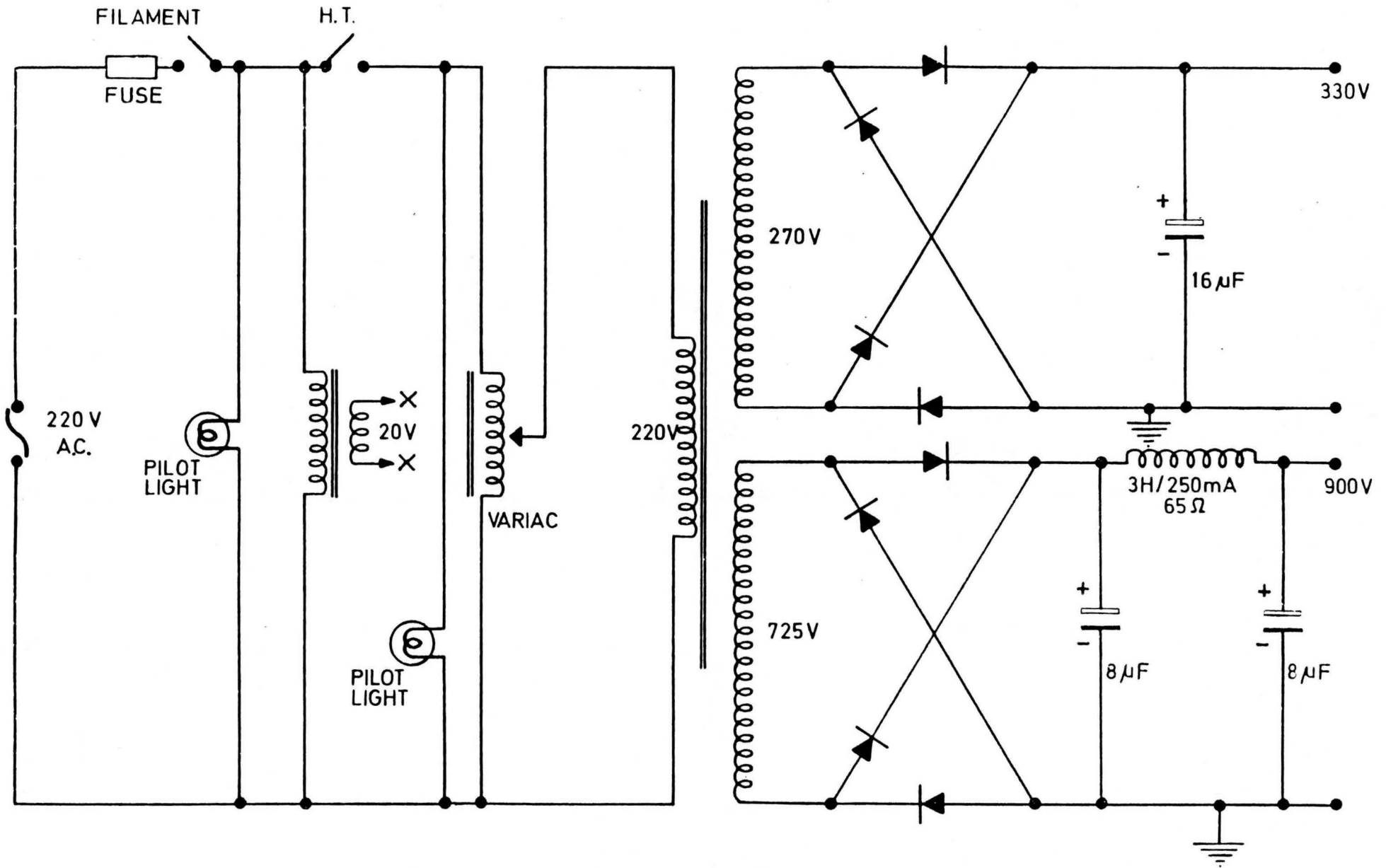
Figure 3.7(a) Power supply circuit

Figure 3.7(b) Oscillator circuit
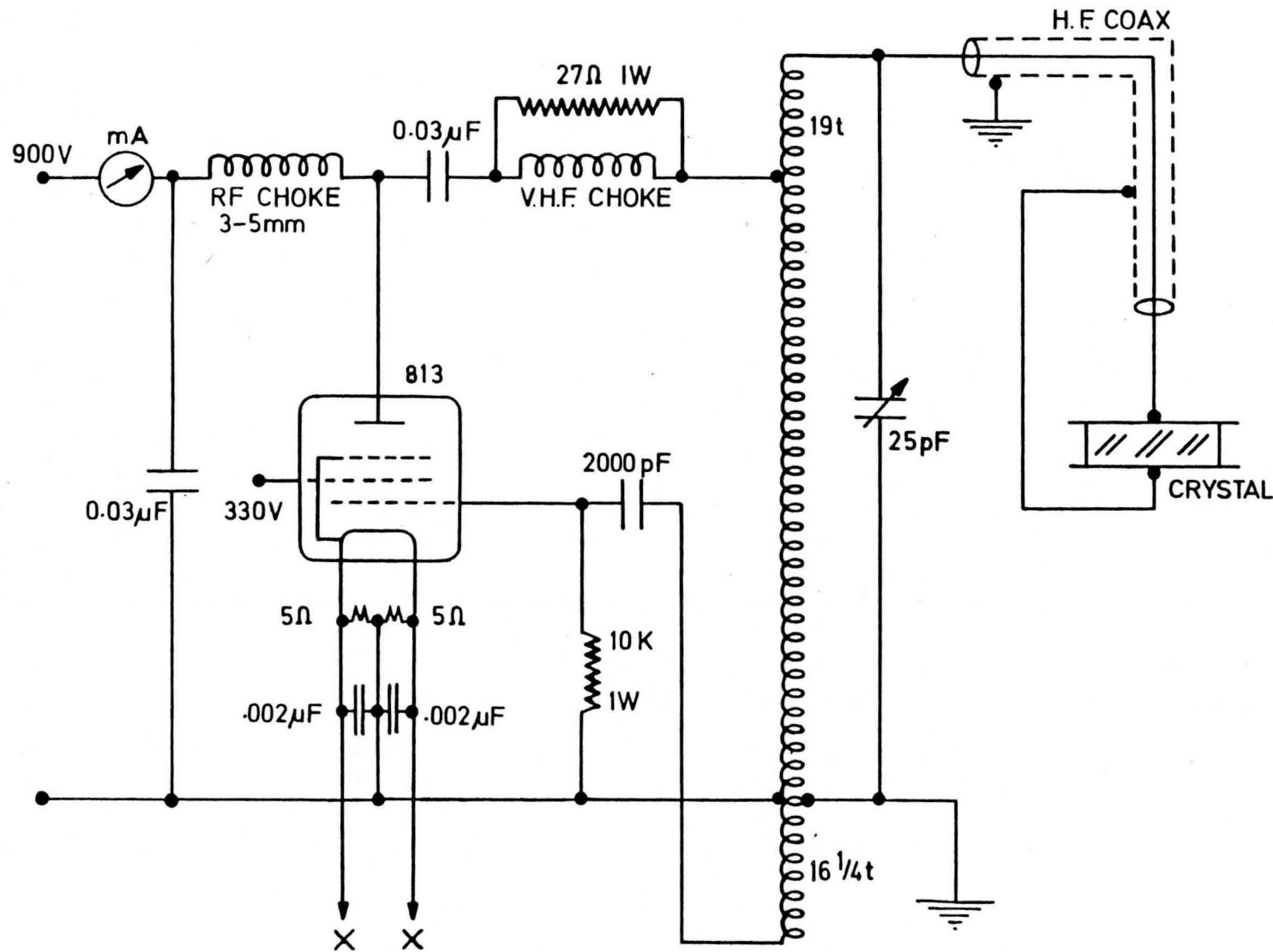
OSC. COIL

$3\frac{1}{8}"$ o.d.

$50\frac{1}{2}$ turns

2.5mm wire

4.5mm between turns

V.H.F. CHOKE

36 turns of 0.5mm wire

close-wound on

17mm o.d. former

reproduceability one needs a constant sample level at exactly the focus point of the crystal. Consistent operation of the ultrasonic nebulizer depends on focussing the beam reproducibly on the sample solution.

Tests were made to assess the uniformity of aerosol production during the course of an analytical measurement. It was found that the quantity of mist produced, did in fact, tend to decrease as the level in the sample container fell. Dunken et al.[48] reported that the amount of spray produced is a function of sample height in the cup. Van Rensburg and Zeeman[136] also supported this and stated that in order to obtain reproducible results, it is essential to have the surface of the solution in the sample cup at exactly the same height for each determination. Hoare et al[75] also used a focussing system and found that the quantity of mist produced tend to decrease as the level in the sample container fell. It seems that the sample height is a problem only associated with focussing devices because Spitz and Uny[126], who used a non-focussing system, showed that the quantity of aerosol produced is constant with time and is independent of the height of the solution. Mermet and Robin[99] as well as Issaq and Morgenthaler[81] also supported this finding.

The sample volume for optimum signal in this work has been determined as 2.5 ml at an input current of 20 mA. However the decrease in sample quantity during the nebulization process influences the production of aerosol. To ensure long term stability in the sample introduction it was necessary to keep the amount of sample constant. A mechanism was therefore developed to retain a constant sample level. The construction of this mechanism and other instrumental arrangements that was used are discussed in Chapter 4.

CHAPTER 4

4. INSTRUMENTATION

4.1 Inductively Coupled Plasma and Nebulizer System

A pure argon plasma was generated by the transfer of RF-energy via the water-cooled coil (three turns) to the argon gas, which flows upwards through a demountable three concentric tube torch. An ultrasonic nebulizer, with and without desolvation, was used to generate a fine aerosol which was fed up the center tube into the plasma. The main characteristics and general operating conditions of the ICP's used in this project are compiled in Table 4.1.

Two separate designs were used to keep the sample volume constant in the sample cup. In the first design, shown in figure 4.1, a syringe was used to keep the sample volume constant. The syringe was filled with sample and then placed in position as shown. The motor was then run at a constant speed to deliver about 0,5 ml.min^{-1} and ensure a constant level in the cup. This mechanism worked very well for diagnostic work e.g. the determination of plasma temperatures and electron densities. After a visit to Mintek it was realized that this design will not serve the requirements for routine service analysis since sample change and washout time requires about 2 minutes.

In the second design the syringe system was replaced by a peristaltic pump to keep the sample volume constant. The peristaltic pump was equiped with two Technicon tubes, the one introducing the sample while the other extracting excess sample. Since a smaller sample volume was maintained the sample cup was lifted until the focus point coincided with the bottom of the cup. A second peristaltic pump was later introduced to cut down on washout times. The one pump was used for sample feeding while the other pump was only used for rinsing. This setup is very similar to the latest commercially available ultrasonic nebulizer.[27] Although this last setup proved to be very efficient it is still inconvenient for routine analysis because it takes more than 1 minute to change samples.

Table 4.1

Generator		
Manufacturer	ARL	Philips
Model	34 000	PV 8490
Oscillator	crystal controlled	Colpitts
Frequency (MHz)	27.1	50
Coil : turns	3	3
Power (kW)	1.2	1.2
Torch		
i.d.outer tube (mm)	17.5	17.5
i.d. inner tube (mm)	14	14
i.d. injector tube (mm)	1.5	1.5
Plasma gasflow (l/min)	12	13
Auxiliary gasflow (l/min)	1	0
Nebulizer gasflow (l/min)	0,65	0.5

Nebulizer

A Batch type ultrasonic nebulizer and a constant feed ultrasonic nebulizer with and without desolvation.

Frequency (MHz)	2
Maximum Acoustic Power (Watt)	80

Meinhard Concentric Nebulizer
Cross-flow Nebulizer with peristaltic pump

Desolvation Apparatus

Heated Chamber wrapped with heating tape.

length (mm)	150
o.d. (mm)	50

Condenser: Modified Friedrichs condenser cooled with tap water
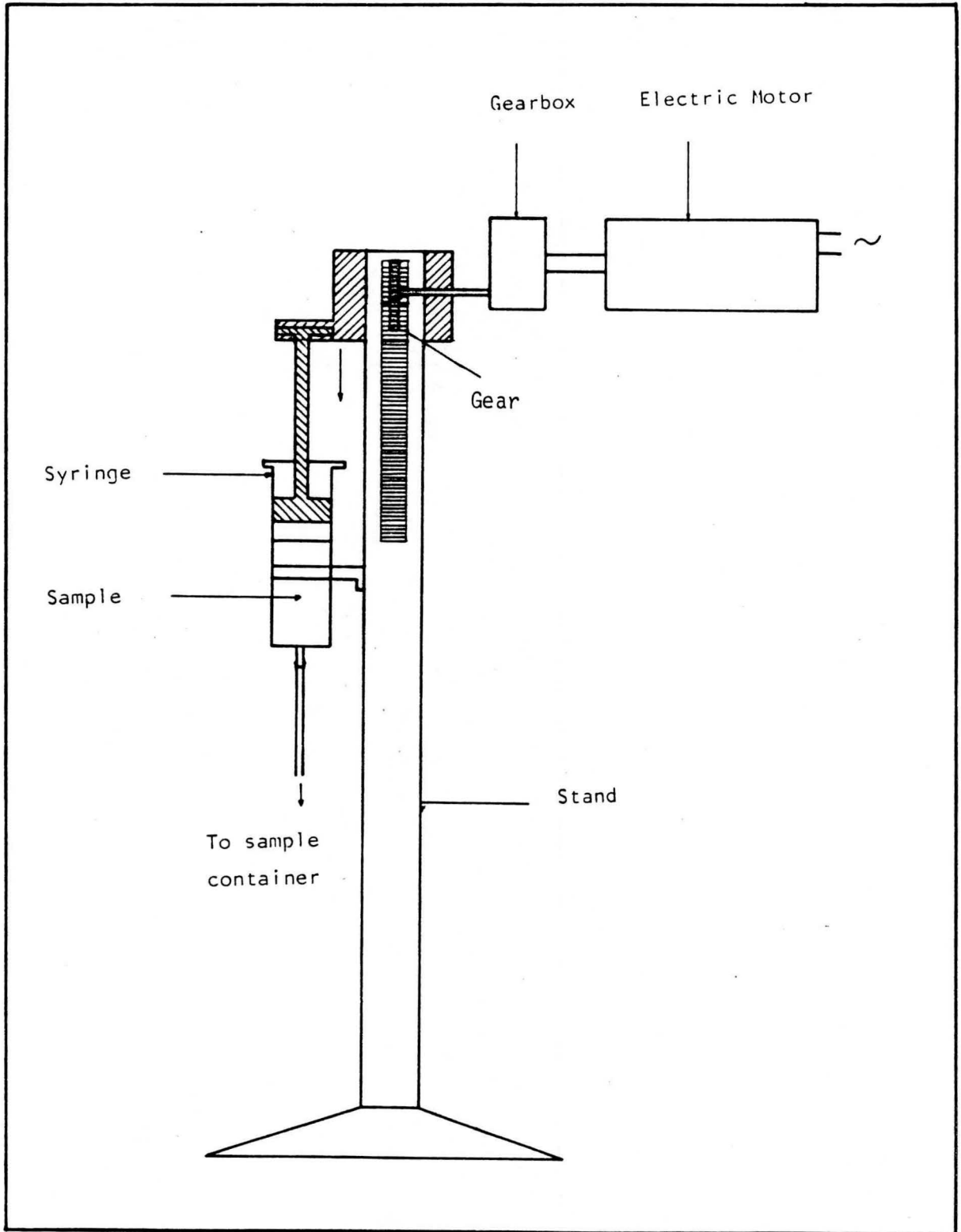
Figure 4.1 The syringe that was used to keep the sample volume constant

Unfortunately the first instrumental arrangement that was tried did not work sufficiently. (Figure 4.2). The desolvation chamber was a new design and consists of a heating tube with a coil that was connected to a power supply (100V/6A) and a glass chamber (length = 300 mm, o.d = 80 mm, spiral i.d. = 5 mm) as shown in figure 4.2. Air was blown across the coil and a thermocouple was used to regulate the temperature. The sample went through the spiral and the hot air was blown in tangentially to secure maximum heat-transfer to the spiral and therefore to the sample. The heating tube and the desolvation chamber were both made of glass and due to tension in the spiral a maximum temperature of only 150 $^{\circ}$C was possible. It was hoped that the longer desolvation path and the shorter total path length would lead to an enhancement in signal without increasing washout time. Unfortunately, a few problems did occur. The first problem was that the spiral started to act as a condenser as soon as the temperature was increased. The spiral was soon full of solvent and the gas flow was therefore obstructed. The second problem followed the first problem in that a drain was now needed for the excess solvent in the spiral. Without the drain all the condensed solvent gathered in the spiral and the upward force of the carrier gas stopped it from running down into the spray chamber. It was possible to get rid of the second problem by increasing the pitch of the turns in the spiral together with an increase in the diameter of the spiral. This was not done because the injection tube and the joint between the torch and the desolvation chamber were not hot enough to prevent condensation and this design was therefore replaced by the heated chamber and condenser used in the second instrumental arrangement. (Figure 4.3).

The condenser is a modified Friedrichs condenser similar to that described by Veillon and Margoshes.[137] Berman et al[12], Dickinson and Fassel[46] and Uchida et al[135] all used similar condensers in their work on ultrasonic nebulizers. The cylindrical heating chamber, 15 cm long and 5 cm in diameter was wrapped with a heating tape. The only modification to the standard 35 cm Friedrichs condenser was the installation of a side arm to allow the dry aerosol to exit to the plasma. The temperature of the heating chamber was varied to determine the optimum desolvation temperature. A thermocouple was used to monitor the temperature. Experiments were done with and without the spray chamber (third instrumental arrangement, Figure 4.4.) to investigate the influence of the spray chamber on the
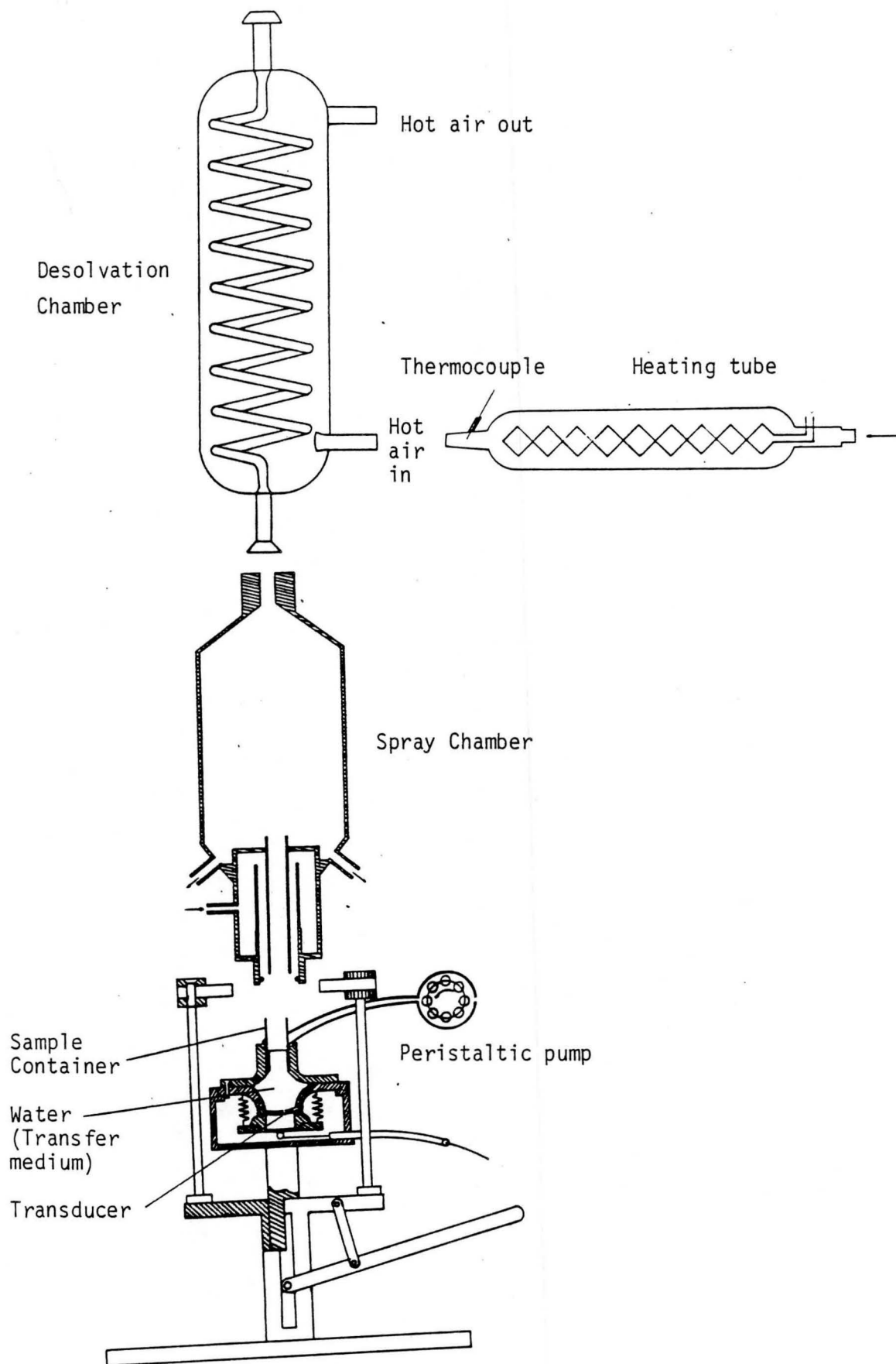
Figure 4.2 The first nebulizer, spray chamber and desolvation chamber arrangement that was used. The nebulizer is a custom built batch-type ultrasonic nebulizer. The desolvation chamber is a new design that was tested.
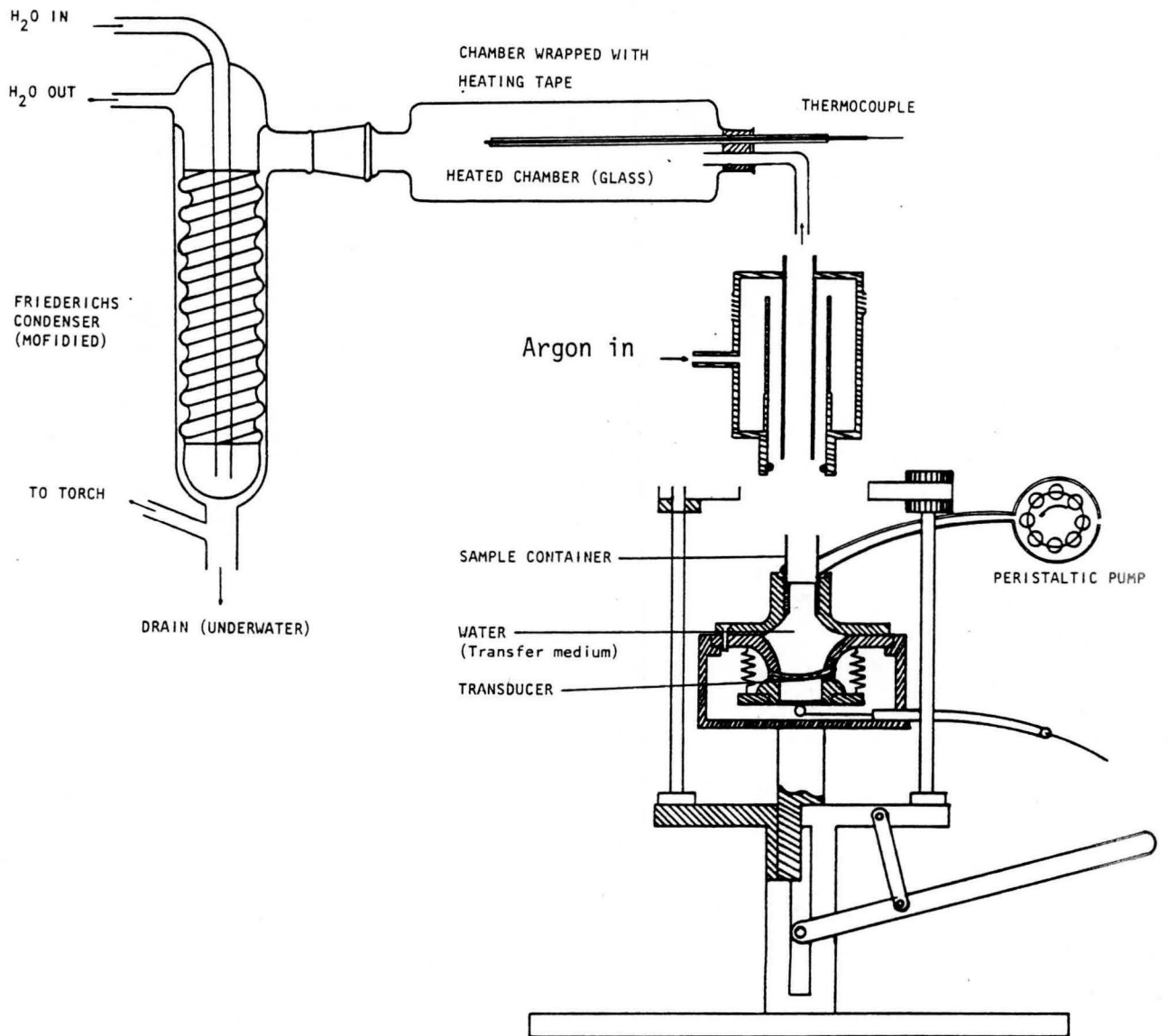
Figure 4.3 The second nebulizer and desolvation arrangement that was used.
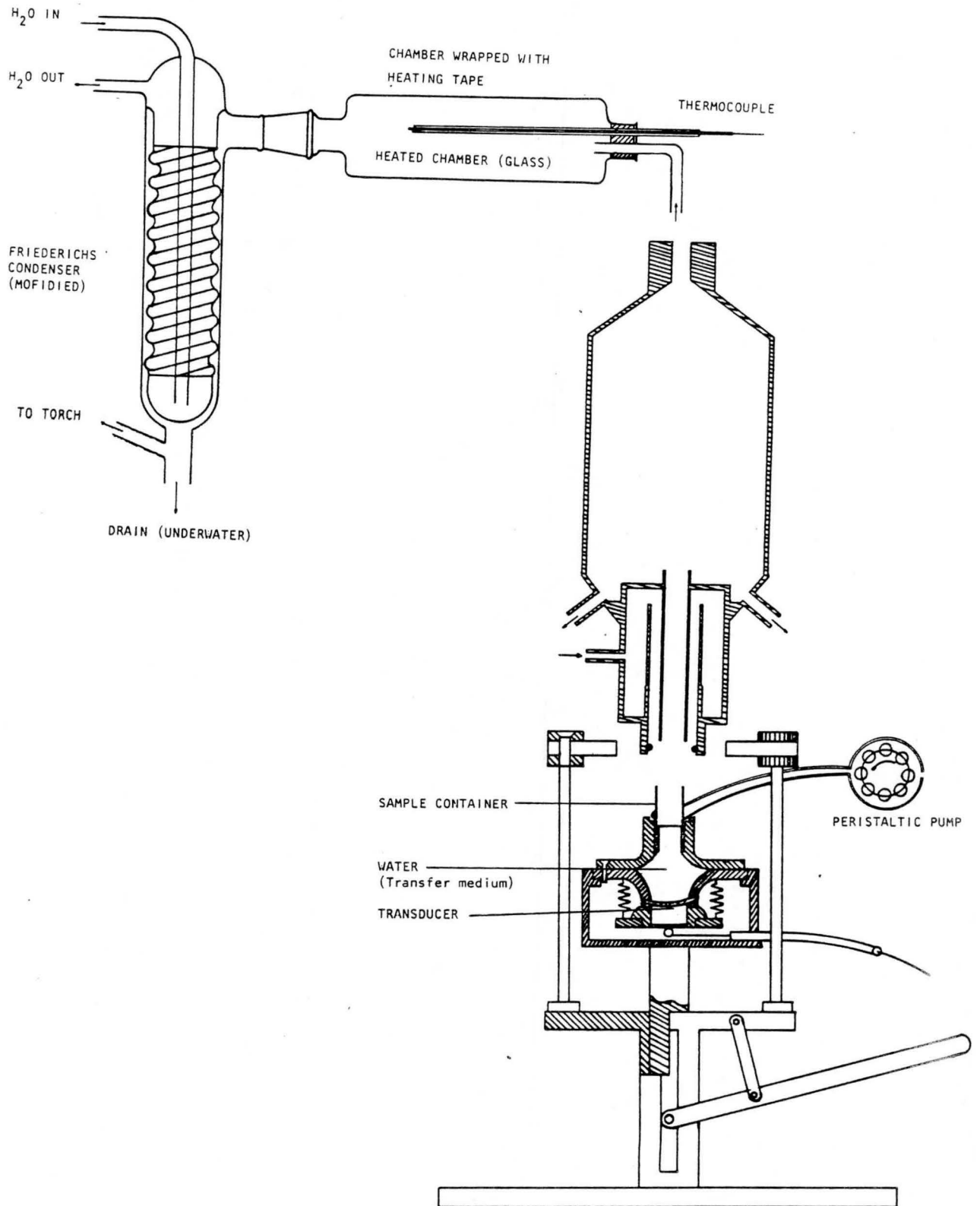
Figure 4.4 The third nebulizer, spray chamber and desolvation arrangement that was used

aerosol. The standard arrangement without desolvation is shown in figure 4.5.

A cross-flow nebulizer (Figure 4.6) and a Babington-type nebulizer (Figure 4.7) (described by Suddendorf and Boyer[129]) was used for the comparative particle size distribution studies. The locally designed demountable torch employed in this study is scematically illustrated in figure 4.8.
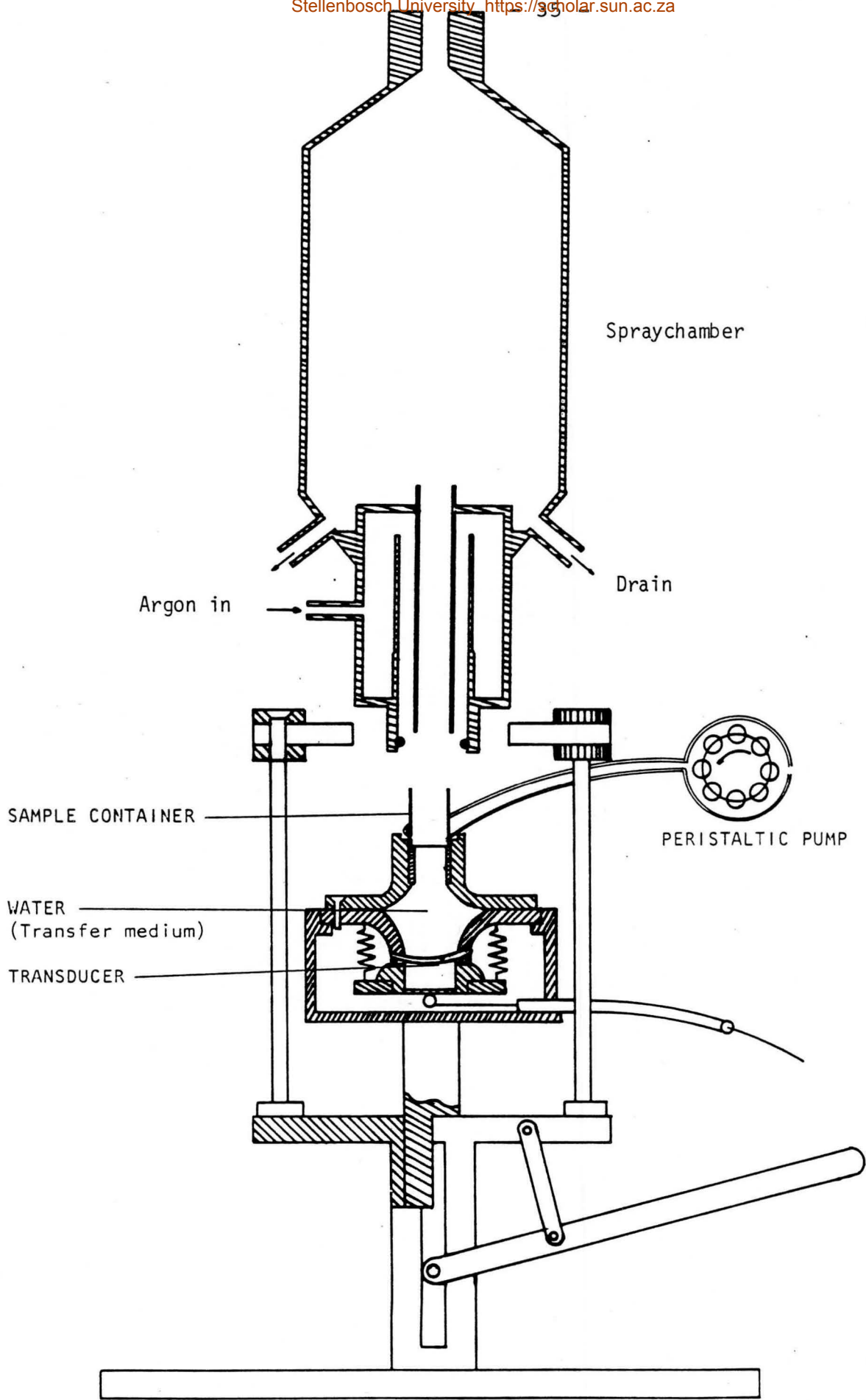
Figure 4.5 The standard instrumental arrangement without desolvation
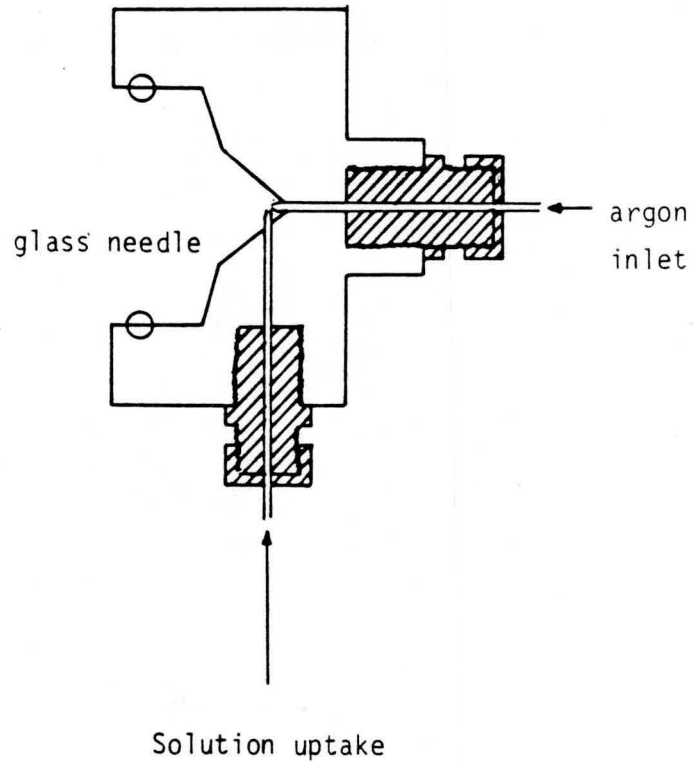
Figure 4.6 The cross flow nebulizer
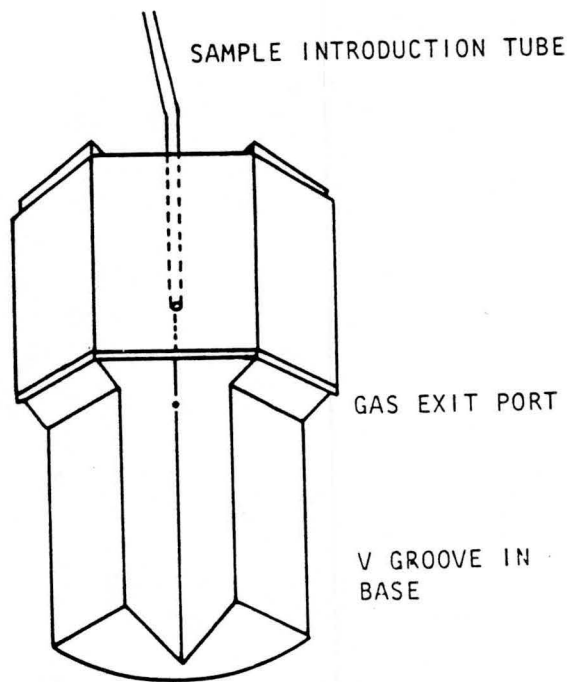
Figure 4.7 The Babington-type nebulizer
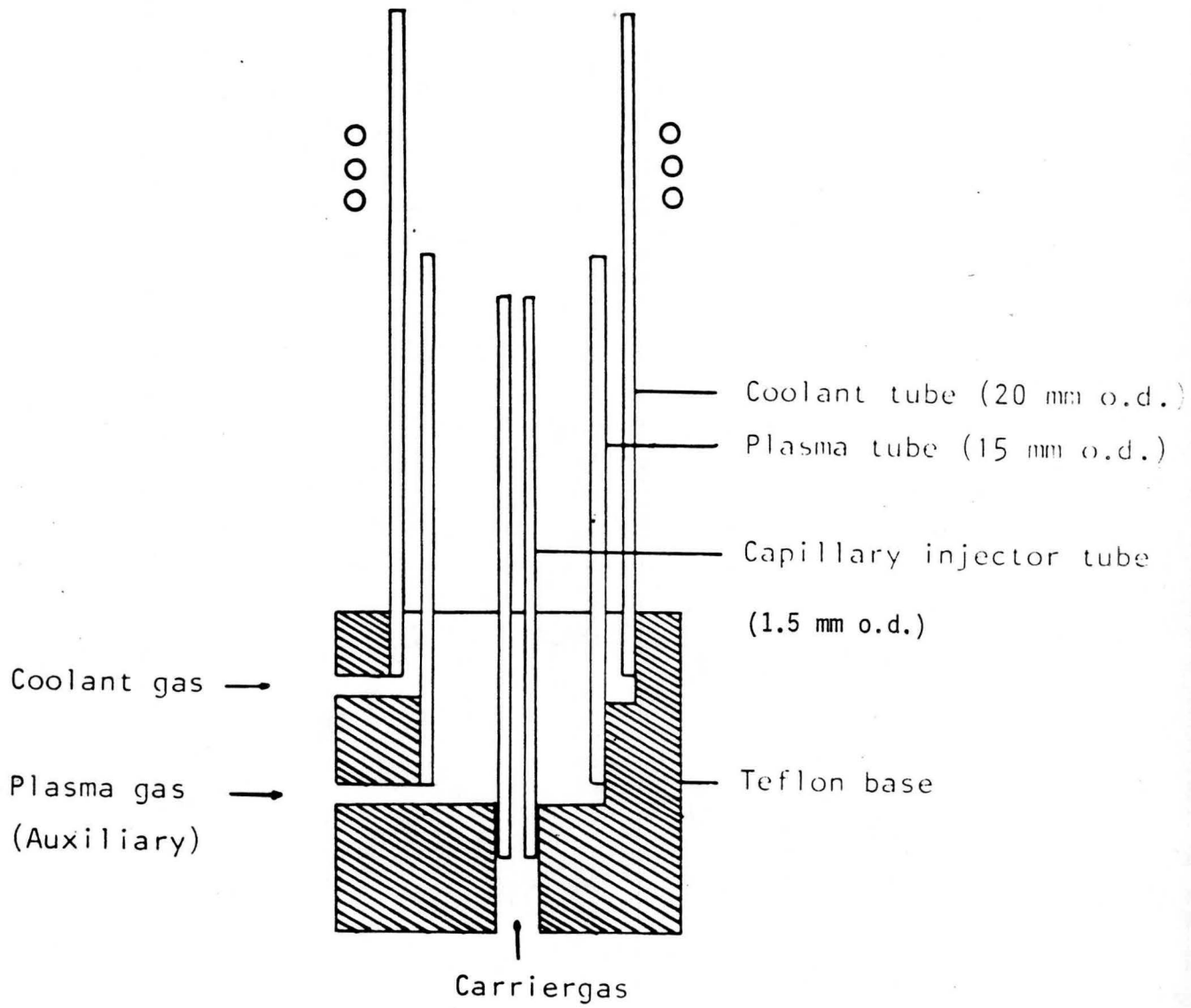
Figure 4.8 The locally designed demountable torch

4.2 *Application of the Ultrasonic Nebulizer to Atomic Absorption*

Virtually all modern flame atomic absorption work uses the pneumatic nebulizer. A significant quantity of sample is lost through the drain with the pneumatic nebulizer, and only about 10% reaches the flame.[75] Of this small percentage reaching the flame, sample is also lost through large droplets, not being desolvated in passing through the flame. Therefore, there is always a need for more efficient sample introduction techniques. The ultrasonic nebulizer was introduced as an alternative sample introduction technique.

The application of ultrasonic nebulizers to atomic absorption spectrophotometry has been discussed by several authors.[10,44,45,75,81,82] Hoare and Mostyn[75] combined an ultrasonic nebulizer with a commercial atomic absorption spectrophotometer and a comparison was made between the performance of the ultrasonic nebulizer and the pneumatic nebulizers with respect to sample consumption, absorbance measurements, stability and droplet size. Their principal finding was that the same sensitivity, given by the standard pneumatic nebulizer, can be achieved on a smaller sample volume with the ultrasonic nebulizer. They also reported that the absorbance measurements given by the two nebulizers on various standard solutions are in close relationship to the respective rates of sample consumption.

Issaq and Morgenthaler[81] discussed the parameters relevant when using the ultrasonic nebulizer in atomic absorption. Their aim was to explore the potential of the ultrasonic nebulizer in atomic absorption by investigating parameters that are affected by heated chamber systems. Their study revealed that the heater temperature is the most critical one. They reported that there is an optimum temperature at which the chamber should be operated.

The aim of this study was to compare the detection limits obtained by the standard pneumatic nebulizer and the ultrasonic nebulizer. Specifications of the apparatus used for the AA-study are summarized in Table 4.2. Certain adjustments were necessary for the use of the ultrasonic nebulizer with the AA-spectrometer. These include a modification of the sample inlet and the gas flow connections due too high

Table 4.2

Atomic Absorption Instrument	Varian Techtron 1275 BD
Optical system	
Single beam arrangement	
Monochromator	
Wavelength range (nm)	185-900
Accuracy (nm)	0.2
Reproducibility (nm)	0.1
Spectral Bandwidth (slit) (nm)	Selectable 0.2, 0.5, 1.0
Dispersing system Grating(in Czerny-Turner mounting)	30mmx35mm 1200 grooves/mm
Blazed wavelength (nm)	250
Focal length (mm)	254
Reciprocal linear dispersion (nm/mm)	2.7 at 250 nm
Burner adjustments	
Vertical range (mm)	20
Lateral range (mm)	14
Nebulizers	
Standard-Fixed Stainless Steel Pneumatic Nebulizer	
Ultrasonic Nebulizer	

pressure. (Figure 4.9). The standard pneumatic nebulizer needs a high primary pressure for nebulization while the ultrasonic nebulizer does not depend on the carrier gas flow rate for sample production. On the other hand a high pressure is also necessary to produce a proper flame. These problems were solved as shown in figure 4.9.
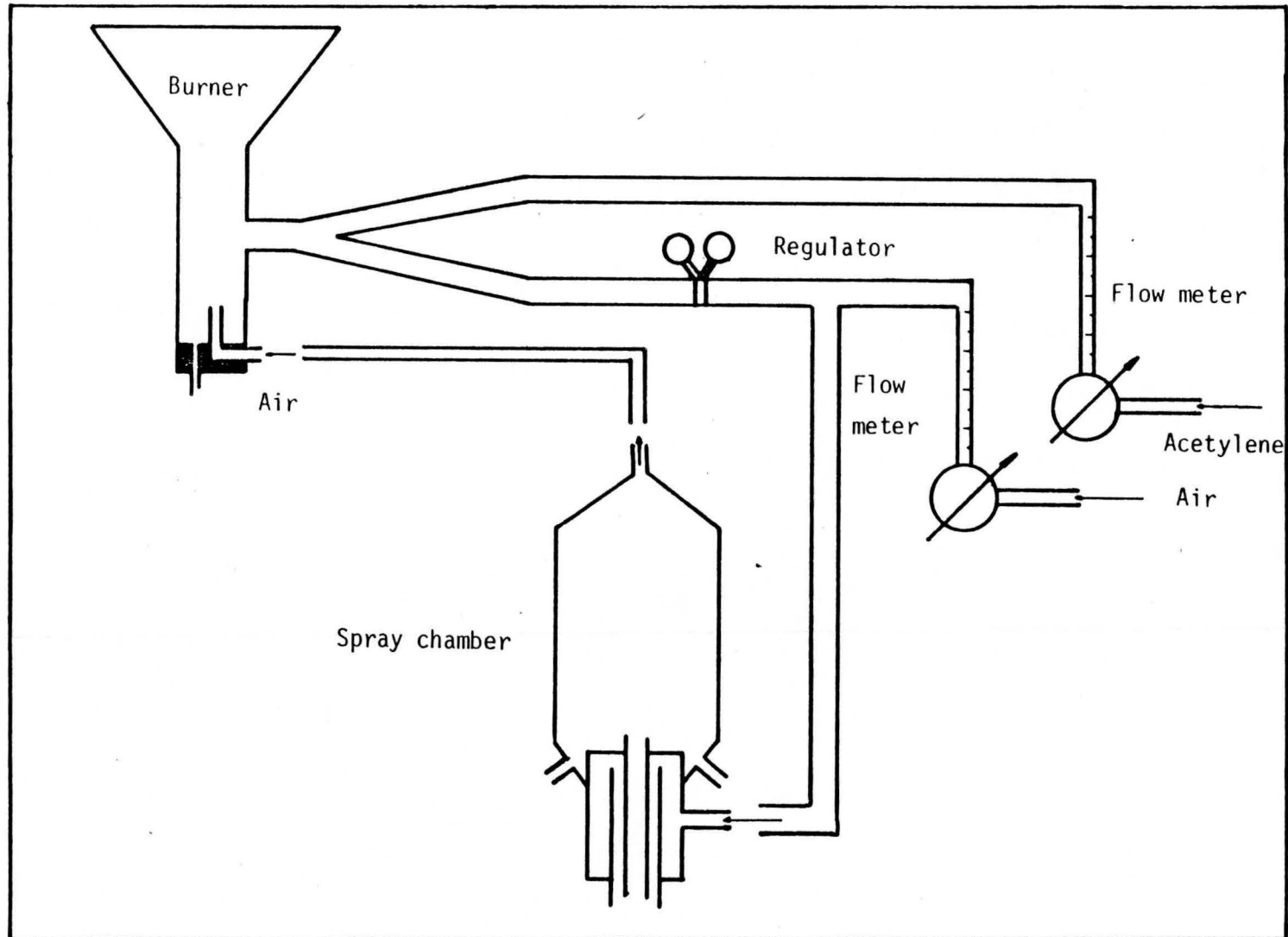
Figure 4.9   The modification of the sample inlet and the gas flow connections for the AA apparatus

4.3 *Optical Imaging System and Dispersion Instruments*

The 3.4 m Ebert spectrometer, built in our workshop, was employed as dispersion instrument.(Figure 4.10). It is equipped with a photo-electrical recording facility and a driving mechanism for spectral scanning by rotation of the grating. It offers a high resolution and low stray light characteristics. It is of the "over-under" type employing a grating of size 102×102 mm^2, with 1200 lines/mm (Bausch and Lomb), blazed at 250 nm in the first order, producing a reciprocal linear dispersion of 0,24 nm/mm. An entrance slit width of 25 μm was used, while the exit slits were 75 μm wide, producing a spectral bandpass of approximately 0,018 nm. Measurements were taken in the first order. The spectrometer is fitted with six independent wavelength channels. The photo current of each photomultiplier tube is fed to a current-to-frequency converter. An image of the ICP source was formed by a spherical lens on a diaphragm situated 5,4 cm from the entrance slit. A quartz convex lens was placed in front of the entrance slit to form an image of the diaphragm on the collimator mirror. (Figure 4.12).

A McPherson model 218 scanning monochromator was also used in the temperature studies. This monochromator is fitted with a 1200 lines/mm grating in a Czerny-Turner mounting, and yields a reciprocal dispersion of 2 nm/mm.(Figure 4.11). The main characteristics of the two spectrometers used are compiled in Table 4.3.

Table 4.3

Characteristics of spectrometers employed

	Ebert "over under"	Czerny - Turner
Manufacturer	Self - built	McPherson
Grating (lines/nm)	1200	1200
Blazed (nm)	250	200
Slit width (μm)		
Entrance	25	25
Exit	75	25
Reciprocal dispersion (nm/mm)	0.24	2.0
Spectral Bandpass (nm)	0.018	0.050
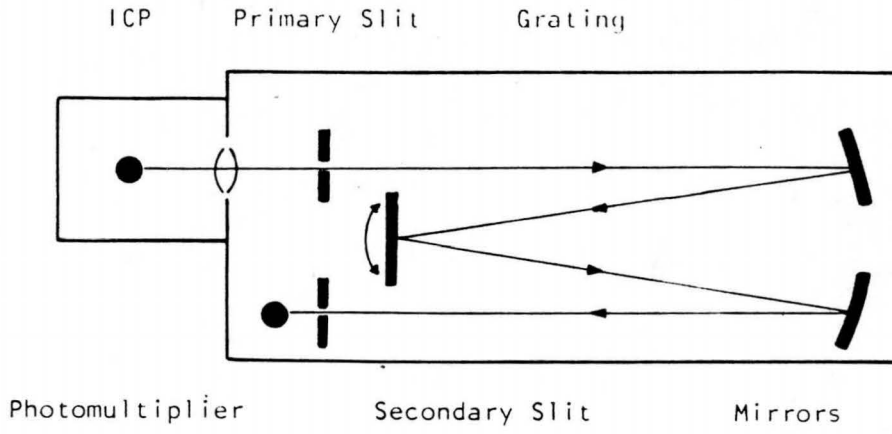
Figure 4.10   The optical system of the scanning monochromator showing (schematically) the Czerny-Turner mounting of the diffraction grating.

1. Primary Slit
2. Concave mirror
3. Collimator section
4. Grating
5. Camera section
6. Focal plane
7. Secondary slit
8. Photomultiplier
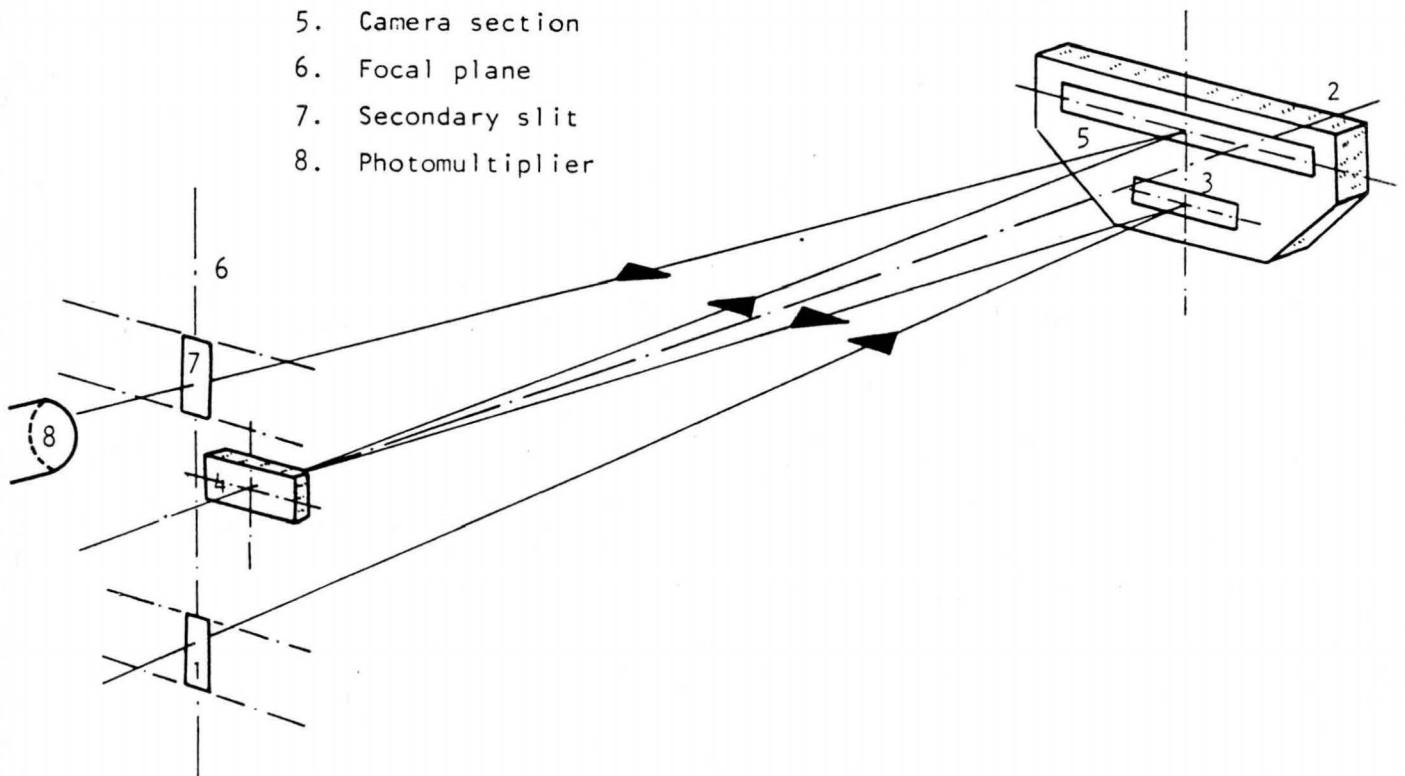
Figure 4.11   The lay out of the Ebert spectrometer

IMAGING SYSTEM
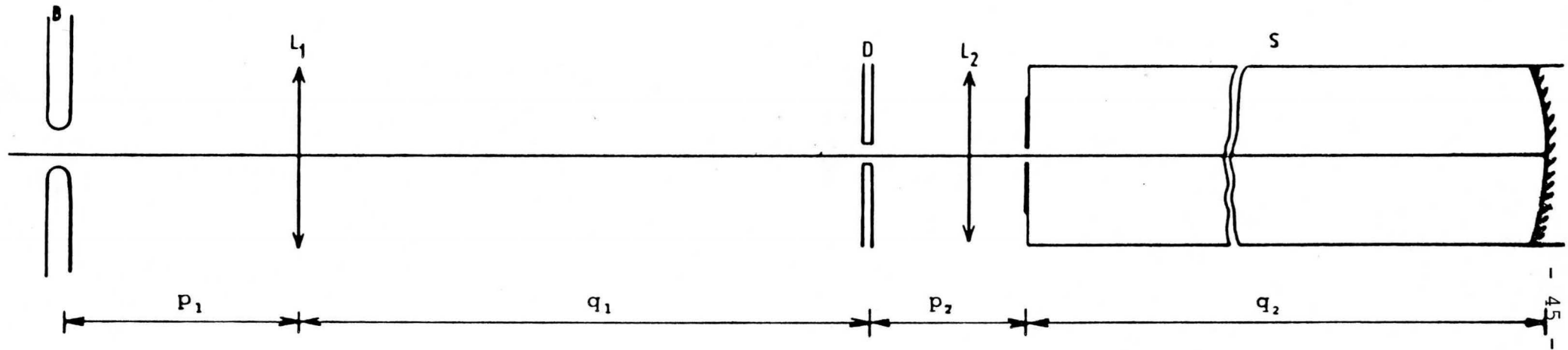
Figure 4.12   Optical Imaging System

f_1	= 21,3 cm	S = spectrometer
$|q_1|$	= 108,5 cm	B = source (ICP)
$|p_1|$	= 26,5 cm	D = diaphragm
f_2	= 5 cm	L_1, L_2 = lenses
$|q_2|$	= 340 cm	
$|p_2|$	= 5,1 cm	

CHAPTER 5

5. *THE INFLUENCE OF NEBULIZER PARAMETERS ON THE DROPLET SIZE*

The aim of this part of the project was to investigate several aspects of the generation and properties of aerosols in the nebulizer. A study was made of the effect of desolvation, nebulizer power and carrier gas flow rate on aerosols generated by the ultrasonic nebulizer. The droplet size from the ultrasonic nebulizer was also compared to the droplet size generated by a Babington-type nebulizer and a crossflow nebulizer. A characteristic sample with 10% HCl was used for all these measurements.

The nebulization of liquid samples is an essential process which has a direct influence on sensitivity and interference effects. Although many aspects of nebulization and the transport process are worthy of detailed investigation, the most important fundamental property of droplet spray is the droplet size because it affects the sample transfer efficiency, magnitude of interference and precision of measurement . The physical parameters of the aerosol should be well characterized and understood in order to fully understand the relative performances of the nebulizer spray chamber systems. Many researchers have worked on the characterization of aerosols.[10,28,35,37,40,74,92,109,110,120,122,123,127] Hieftje et al[10,35] have shown that the size of droplets nebulized, and of the subsequent micro salt crystals formed after desolvation, determines the spatial distribution of atoms in the plasma. Novak and Browner[109] have concluded that the droplet size distribution also affects rate of desolvation, rate of vaporization of the desolvated salt particles, and the magnitude of many interference effects. Stupar and Dawson[127] demonstrated that a relationship exists between the magnitude of certain interference effects and the size of particles remaining after solvent evaporation. Smith and Browner[123] also investigated condensed - phase vaporization interferences (e.g. calcium/phosphate, magnesium/silicon, etc) for a number of elements and matrices in both the air/acetylene and nitrous oxide/acetylene flames. They have examined the performance of several nebulizers and spray chambers and established a clear relationship between droplet size distribution entering the flame and the magnitude of the interferences. Changes in

analytical signal are dependent both on nebulizer properties and the modification in aerosol properties and it is difficult to distinguish between the two.[28] Changes in the one have a direct effect on the other. An example is the effect of change in power to the ultrasonic nebulizer on particle sizes.

A lot of the early workers have not produced reliable results because measurement of droplet size below 10 μm was very difficult, most of the droplet diameters in analytical flames are below 10 μm. Many methods for droplet size measurements exist, and perhaps the most widely utilized method has been a simple microscopic one[35,40]. A microscope slide is coated with magnesium oxide[35,40], mineral oil[75], or carbon black and passed through the droplet cloud. The droplets or their impressions are then observed under a microscope and counted according to size. These sizing techniques are labor intensive and are not well suited to accurate determination on droplets of less than 10 microns in size.

Two promising techniques appear to overcome the handicaps of microscopic techniques, namely cascade impaction and laser light scattering. Near-forward angle Fraunhofer diffraction[28,37,120] has been shown to possess many desirable traits for aerosol size measurements. The principle advantages of exceptional precision, with high accuracy in the 2 - 200 micron range, applicability to any aerosol, regardless of matrix content, speed of measurement and unobtrusiveness make the technique very useful for comparative aerosol size measurements.

5.1 Experimental Method

5.1.1 Particle Sizer Apparatus

A "MALVERN 2 600" particle sizer was used for the measurement of particle sizes. The instrument utilizes the principle of Fraunhofer diffraction of a laserbeam by aerosol particles. The instrumentation is illustrated in Figure 5.1. A low power He-Ne laser produces a parallel, monochromatic beam of light which is arranged to illuminate the aerosol to be studied. The incident light is diffracted by the particles to give a stationary diffraction pattern regardless of particle movement.   As particles enter and leave the illuminated area the diffraction pattern "evolves" always
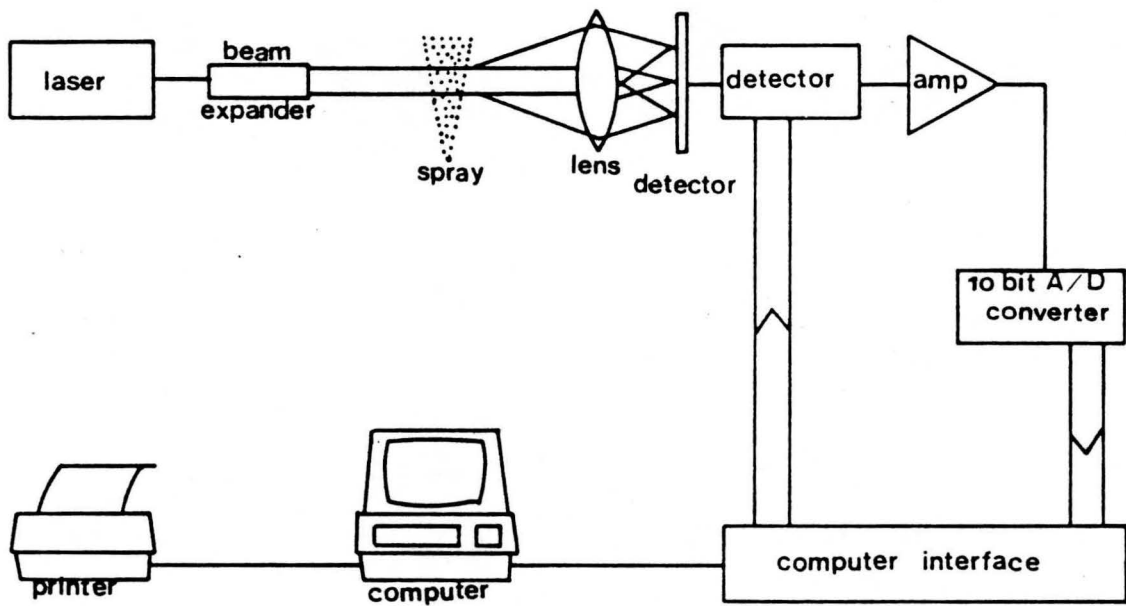
Figure 5.1 The droplet size measurement apparatus (MALVERN INSTRUMENTS 3600)

(a)

(b)
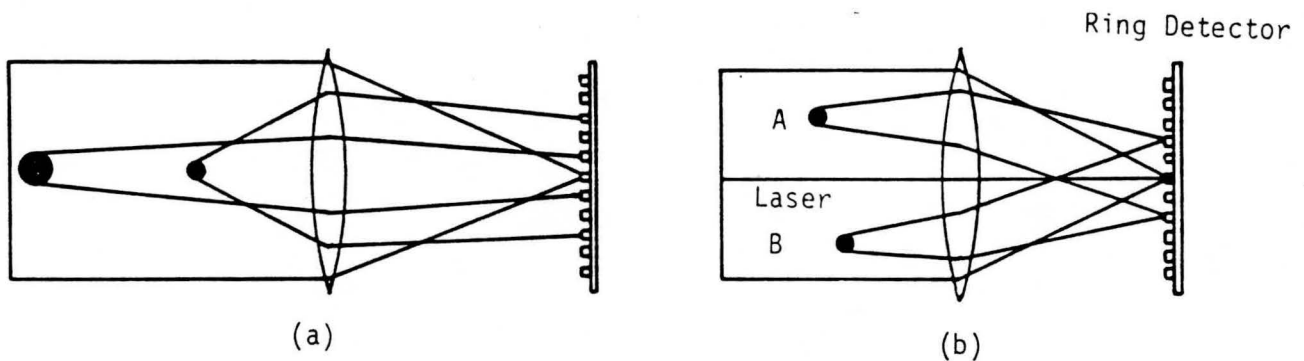
Figure 5.2 (a) Intensity at each detector element is the summation of the
                 intensity from all particles of a given size

          (b) Particles A and B are the same size therefore their diffraction
               angles are the same

reflecting the instantaneous size distribution in this area. (Figure 5.2). Thus by integration over a suitable period and a continuous flux of particles through the illuminated area, a representative bulk sample of particles contributes to the measured diffraction pattern. A Fourier transform lens focusses the diffraction pattern onto a multielement photo-electric detector which produces an analogue signal proportional to received light intensity. This detector is interfaced directly to a desk computer allowing it to read the diffraction pattern and perform the necessary integration. Having measured a diffraction pattern the computer uses the method of non-linear least squares analysis to find the size distribution which gives the closest fitting diffraction pattern. The size distributions can be analytically generated from the three parameter models Rosin Rammler and Log.Normal or Normal or can be obtained by other models under user control. The Rosin Rammler distributions were used in this study. It was originally devised for modelling the size distribution of broken coal. Further work has extended its applicability to many other materials such as sands, ores, clays, etc. However, its most useful area of applicability is in modelling the distribution of droplet sizes in various types of spray atomizers. The cumulative undersize weight distribution is modelled by the equation

$$R = \exp{(-d/x)^N} \qquad\qquad (5.1)$$

The parameter x indicates approximately the position of the peak of the weighted frequency distribution. The x value may range over 1 - 2 000 microns. The N value indicates width with narrow distributions giving high N values and vica versa. The printout of the sizer includes a summary of some derived diameters taken from a numerical integration or interpolation of the cumulative undersize volume (weight) distribution reported. These results are therefore not independently measured but are alternative interpretations of the size distributions obtained by numerical means.

V.M.D represents the Volume Mean Diameter

$$D_{43} = \frac{\sum\limits_{i=1}^{m} N(x_i)x_i^4}{\sum\limits_{i=1}^{m} N(x_i)x_i^3} = \frac{\sum\limits_{i=1}^{m} V(x_i)x_i}{\sum\limits_{i=1}^{m} V(x_i)} \tag{5.2}$$

S.M.D represents the Sauter Mean Diameter.

$$D_{32} = \frac{\sum\limits_{i=1}^{m} N(x_i)x_i^3}{\sum\limits_{i=1}^{m} N(x_i)x_i^2} = \frac{\sum\limits_{i=1}^{m} V(x_i)}{\sum\limits_{i=1}^{m} \frac{V(x_i)}{x_i}} \tag{5.3}$$

where

$N(x)$ = number frequency

$V(x)$ = volume (weigthed) frequency

$\quad x$ = particle diameter

5.1.2 *Nebulizer, Spray Chamber and Desolvation Apparatus*

Three different arrangements of apparatus which were used for measuring droplet sizes are illustrated in figures 4.2, 4.3 and 4.4. A comparison of the droplet size from a cross flow nebulizer and a Babington nebulizer and the ultrasonic nebulizer was also made.

5.2 *Theory of Aerosol Production*

Wood and Loomis (1927) first reported aerosol generation by ultrasonic waves[127]. Lobdell (1967)[92] explained the production of droplets with the aid of ultrasonic waves. Capillary waves, as a result of ultrasonic excitation, reach very high amplitudes so that the wave peaks separate from the liquid or sample by a

process called the geyser mechanism. There is a lot of momentum trapped in such a "geyser" and the waves continue to seperate from the sample and so form a fog of very small droplets.

The cross-flow and the Babington-type nebulizers are both dependent on high pressure gas flow. The particles are formed by a process of impact where the sample stream is broken up into particles by a perpendicular high velocity gas stream crossing it . (Figure 4.6 and Figure 4.7)

Browner et al[28] discussed an "aerosol transport model" to explain processes which occur in aerosol generation and transport. (Figure 5.3) They have divided the processes into three categories namely the "primary" generation step, where the initial sample is broken up into an aerosol by pneumatic, ultrasonic or other means. The "secondary" process is where a impact bead or impact surface is used. The "tertiary" process involves impaction, turbulent and centrifugal loss, gravitational settling, and evaporation. These are all processes which modifies the droplet size distribution prior to entering the plasma. Droplet sizes are in all instances shifted to smaller sizes. In the case of pneumatic nebulizers all the processes, except evaporation, have a negative effect on the analyte transport to the plasma. The sample loss with the batch-type ultrasonic nebulizer used in this project is minimal because most of the excess sample runs back into the sample container and only the large drops from the side of the spray chamber are lost through the drain. The efficiency is much higher in comparison with the pneumatic nebulizers. The "tertiary" drop size is the important one in predicting particle dynamics and ultimate atomization in the plasma. The nebulization efficiency depends on all three processes. Stupar and Dawson[127] discussed the stages whereby an aerosol is transformed into an atomic vapor.(Figure 5.4) One of the proposed mechanisms of droplet formation is that the droplets are set into oscillation by the high velocity gas stream as it leaves the cappilary, and filaments of liquid are sheared off. (Figure 5.5)

No precise theoretical formulas have been discovered which agree with observations of droplet formation. Semi-empirical formulas have been developed which are of value in predicting the consequences of changes in nebulizers, spray chambers or
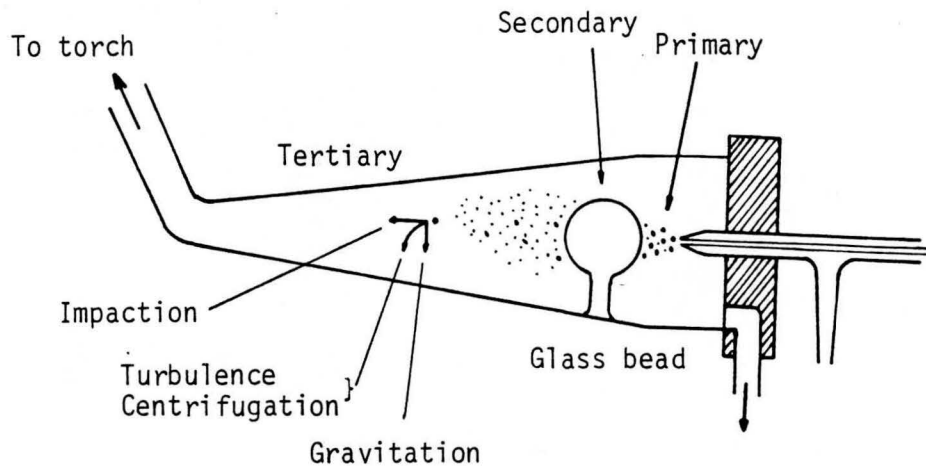
Figure 5.3 Stages in aerosol generation
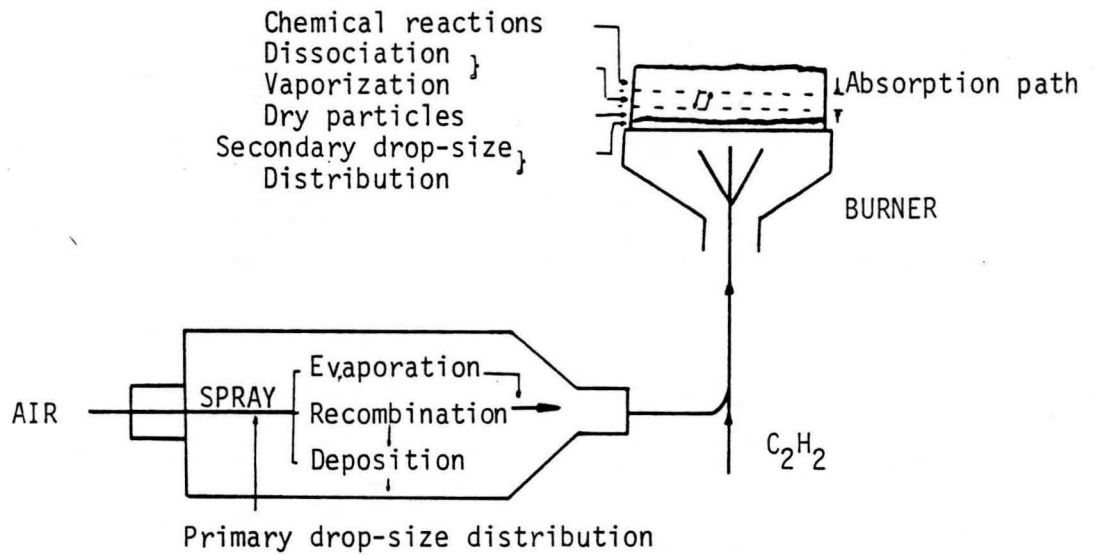
Figure 5.4 The production of an atomic vapor from a solution

Figure 5.5 Breakdown of liquid filament into droplets

solution parameters. The solution flow rate (Q_L) through a pneumatic nebulizer is governed by the Poissuille equation, i.e.

$$Q_L = (R^4 \Delta P/8\eta l) \text{ cm}^3 \text{ sec}^{-1} \tag{5.4}$$

R = radius of capillary (cm)
ΔP = effective pressure difference (dyne cm^{-2})
η = viscosity (g cm^{-1} sec^{-1})
l = length of capillary (cm)

The most satisfactory equation relating to droplet production is an empirical one given by Nukiyama and Tanasawa.[111] It was developed for a specific (concentric) nebulizer.

$$d_o = \frac{585}{(u-v)} (\frac{\eta}{\rho})^{0.5} + 597 (\frac{\eta}{\gamma\rho^{0.5}})^{0.45} (10^3 \frac{Q_L}{Q_G})^{1.5} \tag{5.5}$$

d_o = Sauter mean (volume/surface) diameter (microns)
u = velocity of gas (m sec^{-1})
v = velocity of liquid (m sec^{-1})
γ = surface tension (dyne cm^{-1})
ρ = density (g cm^{-3})
η = viscosity (g.cm^{-1}.sec^{-1})
Q_L = flow rate of liquid (cm^3.min^{-1})
Q_G = flow rate of gas (cm^3.min^{-1}).

Stupar and Dawson[127] used this equation and inserted typical values for a pneumatic nebulizer (u ~ 333 m/sec, v ~ 1 m/sec, Q_G = 8.5 liters/min) and the physical constants of a variety of solutions used in atomic absorption. An interesting result from their work was that at low flow rate an ethanol - water mixture resulted in a significant reduction in d_o when compared to water, whereas at high flow rates, the reverse was true. They explained this phenomenon with the help

of equation (5). At low flow rates, the first term is dominant resulting in d_o being proportional to (surface tension)^{0,5} and inversely proportional to the gas velocity; at high flow rates, the second term makes a significant contribution to d_o. This is mainly attributed to the ratio $Q_L/Q_G{}^{1,5}$ and (viscosity)^{0,45} thus, droplet size increase with flow rate and viscosity. They came to the conclusion that a reduction of the drop size d_o generated by a pneumatic nebulizer may be possible if the velocity of the gas flow can be increased without an increase in volume flow of gas which would offset the gain in sensitivity in atomic absorption. Browner and Boorn[28] also pointed out that improvement in transport efficiency must not be achieved by introduction of large aerosol drops. They stated that for a solution of concentration C (μg/mL), contained in a drop of initial diameter d_0, the dry salt crystal of density ρ (g/cm^3), formed after solvent loss, will have a diameter d_x (μm), given by

$$d^3{}_x = d^3{}_0 (C/\rho) 10^6 \qquad (5.6)$$

Browner et al[28] warns about a serious misconception arising from the fact that the Nukiyama and Tanasawa equation provides data only on the so called "primary" drop size distribution.

The ultrasonic aerosol produced by means of the geyser mechanism led to the following equation:

$$d_o = 0,34 \left(\frac{8\pi\sigma}{\rho f^2} \right)^{1/3} \qquad (5.7)$$

where σ = surface tension of the solution in dyne/cm

ρ = specific gravity in g/ml

and f = frequency in hertz.

Factors such as cavitation, viscosity, vapor pressure, and ultrasonic power also play a part in the nebulization process. Stupar and Dawson[127] felt that it is more likely that these parameters affect the nebulization rate rather than the droplet size.

The droplet size will decrease with an increase in frequency according to Eq.(5.7). At low frequencies (i.e. 50 kHz), cavitation is the main mode of droplet formation and at the high frequencies commonly used in modern ultrasonic nebulizers, typically 1-2 MHz or greater, the mechanism of aerosol production changes from cavitation to the so called geyser formation. Therefore power density in the liquid surface, rather than the operating frequency, becomes of major importance. This is contradictory to what Stupar and Dawson said.

The so called "tertiary" processes are all predominantly aerosol loss processes. Browner et al[28] suggested a more useful criterion for assessing the performance of nebulizers and spray chambers, namely the so called W-parameter. W_u is the usefull mass transport rate given by,

$$W_u = \sum_{o}^{d_{max}} W \tag{5.8}$$

and W_e is the excess mass transport given by,

$$W_e = \sum_{d_{max}}^{\infty} W \tag{5.9}$$

"Useful" analyte is considered to refer to analyte contained in drops sufficiently small ($< d_{max}$) to produce useful analytical signals and "excess" refers to analyte contained in droplets that are too large ($> d_{max}$) to produce useful signals in the atomizer. The transition of "useful" to "excess" occurs in the region of a maximum droplet size (d_{max}) 3 to 5 μm.[28] These cut-off diameters are therefore very much dependent on the "tertiary" processes. Gravitational settling has been used by Skogerboe and Olson[122] to predict cut-off diameters. The model is based on Stoke's law and describes a terminal settling velocity, V_s, such that

$$V_s = \frac{d_a^2 \rho_a g}{18\eta} \qquad (5.10)$$

where g is the gravitational constant, ρ_a = density of the aerosol entities, d_a is the radius of the aerosol droplet, and η is the viscosity of the gaseous transport medium. Browner et al[28] pointed out that a droplet of diameter d_a, initially in the middle of the spray chamber will be removed by fallout to the bottom of the chamber when $V_s \geq D/2t$, where t is the time the aerosol spends in the chamber of diameter D.

Vaporization is another tertiary process that is worth looking at. Together with desolvation is it one of the most important events to convert a sample solution to free atoms. During desolvation, the solvent present in a droplet of solution travelling through a flame is evaporated until one or more solid solute particles remain. Vaporization is the process in which a solid solute particle produced by desolvation is converted to species in the vapor phase. Desolvation therefore plays a significant role in aerosols. The following equation shows how the droplet radius r varies with t, if the initial droplet radius is r_o,

$$r^3 = r_o^3 - 6 D_v \sigma p_s M^2 t (\rho RT)^{-2} \qquad (5.11)$$

where D_v = diffusion coefficient of solvent vapor

   σ = surface tension

   p_s = saturated vapor pressure

   M = molecular weight of the solvent

   ρ = density

   R = gas constant

   T = absolute temperature

   t = time

Cresser and Browner[37] inserted appropriate values for D, σ, p_s, M, ρ, R and T and derived the following equation

$$d^3 = d^3_o - 13.13 \, t. \tag{5.12}$$

We can now calculate how droplet diameters of water droplets change with time in saturated air. Cresser and Browner [37] did this and ended up with the graph given in figure 5.6. This shows that the smaller the diameter the quicker evaporation occurs even in the fraction of a second required for droplets to pass through a spray chamber. Cresser and Browner [37] also calculated and discussed evaporation of salt solution droplets.

It is important to distinguish between desolvation of the droplets in a heated chamber, and desolvation and vaporization in a flame. Hieftje and Malmstadt [74] showed that desolvation rate is a linear function of time in a flame. They used the folowing equation.

$$d^2 = d^2_o - kt \tag{5.13}$$

for their calculations. Attempts to relate rate of desolvation (k) to properties of the droplet, solvent, and the flame led to a model by G.S. Bahn. [74] Clampitt and Hieftje [28] evaluated this theory and did some further work on it. They have summed work as shown in figure 5.7. A droplet is surrounded by a thin film of solvent vapor which spreads by diffusion away from the droplet.

The rate of desolvation of a droplet in a flame is therefore limited by the rate at which heat can be conducted from the flame to the droplet surface. An expression for this heat-transfer controlled evaporation is given by

$$k = \frac{8\lambda M}{c_p \rho} \, \ln \, (1+B) \tag{5.14}$$

where λ = thermal conductivity of the vapour surrounding the drop in cal/sec cm^{o}K

c = heat capacity of the vapor at constant pressure in cal/mole^{o}K

ρ = density of the liquid in g/cm^3

M = molecular weight of solvent

B = transfer number

The transfer number can be expressed as

$$B = \frac{c_p(T_g - T_s) + \gamma Q}{H_v} \qquad (5.15)$$

where T_g = temperature of flame in ^oK

T_s = temperature of droplet surface (boiling point)

H_v = heat of vaporization of the solvent in cal/mole

γ = ratio of amount of oxygen present to that needed for stoichiometric combustion

Q = heat of combustion in cal/mol. (Taken as zero for noncombustible liquids such as water)

Clampitt and Hieftje[35] applied statistical thermodynamic considerations to evaluate the heat capacity and thermal conductivity because they found that for a given solvent vapor, the heat capacity and thermal conductivity are functions of temperature. This was the main problem they encountered with the above theory. They therefore came up with a alternative theory of desolvation. They predicted that the temperature profile near the droplet will appear as shown in figure 5.8.

The resulting model therefore indicates that the solvent is vaporized at the surface of the droplet and then rapidly heated to approximately flame temperature. This then produces a thin film of gas composed of almost entirely of solvent vapor which surrounds the liquid droplet. It is therefore apparent that heat conduction must occur across a region of solvent vapor which is almost completely at the flame temperature. In the region beyond the film of solvent vapor which surrounds each droplet, solvent molecules and flame gas molecules are beginning to diffuse together. (Figure 5.8). By using a heated chamber the residence time of the sample in the chamber is prolongned and therefore completely desolvated droplets reach the

(a)

Flame gases

λ_f

λ_m

λ_v T_s T_g

Droplet

Diffusion Mixture

(b)

Temp

T_g

Droplet

Droplet
Surface

Vapor

Radius
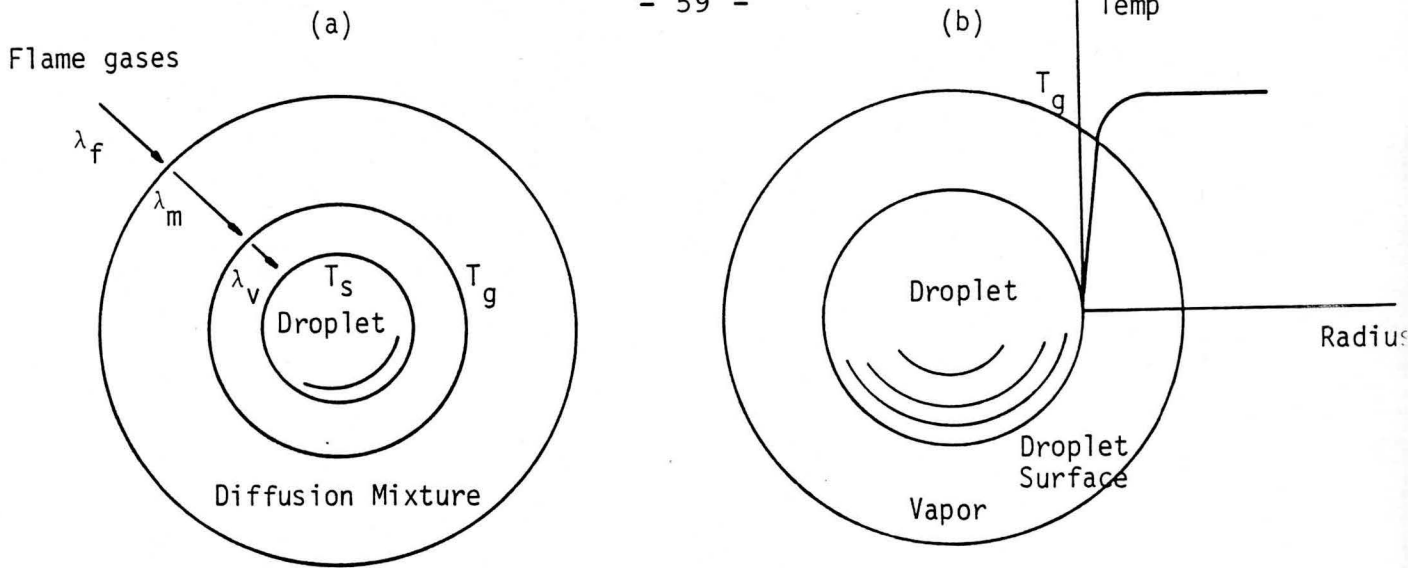
T_s = Temperature at the droplet surface

T_g = Flame temperature

λ_f = Thermal conductivity of flame gases

λ_m = Thermal conductivity of diffusion mixture

λ_v = Thermal conductivity of solvent vapor

Figure 5.7(a)   The processes involved in heat-transfer controlled desolvation of a droplet. (Clampitt & Hiefje)

Figure 5.8(b)   The predicted variation in temperature between the surface of an evaporating droplet and the flame. (Clampitt and Hiefje)

Remaining Droplet

Explosion

Vapor Escape

Crust Formation
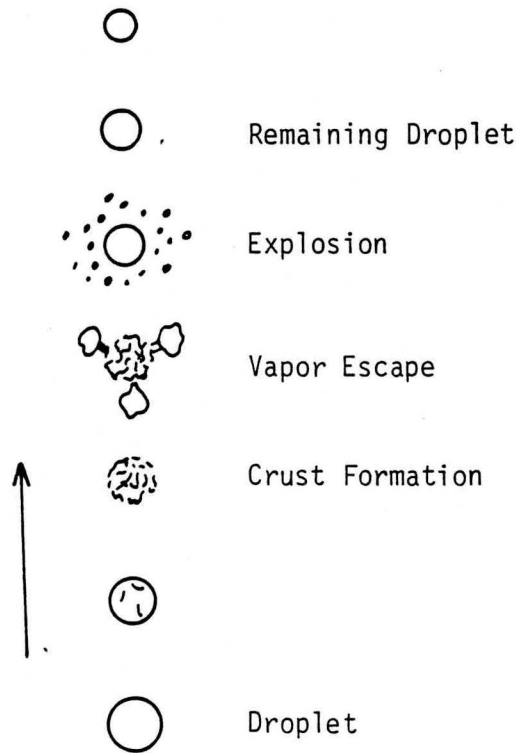
Droplet

Figure 5.9 Graphic illustration of proposed "exploding droplet" desolvation mechanism. (Bastiaans and Hieftje)

plasma.

Bastiaans and Hieftje[10] examined the interaction between desolvation and vaporization in the flame. They wanted to ascertain whether droplets were breaking apart before desolvation was complete and therefore used MgO-coated slides at different positions in the flame. They came up with the following explanation, illustrated in figure 5.9.

The droplet is heated to the solvent's boiling point shortly after the droplet enters the flame. As solvent vapor leaves the droplet, the local concentration of solute at the droplet surface increases, and solid precipitate will eventually begin to appear. It then starts to form a shell which physically impedes the further escape of solvent vapor from the droplet. If the shell eventually completely closes, the enclosed solvent vapor might exert enough pressure to break open the shell and throw fragments of solid away from the remaining droplet. This event would mark the start of vaporization.

5.3 *Data Presentation*

Graphs were drawn to illustrate the influence of carrier gas flow rate, desolvation and nebulizer power on particle sizes.(Figures 5.10 to 5.21)

5.4 *Results and Discussion*

5.4.1 *Influence of Carrier Gas Flow Rate and Desolvation on Droplet Sizes*

The carrier gas was varied from 0,4 l/min to 0,8 l/min and the desolvation temperature from 25°C to 150°C. With the first instrumental arrangement illustrated in figure 4.2, the influence of these variations on the particle size was investigated. The results are shown in Figure 5.10 and Figure 5.11. The mean droplet size is plotted against the carrier gas flow rate and the desolvation temperature. It is clear that the smallest droplets are obtained with low carrier gas flow rate and high desolvation temperature. This phenomenon is selfexplanetory because the residence time in the spray chamber is longer with low carrier gas flow
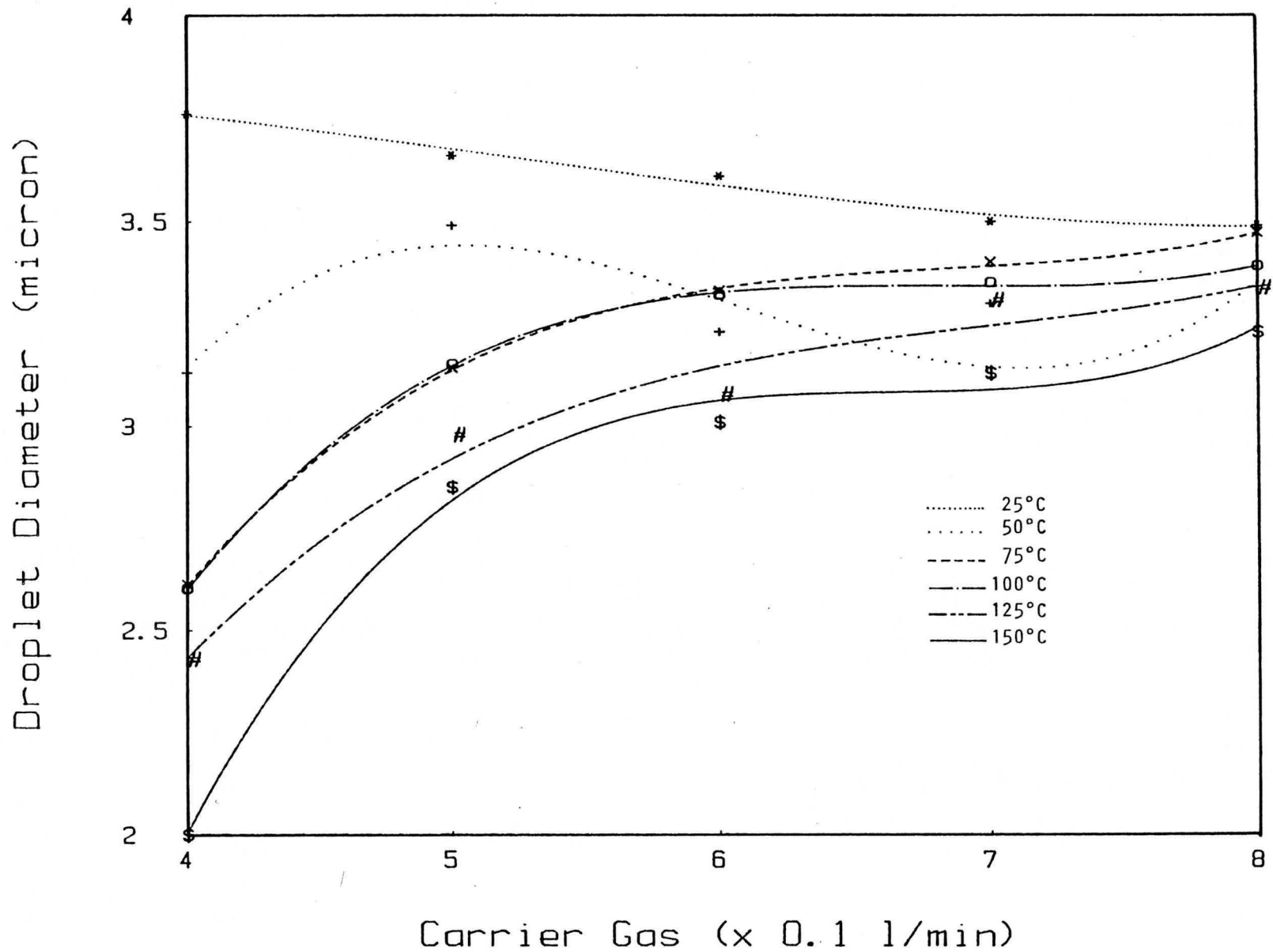
Fig. 5.10   The influence of carrier gas flow rate on particle sizes for different desolvation temperatures for the first instrumental arrangement.
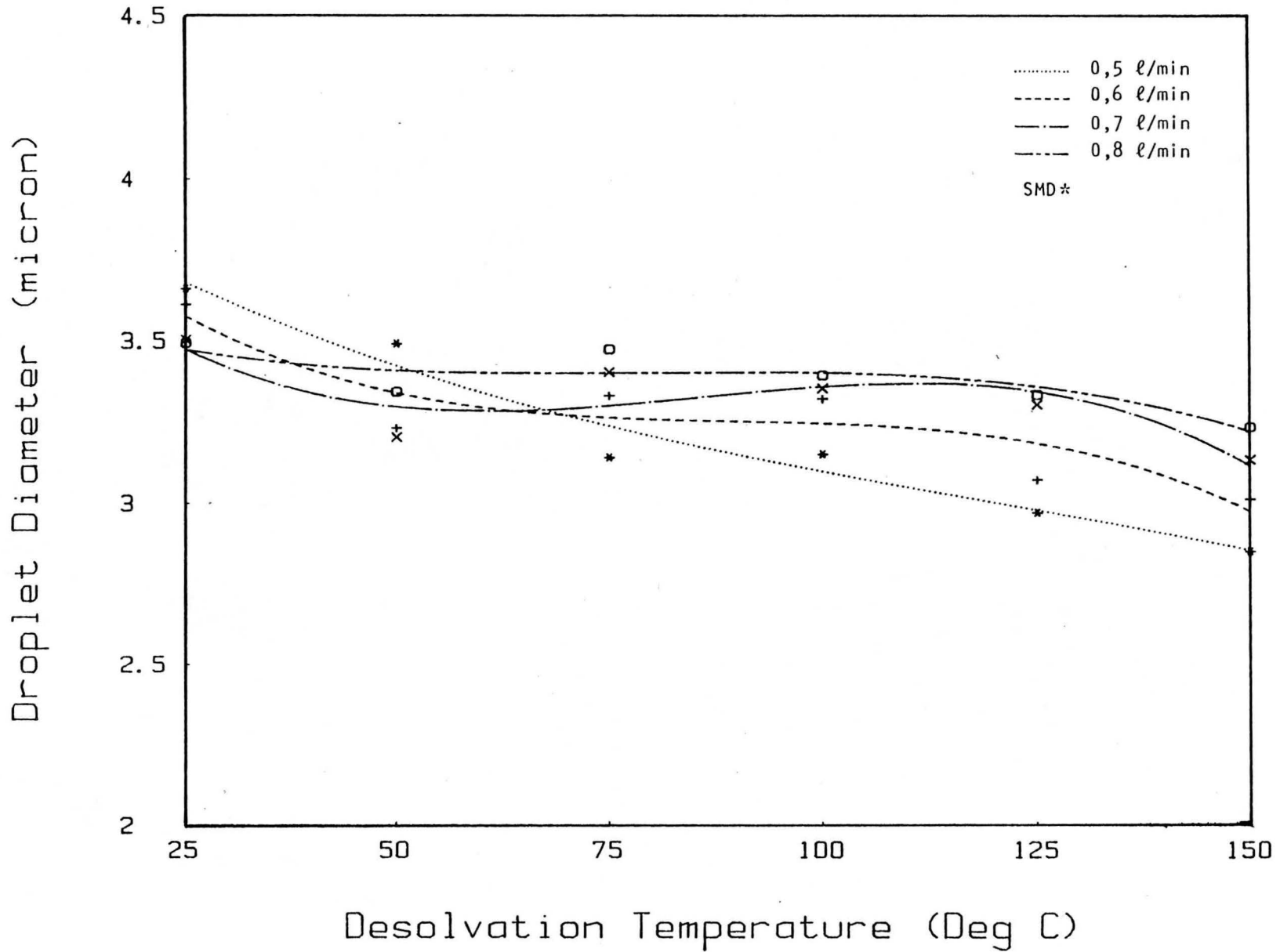
Fig. 5.11   The influence of desolvation on particle sizes for different carrier gas flow rates for the
first instrumental arrangement.

* Sauter Mean Diameter

rate and therefore the smaller droplets will result because of the high evaporation rate with high desolvation temperature. We can also see that at low desolvation temperatures the smallest diameter is obtained with high carrier gas flow rates. This shows that coagulation might be a problem at low carrier gas flow rate when no desolvation is used. This is due to the effective nebulization of the ultrasonic nebulizer. Stupar and Dawson[127] reported the opposite for pneumatic nebulizers, namely that there is a reduction in droplet sizes with decrease in flow rate. The reason for this is that with ultrasonic nebulizers the nebulization of aerosol is indepent of the carrier gas flow rate. This is one of the main advantages of the ultrasonic nebulizer. However, if the flow rate for ultrasonic nebulizers is high (>8 l/min) less uniform droplet sizes were obtained. Lang[89] attributes this non-uniformity to collision of the droplets. We can therefore say that stability increases as flow rate decreases. Mermet and Robin[99] came to the same conclusion. Another interesting obvervation is that the droplet size variation is more sensitive to changes in desolvation temperature than in carrier gas flow rate. This can be attributed to the long desolvation path of the spiral that was used in the first instrumental arrangement.

The graphs for the second instrumental arrangement (Figure 4.3) are shown in figures 5.12 and 5.13. Comparing figure 5.10 with figure 5.12 a difference in slope is apparent for the higher and lower desolvation temperature curves. This phenomenon is attributed to a shorter desolvation path with the instrumental arrangement illustrated in Figure 4.3. The data obtained without desolvation (25°C) shows a good correlation with both graphs indicating a Sauter Mean Diameter of ~ 3,8 microns. Therefore the change in the desolvation path length is responsible for the difference between figure 5.10 and figure 5.12. The difference between figures 5.11 and figure 5.13 is also due to this change. The narrow distribution underlines the earlier statement that desolvation is the dominant variable in reducing droplet diameters. The left and right hand sides of figure 5.13 reflect the contribution of desolvation temperature and carrier gas flow rate respectively. On the right hand side at 150°C the low carrier gas flow rate gives rise to the smallest droplets and on the left hand side the opposite is true.

The graph for the third instrumental arrangement (Figure 4.4) is shown in
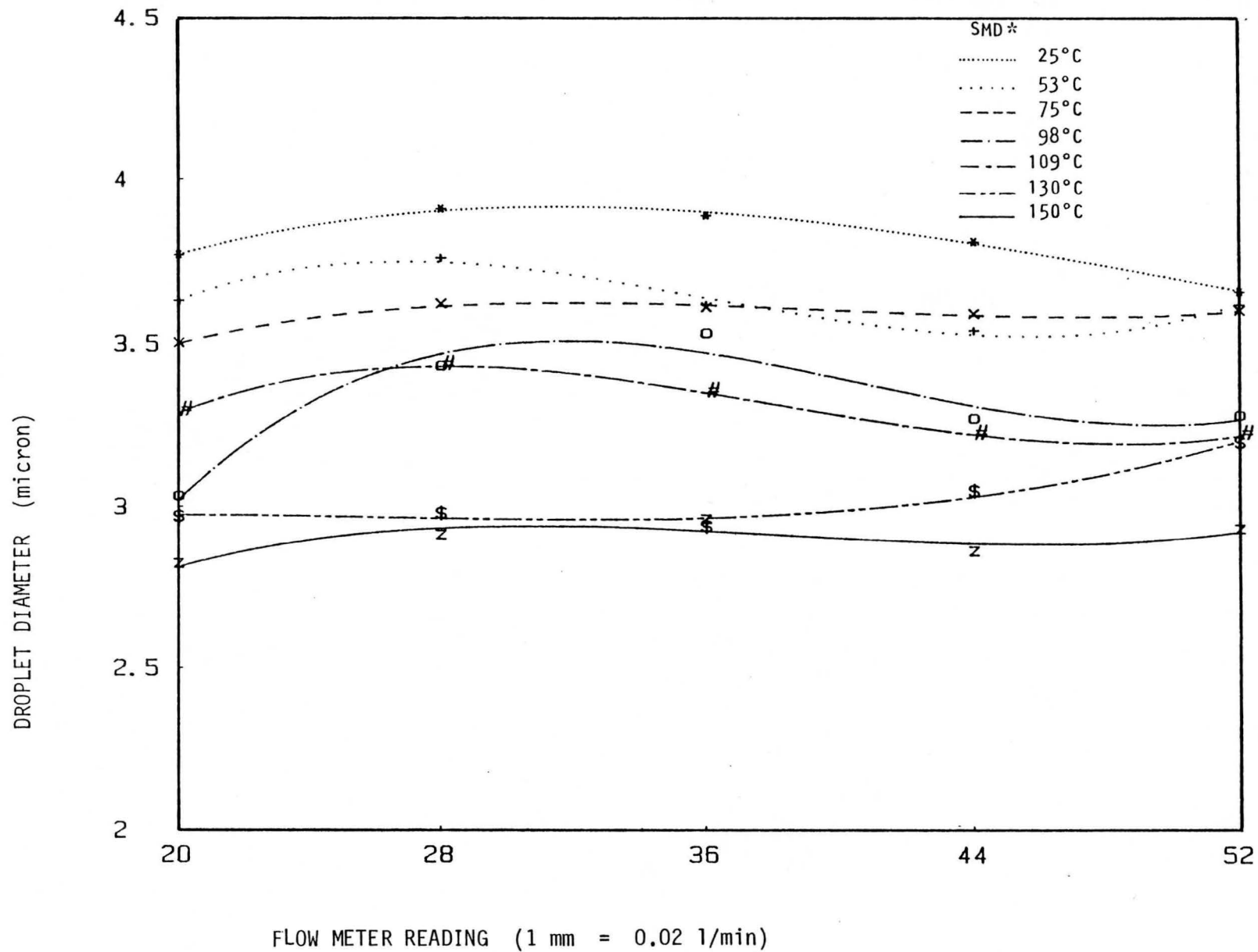
Fig. 5.12 The influence of carrier gas flow rate on particle sizes at different desolvation temperatures for the second instrumental arrangement.

* Sauter Mean Diameter
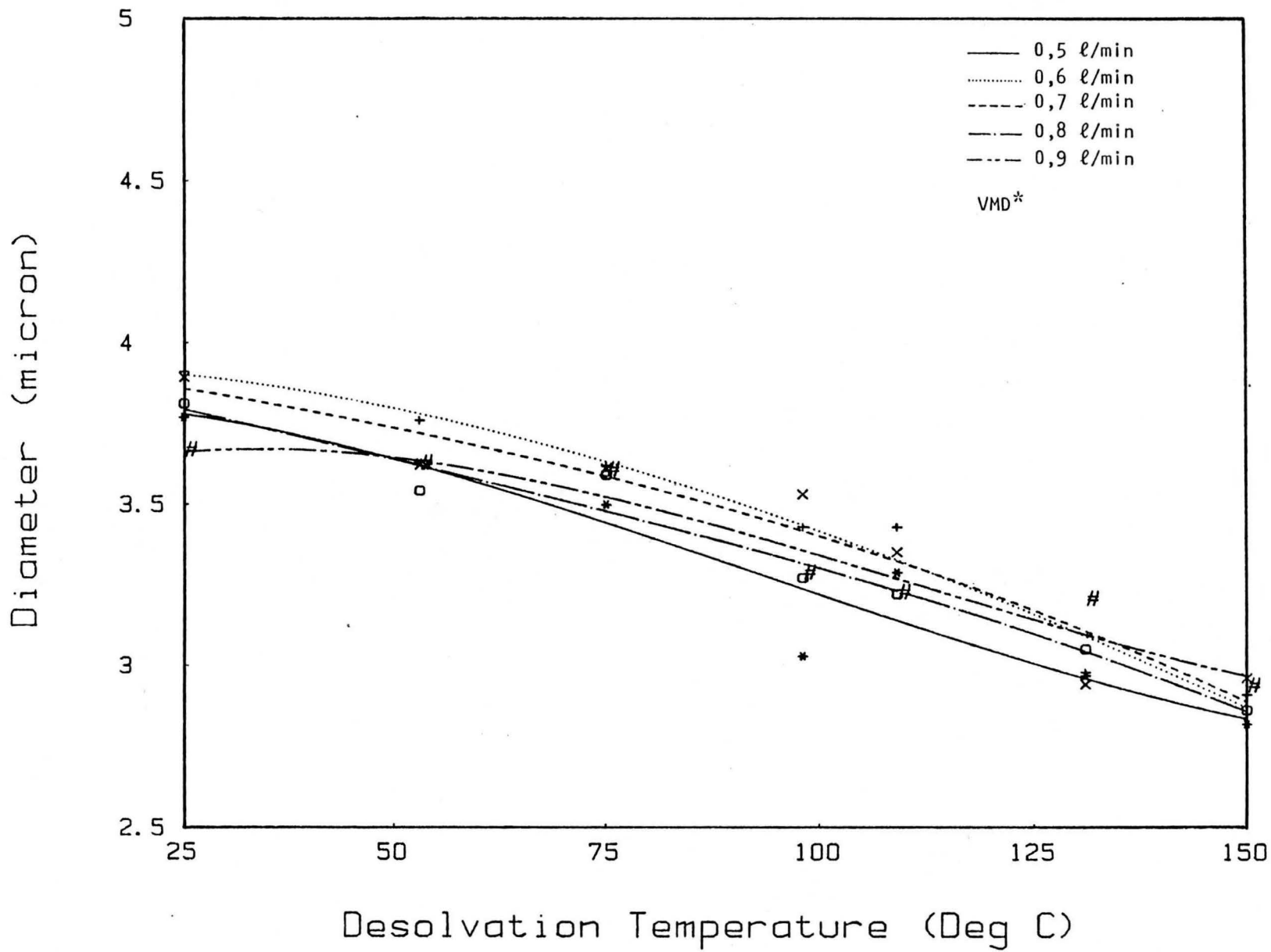
Fig. 5.13 The influence of desolvation on particle sizes for different carrier gas flow rates for the second instrumental arrangement.

* Volume Mean Diameter

figure 5.14. It is clear that the addition of the spray chamber lead to an increase in the particle sizes. This is unexpected as the purpose of a spray chamber is to get rid of the large droplets through the "tertiary" processes mentioned by Browner.[28] An explanation for this can be found in the distribution of the particle sizes. If we look at the histograms of the size distributions of the different nebulizers (see Section 5.4.3) one will notice the significant difference. The distribution for the ultrasonic nebulizer is narrow whereas the distributions for the cross-flow and Babington-type nebulizers are very wide. The use of the spray chamber enhances coagulation of the small droplets rather than extracting the larger droplets. Ham and Willis[73] as well as Goulden and Anthony[64] reported the same result in their work on impact devices and spray chambers. They also felt that recombination is a possible explanation for the larger droplets.

5.4.2 *The Influence of Nebulizer Power on Droplet Sizes*

The results of this investigation is plotted in figure 5.15. It is a well known fact that the droplet sizes decreases with an increase in frequency[43,118,127]. The ultrasonic nebulizer that was used has a fixed frequency of 2 MHz and only the input power can be varied. This was done and the results clearly show an increase in droplet size with increase in nebulizer power. Therefore the height of geyser formation increases with an increase in power. The graph has a maximum between 22.5 mA and 25 mA. The reason for this was clearly visible in practice. At currents above 25 mA the nebulization became more violent, producing large droplets and almost no fog. At this point the trancducer operation becomes unstable and the ICP response decreases because dry spots on the plastic film are alternatively formed and covered with sample. Goulden and Anthony[64] and Mermet and Robin[99] reported the same phenomenon in their work on ultrasonic nebulizers. On the other hand the yield at 15 mA was too low because the sample was not effectively nebulized and the surface of the sample was just broken to form a fine fog. It seems that cohesive forces between the water molecules play a significant role at low power. The optimum input power was found to be at a current of 20 mA. The so called geyser formation is therefore directly dependent on the nebulizer power. This can be expected since the intensity $\propto$ (amplitude)^2.
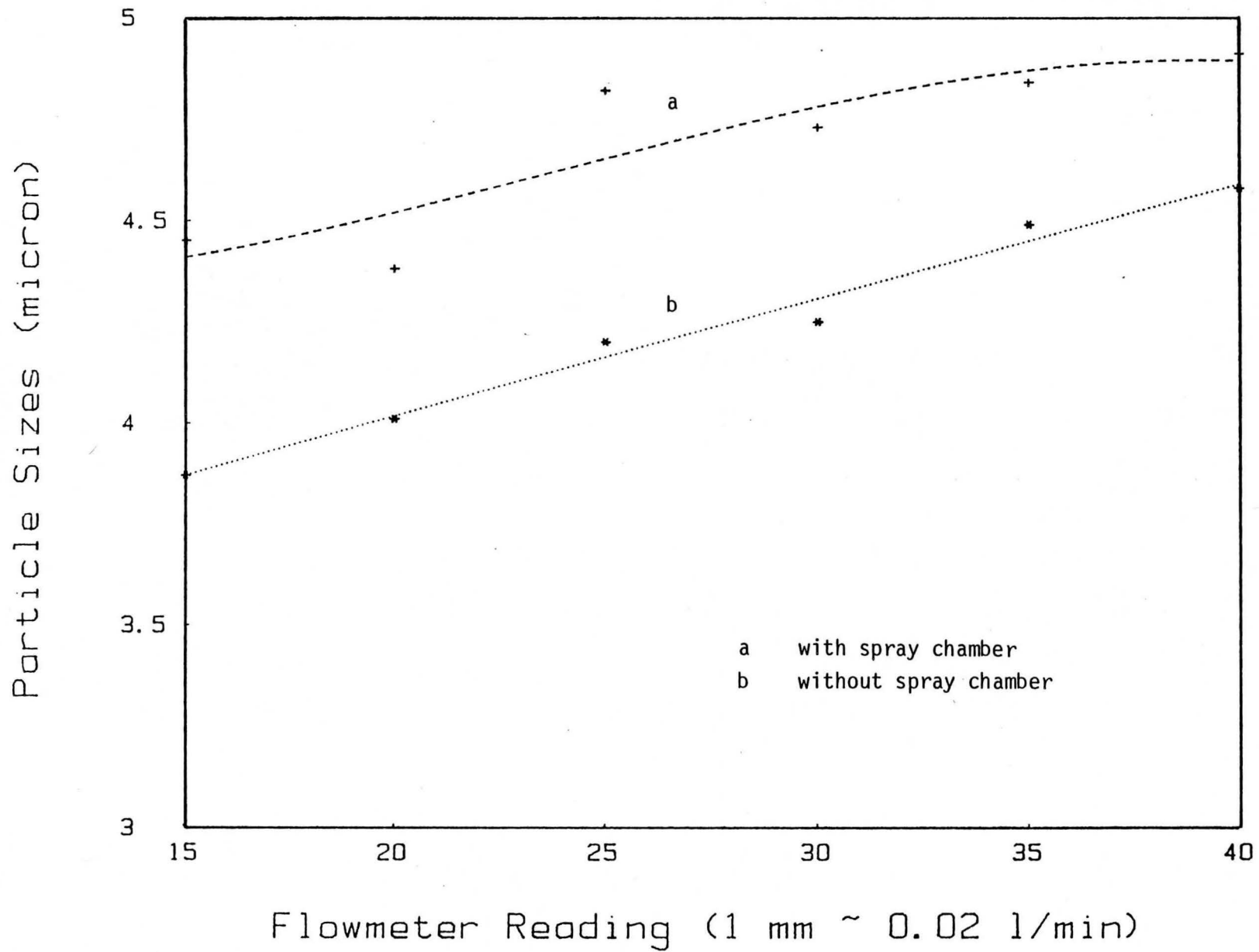
Fig. 5.14   The influence of the spray chamber on the particle size compared to the particle size of the 3rd
arrangement without the spray chamber.
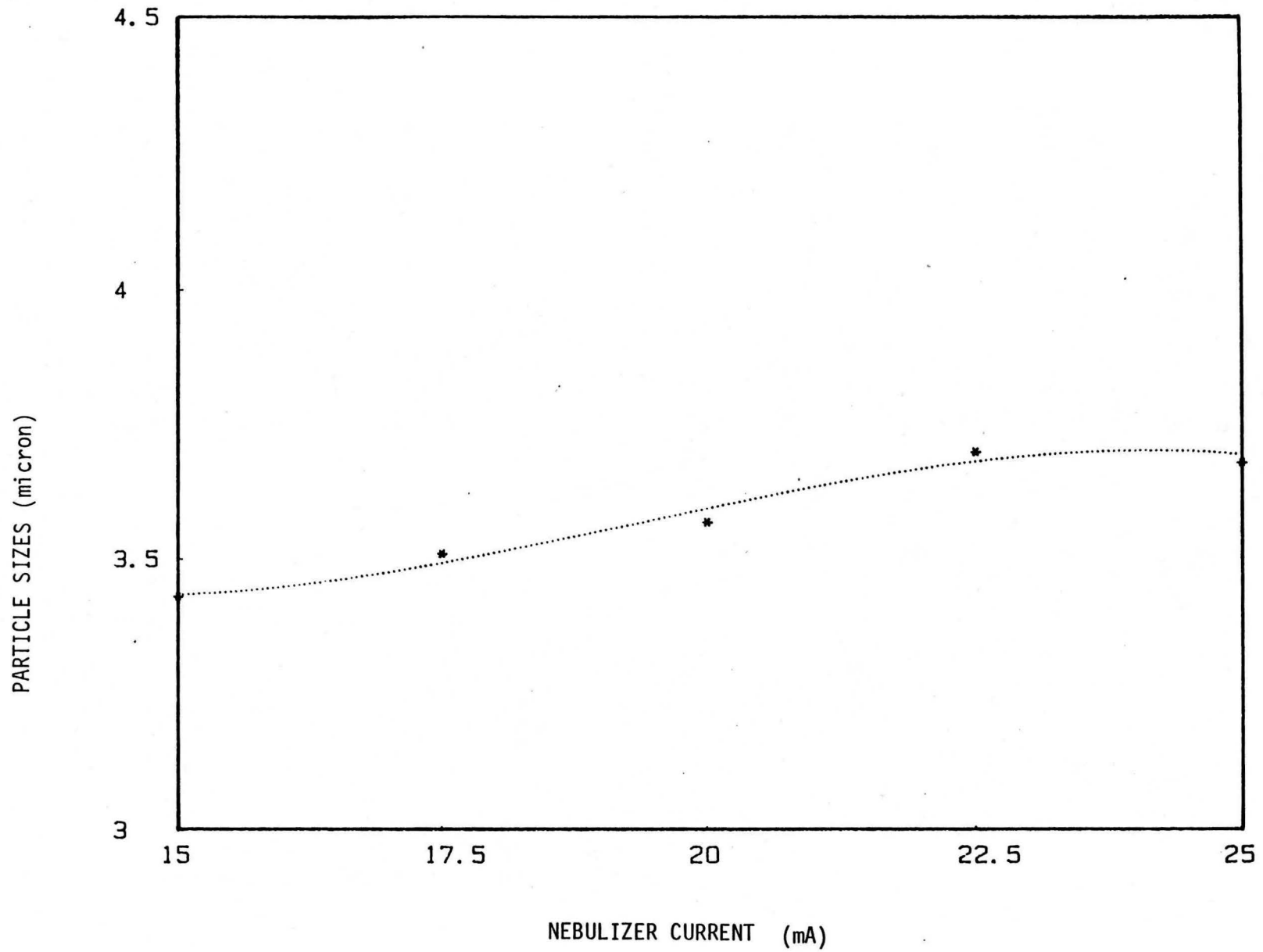
Fig. 5.15   The influence of the nebulizer power on particle sizes

5.4.3 *The Droplet Size Distribution*

The particle size distributions illustrated in figure 5.16 and figure 5.17 are indications of the influence of desolvation on the size distribution for the first and second instrumental arrangements. (Figures 4.2 and 4.3) The distributions are very similar for both arrangements. The carrier gas flow rate (0,6 l/min) and the desolvation temperature (150°C) were the same for both arrangements. The wide distribution without desolvation was shifted to a narrow distribution at the optimum desolvation temperature. Apart from narrower distributions there is also a shift in the mean diameter of about 2 microns towards a smaller size distribution. A further significant feature from these distribution curves is the fact that Browner and Boorn[28] predicted a cut-off diameter of 3 - 5 microns between "excess" and "useful" analyte. Even without desolvation the Sauter mean diameter (50% under) is about 5 microns. It therefore seems that the problem with ultrasonic nebulization is not so much the size of the droplets but rather the large amount of droplets introduced into the plasma. This is well illustrated in the comparative particle size distributions of the Babington-type nebulizer, the cross-flow nebulizer and the ultrasonic nebulizer.(Figures 5.18, 5.19 and 5.20) "Excess" analyte together with a poor signal to background ratio[115] is a serious problem with such wide distributions. Olson et al [113] reported that one of the characteristics of ultrasonic nebulizers is the more uniform particle size obtained. This is well illustrated in figures 5.18, 5.19 and 5.20. The wide size distributions of pneumatic nebulizers also accounts for the poor efficiency because a lot of sample is lost through too large droplets.

The addition of the spray chamber to the third instrumental arrangement is illustrated in figure 5.21. The size distribution was shifted towards the larger droplet side when the chamber was used. This can be ascribed to coagulation of the small droplets.
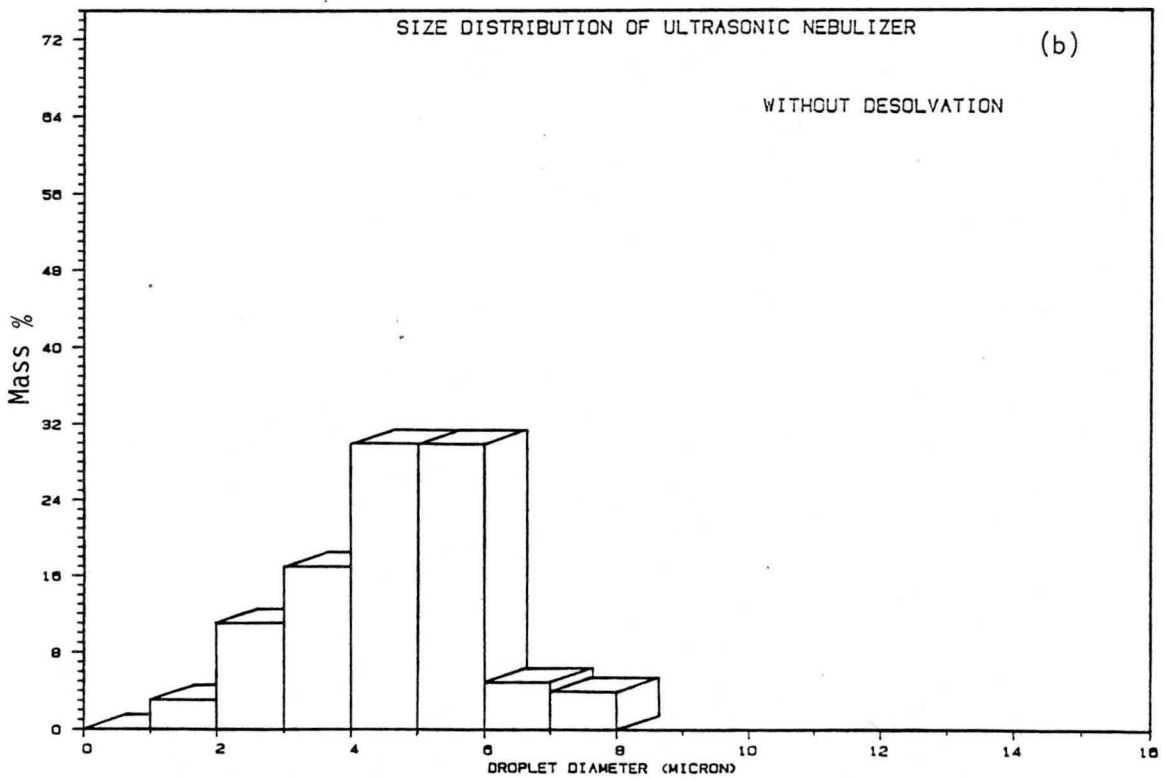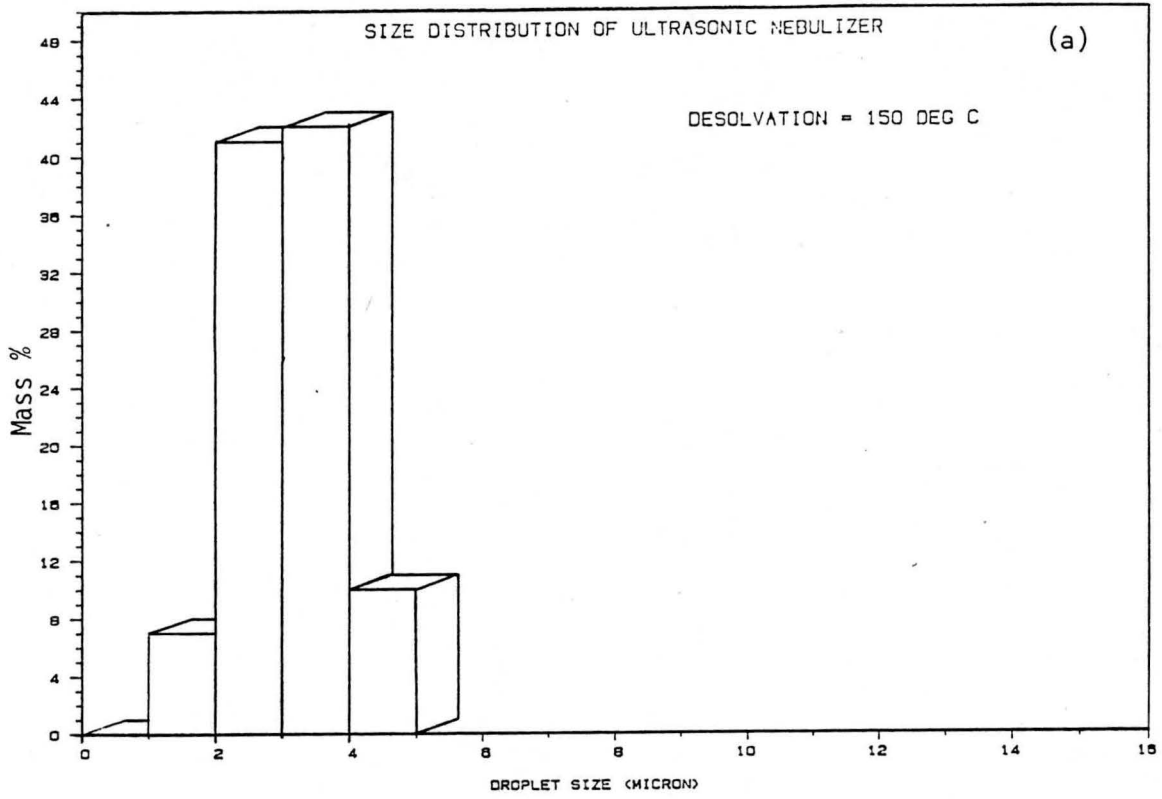
Fig. 5.16   The size distributions, with (a) and without (b) desolvation, for the first instrumental arrangement
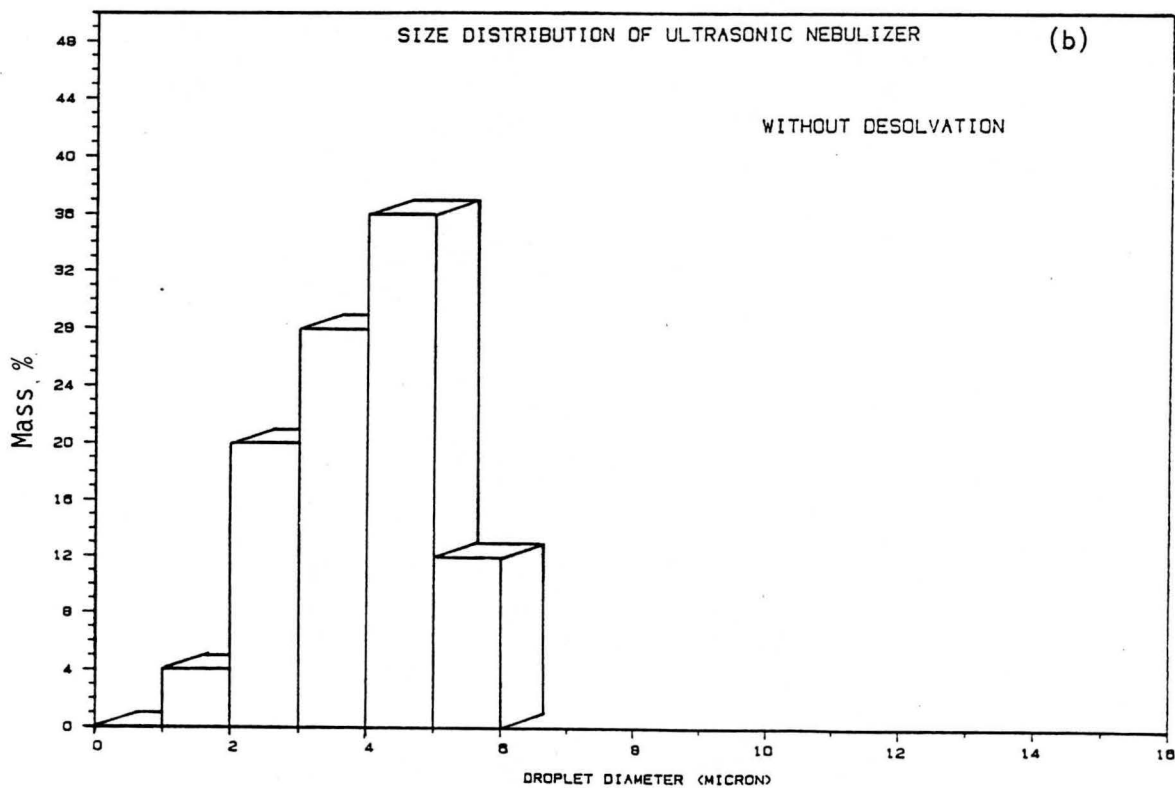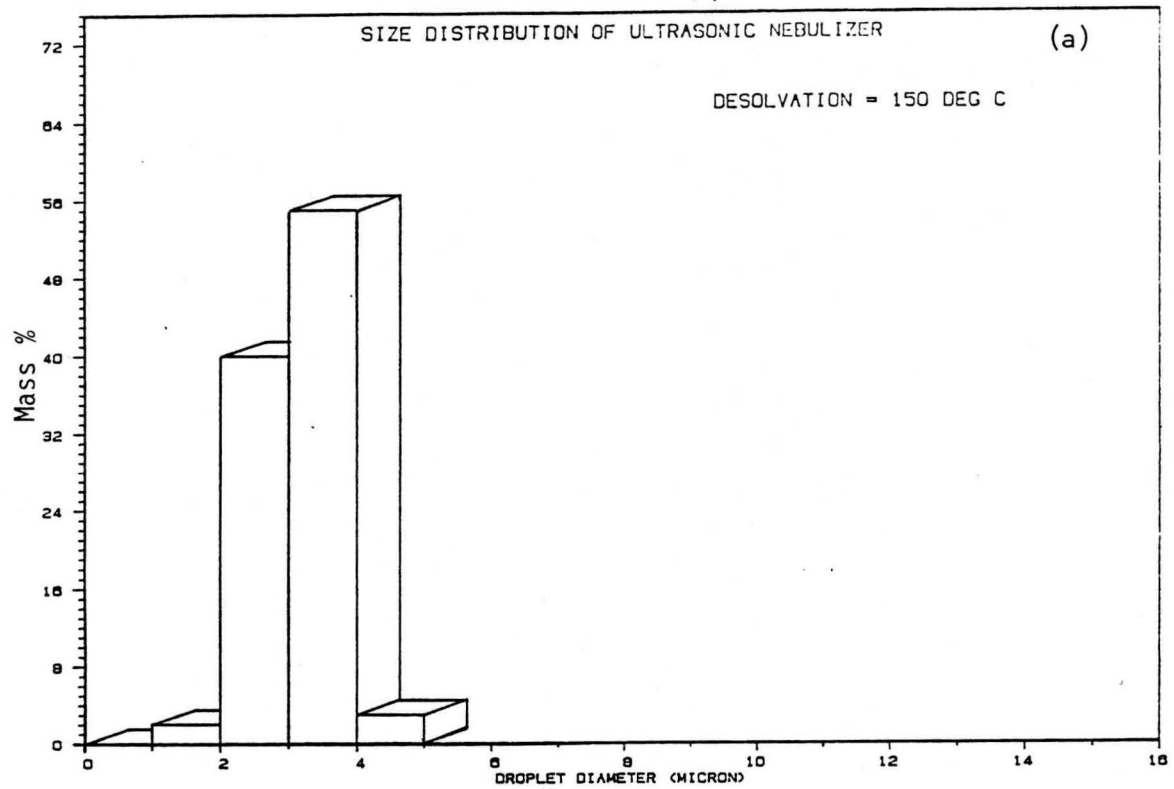
Fig. 5.17   The size distributions, with (a) and without (b) desolvation for the second instrumental arrangement.
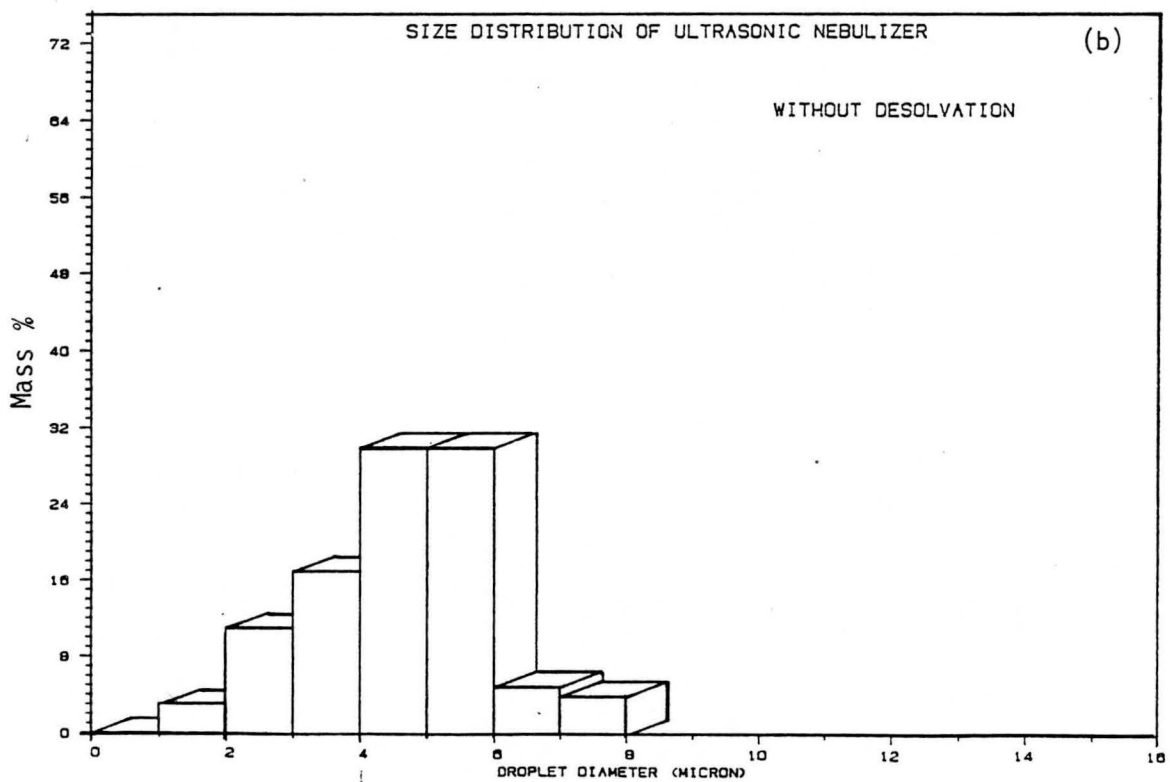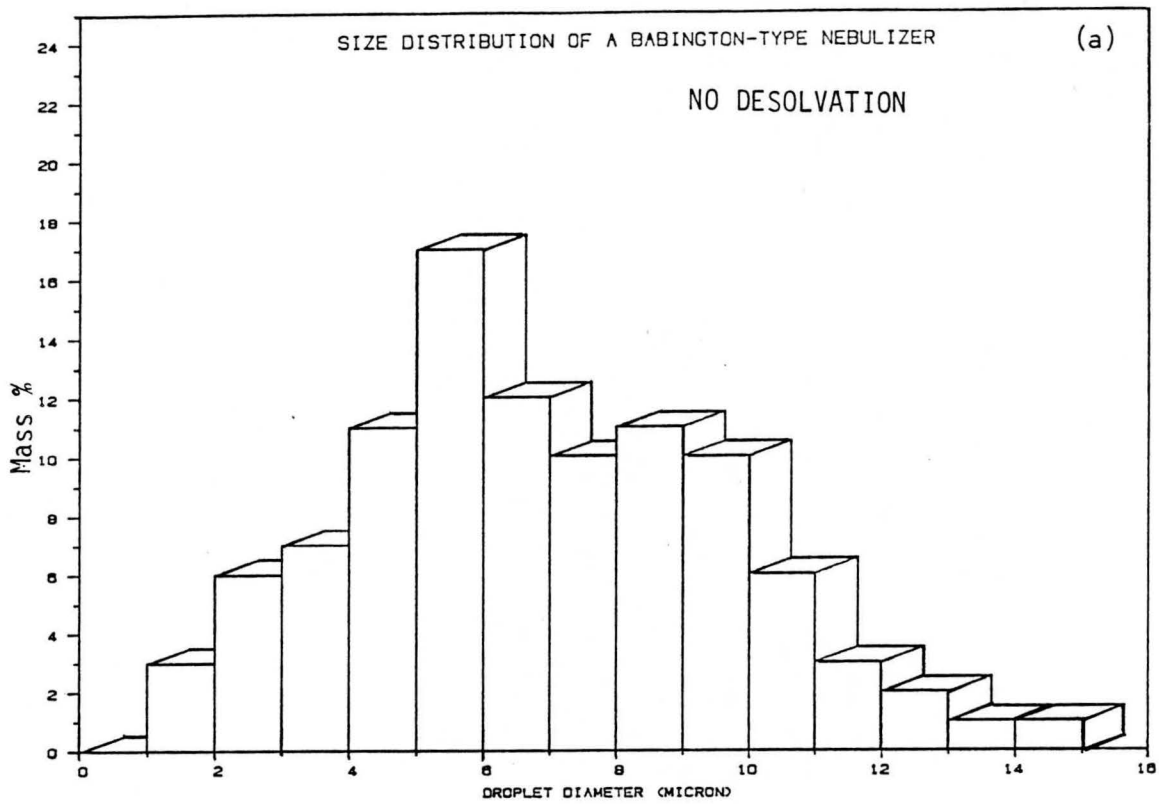
Fig. 5.18 The comparison of the size distributions for a Babington-type[a] and the ultrasonic[b] nebulizer. No desolvation was used.
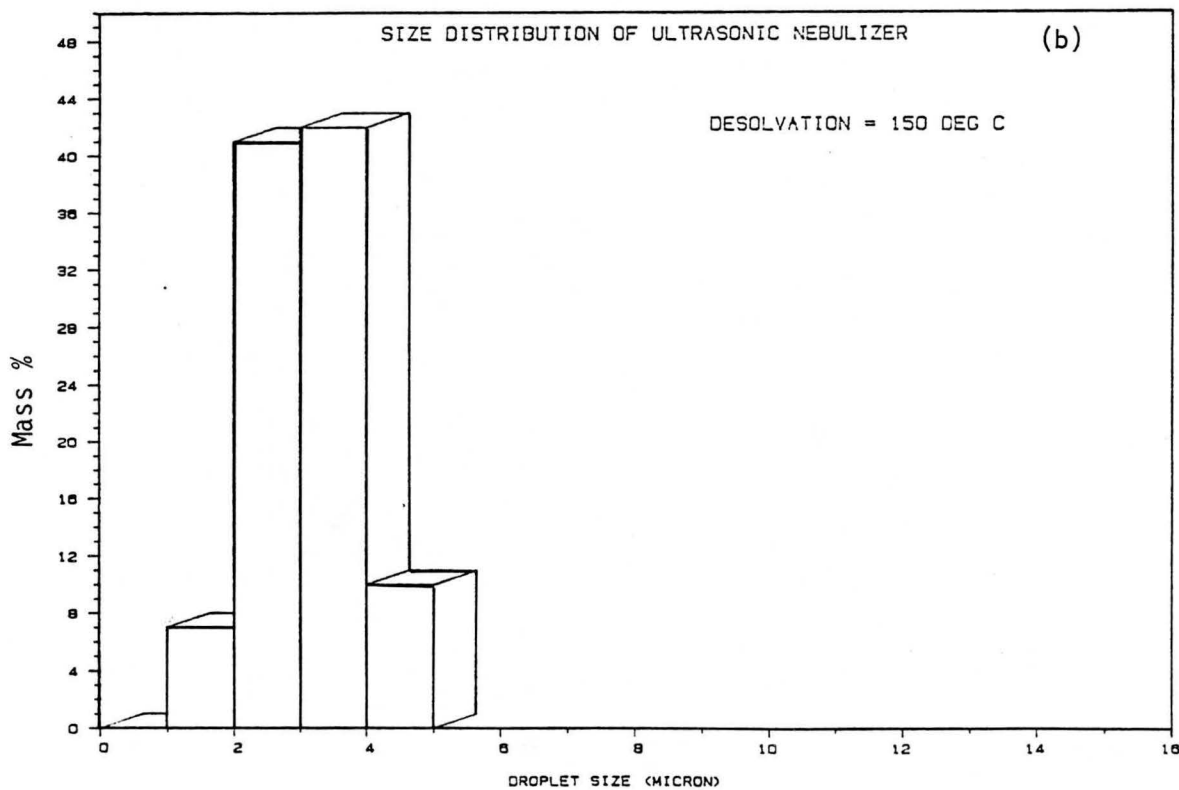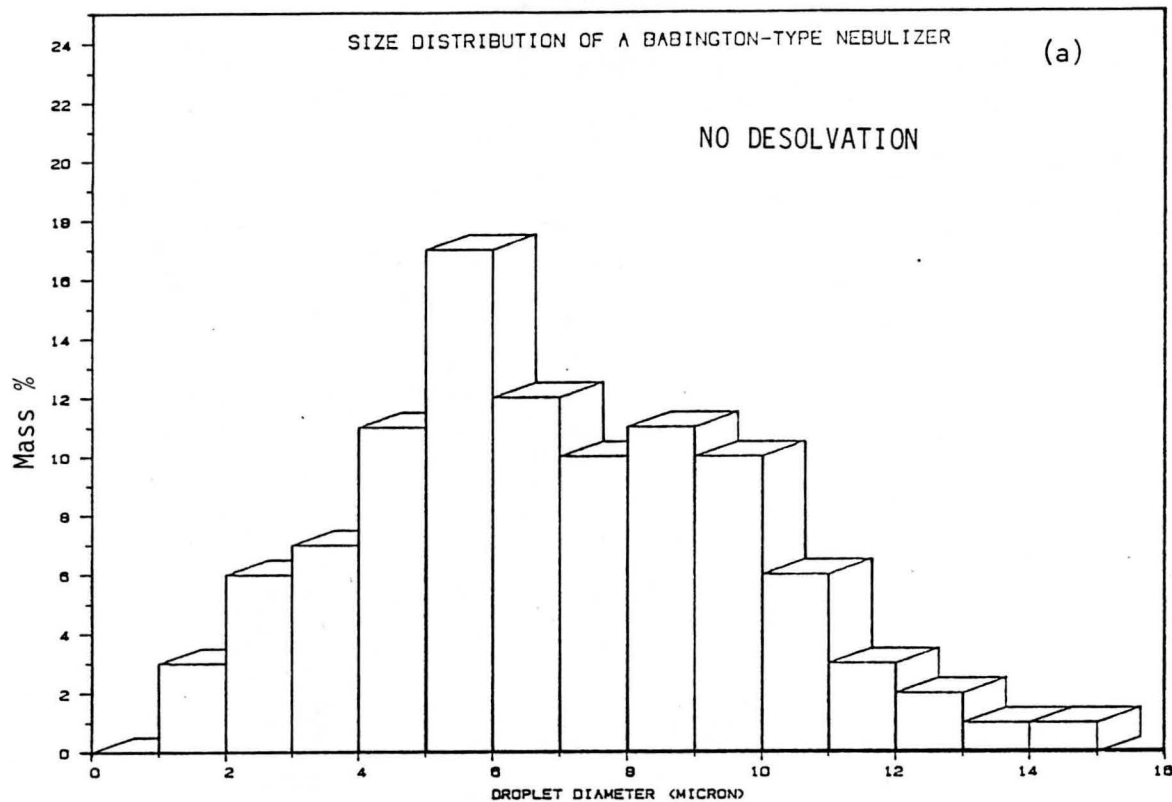
Fig. 5.19 A comparison of the size distributions of the Babington-type nebulizer[a] and the ultrasonic nebulizer[b]. A desolvation temperature of 150°C was used.
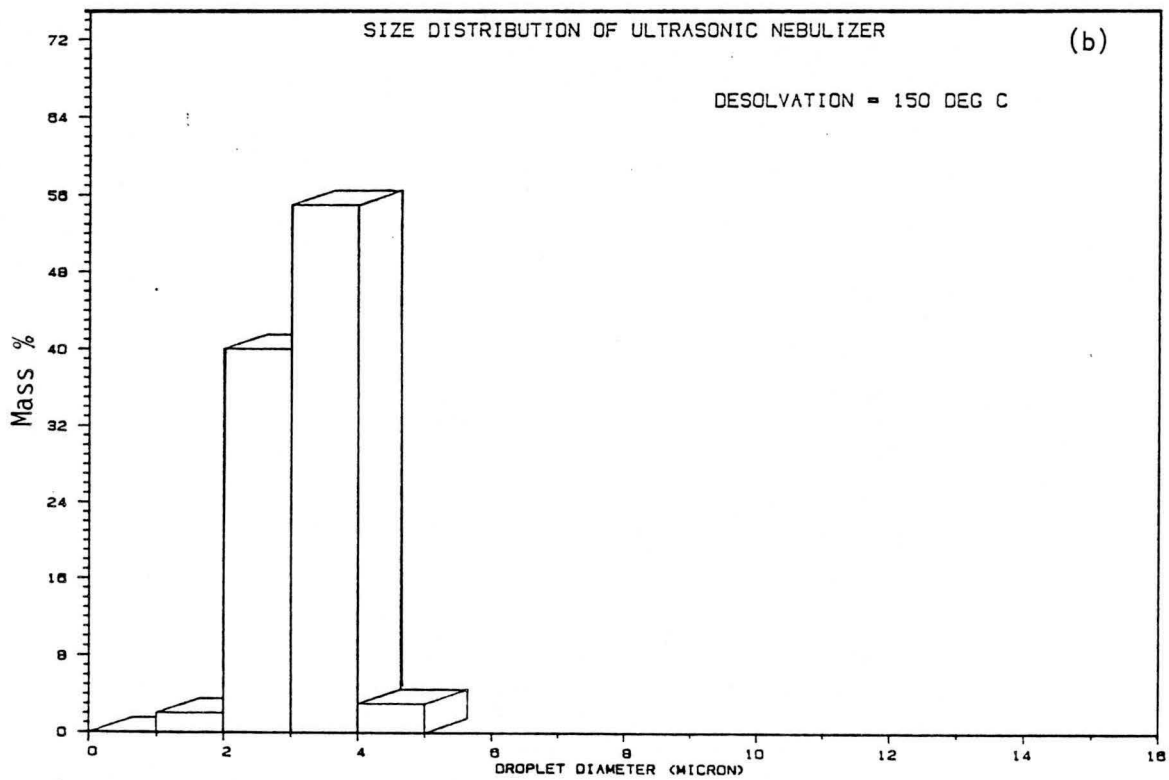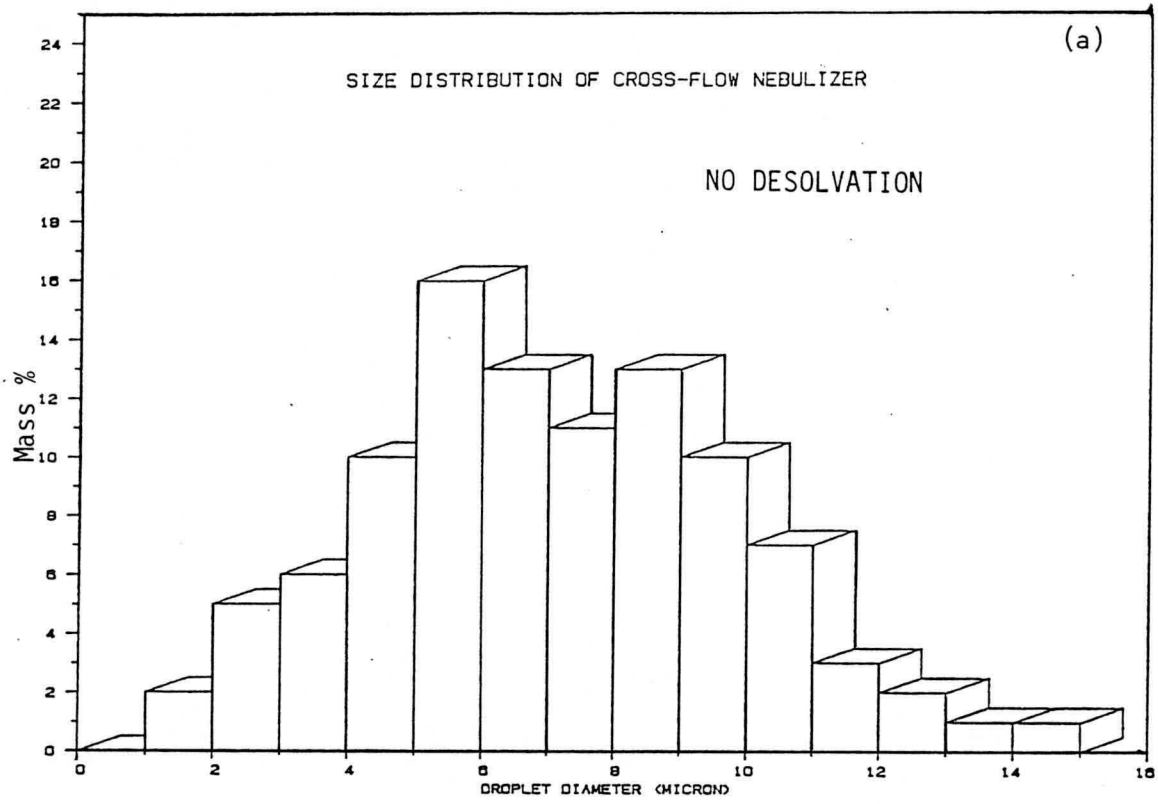
Fig. 5.20 A comparison between the size distributions for a cross-flow nebulizer [a] and the ultrasonic nebulizer [b] with desolvation.
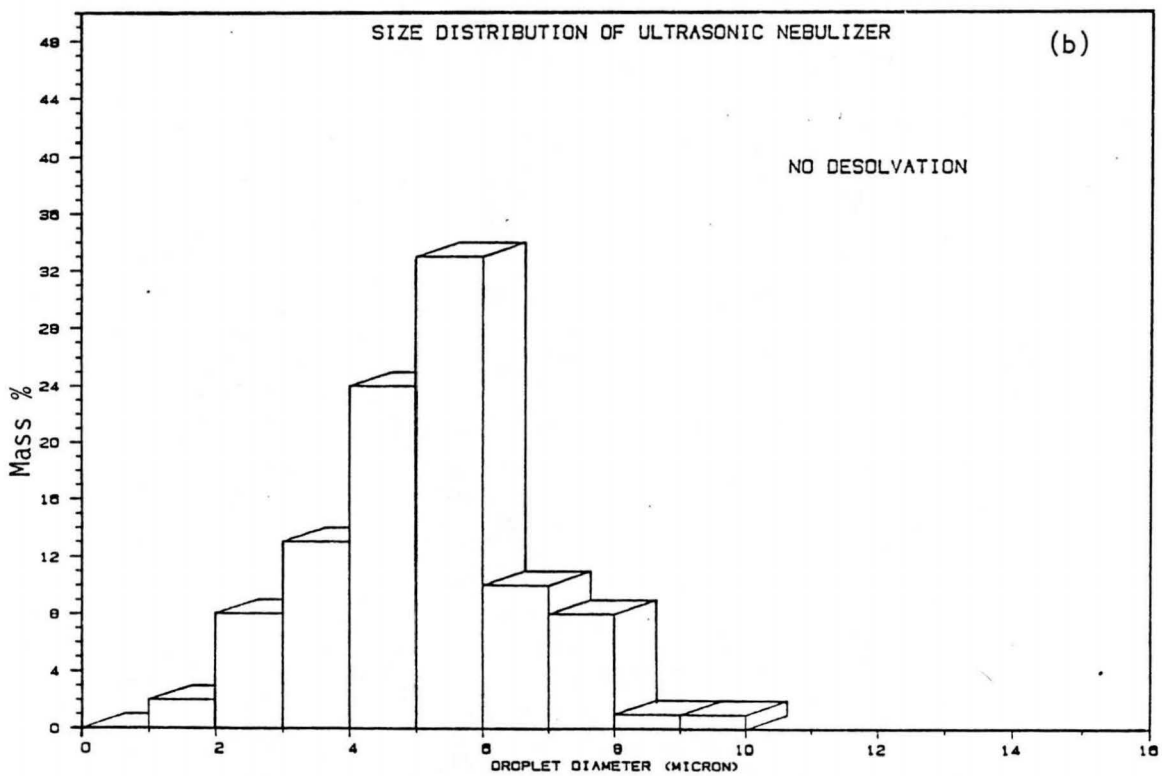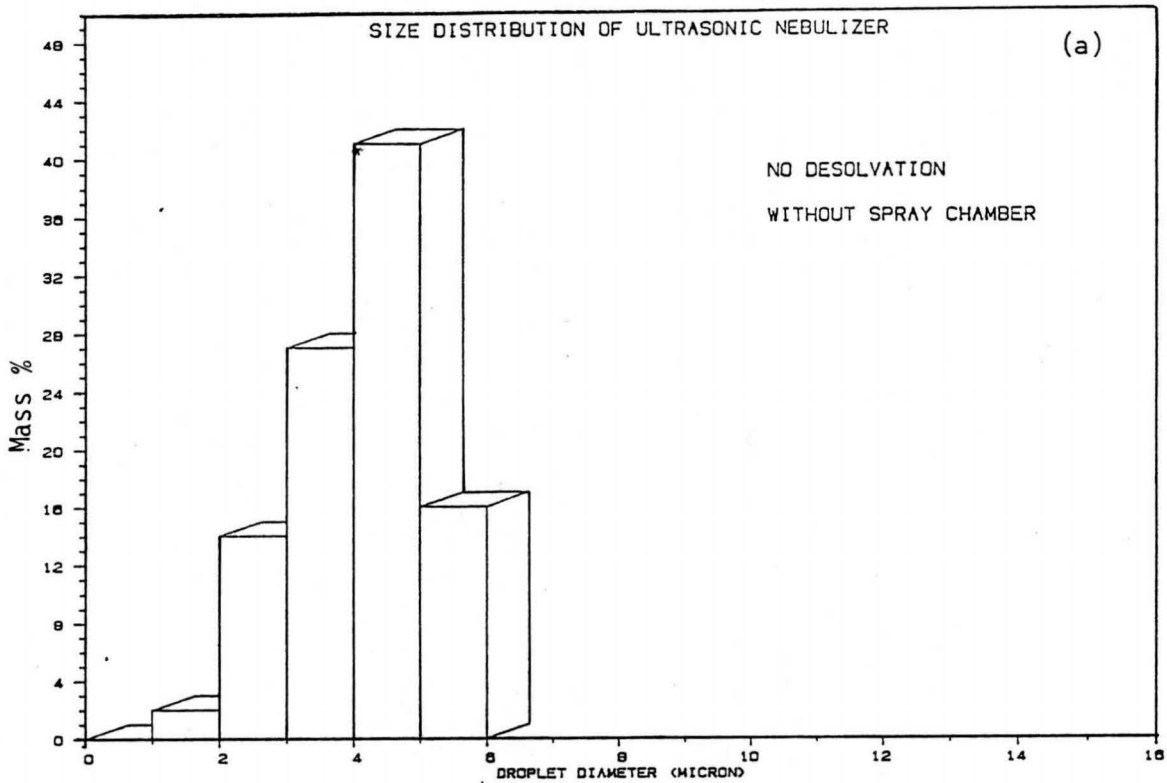
Fig. 5.21 A comparison of the size distribution when the spray chamber was left out (a) and when the spray chamber was used (b).

CHAPTER 6

6. *THE INFLUENCE OF DESOLVATION ON THE TEMPERATURE AND ELECTRON DENSITY DISTRIBUTION IN THE PLASMA.*

A considerable amount of effort is spent in determining the thermodynamic status of plasmas, since the degree of thermodynamic equilibrium determines the analyte emission characteristics. A better understanding of the basic processes leading to emission is therefore necessary to manipulate and control the source in order to improve and extend its analytical capability. In spite of the importance of the solvent/plasma interaction process, it has received relatively little attention to date. Work recently done includes articles by Alder et al[3], Long and Browner[94], Magyar et al[98], Tang and Trassy[131] and Kirkbright.[86] Parameters that will be discussed are the influence of the ultrasonic nebulizer, with and without desolvation, on the plasma temperature, the electron density and the emission profiles of calcium.

General theory

Theory on the interaction of solute with the plasma is very limited. A possible reason for this is the limited knowledge of the precise mechanisms and the kinetics of sample interaction with the plasma[94]. Most of the models mentioned in the literature are models of excitation mechanisms.[3,16,41,86,97] Although this work concentrated on a model for the processes before excitation is it still important to know about the existing excitation mechanisms. De Galan[41] has summarized and discussed the different excitation models:

1. The argon-metastable model, whereby a high population of metastable argon energy levels is responsible for the observed ion/atom intensity ratios.

2. The radiation trapping model that attempts to explain the overpopulation of high energy levels, notably of argon metastable levels.

3. The reaction rate model, where the level population is derived from the excitation and de-excitation reactions occuring in the plasma.

4. The ambipolar diffusion model, where the conditions in the hot plasma region inside the rf-coil are responsible for the phenomena observed in the analytical observation region.

Long and Browner[94] adopted a model for the transformation of the sample in the plasma. This model is summarized in Figure 6.1. The different transformation stages before excitation were discussed by them. The solvent must first evaporate from the aerosol drops. The conversion of the solid desolvated material into the gaseous state is the second stage in this so called sample introduction/excitation process. The energy absorption characteristic of the molar heat of vaporization and bond dissociation of the solute are part of this process.

In the plasma, the dissociation of water is a predominant phenomenon. The dissociation requires much more energy than evaporation.[131] The following equilibria are involved:

$$2H_2 + O_2 \rightleftharpoons 2H_2O$$

$$H_2 + O_2 \rightleftharpoons 2OH$$

$$O_2 \rightleftharpoons 2O$$

$$H_2 \rightleftharpoons 2H$$
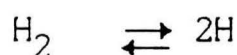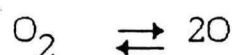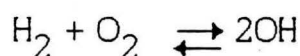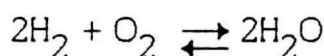
Water in the central channel is essentially present in the forms of atomic hydrogen and atomic oxygen.[4,86,131] Alder et al[3] has stated that for a nebulizer working at 3% efficiency and a carrier gas flow rate of 1.0 l/min, the mole ratios of argon, hydrogen and oxygen atoms in the plasma are in the ratio Ar:H:O as 89,9:6,7:3,4. The water will therefore modify the conditions in the analytical zone. The different zones of the plasma are illustrated in Figure 6.2.

Both processes mentioned by Long and Browner[94] would drain a lot of power from the toroidal area. They felt that the energy necessary may represent a large
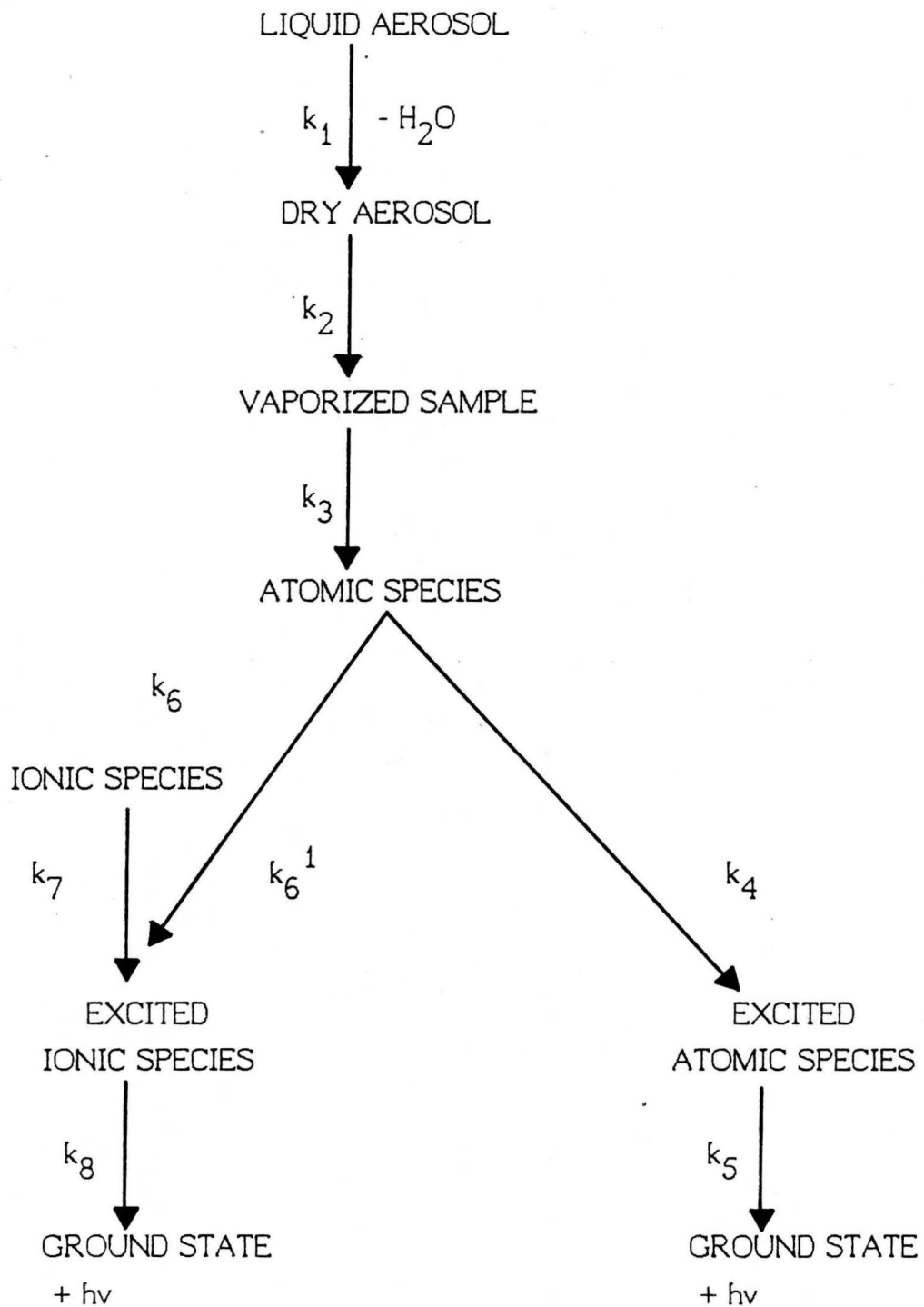
Fig. 6.1 Sample transformation steps in a plasma. k_1 .... k_8 represents rate constants for the processes indicated. (Long and Browner[94]).
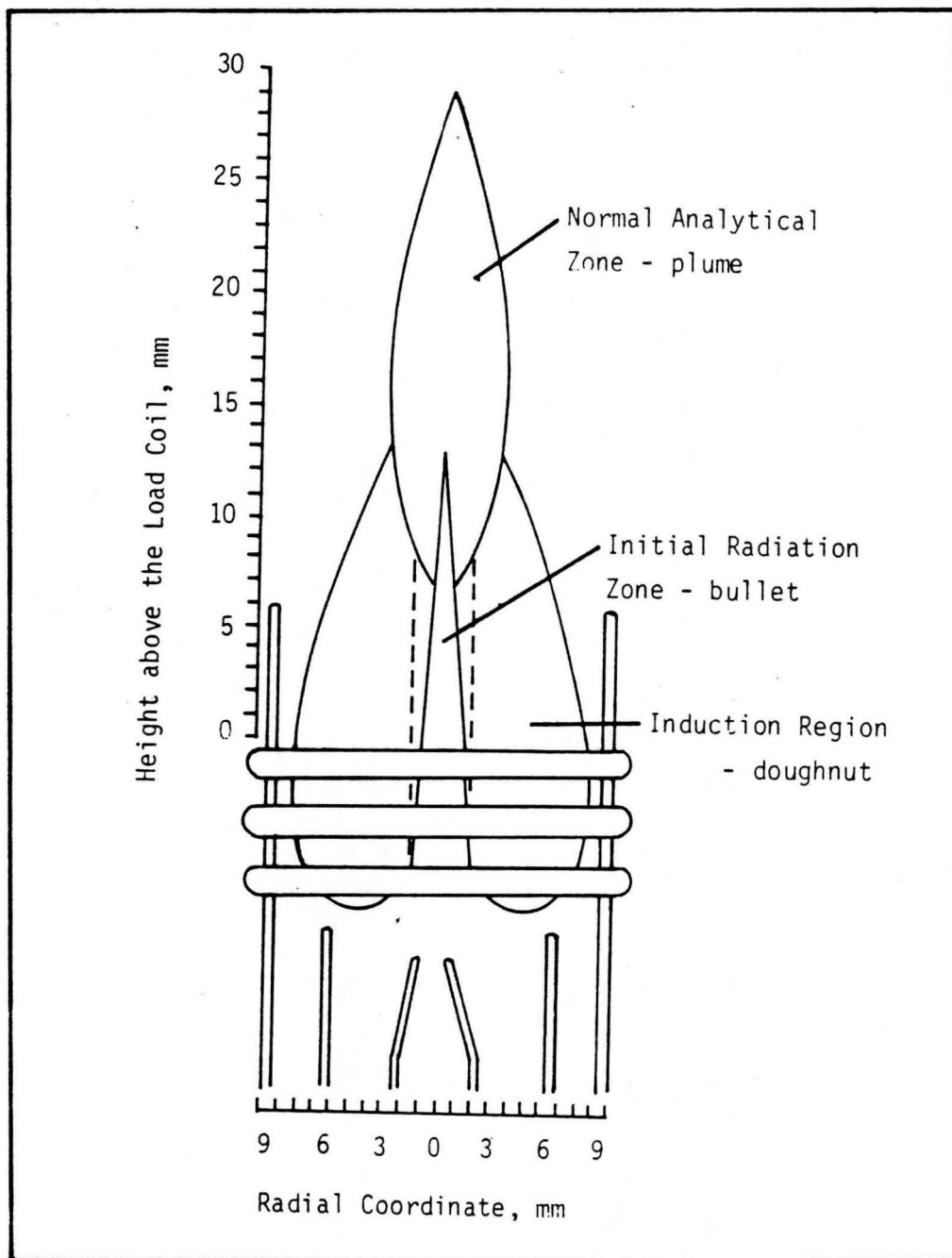
Figure 6.2   The different zones of the plasma

fraction of the total energy available for excitation. Boumans and De Boer[19] estimated that the water would consume about 20% of the total power and predicted a decrease in temperature. The lost energy can only be replaced by conduction from the outer zone of the plasma. Tang and Trassy[131] discussed the influence of thermal conductivity. They estimated the thermal conductivity between the toroidal plasma and the central channel as from the rate equation:

$$\frac{dQ}{dt} = \Theta \frac{\delta T}{\delta x} dS \qquad (6.1)$$

where $\frac{dQ}{dt}$ = rate of thermal energy transfer

Θ = thermal conductivity

$\frac{\delta T}{\delta x}$ = the thermal gradient

dS = the exchange area

The following assumptions were made because of the difficulty of integrating equation (6.1).

(i) The thermal gradient is constant

(ii) The hottest zone of the plasma has a toroidal shape; estimation of the mean thermal gradient in the axial zone of the plasma is possible.

(iii) The energy transfer between the electric field and the central channel is negligible; the electric field on the axis is zero and the channel diameter is small.

(iv) The radiative transfer is negligible.

The exchange area is taken as the area of a cylinder with channel diameter d_c and height h and is given by :

$$S = \Pi d_c h \qquad\qquad (6.2)$$

Tang and Trassy[131] therefore have written the equation for heat transfer by conduction as

$$\frac{dQ}{dt} = \Theta \frac{\delta T}{\delta x} \Pi d_c h \qquad\qquad (6.3)$$

The thermal conductivities of water, hydrogen and argon are shown in Figure 6.3. It is clear that hydrogen and water have maximum conductivities at 3500 K. At the same temperature the thermal conductivity of an argon-water mixture is about 4,5 to 18 times higher than argon.[131] Alder et al[3] raised another point about the different atoms in the central part of the plasma. The ionization energies of hydrogen and oxygen are about 2eV below that of argon. They therefore stated that the degrees of ionization of hydrogen and oxygen at 6000 K would be about five times higher than that of argon. An increase in electron density should thus be expected when water is present. Kirkbright[86] agreed with this but doubted if it would be the same with ultrasonic nebulization. Still on the subject of conductivity. Goldfarb[63] raised the question of the high heat capacity of water.[114,131] (See figure 6.4) It is clear that water has a very high heat capacity between 3000 and 4000 K. The high water vapor concentration means a two-to eight-times increase in heat capacity in the central channel.[63] We therefore expect a decrease in temperature when the water vapor concentration is high. Due to the high temperature gradient we would also expect the migration of energetic Ar, Ar^+ and Ar^{2+} towards the aerosol channel. (Figure 6.2.) Olson and Böhmer[114] suggests that energy transfer occurs by the following means:

$$Ar^+ + H_2O \rightleftharpoons ArH^+ + OH$$
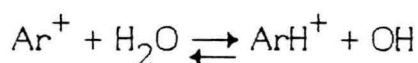
The hydroxyl radical would then transfer its energy to the sample species. It is
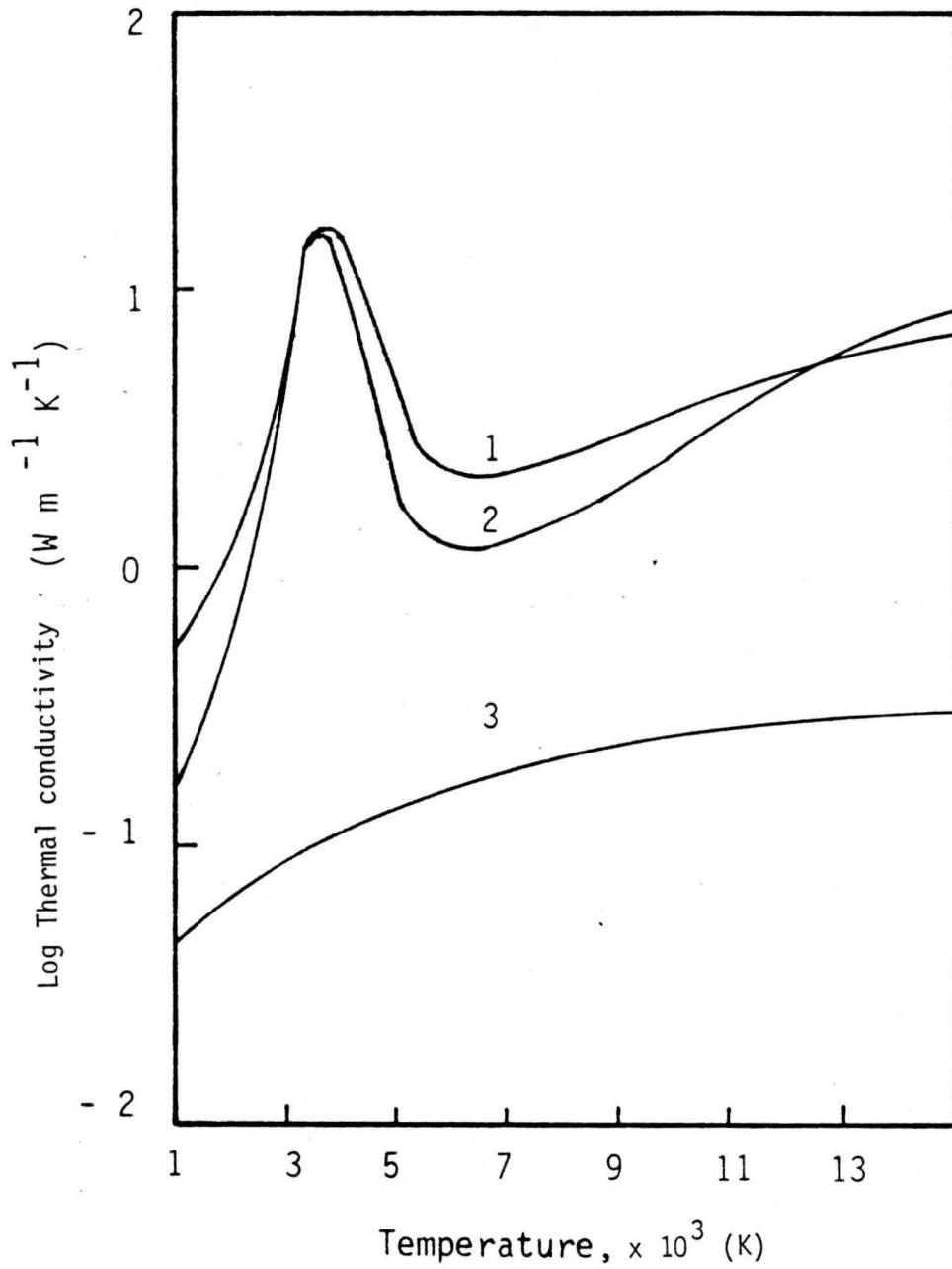
Figure 6.3 Thermal conductivities of water (2),
hydrogen (1) and argon (3) as functions of tem-
peratures
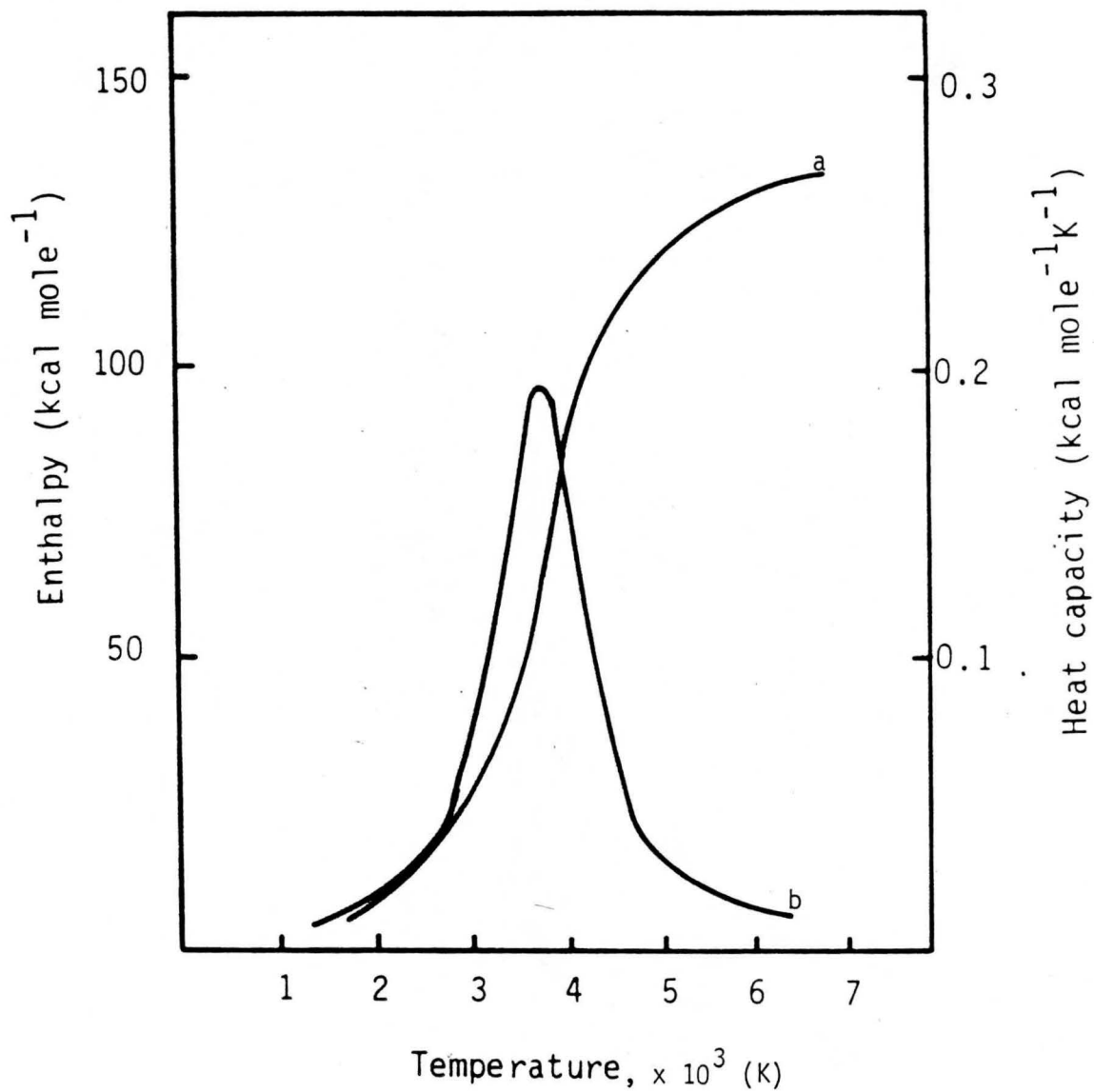
Figure 6.4 Enthalpy (a) and heat capacity (b) of water

clear that several processes have to take place before excitation. The sample/plasma interaction model is not complete without a detailed investigation of the influence of particle sizes on the emission profiles. The particle size is a function of the type of nebulizer and the degree of desolvation. (Chapter 5). Another influence that can be incorporated into this model is the influence of solvent type (i.e. organic samples) on the sample/plasma interaction[14,96].

6.1 *The Plasma Temperature*

Theory

A number of researchers have done work on plasma temperatures.[3,4,14, 15,39,49,52,59,61,66,68,69,83,84,131,134] Temperature as a variable is dependent on thermodynamic equilibrium. A state of thermodynamic equilibrium will be attained by an undisturbed closed system when surrounded by a heat bath at uniform temperature, T.[68] Complete thermodynamic equilibrium in a system requires that: (i) the spectral radiance at all wavelengths must obey Planck's radiation law; (ii) the velocity distributions of the particles must obey Maxwell's distribution law; (iii) the internal energy states of the particles (vibration and rotation) must be occupied according to Boltzmann's formula; and (iv) the ionization and the dissociation of the molecules must correspond to the appropriate mass action laws.[4] At complete thermodynamic equilibrium the temperature, T, in these distributions and equilibrium laws must have one and the same value. These laws are summarized in Table 6.1.

The Saha Law relates the concentration of neutral species to those of the ionized products in thermodynamic equilibrium. These requirements for general equilibrium can only be satisfied exactly if the system is isolated from the environment and enough time is allowed for the separate kinds of equilibria to be established. That implies that the forward process (radiative or collisional) must correspond exactly to the reverse process.[4] Therefore, in principle, if the energy distribution of one degree of freedom is disturbed, then the other distributions are also affected and the thermodyamic system deviates from equilibrium.

In a flame these equilibrium conditions are obviously not met. The determination of whether thermodyamic equilibrium can exist in a flame is necessary for the determination and interpretation of the flame temperature. Elder and Winefordner[52] summarized the difficulties in applying the concept of thermodynamic equilibrium to a flame system, (See Table 6.2.)

The ICP is also not isothermal and cannot be described by one temperature. But, if the rates of the transport processes are slow relative to all the transport rates at which energy is locally partitioned over the various degrees of freedom, it is still meaningful to speak of a local state of equilibrium characterized by a local temperature[3] (LTE). Winefordner and Elder[52] gave a summary of the local thermodynamic considerations, summarized in Table 6.3.

TABLE 6.1

THERMODYNAMIC EQUILIBRIUM REQUIREMENTS

1. Planck's Law — The distribution of the electromagnetic radiation energy.

2. Maxwell's Law — The velocity distribution function of all gas particles.

3. Boltzmann's Equation — The population distribution of the excited energy states.

4. Mass-Action Law — The distribution of molecules and their dissociation products.

5. Saha-Eggerts' Equation — The distribution of atomic and ionization products.

TABLE 6.2

FLAME DEVIATIONS FROM THERMODYNAMIC EQUILIBRIUM

1. Absence of well defined boundaries (open system)

2. Net transfer of heat, mass and energy.

3. Temperature and concentration gradients in vertical and radial directions.

4. Radiative disequilibrium (not black body radiator).

5. Nonthermal radiation (chemiluminescence from metals, OH, C_2, CH etc in reaction zone).

TABLE 6.3

LOCAL THERMODYNAMIC EQUILIBRIUM CONSIDERATIONS (LTE)

1. Local T - describes particle velocity distribution and energy distributions over degrees of freedom corresponding to Boltzmann's law.

2. Radiation LTE is not necessary.

3. Existence of temperature gradients is acknowledged.

4. Transient local T possible.

5. Different "temperatures" for different degrees of freedom in any one species considered.

Local thermal equilibrium means a volume-element in a non-isothermal plasma with the same temperature as an isolated volume element with the same chemical composition. The chemical equilibrium of a system means that we would get the same temperature from temperature dependent equations as the kinetic temperature of the gas. As stated in Table 6.3 there is an existing temperature gradient in the ICP which leads to non-equilibrium conditions. It is only possible to isolate the volume elements if the temperature gradients are not too steep.[68] The steepness of the gradient is determined by the variation in temperature along the mean path length of the particle described by the volume element. The influence of the temperature gradient on the equilibrium can be disregarded if the temperature variation is small in comparison with the average temperature of the volume element.[68] A criterion for the gradient is

$$\frac{T(r+\Delta r) - T(r-\Delta r)}{T(r)} \ll 1 \tag{6.4}$$

with $2.\Delta r$ = average free pathlength of the particle

$T(r)$ = radial temperature.

It is necessary to divide the plasma into isothermal rings in order to describe the temperature gradient. (Figure 6.5) Several investigators have shown that if the medium is optically thin and displays at least cylindrical symmetry then the problem may be reduced to the solution of a simple integral equation.[2,34,36,57] However, it is the rule rather than the exception that the distribution will be more or less assymmetric and the centre of the distribution will be somewhat indeterminate. Various investigators such as Algeo and Denton[2], Freeman and Katz[57] and Cremers and Birkebak[36] differ greatly about how to treat this problem.

6.1.1 *The Transformation of the Lateral Radiation Profile to a Radial Radiation Profile*

To determine the true temperature of a volume element in a cylindric symmetric plasma like the ICP, the image of the plasma is scanned across the diaphragm in front of the entrance slit of the spectrometer in a horizontal plane. Thereby the spectral radiance is measured along lateral segments through the plasma as shown
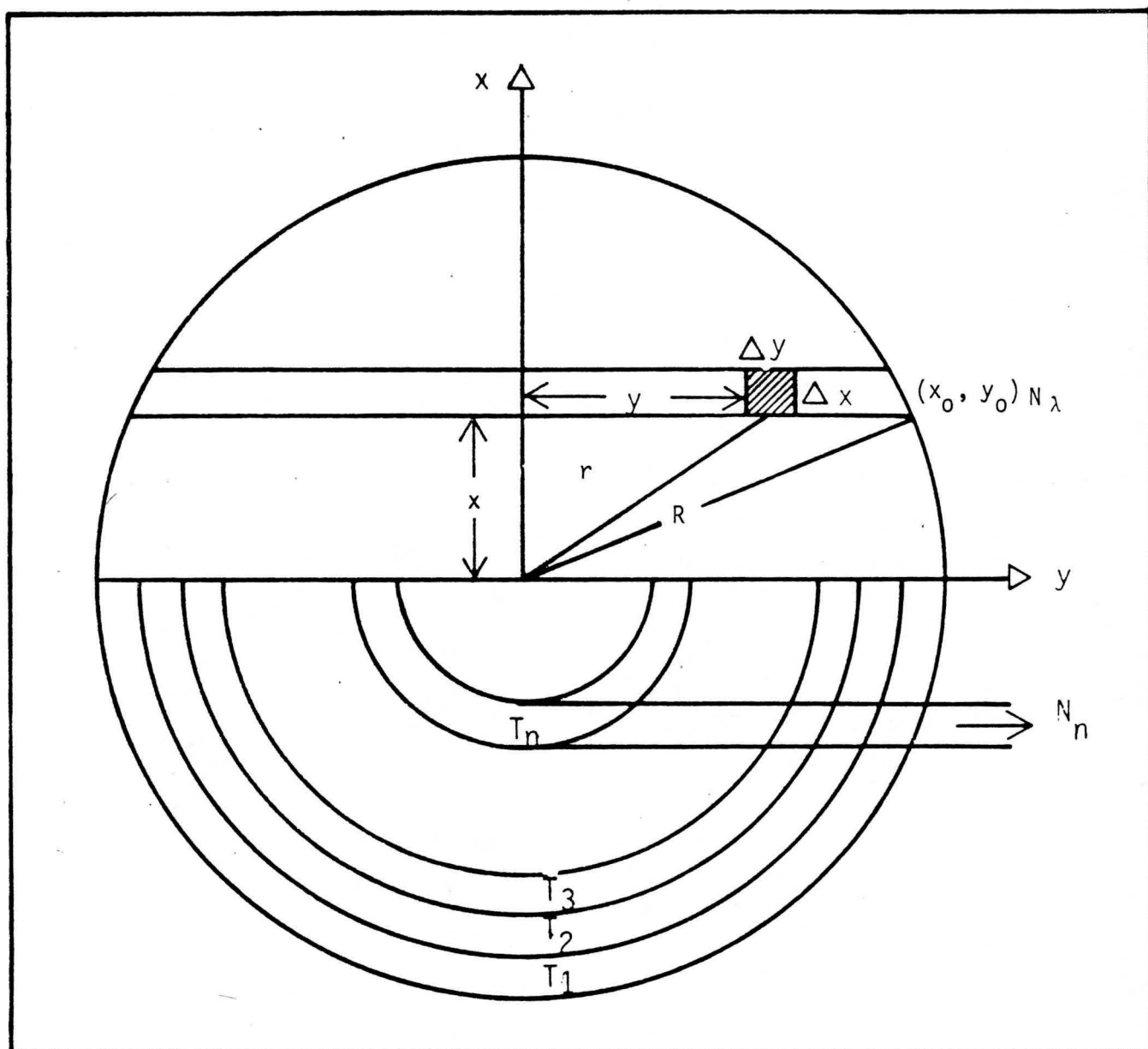
Figure 6.5 Schematic diagram for spatial resolution of cylindrically
            symmetrical sources

in figure 6.5. In order to obtain the absolute spectral radiance from each radial shell, the lateral integrated values are transformed to radial values with Abel inversion integrals. This method is fully described in Appendix 2.

6.1.2 *Determination of the Radiation Profiles*

6.1.2.1 *Measurement Procedure*

The difference between the upper energy states must be as large as possible for species to be used in the two-line method. The method is also critically sensitive to errors in the ratio of transition probabilities. It was therefore decided to use the atom lines Ca I 445,5 and 422,6 nm and the ion lines Ca II 373,7 and 393,3 nm, because the spectroscopic constants of these lines are well known. (Table 6.4)

TABLE 6.4

SPECTROSCOPIC CONSTANTS FOR THE CALCIUM TRANSITIONS

State	Energy (cm^{-1})		Wavelength	$G_n A_{nm}$	Transition
	E_m	E_n	(nm)	(s^{-1})	
Ca I	15316	37757	445,478	$6,02 \times 10^8$	$^3P^0 \rightarrow {}^3D$
Ca I	0	23652	422,673	$6,54 \times 10^8$	$^1P^0 \rightarrow {}^1P^o$
Ca II	0	25414	393,366	$6,0 \times 10^8$	$^2S^2 \rightarrow {}^2P^o$
Ca II	25414	52167	373,690	$3,3 \times 10^8$	$^2P^0 \rightarrow {}^2S$

Solutions of 10 μg/ml Ca were made up from a standard $Ca(NO_3)_2$ solution. Deionised water were used for the background measurements. Lateral scanning is essential for the determination of the absolute temperature. It requires the movement of the image of the plasma across the entrance slit. This was done by means of a stepper-motor which was connected to a lead screw, with a 0,5 mm pitch. Intervals of 0,25 mm were used and with the one second integration time used

in this study, the plasma source was sampled in about 54 lateral steps. The electronic circuit of the steppermotor control unit allowed both forward and backward movement. The speed of movement is controlled by the variation of the pulse frequency to the steppermotor, and limit switches were used to confine the ICP movement to the usefull region. The six-channel counter system was interfaced with either a HP-86 microcomputer or a HP-1000 minicomputer for on-line data compiling. Programs in BASIC were used to handle incoming data arrays in the case of the HP-86, while FORTRAN was used in the case of the HP-1000.

6.1.2.2 *The Lateral and Radial Radiation Profiles*

The net lateral radiation profiles for CaI and CaII were obtained by subtraction of the background from each spectral line. This was done for each corresponding lateral position. The method of Freemand and Katz,[57] as described in (Appendix 2), was used for transformation of the lateral data to radial radiation profiles. The centre of the profile was chosen at the maximum point of the lateral radiation profile. (Figure 6.6) See Appendix 2 for further discussion. A least-square polynomial fit across the lateral radiation profile was made for the determination of seven coefficients of the 6th order polynomial. This together with the lateral radiation data was used for the determination of emission coefficients according to equation (6) in Appendix 2. This procedure was repeated for each spectral line of Ca at different desolvation temperatures.

6.1.3 *Spectral Calibration*

The measured radiation values are relative values and it is therefore necessary to calibrate them in terms of absolute values for the determination of the temperature and electron density. A secondary radiation standard in the form of a tungsten ribbon filament lamp was used to calibrate the response of the detection system at different wavelengths and all measured intensities were corrected. The lamp, No EPUV - 1160, was supplied and calibrated in units of microwatts per sterradian per square millimeter of projected source area per nanometer wavelength interval by the Eppley Laboratories, U.S.A. It was calibrated for the wavelength region
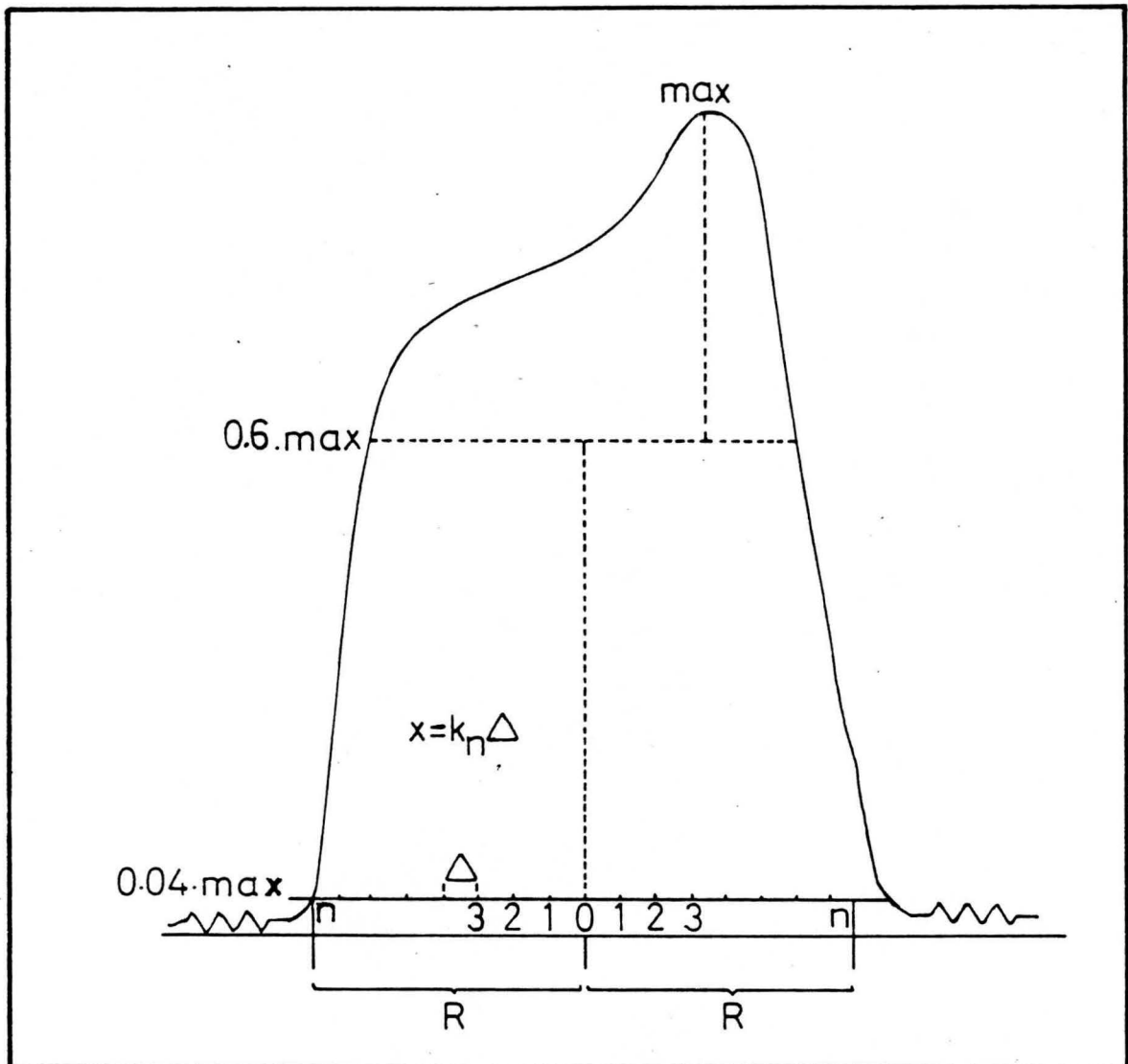
Figure 6.6 The determination of the centre of the lateral data profile

250- 750 nm. (See Table 6.5) A forth order polynomial was fitted through the wavelengths 300 - 500 nm. The constants for this polynomial fit are listed in Table 6.6. The polynomial fit is illustrated in figure 6.7. It is now possible to calculate the absolute radiation values at the Ca-wavelengths that were used. The formula used for this calculation is as follows:

$$R = i_4\lambda^4 + i_3\lambda^3 + i_2\lambda^2 + i_1\lambda + i_0 \tag{6.5}$$

The tungsten ribbon lamp was placed at the same position as the ICP, and the optics were the same as for the ICP. The photo-electric system used with the ICP was also used for the radiation standard. It is therefore possible to calibrate the spectral radiation to absolute values by using the absolute values calculated from the forth order polynomial. (See Table 6.7.) The measured mean spectral radiations were calculated from 150 radiation measurements. The calibration constants (K_i) for the transformation of relative spectral radiations to absolute radiations are listed in Table 6.8, and used in this work to transform all relative radiations to absolute values. This is necessary for temperature and electron density determinations.

6.1.4 Temperature Determinations

Theory

Temperature is an important parameter which governs the excitation mechanism of the ICP. The importance of temperature determinations for a better understanding of the basic processes leading to emission was mentioned earlier in this chapter. A large variety of literature exists on temperature determinations.[3,4,14,39,59,66, 68, 83,84,131,134] Care must always be exercised in the comparison of reported values of measured temperatures. The measured temperatures vary not only with the calculation method, but also with ICP operating conditions such as frequency, power, load coil number of turns, plasma torch configuration, gas composition, gas flow rates and solute volume and composition.

Elder and Winefordner[52] distinquished two categories of temperature measurement techniques, namely with intrusive and nonintrusive probes. Intrusive

TABLE 6.5

SPECTRAL RADIATIONS FOR THE TUNGSTEN RIBBON LAMP NO EPUV 1160 OPERATED AT 35 A IN $Watt.sterrad.^{-1}nm.^{-1}mm^{-2}$

λ(nm)	Standard Radiation
250	0.0140
260	0.0303
270	0.0545
280	0.0960
290	0.1580
300	0.2480
320	0.5430
350	1.4900
370	2.5800
400	5.2000
450	12.6000
500	25.3000
550	41.9000
600	61.9000
650	83.1000
700	103.0000
750	120.0000

TABLE 6.6

THE POLYNOMIAL COEFFICIENTS (Ci) FOR THE DETERMINATION OF THE SPECTRAL RADIATION VALUES

i	C_i
0	$6.960480129 \times 10^{-1}$
1	$2.121801794 \times 10^{-2}$
2	$-4.493831222 \times 10^{-5}$
3	$-5.585220285 \times 10^{-7}$
4	$1.520697835 \times 10^{-9}$

TABLE 6.7

ABSOLUTE SPECTRAL RADIATIONS FOR THE EPPLY STANDARD AND THE CA-WAVELENGTHS CALCULATED

N_E	N_{Abs}	λ(nm)
0.248	0.25	300
0.54	0.53	320
1.49	1.49	350
2.58	2.60	370
-	2.86	373.7 (Ca II)
-	4.51	393.4 (Ca II)
5.18	5.20	400
-	8.00	422.7 (Ca I)
-	11.75	445.5 (Ca I)
12.6	12.60	450
25.3	25.30	500

TABLE 6.8

CALIBRATION CONSTANTS FOR THE CA-WAVELENGTHS

Wavelength (nm)	N_{Abs} W.ster^{-1}.nm^{-1}.mm^{-2}	N_{Rel}	K_i
393.3	4.51	23	1.955×10^{-1}
422.6	8.00	177	4.52×10^{-2}
445.5	11.75	588	2.0×10^{-2}
373.7	2.86	26	1.115×10^{-1}

where N_{Abs} = the calculated absolute radiation

N_{Rel} = the measured radiation

$$N_{Abs} = N_{Rel} \cdot K_i$$
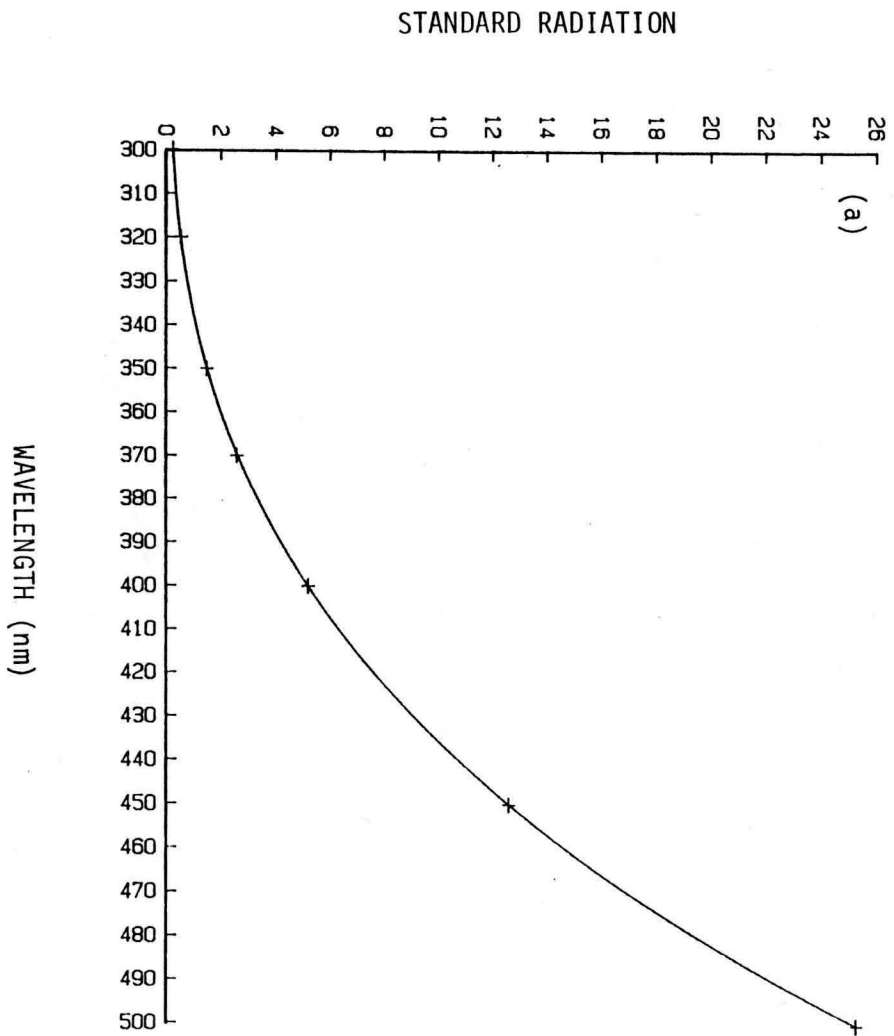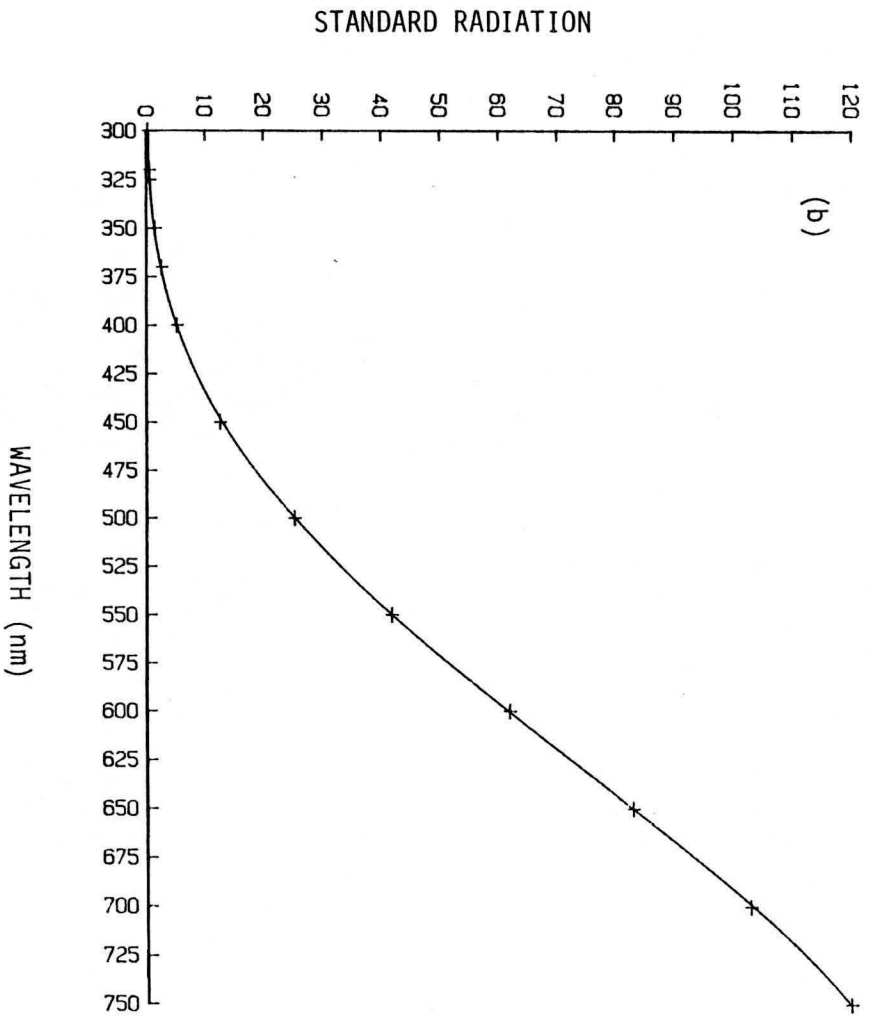
Figure 6.7 The polynomial fitted through the wavelengths (a) 300 - 500 and (b) 300 - 750 nm

probes include thermocouples, resistance thermometers, the ultrasonic thermometer and many others. The problem with intrusive probes is that their measurement range is generally below 3000 K. Non-intrusive or spectrometric methods do not have this limitation and include measurements of the spectral radiance corresponding to transitions (emmission, absorption, fluorescence) from populated levels of the internal energy distributions within the atomic species. This approach to temperature determination depends on measurement of a single line or band or on some relation (Maxwell and Bolzmann distributions) between the spectral lines. An advantage of spectrometric methods is that it does not have a high-temperature limit, however LTE within the flame volume is assumed as well as negligible self-absorption of the measured lines. Tourin[134] and Elder and Winefordner[52] discussed the different methods of measuring plasma temperatures. The two-line ratio method was used for temperature determinations in this project.

The radiation of an atomic emission line, when self-absorption is negligible is given by[134]

$$N_{nm} = \frac{1}{4\Pi} L \rho_n A_{nm} h\nu \qquad \text{erg sec}^{-1}\text{cm}^{-1}\text{steradian} \qquad (6.6)$$

Where n and m refer to the upper and lower energy states, respectively

N_{nm} = wavelength integrated radiation

A_{nm} = Einstein's coefficient of spontaneous emission (transition probability)

ν_{nm} = the wavenumber of the line in cm^{-1}

L = pathlength

h = Planck's constant

c = velocity of light

ρ_n = the number density of atoms in state n, given by the Maxwell-Boltzmann relation

$$\rho_n = \rho_o \frac{g_n}{Q} e^{-E_n/kT} \qquad (6.7)$$

where ρ_o = the number density of atoms
g_n = the statistical weight of the upperstate of the transition n m
Q = partition function

where $Q = \sum_n g_n e^{-E_n/kT}$ $\qquad (6.8)$

E_n = the energy of the upper state.

Substituting equation (6.7) into equation (6.6), and substituting $\nu_{nm} = \frac{c}{\lambda}$, we have

$$N_{nm} = \frac{hc}{4\pi} L\rho_o \frac{g_n A_{nm}}{Q\lambda_{nm}} e^{-E_n/kT} \qquad (6.9)$$

If the transition probability, statistical weight of the upper state, energy of the upper state, and wavelength of each of the two atomic lines are known, it follows from equation (6.9) that

$$\frac{N_1}{N_2} = \frac{g_1 A_1 \lambda_2}{g_2 A_2 \lambda_1} e^{-(E_1 - E_2)/kT} \qquad (6.10)$$

The temperature (T) can then be determined from equation (6.10);

$$T = (E_1 - E_2)/k \ln \frac{N_2 g_1 A_1 \lambda_2}{N_1 g_2 A_2 \lambda_1} \qquad (6.11)$$

Equation (6.11) is the atomic excitation temperature according to the two-line method, i.e. a temperature corresponding to equilibrium population of neutral atom electronic energy levels. If both lines are from an ion, we obtain an ionic excitation temperature.

6.2 *Electron Density*

The electron density, similar to the plasma temperature, is an important parameter which governs the excitation and pre-excitation mechanisms in the ICP. Electron density measurements in the ICP have been made by several workers over a range of operating and observation conditions. Blades and Caughlin[14] published excitation temperatures and electron densities for both water and organic solutions. Alder et al[3] measured the vertical electron densities at three different heights for different carrier gas flow rates. The measured electron densities varied from 1.77×10^{14} to 3.34×10^{15} cm^3. Furuta et al[60] measured a large number of emission profiles at different heights. They then built up complete contour maps of electron densities. The maximum electron density was 4×10^{15} cm,$^{-3}$ occuring low in the plasma and 5 mm of axis. Gunter et al[69] calculated the electron densities in the 9, 27 and 50 MHz ICP's. The measured electron densities were in the range from $4,3 \times 10^{14}$ cm^{-3} for the 50 MHz to $1,2 \times 10^{15}$ cm^{-3} for the 9 MHz to $2,0 \times 10^{15}$ cm^{-3} for the 27 MHz ICP. Kalnicky et al[84] calculated the electron densities experienced by analyte species in the ICP with and without the presence of an easily ionized element. A comparison of radial electron density distributions measured with the Saha-Eggert ionization and with Stark broadening methods is also given for an observation height of 15 mm above the load coil. Montaser and Fassel[104] reported electron densities measured in a Ar and Ar-N$_2$ ICP. Electron densities were reported and discussed for the two systems.

Theory

Ionization equilibrium is controlled by the Saha- equation.[134] Apart from atoms in the ground state or excited state there are also ions of the same element present in any flame, with a certain equilibrium existing between the two species at each temperature. The Saha-equation, which relates this ionization equilibrium, is

based on the law of mass action. The equilibrium is pictured by the following equation.

$$a \underset{k_r}{\overset{k_i}{\rightleftarrows}} i^+ + e^-$$
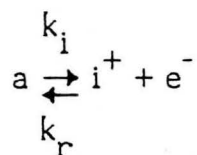
where k_i = velocity constant for the dissociation process, and

k_r = for the recombination process

a = atoms

i^+ = ions

e^- = electrons

For a specific temperature of the radiation source there is a so called ionization equilibrium constant, K_i

$$K_i = \frac{\rho_i \rho_e}{\rho_a} \tag{6.12}$$

where ρ_i = ion density
ρ_a = atom density
ρ_e = electron density

The electron density is calculated in terms of number of electrons per m^3. It is difficult to determine ρ_i and ρ_e directly and we therefore use the Saha-equation. The Saha equation is derived from the equilibrium constant K_i (equation 6.12), which is expressed in terms of the atom state, Q_a, and the ion state, Q_i, the temperature of

the source T and the ionization energy, χ, of the particular species, i.e. Ca. Therefore,

$$K_i = \frac{\rho_i \rho_e}{\rho_a}$$

$$= \frac{2(2\Pi m_e kT)^{3/2}}{h^3} \frac{Q_i}{Q_a} e^{-\chi/kT} \qquad (6.13)$$

where m_e = mass of the electron

   Q_i = partition function of the ion

   Q_a = partition function of the atom

   χ = ionization energy

   k = Boltzmann constant

   h = Planck's constant

   T = absolute temperature

The radiation from a spectral line of an atom in terms of the Boltzmann equation is given by equation 2 in Appendix 2 as:

$$N_{nm} = \frac{hc}{4\Pi} L \rho_a \frac{g_n A_{nm}}{Q_a \lambda_{nm}} e^{-E_n/kT} \qquad (6.14)$$

The equation for the radiation for a spectral transition $(k \rightarrow j)$ of an ion of the same element is very similar.

$$N_{kj}^+ = \frac{hc}{4\Pi} L\rho_i \frac{g_k^+ A_{kj}^+}{Q_i \lambda_{kj}^+} e^{-E_k^+/kT} \tag{6.15}$$

The ratio of the spectral radiations for the transitions (n → m for atom, k → j for ion) for successive ionization states of the same element will be as follows:

$$\frac{N_{nm}}{N_{kj}^+} = \frac{\rho_a g_n A_{nm}}{\rho_i g_k^+ A_{kj}^+} \frac{Q_i}{Q_a} e^{\{-(E_n - E_k^+)/kT\}}$$

Thus,

$$\frac{\rho_a}{\rho_i} = \frac{N_{nm} g_k^+ A_{kj}^+ Q_a \lambda_{nm}}{N_{kj}^+ g_n A_{nm} Q_i \lambda_{kj}^+} \exp\{-(E_k^+ - E_n/kT)\} \tag{6.16}$$

Equation (6.16) substituted into the Saha-equation (6.13) gives;

$$\rho_e = 2 \frac{2\Pi m_e kT)^{3/2}}{h^3} \frac{N_{nm} \lambda_{nm} g_k^+ A_{kj}^+}{N_{kj}^+ \lambda_{kj}^+ g_n A_{nm}} \exp\{-(E_k - E_n^+ + \chi)/kT\} \tag{6.17}$$

Therefore,

$$\ln \rho_e = \ln 2 \left\{ \frac{(2\Pi m_e kT)^{3/2}}{h^3} \right\} + \ln \left\{ \frac{N_{nm}}{N_{kj}^+} \right\} + \ln \left\{ \frac{g_k^+ A_{kj}^+ \lambda_{nm}}{g_n A_{nm} \lambda_{kj}^+} \right\} - \left\{ \frac{E_k - E_n^+ + \chi}{kT} \right\}$$

$$........(6.18)$$

It is thus possible to determine the value of the electron density, ρ_e. The value of T, determined with the two-line method, together with the measured radiation values, N_{nm} and N_{kj}^+, and the values for other parameters gathered from tables are substituted in equation (6.17) or (6.18). This method is based on the acceptance of thermal equilibrium.

Another popular method for the determination of electron densities is through Stark broadening of spectral lines. [3,84,104] Atomic hydrogen lines are most frequently employed for these calculations because of the availability of extensive tables of Stark broadening parameters for the complete line profiles. This technique was not used in this work and for further discussion on this and other electron density measurement techniques the reader is referred to the discussions by Griem. [66]

Results and Discussion

Plots of excitation temperature, as measured radially outwards in the plasma at three different heights, are shown in figures 6.8 and 6.9 for no desolvation and 150°C pre-desolvation temperature applied respectively. The off-axis peak of the 7 mm radial measurement illustrates the cooling effect of plasma penetration by the sample. There is no difference in the relative position of the profiles for the different heigths with and without desolvation. The major difference between the two figures is the overall increase in plasma temperature with pre-desolvation. Less power is therefore drained from the plasma for the desolvation process, normally the major consumer of energy in the plasma. This is illustrated in figure 6.10, where the excitation temperature versus height above the coil along the plasma axis is shown for the two cases. In both cases the temperature peaks at 15 mm above the coil after which it drops off rapidly with increasing height. This phenomenon was also reported by Furuta and Horlick[61] and Alder et al.[3]

Alder et al[3], Tang and Trassy[131] and Kirkbright[86] however all reported a decrease in excitation temperature if most of the water was removed from the sample by desolvation before injection. A similar excercise was carried out with the only difference that we increased the pre-desolvation temperature in small increments. (Figure 6.11) From the graph it can be noticed that an optimum pre-desolvation temperature is encountered at approximately 150 $^\circ$C, which corresponds to the highest plasma excitation temperature. Venghiattis[138] and Boumans and De Boer[19] mentioned "best" settings of 200 $^\circ$C and 140 $^\circ$C respectively, but they gave no explanation for this phenomenon. Issaq and Morgenthaler[81,82] suggested a
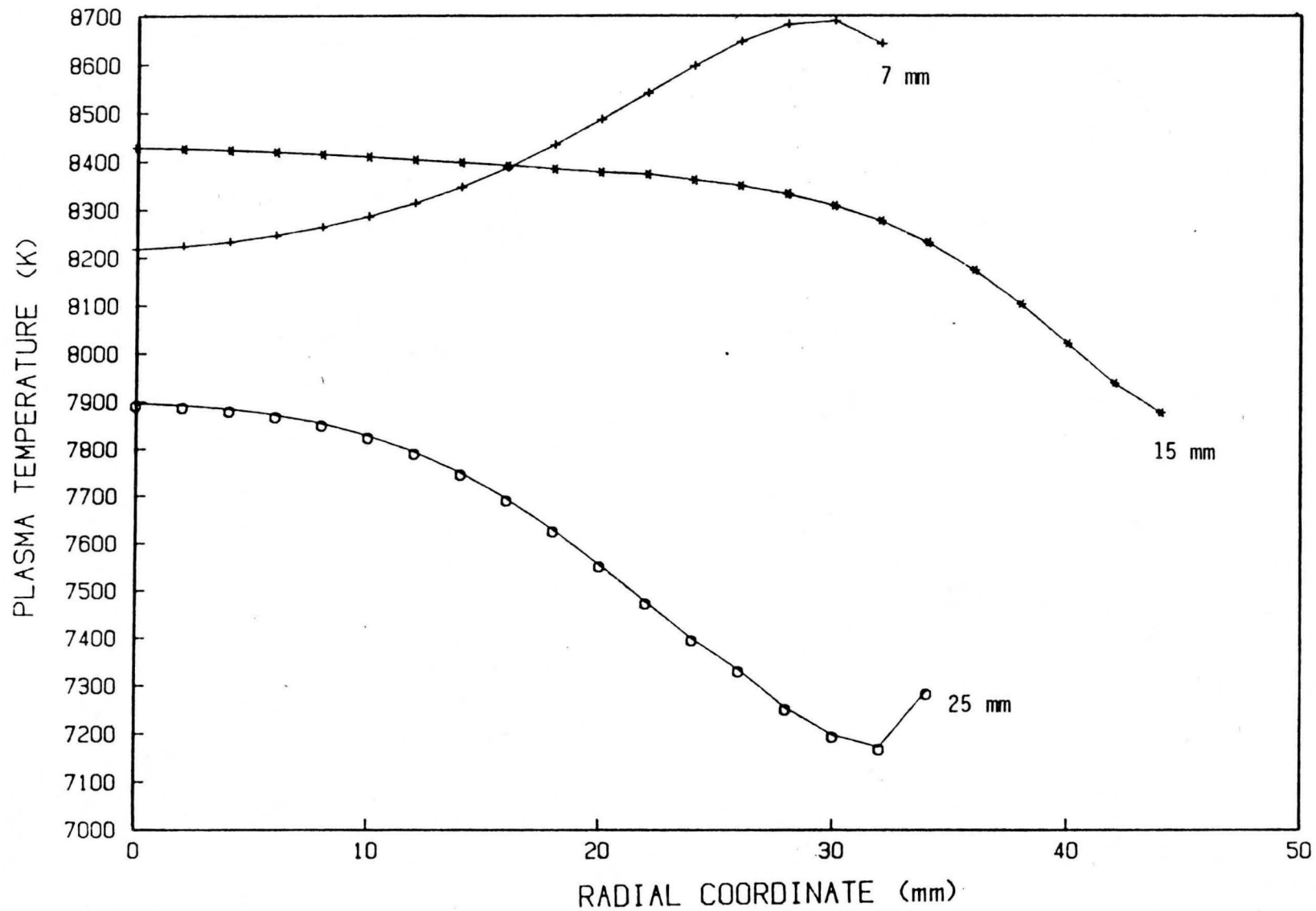
Figure 6.8 Excitation temperatures measured, without pre-desolvation, using Ca II spectral lines at different heights above the coil
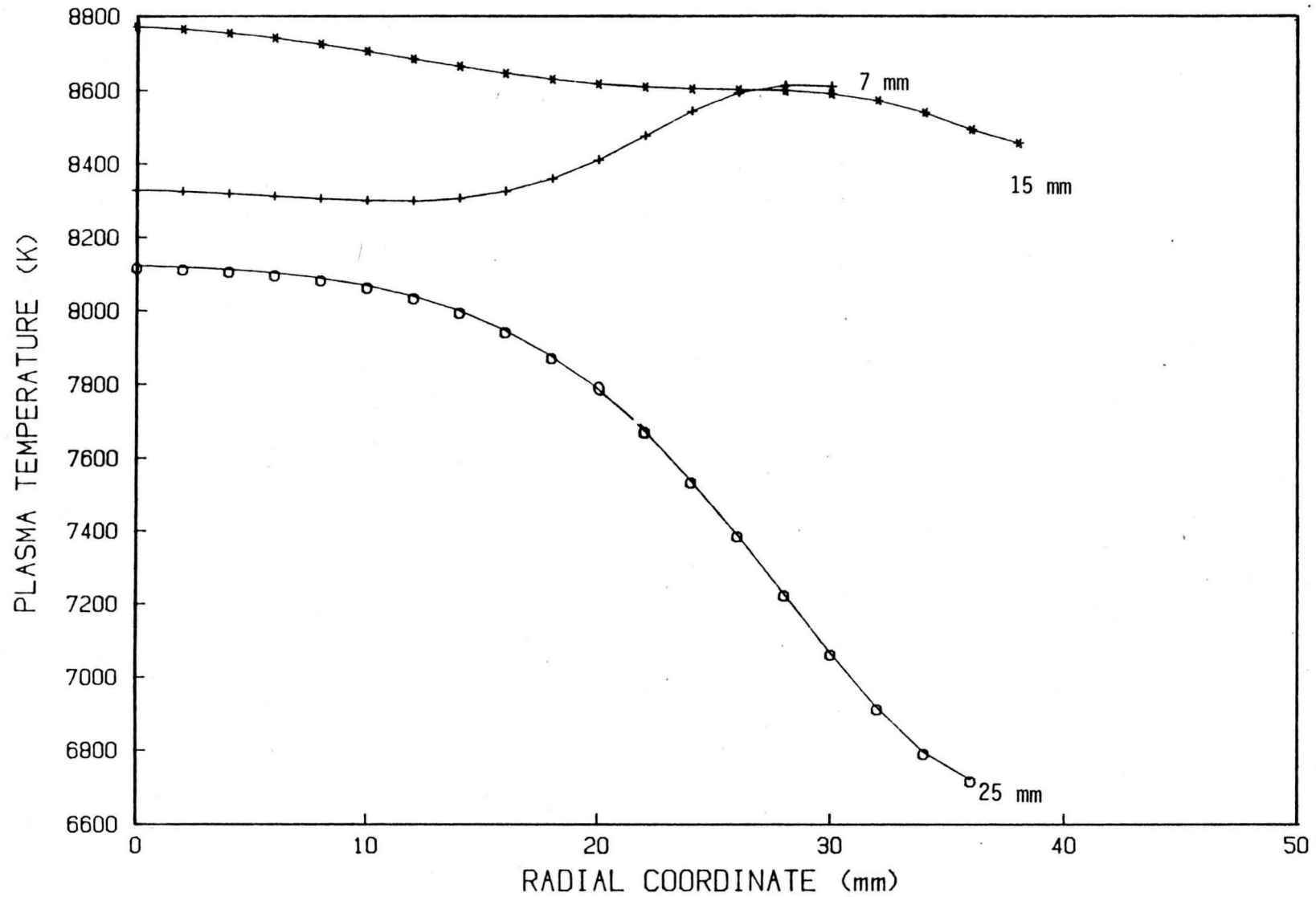
Figure 6.9 Excitation temperatures measured, with pre-desolvation, using Ca II spectral lines at different heights above the coil
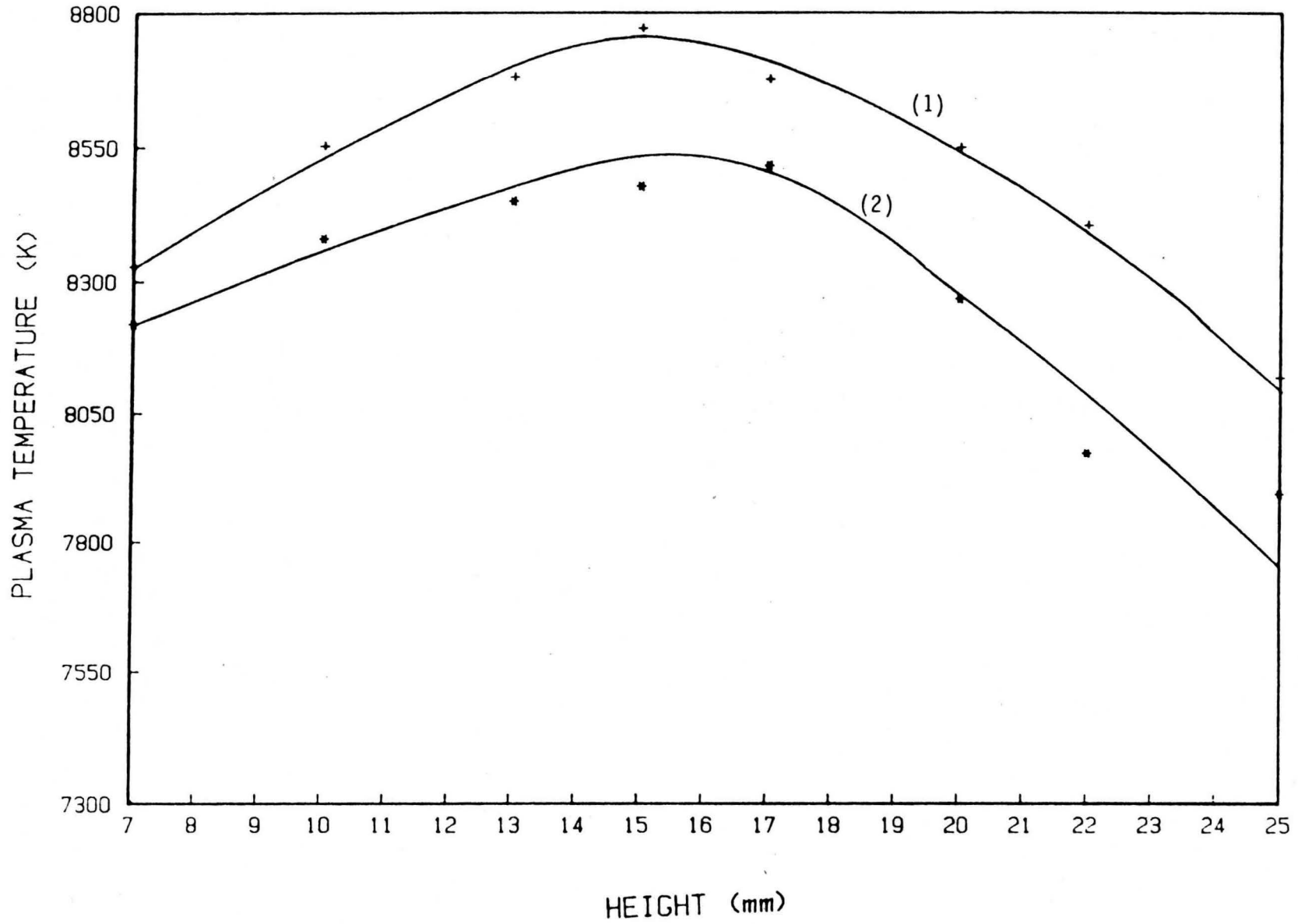
Figure 6.10 The excitation temperature as a function of height above coil with .(1) and without (2) pre-desolvation
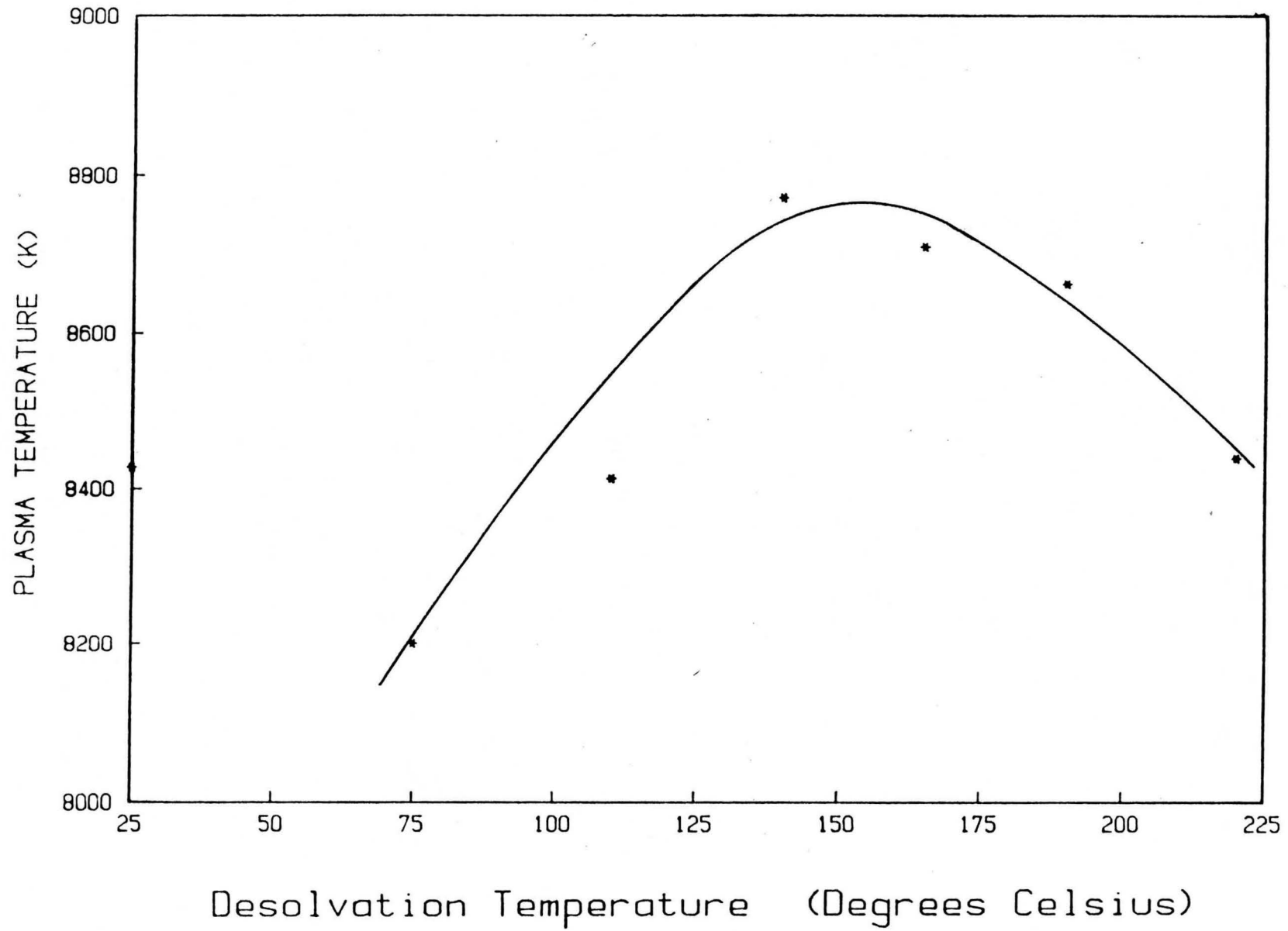
Figure 6.11 Excitation temperatures measured at different pre-desolvation temperatures (15 mm above coil)

relatively high pre-desolvation temperature of $350^{\circ}C$, but due to difficulties with solutions of high salt content at temperatures of $250-350^{\circ}C$, a high pre-desolvation temperature seems inappropriate.

Plots of the electron density as a function of pre-desolvation temperature and plasma height are given in figures 6.12, 6.13 and 6.14 and figure 6.15 respectively. The electron density variation across the diameter of the plasma shows the same tendency as the plasma excitation temperature, namely a significant increase in the electron density at 15 mm height with pre-desolvation. This is also attributed to the addition of energy via the heating chamber. The same optimum predesolvation temperature of 150 $^{\circ}C$ is found as for the temperature data. (Figure 6.15) It is clear that an optimum pre-desolvation temperature is characteristic of a spesific height above the coil. (Figure 6.10)

6.3 *The Influence of Solvent on the Emission Profiles*

The spatial emission behaviour of solutes in the presence and absence of water is another aspect which may help in the understanding of the influence of solvent on plasma parameters and to further expand the solvent/plasma interaction model. Water was selected as the solvent of study because of its almost universal use in ICP spectrometry. Many investigators have done some spatial characterization of analyte emission for different reasons. Edmonds and Horlick[51] measured the profiles for both atom and ion lines of several elements as a function of plasma power, central axial flow rate, and coolant flow rate. They acquired analyte emission intensity information as a function of vertical height above the load coil. The position of the peak maximum was found to shift upward as the aerosol flow rate was increased.

Boumans and De Boer[18,20] also investigated the influence of parameters such as RF-power coupled with the plasma, carrier gas flow rate and observation height on emission profiles. In these early investigations they found, in general, that the emission intensity increases with power and decreases with observation height. They further stated that the shape of emission profiles depend to only a small extent on carrier gas flow. They also experienced an optimum value with increasing carrier
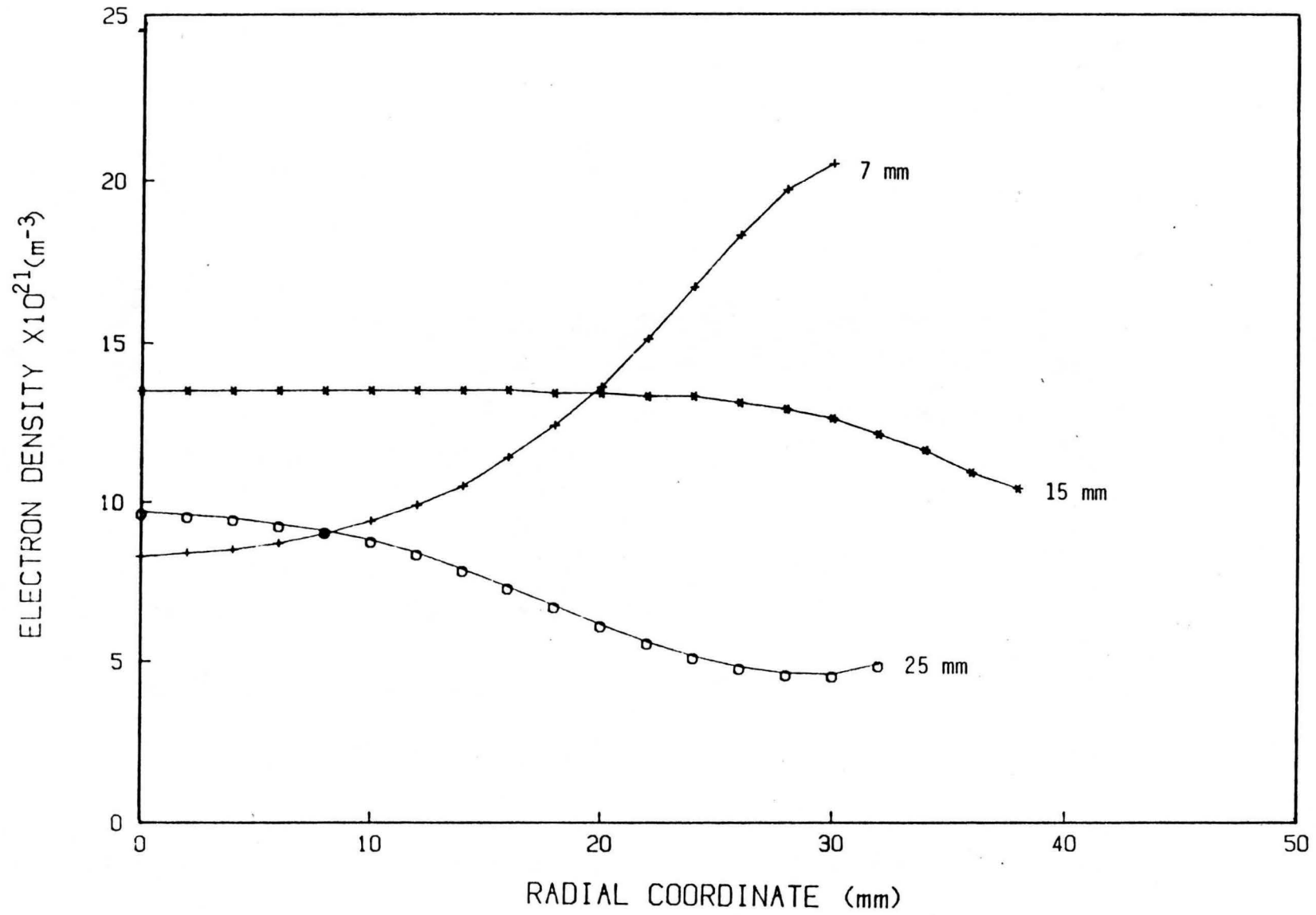
Figure 6.12 Electron densities obtained without pre-desolvation at a height of 7, 15 and 25 mm above coil
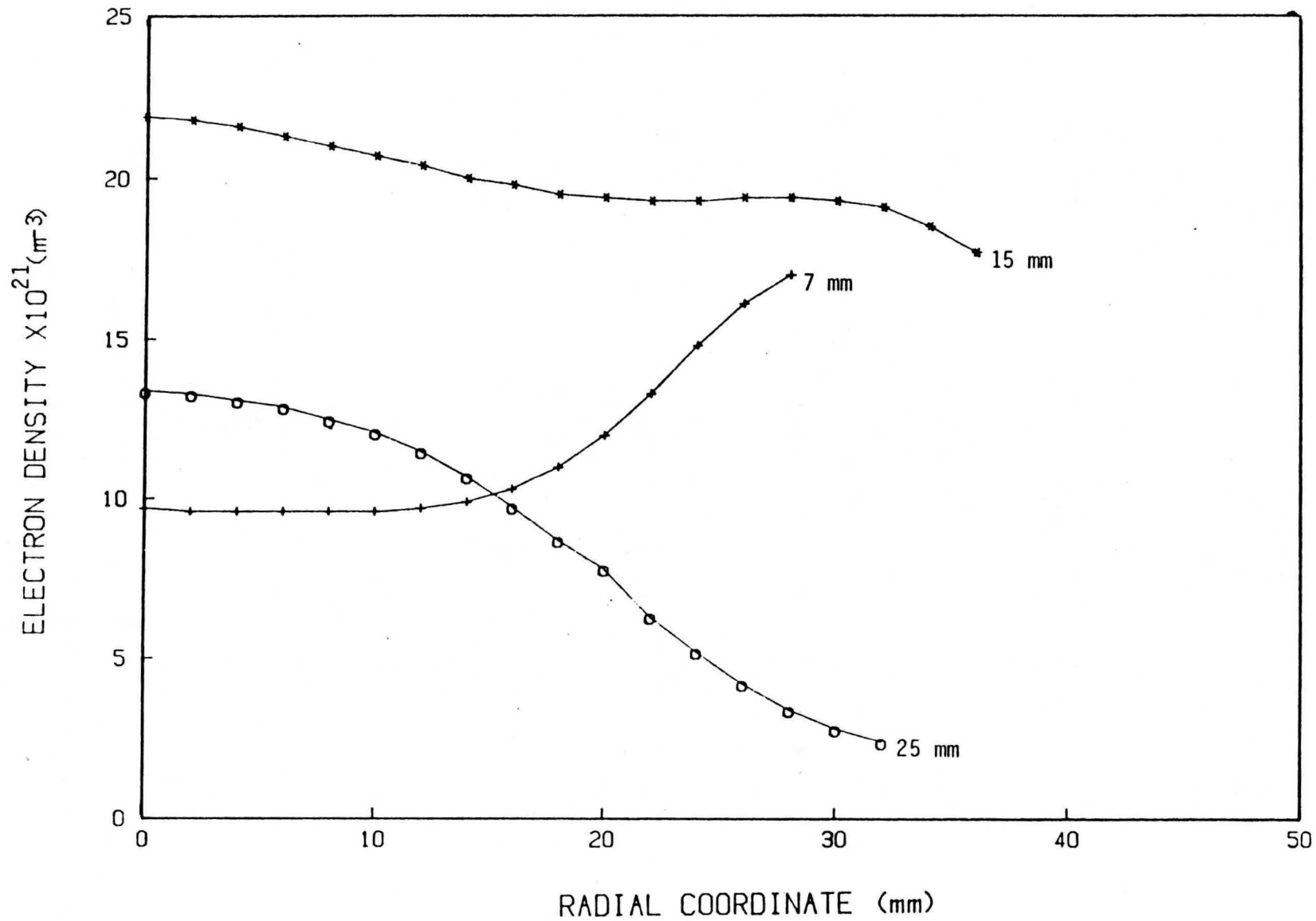
Figure 6.13 Electron densities obtained with pre-desolvation (150°C) at a height of 7, 15 and 25 mm
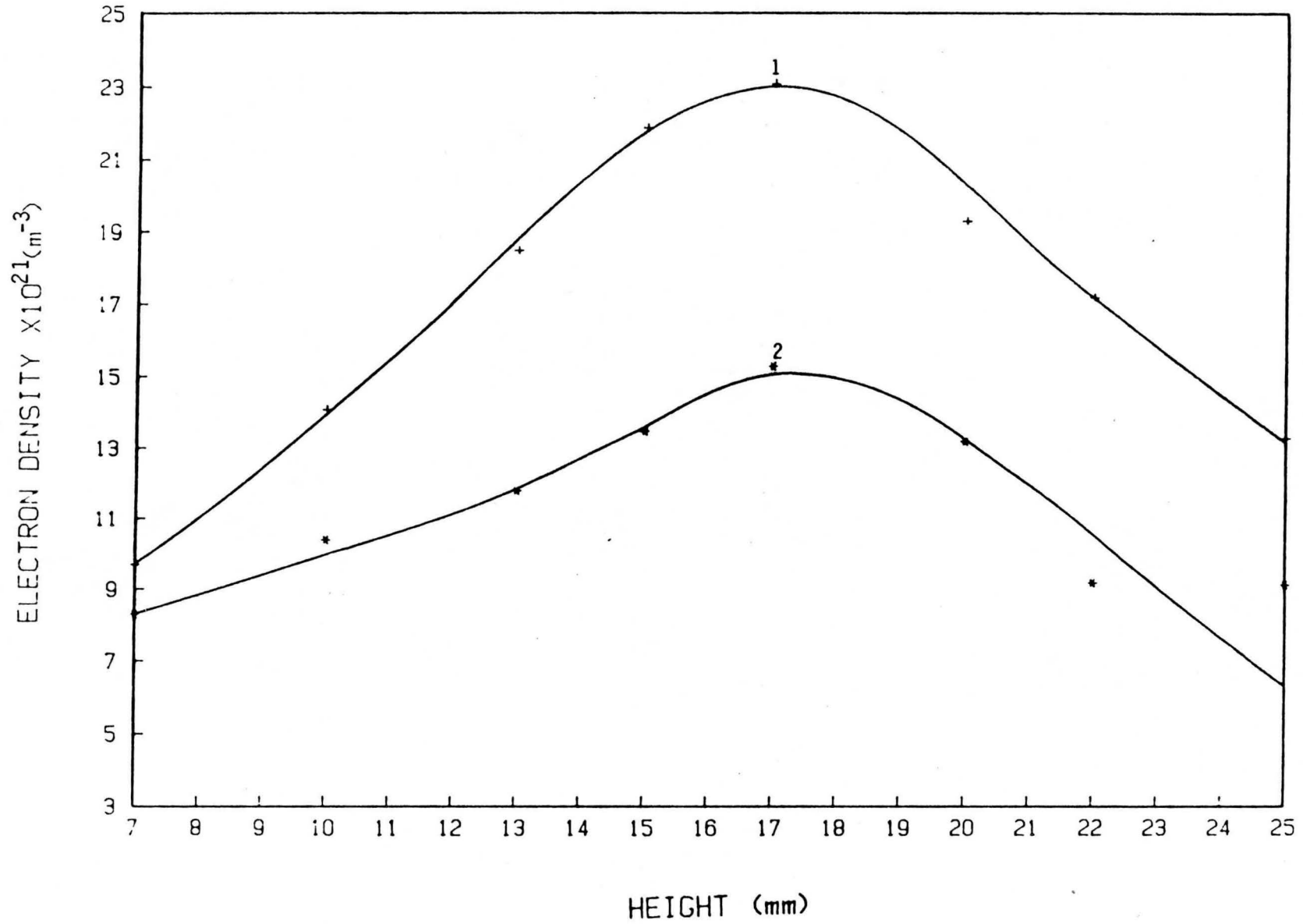
Figure 6.14   The electron density as a function of height above coil with (1) and without (2) pre-
desolvation
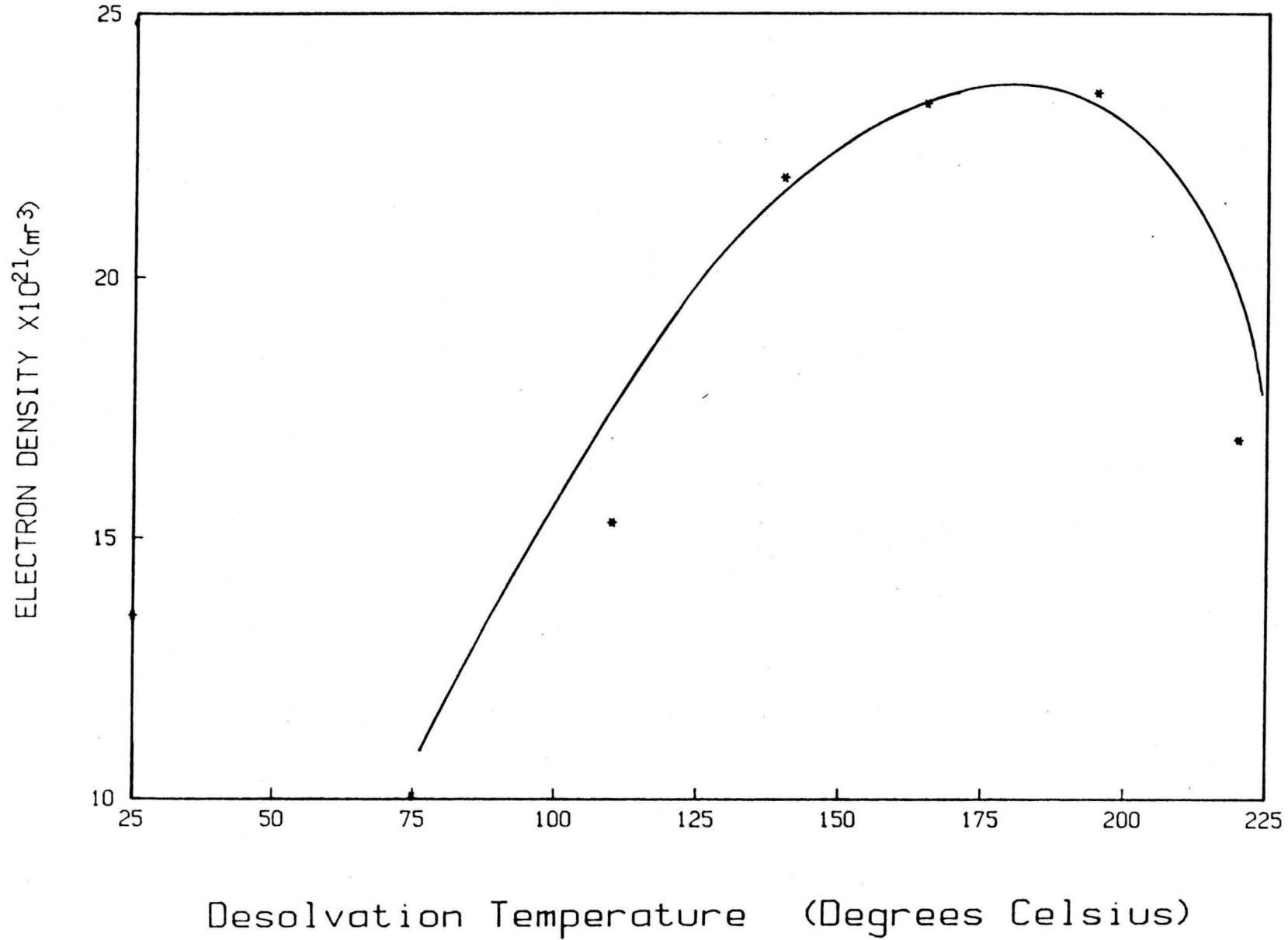
Figure 6.15 The electron density as a function of pre-desolvation temperature (15 mm above coil)
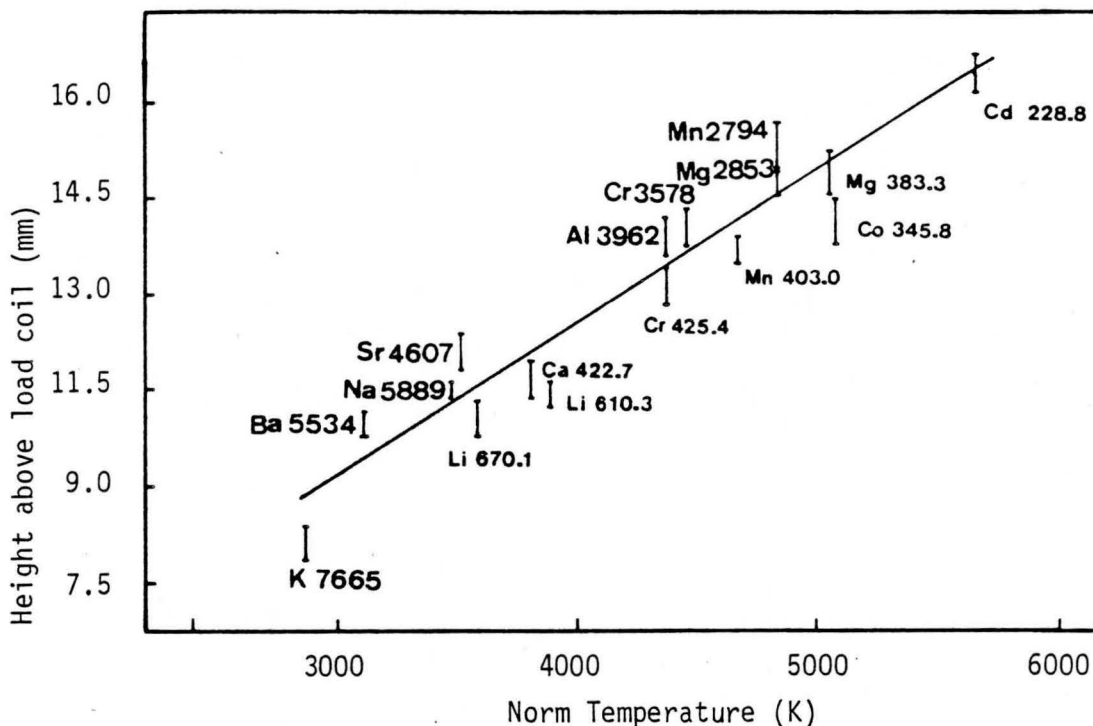
Figure 6.16   Position of vertical profile peak as a function of
norm temperature (in K) Blades and Horlick(
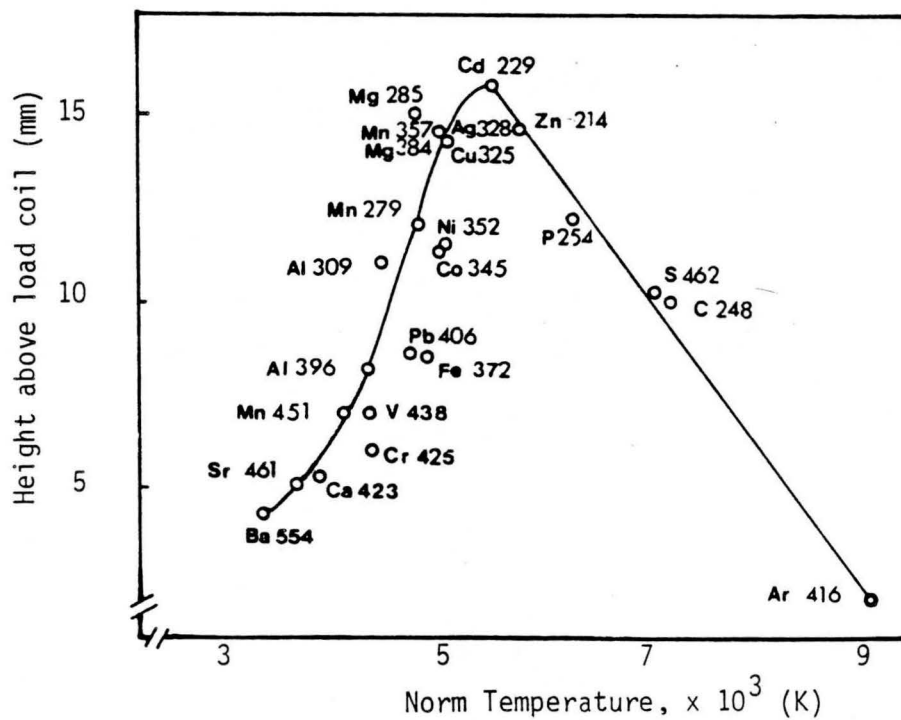
Figure 6.17   The observed position of peak emission vs normal
temperature plot. (Furuta and Horlick(

gas flow. Edmonds and Horlick[51] further found that the analyte spatial emission profiles fell into two distinct plasma zones based on these responses to applied power at a fixed aerosol flow rate. Furuta and Horlick[61], Blades and Horlick[16] and Kawaguchi et al[85] all shared this idea. It was shown that the ICP discharge could be divided into two zones, a lower region that is thermal in nature and where the peak emission position of neutral atom line (soft lines) can be related to normal temperature and an upper non-thermal region where ion and energetic neutral atom line emission occurs. This region are characterized by spatial behaviour insensitive to the analyte excitation parameters[16]. It was shown that the effect of an increase in load power is to shift the "thermal" zone downwards to the load coil and to slightly increase the energy of the electrons. This leads to a downward spatial profile shift and an overall increase in the emission intensity. Blades and Horlick[16] showed in their work that the position of the emission peaks observed in the ICP are strongly related to the norm temperature where the line is best excited. (Figure 6.16) Similar plots by Furuta and Horlick[61] clearly show that species such as (Zn, P, C, H and Ar) do not appear to follow the correllation proposed by Blades and Horlick[16]. The correlation for lower energy lines is confirmed but when the norm temperature exceeds about 5500K the correlation reverses in trend. It is therefore clear that a detail zoning of the plasma must include vertical spatial profiles as well as off-axis profiles. The temperature variation reported by Furuta and Horlick[61] is illustrated in figure 6.17.

General Theory

From the literature[16,51,61,85,94] it is clear that the peak position of neutral atom emission always occurs lower in the plasma than that of the corresponding ion line except where high energy neutral atom lines are involved i.e. Zn and Cd[61]. Blades and Horlick[16] refer to the two zones as the "thermal" (0 15 mm) and "non-thermal" zone (15 - 25 mm). No definitions for this "thermal" and "non-thermal" terms are represented in the papers although the processes in this regions are postulated. It is believed that neutral atom excitation is a result of electron collision and that ionic species generation and excitation is a result of collision with energetic argon species.[16,61,94]

The processes of desolvation, vaporization and dissociation of the analyte in the

region of the load coil result in ground state atomic species travelling up the analyte channel. As the atom moves up the central channel the rise in temperature will result in an increase in emission intensity due to an increase in excited state population according to the Boltzmann distribution. An increase in ionization will result in an opposing reaction due to a decrease in the atom population as described by the Saha equation. We can therefore expect an emission intensity maximum at some position above the load coil. This will occur at the so called norm temperature. This transition zone is the border between the "thermal" and the "non-thermal" zone. This border is reported to be at a height of about 15 mm.

Long and Browner[94] measured the emission profiles with and without water and experience a shift in emission intensity. They also found a shift in emission profiles with a variation in applied power. As a consequence of this spatial shift they presented two possible mechanisms, one a kinetic and one of thermal origin.

The kinetic process is the process whereby the electrons receive their kinetic energy from the induced electromagnetic force. The processes that follow thereafter are called thermal processes. These processes include elastic collision between low energy electrons and ground-state atoms, secondary collisions between low energy electron and excited atoms, recombination between ions and atoms, triple collisions etc.

(1) If the kinetic process dominates Long and Browner predicted a delay between the moment of aerosol entry and atomic excitation in the presence of solvent. It is therefore a function of desolvation.

(2) If the thermal process dominates it implies a decrease in power in the presence of water in the central channel. The maxima is therefore a function of applied power.

No further explanation or definition for this processes is given and it is felt that both kinetic and thermal processes occur in the lower region (0 - 15 mm).

It was found that the influence of power was only significant low in the plasma (0-15 mm).[16,85,94] Long and Browner[94] did however find that water has

an influence on the upper region (15 - 25 mm). The upper region is therefore insensitive to energy changes but sensitive to the amount of solvent. The extraction of solvent causes an apparent shift of the ion profile out of the "non-thermal" zone into the "thermal" zone[94] Long and Browner[94] suggested two possible reasons for this behaviour.

(1) the species responsible for ionic emission profiles are themselves directly or indirectly affected by the presence or absence of solvent.

(2) the phenomenon is primarily one of sample excitation kinetics.

Reason (2) may lead to reason (1). One expects the border zone between the "thermal" and "non-thermal" zone to shift as a function of amount of solvent. According to our definition of "thermal" processes the upper region (15 - 25 mm) is also characterized by thermal processes. A better definition for the two regions might be a kinetic zone (0 - 15 mm) and a non-kinetic zone (15 - 25 mm).

Results and Discussion

Plots of the radial emission as a function of the plasma radius, height above coil and pre-desolvation temperature are shown in figures 6.18, 6.19, 6.20 and 6.21. Figures 6.18 and 6.19 shows the influence of pre-desolvation (Figure 6.19) on the radial emission along the axis of the plasma. It is clear that the region which emits the optimum signal shifts towards the load coil with increasing predesolvation temperature. This is attributed to the availibility of more energy for the processes of dissociation and subsequent atomization. This was expected and is supported by the results reported on plasma temperature and electron number densities. There is also a noticeable increase in the spectral emission. In figure 6.20 the radiation intensity of Ca II 393,3 nm at 15 mm in the centre of the plasma at different desolvation temperatures is displayed. The emission intensity of the ion line peaks around an optimum desolvation temperature of 150°C. These results can lead to improvements in the analytical working range of factors between 1.1 - 12 as have
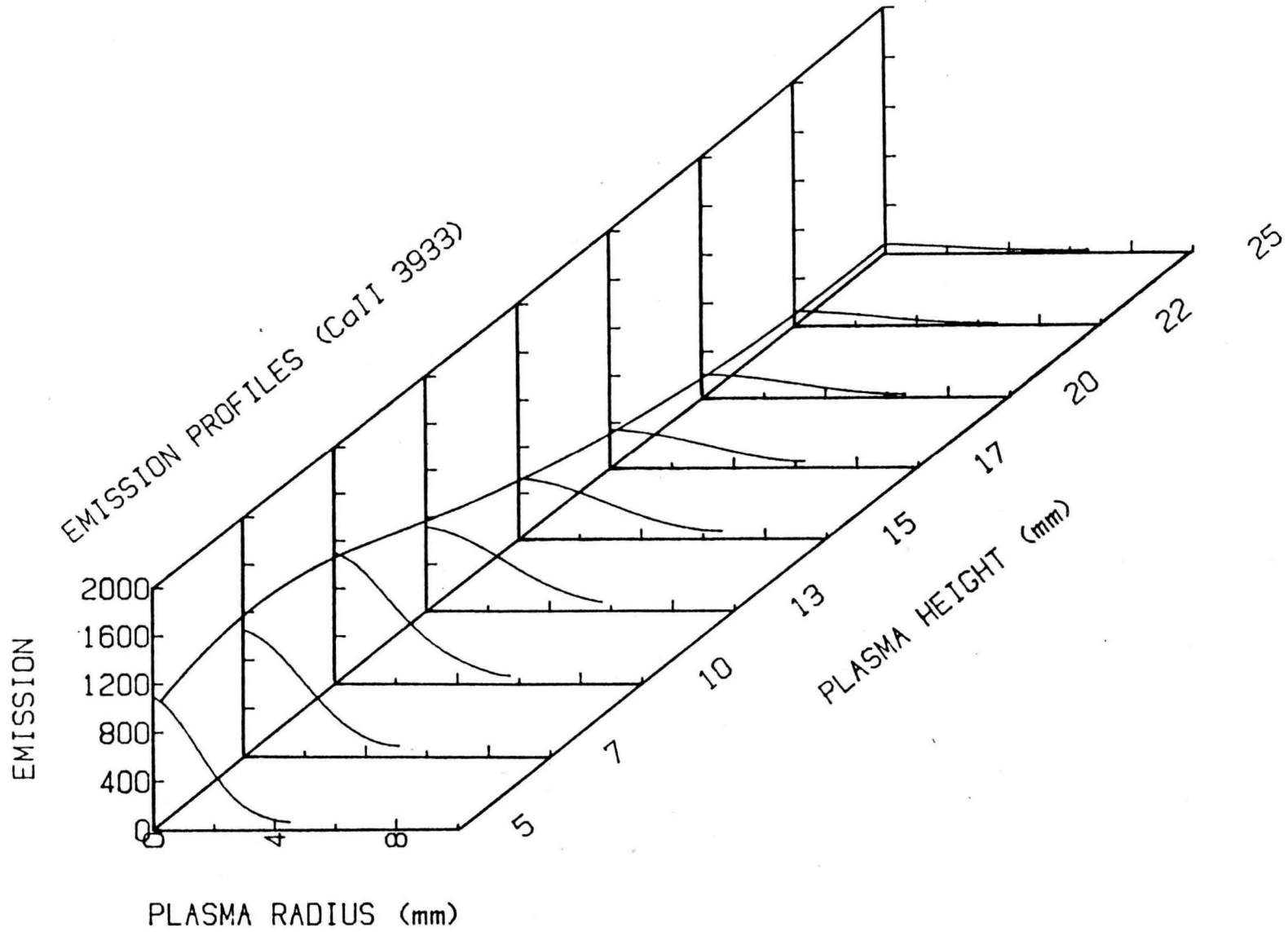
Figure 6.18 Emission Profiles of the CaII line at different heights above the coil, obtained without pre-desolvation
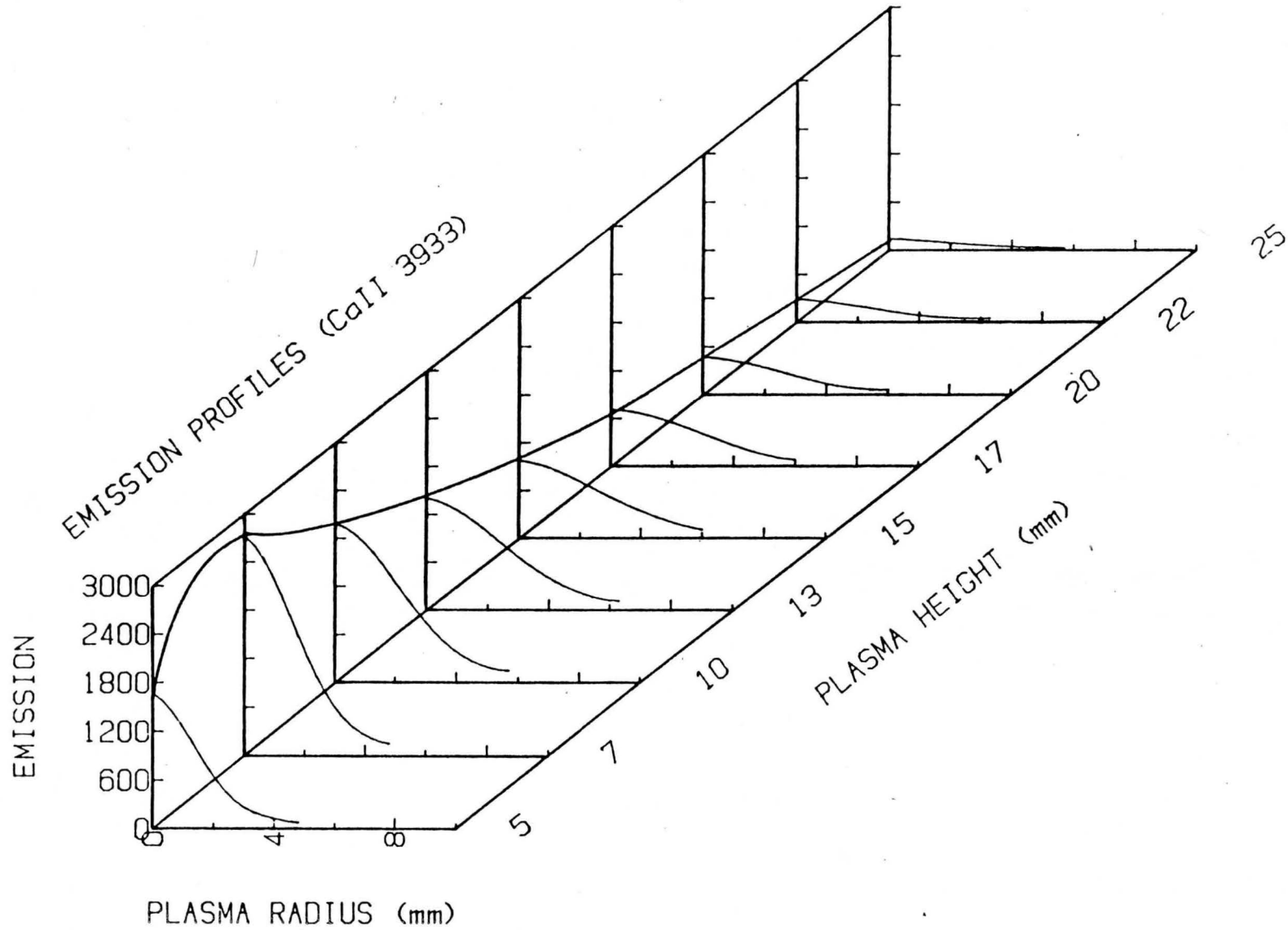
Figure 6.19 Emission Profiles of the CaII line at different heights above the coil, obtained with desolvation (150°C)
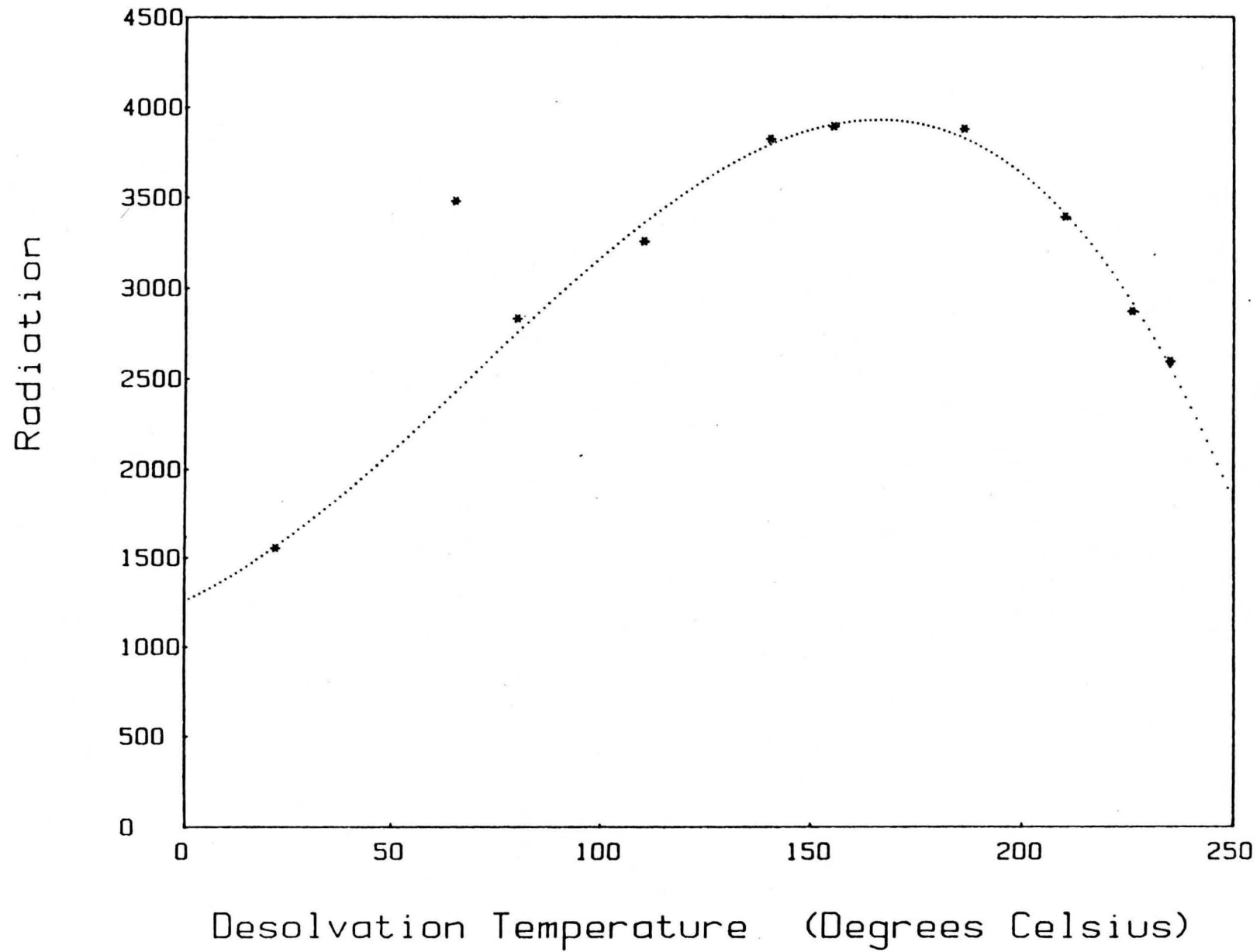
Figure 6.20   The radiation of the CaII393,3 line as a function of pre-desolvation temperature
(15 mm above coil)
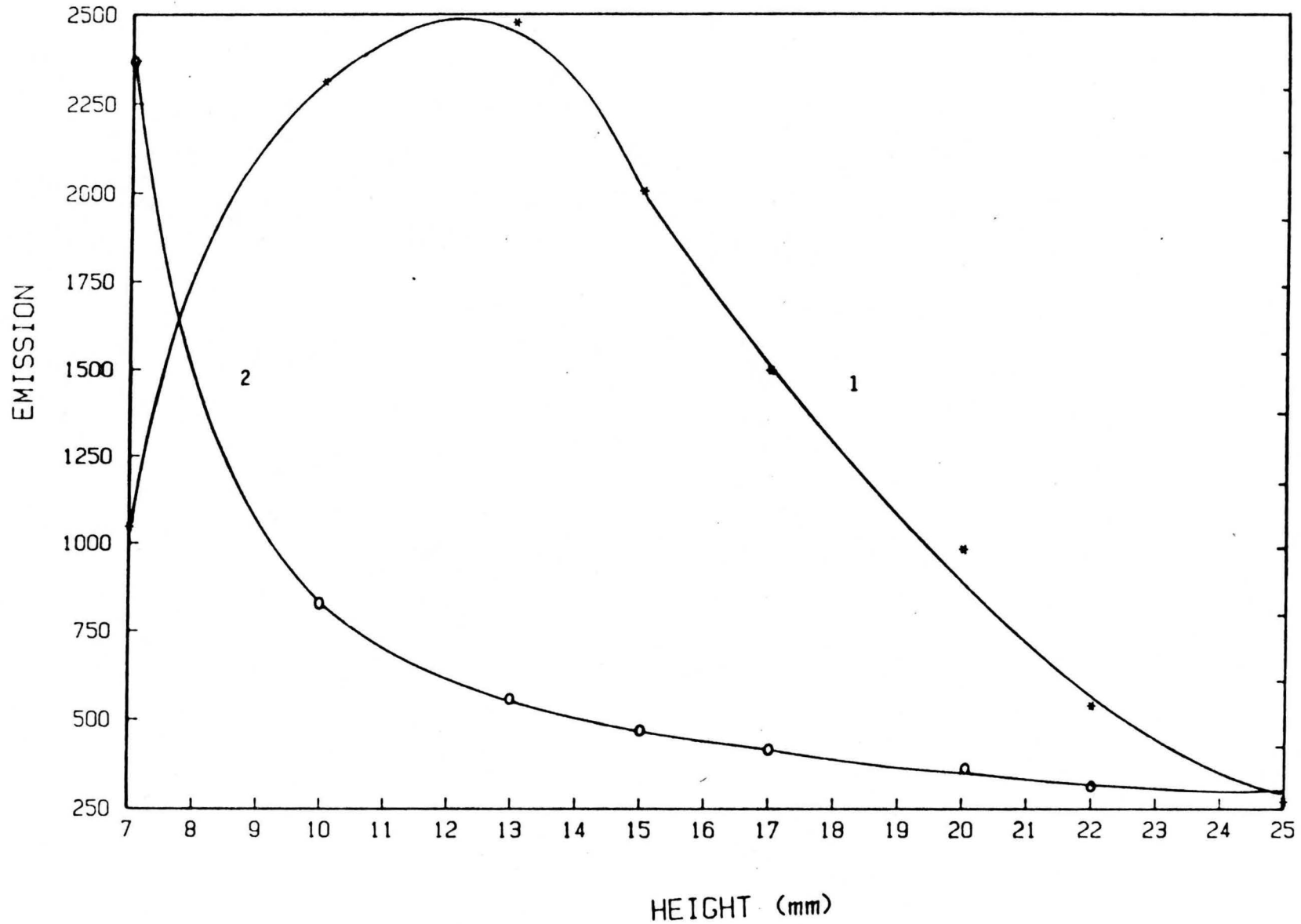
Figure 6.20 The spacial behaviour of the Ca II 393,3 nm (1) and the Ca I 422,6 nm (2) along the vertical axis of the plasma

been reported by Taylor et al.[132] It is therefore possible to increase W (the analyte transport rate) by a factor of about ten without having a negative effect on the plasma.[113]

The observed decrease in line intensity (Figure 6.21) above 150°C could perhaps be the result of sample not reaching the plasma, i.e. lost via the drain at higher temperatures. This possibility was verified by means of atomic absorption. The ultrasonic nebulizer and desolvation system was connected to a Varian Techtron 1275 BD spectrophotometer and the absorbance was monitored with increasing pre-desolvation temperature. However no decrease in the absorbance was found . This interesting result confirmed that the sample was actually still introduced into the ICP plasma, but due to change in the excitation mechanisms a decrease in line intensity was observed. From the results it can be deduced that water is essential for the excitation process. This result agrees with these of Tang and Trassy,[131] Olson and Böhmer[114] and Alder et al[3] as discussed in the introduction of this chapter, but not with their conclusion that pre-desolvation always leads to a decrease in the plasma temperature. The excitation temperature depends on the desolvation temperature, as is shown in figure 6.11. However we agree that excessive pre-desolvation can lead to a lower temperature. It is therefore clear that too much water can drain up to 20% of the available energy, as reported by Boumans and De Boer[19], due to the very high heat capacity of water. On the other hand we know that water is dissociated and essentially present in the form of atomic hydrogen and atomic oxygen.[3,86,131] As mentioned in the theory discussed earlier the thermal conductivity of hydrogen is about ten times higher than that of argon, while a water-argon mixture is about 4,5-18 times higher than that of argon[131] and it is therefore clear that the presence of hydrogen is very important for proper excitation of the analyte.

The presence of hydrogen will also influence the electron density in the plasma since the ionization energies of hydrogen and oxygen are about 2 eV below that of argon. (Figure 6.15) Two extremes are therefore responsible for the observed optimum pre-desolvation temperature. On the one hand the high efficiency of the ultrasonic nebulizer introduces a large amount of water into the plasma causing cooling . On the other hand too much desolvation extracts all the water, which then

decreases the amount of hydrogen, necessary for the energy transport to the sample, to such an extent that a decrease in line intensity and temperature is again observed. It is therefore clear that one needs to work at an optimum pre-desolvation temperature to ensure an optimum signal. Atom and ion lines display different spatial behaviour in a plasma, as discussed earlier in section 6.3. In figure 6.21 the spatial behaviour of Ca (II) 393,3 and Ca (I) 422,6 is shown along the vertical axis of the plasma. It is clear that the atom line peaks lower in the plasma than the ion line. This is because of the greater energy required for ionization. However one must bear in mind that other processes such as transition probability, norm temperature and ionization potential also influence the spatial distribution of emission line intensity in the plasma. One should never measure spectral line intensities below 12 mm in the plasma, even if some atom or ion lines show optimum intensities there, because in this so-called initial radiation zone (IRZ) where desolvation and dissociation take place interelement effects can be a problem. The normal analytical zone (NAZ) is usually about 15 mm above the load coil in plasmas without pre-desolvation. With pre-desolvation the position of optimum ion line intensity shifts to lower heights, coinciding with that of the atom line. In fact the normal analytical zone will also be nearer to the load coil.

CHAPTER 7

7. OPTIMIZATION

The ultimate goal of most researchers is to determine the optimum combination of parameters for his apparatus. In spectroscopic analysis the parameters to be optimized are those that determine the number of free atoms produced, as well as those that determine the effective excitation of these free atoms. To use the ICP in the most efficient and cost-effective manner a knowledge of the optimum operating conditions for the plasma is required. Comparisons between different instruments or nebulizers are meaningless unless a complete optimization is done[47] on each.

If the different parameters are linear and independent of the other variables it is possible to optimize each parameter separately by measuring the response of a sequence of values for each parameter. However, in spectrochemical analysis, the variables are interdependant. A sequential simplex method is therefore necessary for optimisation. A simplex is a geometrical figure defined by a number of points which is one greater than the dimensional number of the space containing the simplex. The simplex method implies the tracking of optimum conditions by evaluating the output from a system at a set of points forming the simplex in the factor-space, and continually forming new simplices by reflecting one point in the hyperplane of the remaining points to eventually yield a minimum or maximum of a certain mathematical function. Spendley et al[125] proposed a basic sequential simplex method in 1962. The attractive features of this method are the simple calculations involved and the speed with which optimum conditions can be established.

The modified simplex method of Nelder and Mead[106] represents an improvement on the basic method in that the simplex can be expanded and contracted allowing optimum conditions to be achieved in a shorter time. There are many possible response functions one can use although the most commonly used is the net signal-to-background ratio (SBR). The particle size was used as a response function for the optimization of the ultrasonic nebulizer in this study. The influence of the nebulizer power and the spray chamber dimensions was investigated. The carrier gas flow

rate and plasma height were also optimized with the simplex program, by using the radiative emission as the response function. The simplex method is described in Appendix 1.

7.1 *Experimental Results*

Three variables were chosen for investigation: power, observation height, and flow rate of the aerosol carrier gas. The modified simplex method was used to determine the optimum plasma-operating conditions for the spectral line Mn (II) 257.61 nm, first on the basis of the maximum SBR and then on the basis of net signal. Boumans and Lux-Steiner[23] proposed that this manganese ion line can be regarded as being representative of all lines, and that the optimum conditions determined for that line can be used with confidence for all other lines. The setting of boundary limits is essential to the operating of the simplex method, since the simplex may well move outside the permissible factor space. From the graph of response versus vertex number (Figure 7.1) one can see how the simplex moves and when it reaches the maximum. The optimum settings are listed in Table 7.1.

Table 7.1

Optimum parameters			
	min	opt	max
Power (kW)	1.050	1.177	1.250
Carrier Gas Flow Rate (l/min)	0.5	0.7	0.9
Observation Height (mm)	10	13	25

CHAPTER 8

8. DETECTION LIMITS AND ANALYTICAL PERFORMANCE ON METALLURGICAL SAMPLES

The definition and quantification of detection limits is a problem felt by most analysts. The main problem, as Boumans[24] has stated it, is one of " bringing together the theory and practice in an integral and uniform picture which is both understandable and effective." The quantification of an element is often viewed in terms of the limit of detection. Particularly in the analysis of trace constituents, the minimum detectable amount or concentration of the analyzed component is of great interest. The limit of detection is expressed in units of concentration that describes the lowest concentration level of the element which an analyst determines to be statistically different from an analytical blank.

The various approaches to statistics are the main reason for the problems that are encountered in expressing these values. The calculated limit of detection may vary by an order of magnitude depending on the method of computation. The International Union of Pure and Applied Chemistry (IUPAC) adopted a model for limit of detection calculation in 1975[80], but it seems that the awareness and acceptance of this model by the analytical community has been slow if one looks at all the different approaches currently used for the determination of detection limits. Comparison between various analytical procedures, methods and analytical instruments on the basis of detection limits must therefore be treated with a great deal of caution. Comparisons are meaningless unless the detection limits are calculated in a consistent manner. Detection limits can also be one of the most misleading parameters for judging the results that will be obtained in routine analysis.

It is a well established practice to calculate a detection limit by the determination of the noise on the background signal as a standard deviation, σ. This standard deviation is then converted to a concentration equivalent and a detection limit is then quoted as a 2σ or as a 3σ concentration equivalent.

The sample introduction method naturally has an important influence on the detection limits, as do the gas flow rates, and a complete optimization is therefore important. Detection limits in high power, argon-nitrogen ICP's are an order of magnitude poorer than those of argon ICP's.[70] This is attributed to the more efficient non-thermal excitation of ionic spectral lines, in the argon ICP. The detection limit data can be obtained under either single element optimized conditions or multi-element compromized conditions.[113] Numerous lists of detection limits attained in ICP have been published and comparisons have been made with detection limits reached in other sources and in AAS and AFS.[7,20,22,26,33,46,54,55,62,64,65,75,77,88, 100,102,112,113,132,139,146] The theory and definitions of detection limits are thoroughly discussed in Appendix 3.

8.1 *Determination of the Detection Limits for the ICP and AA.*

Six Mintek-type samples were chosen for the evaluation of the ultrasonic nebulizer. Detection limits were determined and compared with the detection limits obtained with a cross flow nebulizer and a Meinhard nebulizer. The observed detection limits were also compared with detection limits obtained by other authors. It is recognized that detection limits are influenced by many experimental factors and that comparison of values measured by other investigators is possible only on a semi-quantitative basis. In spite of this limitation, it is instructive to compare the values with those reported in the literature. Twenty 1-second integrations were used for the calculation of each detection limit for both the ultrasonic nebulizer and the pneumatic nebulizers. The spectrometer is described in Chapter 4. It is important to note that this spectrometer is not as light sensitive as the spectrometers that are being used in most laboratories, because it is more suited for diagnostic work. Detection limits were also determined for atomic absorption. The equations used for the calculation of the detection limits are listed in Table 8.0 and explained in Appendix 3.

Table 8.0

EQUATIONS USED FOR THE DETERMINATION OF THE DETECTION LIMITS

A	B	C	D
$C_L = \dfrac{2S_B C}{X_{S+B} - X_B}$	$C_L = \dfrac{3S_B C}{X_{S+B} - X_B}$	$C_L = \dfrac{3(0.01X_B)C}{X_{S+B} - X_B}$	$C_I = \dfrac{6S_B C}{X_{S+B} - X_B}$

8.1.1 Preparation of the Samples.

The six elements chosen were lead, gold, aluminium, chromium, scandium and tin. A summary of the elements, the Reference Material No., the concentration in the sample, the concentration in the solution and the dissolution methods are given in Table 8.1.

The procedure for the dissolution of the samples was as follows,

STEP 1: 10 ml HNO_3 and 10 ml $HClO_4$ were added to 2 gram of the sample in a Teflon beaker. The beaker was then placed on a hot plate, whose surface temperature was raised from 150 to 225 $^{\circ}C$. The beaker was kept at this temperature till the volume was reduced to $\leq$ 3 ml. The beaker was then removed and cooled.

STEP 2: The temperature cycle used in STEP 1 was repeated after the addition of 5 ml $HClO_4$ and 10 ml HF. The final volume was again $\leq$ 3 ml. 20 ml water was then added, covered with a watch glass and boiled for 10 min. A precipitate formed and was filtered off.

Step 1 in the procedure allows for the destruction of any organic material that might be present in the samples. This treatment also oxidizes the sulfides. Step 2 attacks the silicates and removes the silicon from the solution as SiF_4. The resin and steels were treated differently. The resin was ashed and sodium peroxide was added. It was then dissolved in HNO_3 and H_2SO_4. The steels were dissolved in 20 ml HCl, 20 ml H_2O and 5 ml HNO_3. The residue was then filtered off and the paper ashed and dissolved in acid.

Table 8.1

STANDARDS USED FOR THE DETERMINATION OF DETECTION LIMITS

Elements	Fef. Mat. No.	Conc. in Sample	Conc. in Solution	Diss. Method
Pb	MRG 1(A229)	10 ppm	0.01 ppm	Acid Digestion
	GSP 1(A428)	51 ppm	0.51 ppm	Acid Digestion
Au	19/82(Resin)	30 ppm	0.30 ppm	Ashed,Fusion
	ASK 3(A414)	60 ppm	0.60 ppm	Fusion
Al	Steel(A560)	420 ppm	0.21 ppm	Acid Digestion
	Steel(A600)	31 ppm	0.31 ppm	Acid Digestion
Cr	SY 3 (A345)	10 ppm	0.10 ppm	Acid digestion
	MAG 1(A435)	105 ppm	1.05 ppm	Acid Digestion
Sn	ASK 3(A414)	460 ppm	4.60 ppm	Fusion
	GSP 1(A428)	5 ppm	0.05 ppm	Fusion

8.1.2 *Profiling of Spectral Lines*

A 35 mm photographic film was placed in the focal plane of the spectrometer. A sample containing all the analyte elements was aspirated and the film exposed for 45 seconds. The different spectral lines were identified and 2 mm wide slits were punched out of the film at the appropiate places. The film was then sprayed with matt black paint and placed back in the focal plane. The film then served as a mask to eliminate all unwanted parts of the spectrum. The slits were placed in position with the photomultipliers behind them. The sample was again aspirated and the slits were adjusted to the optimum position. The tilt of each slit was also adjusted so that the slit was parallel to the spectral line.

8.1.3 *Detection Limits for the ICP.*

The elements with their wavelengths are listed in Table 8.2. The detection limits obtained are listed in Table 8.3.2. The general statistics are listed in Table 8.3.1.

<div align="center">

Table 8.2

WAVELENGTHS USED FOR ICP

Elements	Wavelength (nm)
Au(I)	267.5
Al(I)	308.2
Cr(II)	283.5
Pb(II)	220.3
Sn(I)	303.4
Sc(II)	255.2

</div>

8.1.4 *The Detection Limits Determined for Atomic Absorption.*

The application of the ultrasonic nebulizer to Atomic Absorption has been discussed by several authors.[44,45,75,81,82] The merits of the conventional pneumatic nebulizer and the ultrasonic nebulizer have been examined with respect to sample

Table 8.3.1

GENERAL STATISTICS OBTAINED WITH ULTRASONIC AND PNEUMATIC NEB.

Element	(Desolvation) Ultrasonic Nebulizer						(No Desolvation) Ultrasonic Nebulizer					
	Background		Net Signal		S/B		Background		Net Signal		S/B	
	Mean	$\%S_B$	Mean	$\%S_B$			Mean	$\%S_B$	Mean	$\%S_B$		
Al	57	1.9	426	2.4	7.47		90.2	0.7	149	1.4	1.66	
Au	103	1.3	1665	1.0	16.17		94	0.8	429	0.3	4.56	
Cr	135	1.1	12599	1.1	93.33		159	0.6	6285	0.4	39.53	
Sc	96	1.2	4162	1.0	43.35		130	0.6	1810	1.5	13.92	
Sn	125	0.9	418	1.4	3.34		150	0.6	38	2.6	0.25	
Pb	53	1.1	368	1.1	6.94		54	0.9	154	1.1	2.85	

Element	Cross Flow Nebulizer						Meinhard Nebulizer					
	Background		Net Signal		S/B		Background		Net Signal		S/B	
	Mean	$\%S_B$	Mean	$\%S_B$			Mean	$\%S_B$	Mean	$\%S_B$		
Al	92	0.7	30	4.4	0.03		113	0.9	14	11	0.12	
Au	76	0.7	50	2.9	0.66		150	0.8	54	4.2	0.28	
Cr	119	1.1	1041	3.4	8.75		174	0.4	357	2.5	2.05	
Sc	165	0.9	639	5.0	3.87		91	1.0	285	2.8	3.13	
Sn	219	0.6	47	3.5	0.21		270	0.5	23	7.5	0.09	
Pb	73	1.3	34	3.3	0.5		76	1.1	21	3.5	0.28	

Table 8.3.2

DETECTION LIMITS OBTAINED FOR THE ICP (ng /ml)

Element	Ultrasonic Nebulizer (Desolvation)			Ultrasonic Nebulizer (No Desolvation)		
	$\dfrac{2S_BC}{X_S-X_B}$	$\dfrac{3S_BC}{X_S-X_B}$	$\dfrac{3S_BC}{S/B}$	$\dfrac{2S_BC}{X_S-X_B}$	$\dfrac{3S_BC}{X_S-X_B}$	$\dfrac{3S_BC}{S/B}$
Al	51	76	40	91	136	181
Au	16	24	19	37	56	66
Cr	2	4	3	3	5	5
Sc	3	8	7	4	13	22
Sn	262	390	90	478	717	1200
Pb	30	45	43	63	95	105

	Cross Flow Nebulizer			Meinhard Nebulizer		
	$\dfrac{2S_BC}{X_S-X_B}$	$\dfrac{3S_BC}{X_S-X_B}$	$\dfrac{3S_BC}{S/B}$	$\dfrac{2S_BC}{X_S-X_B}$	$\dfrac{3S_BC}{X_S-X_B}$	$\dfrac{3S_BC}{S/B}$
Al	463	686	1000	1386	2060	2500
Au	207	310	455	429	642	1071
Cr	25	37	34	42	62	146
Sc	49	73	78	63	95	96
Sn	2704	4073	1428	-	-	-
Pb	565	833	638	787	1250	1071

Table 8.3.2 cont.

	Mintek		Ames[55] Laboratory	Winge[146] et.al.	Taylor and Floyd[132]	
	Pneumatic Neb		Pneumatic Neb.	Pneumatic Neb.	Ultrasonic Neb.	Pneumatic Neb.
	$\dfrac{2S_B C}{X_S - X}$	$\dfrac{3(0.01X_B)C}{X_S - X_B}$	$\dfrac{2S_B C}{X_S - X_B}$	$\dfrac{3(0.01X_B)C}{X_S - X_B}$	$\dfrac{3S_B C}{X_S - X_B}$	$\dfrac{3S_B C}{X_S - X_B}$
Al	54	110	2	45	3.0	40
Au	8	10	40	31	-	-
Cr	2	5.3	1	7.1	0.3	5
Sc	5	9.4	3	4.6	-	-
Sn	140	440	300	25	4	60
Pb	250	540	8	42	2	30

consumption and analytical performance. The elements used for the determination of the detection limits are listed in Table 8.4. The conditions used for the determinations are listed in Table 8.5. The absorbance values, standard deviations of the background for the ultrasonic nebulizer and for the conventional pneumatic nebulizer are listed in Table 8.6. The comparative detection limits are listed in Table 8.7. The sample consumption results are listed in Table 8.8. For each atomizer, measurements were made to determine the proportion of the sample solution actually reaching the flame. A known volume of solution was atomized for a fixed time. The volume retained was measured and the rest was taken to be the volume consumed in the flame.

Table 8.4

WAVELENGTHS USED FOR AA

Elements	Wavelength(nm)
Au	242.8
Cr	357.9
Mo	313.3
Pb	217.0

Table 8.5

CONDITIONS USED FOR ATOMIC ABSORPTION DETERMINATIONS

Element	Lamp Current	Fuel	Support	Flame Stoichiometr	Spectral Bandpass	Flame Height USN	Pneum
	(mA)				(nm)	(mm)	
Au	4.0	acetylene	air	oxidizing	0.1	11	10
Cr	7.0	acetylene	air	reducing	0.2	14	12
Mo	7.0	acetylene	air	reducing	0.5	12	10
Pb	6.0	acetylene	air	oxidizing	1.0	14	13

Table 8.6

ABSORBANCES WITH ULTRASONIC AND PNEUMATIC NEBULIZERS

Element	Conc	S_B	Abs	Conc	S_B	Abs
	Ultrasonic Nebulizer			Pneumatic Nebulizer		
Au	5 ppm	0.0004	0.125	10 ppm	0.0003	0.120
Cr	5 ppm	0.0003	0.289	5 ppm	0.0003	0.160
Mo	25 ppm	0.0005	0.236	25 ppm	0.0005	0.165
Pb	10 ppm	0.0004	0.280	10 ppm	0.0003	0.136

Table 8.7

COMPARISON OF DETECTION LIMITS FOR AA

Element	Ultrasonic Nebulizer $\dfrac{3S_B C}{X_{Abs}}$	Pneumatic Nebulizer $\dfrac{3S_B C}{X_{Abs}}$
Au	0.048 ppm	0.075 ppm
Cr	0.016 ppm	0.028 ppm
Mo	0.162 ppm	0.227 ppm
Pb	0.043 ppm	0.066 ppm

Table 8.8

EFFICIENCY OF ULTRASONIC AND PNEUMATIC NEBULIZERS

	Nebulizer	
	Ultrasonic	Pneumatic
Total nebulizing time (min)	10	10
Total volume consumed (ml)	6	28
Volume lost (ml)	1.5	25
Volume reaching flame (ml)	4.5	3
Efficiency (%)	75	12

8.2 General Discussion.

The determination of detection limits provided a way of comparing the ultrasonic nebulizer with standard pneumatic nebulizers. The detection limits were of primary interest but it was also instructive to compare the efficiency of the different nebulizers. The influence of the different nebulization methods on the detection limits is quite significant. However, it is difficult to pinpoint the reasons for the differences. It is usually a conglomerate of parameters that causes the difference between nebulization systems. The influence of desolvation on the detection limits is the most significant. (Table 8.3.2) The detection limits obtained for the ultrasonic nebulization without desolvation are superior by a factor of 5 to 10. This corresponds with the results listed in the literature.[1,12,22,45,64,110,132] The detection limits obtained for ultrasonic nebulization with desolvation are even better. The data clearly shows that the ultrasonic nebulizer provides sensitivities superior to those obtained with the pneumatic nebulizers for the ICP, either with or without desolvation. The superior sample delivery rate of the ultrasonic nebulizer is primarily responsible for the improved sensitivity that was achieved. Berman et.al.[12] reported that the detection limits attainable with ultrasonic nebulizers without desolvation are not significantly better than can be achieved by pneumatic nebulization. This is contradicted by the results listed in Table 8.3.2. Olson et.al.[113] commented on the possible cooling of the plasma by the large amount of aerosol introduced into the plasma. Berman et.al [12] thought that this might be the reason why they did not get a significant improvement in the detection limits without desolvation. It is clear from the results in listed Table 8.3.2 that the detection limits obtained with desolvation are superior. However without desolvation the detection limits are still superior by a factor 5 to 10. It is clear that the large amount of aerosol does play a part in the excitation mechanism, but it is the smaller droplets which give rise to the better detection limits. The smaller and more uniform particle sizes produced by the ultrasonic nebulizer greatly enhances signals and reduces interferences.[10,30,81,122,127,149] The smaller particles increase the efficiency of vaporization of the particles in the flame or plasma.[10] The smaller particles also increase the efficiency of atomization.

The aerosol characterization is very helpful and important in the understanding of the

results obtained.   The narrow size distribution from the ultrasonic nebulizer corresponds to a high signal-to-noise ratio.[115] This is reflected in Table 8.3.1.

A further contribution to the superior sensitivity is the independent carrier gas flow rate. This means that the residence time of the analyte in the plasma and flame is controllable, which is not possible with the pneumatic nebulizers. The input power to the crystal of the ultrasonic nebulizer is a second variable which can control the amount of aerosol reaching the flame or plasma. The larger amount of aerosol can thus be reduced by decrease in power. The influence of the aerosol with and without desolvation on the excitation mechanism of the plasma were discussed in Chapter 6.

The detection limits obtained with the ultrasonic and conventional pneumatic nebulizers for the AA did not show a significant difference. The absorbances for the ultrasonic nebulizer are superior but the statistics are poorer. (Table 8.6) This can be attributed to the more uniform feed of the pneumatic nebulizer to the burner. The ultrasonic nebulizer tends to produce a pulsating stream and this has a more significant influence on the AA than on the ICP. There was a small difference in the amount of sample reaching the flame. (Table 8.8) The better absorbances are attributed to better aerosol characteristics, i.e. smaller droplets. With a fixed rate of aerosol production and an independent carrier gas the solution delivery is more per unit volume of flame gas.[44] From Table 8.8 we can see that the optimum aspiration rate for the ultrasonic nebulizer is 0.6 ml/min with an efficiency of 75%. This means that the best rate of sample supply to the burner, i.e. the amount of sample reaching the flame , is equivalent to approximately 0.45 ml/min. The amount of sample reaching the flame with the pneumatic nebulizer is calculated at 0.3 ml/min. Issaq et.al.[82] reported an aspiration rate of 0.75 ml/min and an efficiency of 86% for the ultrasonic nebulizer they used in Atomic Absorption.. This means that the amount of sample reaching the flame is equal to 0.65 ml/min. Hoare et.al.[75] reported an efficiency of 75% and 15% for the ultrasonic and pneumatic nebulizers respectively. The volumes reaching the flame are reported as 0.41 ml/min and 0.6 ml/min respectively. This is in contradiction with the results in Table 8.8 and the results reported by Issaq et.al.[82] With an increase in the flow rate, both the sensitivity and the stability deteriorate. The sensitivity is decreased as a result of a loss in aerosol density and the stability is poorer because the pulsating action is carried over into the flame as the nebulization

rate is no longer buffered within the chamber.

8.3 Conlusion

The detection limit is an analytical figure of merit which is valid for a given analytical procedure, a given operator, and a given time interval. The factors that influence the detection limit include:

1. Transport rate
2. The efficiency of nebulization and desolvation
3. The efficiency of atomization of particles in flame or plasma
4. Particle sizes
5. Gas flow rate
6. Desolvation temperature
7. Height in plasma or flame
8. The amount of solvent present

CHAPTER 9

9. _THE APPLICATION OF THE ULTRASONIC NEBULIZER FOR THE DETERMINATION OF RARE EARTH ELEMENTS_

The determination of rare earth elements (REE) by inductively coupled plasma is widely reported in the literature.[5,17,25,32,38,50,108,121] The rare earth group is made up of 17 elements, as shown in Table 9.1.

TABLE 9.1
RARE EARTH ELEMENTS

Element	Z	Valency
Scandium	21	3+
Yttrium	39	3+
Lanthanum	57	3+
Cerium	58	3+, 4+
Praeseodymium	59	3+, 4+
Neodymium	60	3+
Promethium	61	3+
Samarium	62	2+, 3+
Europium	63	2+, 3+
Gadolinium	64	3+
Terbium	65	3+, 4+
Dysprosium	66	3+
Holmium	67	3+
Erbium	68	3+
Thulium	69	3+
Ytterbium	70	2+, 3+
Lutetium	71	3+

An increasing demand exists on the part of geologists for the determination of REE

in geological materials at relative low concentrations (chondrite levels) suitable for studies of petrogenesis. REE geochemistry is of fundamental importance to modern petrological studies on the origin of igneous, metamorphic and sedimentary rocks. The understanding of the processes by which rocks have been formed has greatly improved in many instances by a knowledge of the REE geochemistry. The accurate and precise measurement of the concentrations of these elements in a wide diversity of rock types has formed the basis for many research efforts by geochemists in recent years.

The usefulness of the REE derives from the close similarities in their chemical properties and the gradual changes in ionic ratio for the trivalent cations in octahedral coordination. There is a progressive decrease in radius from 1.03 A for La to 0,861 A for Lu. This leads to a preferential uptake by some minerals for heavy rare earths relative to the light rare earths, or vice versa. Garnet and Zircon are examples as they are enriched in the heavy rare earths. There is also the special feature of Eu geochemistry. It is the ability of Eu to exist in the divalent as well as the more common trivalent state. When Eu is present as a divalent ion it can readily substitute for Ca in feldspar resulting in anomalous Eu contents relative to the other rare earths.

The analytical requirements for the determination of the REE presents serious difficulties because of the low working detection limits needed. Concentration levels in samples can be compared to the chondrite levels i.e. La (0.33 $\mu g.g^{-1}$), Ce (0.865 $\mu g.g^{-1}$) etc. The chondritic abundance is taken as the abundance found in chondritic meteorites. The abundance is nearly constant and can be taken as the lowest level normally encountered in terrestrial rocks. The values obtained for each element in a sample is plotted as a ratio with the chondritic values so that any anomalies can be seen. The degree of fractionation can be estimated by the slope of plots of the elements against sample concentration divided by the chondritic abundances.

Before the ICP was introduced, most of the REE analysis were determined by neutron activation or isotope dilution - mass spectrometry. The ICP-AES came as a valuable alternative to these techniques. The availability of rapid and reliable methods is of great importance and benefit in geochemistry. The ion lines are normally used for

analysis with the ICP. The spectra of the 15 elements are very complex and the differences in their intensities are small. Moreover, major analytical lines of the REE exists in the CN band region. Although there are many lines to choose from, several of them are useless due to spectral overlap. Since the spectra of the 15 elements are very complex, spectrometers having a high degree of dispersion and high resolution are required.

Three geological samples were chosen for REE analysis. The samples came from the Coretsi Mine north of Kuruman. The three samples were riebeckite (31RIB), crocidolite (31K1B) and stilpnomelane (31CW1B). Detection limits were also determined for the REE and are listed in Table 9.2. The statistics were also calculated and shown in Table 9.3. The results obtained with the ultrasonic nebulizer were compared to the results obtained with a cross flow nebulizer. The concentrations obtained for the three samples are listed in Table 9.4.

9.1 *Sample Preparation*

The complexities of the REE emission lines, the very low levels at which the elements are sought and the potential interferences from the major elements, have led to the use of separation methods to remove the bulk of the major elements and at the same time to concentrate the REE's from the rock sample into a small volume of solution. The method used uses a digestion and a bomb step for the dissolution and an ion exchange chromatography for the separation of the REE.

9.1.1 *Sample Dissolution*

The dissolution is achieved in three steps;[133]

(a) an HF digestion in which Si is fumed off as volatile SiF_4,

(b) a bomb step in which resistant minerals such as zircon and garnet are dissolved,

Table 9.2

DETECTION LIMITS DETERMINED FOR THE 50 MHZ ICP (ng/ml)

Elements	Ultrasonic Neb. $\dfrac{3S_BC}{X_{S+B}-X_B}$	Cross Flow Neb $\dfrac{3S_BC}{X_{S+B}-X_B}$	Ultrasonic Neb[55] $\dfrac{3S_BC}{X_{S+B}-X_B}$
La	2.9	28	3
Ce	19	92	7
Pr	5	24	-
Nd	6	38	-
Sm	2	9	-
Eu	0.4	0.9	-
Gd	4	20	-
Dy	1.7	15	-
Ho	1.6	17	-
Er	59	180	-
Yb	0.9	16	-
Lu	3	90	-
Ba	40	260	0.1
Sc	1.5	2	-
Th	5	4	3
Ca	70	1900	-

Table 9.3

THE GENERAL STATISTICS FOR THE 50 MHZ ICP

	Ultrasonic nebulizer				Cross Flow Nebulizer			
	Background		Net Signal		Background		Net Signal	
Element	Mean	%S	Mean	S/B	Mean	%S	Mean	S/B
La	30	1.3	19142	638	36	0.2	3027	84
Ce	56	1.1	11794	211	60	0.9	2043	34
Pr	277	0.9	47076	170	358	0.5	6872	19
Nd	107	1.4	24901	233	136	0.9	3588	26
Sm	212	0.7	135100	637	254	0.6	17018	67
Eu	204	1.4	284740	1396	250	0.7	24463	98
Gd	121	0.7	42772	353	136	1.0	6931	51
Dy	103	1.6	38169	371	147	0.7	5282	36
Ho	117	1.5	42244	361	147	1.0	5970	41
Er	103	1.4	40290	391	120	1.1	5958	50
Yb	33	1.6	65430	1983	38	1.9	11209	295
Lu	170	0.7	10514	62	201	0.5	2104	10
Ba	122	0.8	16640	136	131	1.0	3401	26
Sc	114	0.9	39031	342	116	0.6	6987	60
Th	100	1.2	31973	320	124	1.2	4411	36
Ca	173	0.5	3066	18	52	1.5	692	13

TABLE 9.4

CONCENTRATIONS FOR THE REE ELEMENTS (μg/ml)

Elements	31R1B	31K1B	31CW1B
La	16.78	2.02	17.89
Ce	48.26	11.77	44.40
Pr	5.58	1.54	4.18
Nd	11.63	1.44	9.36
Sm	0.73	0.47	1.73
Eu	0.34	0.09	0.53
Gd	2.25	0.77	2.09
Dy	1.34	0.35	1.50
Ho	0.36	0.14	0.34
Er	3.02	0.93	1.41
Yb	0.64	0.46	0.78
Lu	0.9	0.5	0.53
Ba	161.81	109.65	246.14
Sc	1.38	0.28	3.06
Ca	1049.56	981.87	1034.11

(c) Dissolution in HCL which dissolves insoluble fluorides produced in the bomb step, and enables the use of glass vessels. Batches of six samples are processed together with a standard on a blank. The solutions are loaded on the chromatography columns, the major are eluted with 1.7 N HCL. The REE, Sc, Y and Ba as well as most of the Sr, Zr, Hf and Th are then eluted with 4 N HCL. The flow rate of the columns is about 140 ml/h.

9.2 *Instrumentation*

The instrumental arrangement used for this study is the same as illutrated in figure 4.4. No desolvation was used. The rest of the instrumentation is described in Chapter 4.

9.3 *Results and Discussion*

The influence of the different nebulization methods on the detection limits is again quite significant. The statistics in Table 9.3 clearly show the superior sensitivity of the ultrasonic nebulizer. The detection limits were determined without desolvation but still were a factor 5 to 10 better than the commercial cross flow nebulizer (Table 9.2). As noted earlier (Chapter 8) this could still be improved using desolvation. The possible reasons for this improvement were discussed in paragraph 8.2.

The concentration values are listed in Table 9.4 levels are very low. Using the equation for the limit of identification as discussed in Appendix 3, namely six times the standard deviation, for the determination of the detection limit the need for better sensitivity is clear. Take for instance Nd (1.44 ppm) in sample 31K1B as an example. With the cross flow nebulizer a detection limit of 1.17 ppm is attained, which is very close to the actual concentration level in the sample. While with the ultrasonic nebulizer the concentration is still a factor 10 above the detection limit. The ultrasonic nebulizer is therefore very suited for low concentration levels such as encountered with the REE.

CHAPTER 10

10. GENERAL CONCLUSION AND RECOMMENDATIONS

Many promising results were obtained in this project. The ultrasonic nebulizer undoubtedly proved to be superior to the commercial pneumatic nebulizers. It yielded much lower detection limits which is of great importance to certain geological investigations which are hampered by the low concentration levels of the elements being monitored.

Different aspects of the batch type ultrasonic nebulizer was thoroughly investigated. A great deal of time was spent on the design of the ultrasonic nebulizer chamber to ensure a constant sample vapour transport to the ICP. Different designs were evaluated by applying the Simplex optimization technique to the statistics and signal to background ratios obtained from the emission output.

Since the volume of sample introduced into the plasma was much more than in the case of pneumatic nebulizers, like the cross flow and Meinhard nebulizers, the plasma was cooled down, especially at lower heights above the load coil. This could lead to possible chemical and physical interferences, which are more probable at lower temperatures. To reduce this problem a desolvation system, consisting of a heated chamber and condenser, was installed between the nebulizer and the ICP. This system proved to be a vital part of this project, since it was possible to control firstly the droplet size, thereby assisting the desolvation process in the plasma and secondly the amount of water vapour, and subsequently the amount of hydrogen, which seemed to be a basic element. It was verified by means of atomic absorption measurements that the decrease in emission of an analyte element at very high desolvation temperatures ($>150^{\circ}$C) was not due to loss of the sample in the desolvation process but rather to a change in the energy transfer and excitation processes in the plasma. It was concluded that in the case of the current system, if one works at about 15 mm above the load coil in the analytical zone, the optimum desolvation temperature in the heated chamber should be about $150\,^{\circ}$C.

Pre-desolvation of the sample vapour also affected the plasma temperature and

electron density at the analytical observation height as can be expected. Interestingly the plasma temperature and electron density both show maxima when a pre-desolvation temperature of 150 $^{\circ}$C was used.

The ultrasonic nebulizer ICP system was applied to both metallurgical and geological samples. The detection limits were determined for six elements in metallurgical samples supplied by MINTEK. Even with no desolvation applied the detection limits were a factor 5 to 10 better than those obtained with the commercial cross flow nebulizer. The narrow size distribution of the small droplets produced by the desolvating ultrasonic nebulizer yielded far better signal-to-background ratios than the cross flow (a factor 10 - 25) and the Meinhardt (a factor 14 - 65). Also with the determination of 16 rare earth elements in geological samples the ultrasonic nebulizer without desolvation was superior to the cross flow nebulizer with respect to detection limits by factors ranging between 5 and 10. When the ultrasonic nebulizer without desolvation was attached to the atomic absorption spectrophotometer the detection limits were only slightly better (a factor of about 1,5).

A major drawback for the nebulizer if it is to be used in routine service analysis is the problem of slow sample changeover. Certain modifications did however partially solve the problem. The addition of the peristaltic pump system made the sample changeover a lot easier and faster as compared to the system when it is strictly used as a batch type nebulizer. The modifications made to the apparatus were similar to those on the ultrasonic nebulizer that recently became commercially available. It is therefore felt that with further modifications, the system can be used in routine analysis.

Finally it is recommended that the ultrasonic nebulizer should definitely be used where problems with low concentration level samples are encountered. The modified nebulizer can serve as a starting point on which further improvements should be made and assessed. Further investigations with the ultrasonic nebulizer can also include studies on the influence of different solvents with different viscosities, and even slurries.

REFERENCES

1. Abercrombie, F., "*ICP Newsletter*", *Vol.3, No.11, pp.458, 1978.*

2. Algeo, J.D. and Denton, M.B.: "On the Use of the Inverted Abel Integral for Evaluating Spectroscopic Sources." *Applied Spectroscopy, Vol. 35, No. 1, pp. 35 - 42, 1981.*

3. Alder, J.F., Bombelka, R.M., and Kirkbright, G.F., "Electronic excitation and ionization temperature measurements in a high frequency inductively coupled argon plasma source and the influence of water vapour on plasma parameters". *Spectrochimica Acta, Vol. 35B, pp. 163 - 175.*

4. Alkemade, C.Th.J. and Herrmann, R. *Fundamentals of Analytical Flame Spectroscopy. Adam Hilger LTD, Bristol. pp. 20-24, 1979*

5. Aulis, R., Bolton, A., Doherty, W., v.d. Voet, A and Wong, P.: "Determination of Yttrium and selected REE in geological materials using high performance liquid chromatographic separation and ICP spectrometric detection". *Spectrochimica Acta, Vol. 40B, No's 1/2 pp. 377 - 387, 1985.*

6. Baginski, B.R., and Meinhard, J.E.: "Some effects of High-Solids Matrices on the Sample Delivery system and the Meinhard Concentric Nebulizer During ICP Emission Analyses." *Applied Spectroscopy, Vol. 38, No. 4, pp. 568 - 572, 1984.*

7. Barnes, R.M., Fernando, L., Jing, Lu S., and Mahanti, H.S.: "Analysis of Aluminium by Inductively Coupled Plasma-Atomic Emission Spectroscopy". *Applied Spectroscopy, Vol. 37, No. 4, pp. 389 - 395, 1983.*

8. Barnes, R.M.: "Progress in Inductively Coupled Plasma Analytical Spectroscopy". *Journal of Testing and Evaluation, Vol. 12, No. 4, pp. 194 - 202, 1984.*

9. Barnes, R.M.: ICP - AES: A Review. *Trends in Analytical Chem.*, *Vol. 1, No. 2, pp. 51 - 55, 1981.*

10. Bastiaanse, G.J., and Hieftje, G.M.: "Investigation into the Vaporization of Individual Solute Particles in Flame Spectrometry". *Anal Chem.*, *Vol.46, No.7, pp. 901 - 910, 1974.*

11. Belchamber, R.M., Betteridge, D., Wade, A.P., Cruickshank, A.J. and Davidson, P.: "Removal of a matrix effect in ICP-AES multi-element analysis by simplex optimization." *Spectrochimica Acta, Vol.41B, No. 5,pp. 503 - 505, 1986.*

12. Berman, S.S., McLaren, J.W., and Willie, S.N.: "Simultaneous Determination of Five Trace Metals in Seawater by Inductively Coupled Plasma Atomic Emission Spectrometry with Ultrasonic Nebulization." *Anal Chem.*, *Vol.50, pp. 488 - 492, 1980.*

13. Blades, M.W. and Horlick, Gary.:" Photodiode Array Measurement System for Implementing Abel Inversions on Emission from an ICP." *Applied Spectroscopy, Vol. 34, No. 6, pp. 696 - 699.*

14. Blades, M.W. and Caughlin, B.L. " Excitation temperature and electron density in the ICP - aqueous vs organic solvent introduction." *Spectrochimica Acta, Vol. 40B, pp. 579-591, 1985.*

15. Blades, M.W. "Some considerations regarding temperature, electron density, and ionization in the argon - ICP." *Spectrochimica Acta, Vol.37B, No.10, pp. 869 - 879, 1982.*

16. Blades, M.W. and Horlick, G. "The vertical spatial characteristics of analyte emission in the ICP." *Spectrochimica Acta Vol.36B, No.9, pp.861-880.*

17. Bo Hong, A., Hwang, J and Van Der Voet, Anthony "The determination of Scandium, Yttrium and Selected Rare Earth Elements in Geological materials by ICP-OES.", *Spectrochimica Acta, Vol. 38B, Nos. 1/2, pp. 165 - 174, 1983.*

18. Boumans, P.W.J.M., and De Boer, F.J.: "Studies of flame and plasma torch emission for simultaneous multi-element analysis - I." *Spectrochimica Acta, Vol.27B, pp. 391 - 414.*

19. Boumans, P.W.J.M., and De Boer, F.J.: "Studies of a radio frequency inductively coupled argon plasma for optical emission spectrometry. III Interference effects under compromise conditions for simultaneous multi-element analysis." *Spectrochimica Acta. Vol.31B, pp. 355 - 375.*

20. Boumans, P.W.J.M., and De Boer, F.J.: "Studies of an inductively- coupled high-frequency argon plasma for optical emission spectrometry II. Compromise conditions for simultaneous multi-element analysis." *Spectrochimica Acta, Vol.30B, pp.309 - 334.*

21. Boumans, P.W.J.M.: "A Look at ICP Detection Limits" *ICP Information Newsletter, Vol.1, No.4, pp.8 - 71, 1975.*

22. Boumans, P.W.J.M.: "Inductively Coupled Plasma-Atomic Emission Spectroscopy: Its present and Future Position in Analytical Chemistry". *Fresenius Z. Anal. Chem., Vol.299, pp.337 - 361, 1979.*

23. Boumans, P.W.J.M., and Lux-Steiner, M.Ch., "Modification and optimization of a 50 MHz inductively coupled argon plasma with special reference to analysis. Organic Solvents". *Spectrochimica Acta, Vol.37B, No.2, pp.97 - 126, 1982.*

24. Boumans, P.W.J.M.: "A tutorial review of some elementary concepts in the statistical evaluation of trace element measurements". *Spectrochimica Acta, Vol. 33B, pp. 625 - 634, 1978.*

25. Broekaert, J.A.C., Leis, F., and Laqua, K.: "Application of an inductively coupled plasma to the emission spectroscopic determination of REE in mineralogical samples." *Spectrochimica Acta, Vol.34B, pp.73 - 84.*

26. Broekaert,J.A.C.: "The application of ICP-OES to industrial analytical problems" *Trends in Analytical Chemistry, Vol.1, No.11, pp.249 - 253, 1982*

27. Broekaert, J.A.C. Ultrasonic Nebulizer (Instruments S.A.): *Instrument Column, Spectrochimica Acta, Vol.41B, No.5, pp. 493-501, 1986*

28. Browner, R.F., Boorn, A.W. and Smith, D.D.: "Aerosol Trnsport Model for Atomic Spectrometry". *Anal. Chem., Vol.54, pp.1411 - 1419, 1982.*

29. Browner, R.F., Novak, J.W., and Dillard, J.H.: "The chemistry of aerosol transport and characterization of droplet sizes". *ICP Information Newsletter, Vol.5, No.3, pp.137 - 138, 1979.*

30. Browner, R.F., and Boorn, A.W.: "Sample Introduction: The Achilles' Heel of Atomic Spectroscopy?" *Anal. Chem., Vol.56, No.7, pp.787A - 798, June 1984.*

31. Browner, R.F., and Boorn, A.W.: "Sample Introduction Techniques for Atomic Spectroscopy". *Anal. Chem., Vol.56, No. 7, pp. 875A - 888A, 1984.*

32. Buchanan, S.J. and Dale, L.S. : "ICP-AES determination of rare earth elements in geological materials." *Spectrochimica Acta, Vol. 41B, pp. 237-242, 1986.*

33. Butler, C.C., Kniseley, R.N., and Fassel, V.A.: "Inductively Coupled Plasma-Optical Emission Spectrometry: Application to the Determination of Alloying and Impurity Elements in Low and High Alloy Steels". *Anal. Chem., Vol. 47, No.6, pp. 825 - 829, May 1975.*

34. Choi, B.S., and Kim, H.: "On Abel Inversions of Emission Data from an Inductively Coupled Plasma". *Applied Spectroscopy, Vol. 36, No. 1, pp. 71 - 74, 1982.*

35. Clampitt, N.C., and Hieftje, G.M.: "Investigation into the Mechanism of Desolvation of Samples Droplets in Flame Spectrometry." *Anal. Chem., Vol.44, No.7, pp.1211 - 1219, June 1972.*

36. Cremers, Clifford.J. and Birkebak, Richard.C.: "Application of the Abel Integral Equation to Spectrographic Data." *Applied Optics, Vol. 5, No. 6, pp.1057 - 1064, 1966.*

37. Cresser, M.S., and Brower, R.F.: "A method for investigating size distributions of aqueous droplets in the range 0,5 - 10 um produced by pneumatic nebulizers." *Spectrochimica Acta, Vol.35B, pp.73 - 79.*

38. Crock, J.G., and Lichte, F.E.: "Determination of Rare Earth Elements in Geological Materials by Inductively Coupled Argon Plasma/Atomic Emission Spectrometry." *Anal. Chem., Vol.54, pp.1329 - 1332, 1982.*

39. Davies, John, Dean, John.R. and Snook, Richard.D. : "Axial view of an inductively coupled plasma." *Analyst, Vol. 110, pp. 535-540, 1985.*

40. Dean, J.A., and Cames, W.J.: "Drop Size of Aerosols in Flame Spectrophotometry" *Anal. Chem., Vol.34, No.2, pp.193 - 194, 1962.*

41. De Galan, L. "Some considerations on the excitation mechanism in the inductively coupled plasma." *Spectrochimica Acta, Vol. 37B, No. 10, pp. 537 - 550, 1984.*

42. Deming, S.N., and Morgan, S.L.: "Simplex Optimization of Variables in Analytical Chemistry". *Anal. Chem., Vol. 45, No.3 pp. 279A - 283A, 1973.*

43. Denton, M.B., and Swartz, D.B.: "An improved ultrasonic nebulizer system for the generation of high density aerosol dispersions." *Rev. Sci. Instrum.*, *Vol.45, No.1, pp.81 - 83, Jan 1974.*

44. Denton, M.B., and Malmstadt, H.V.: "Burner and Ultrasonic Nebulizer Improvements for AAS." *Anal. Chem., Vol.44, No.2, pp.241 - 247, 1972*

45. Denton, M.B., and Malmstadt, H.V.: "Ultrasonic Nebulization in a Low-Emission Flame for Atomic Fluerescence Spectrometry." *Anal. Chem., Vol.44, No.11, pp.1813 - 1818, 1972.*

46. Dickinson, G.W., and Fassel, V.A.: "Emission Spectrometric Detection of the Elements at the Nanogram per milliliter Level Using ICP Excitation." *Anal. Chem., Vol.41, No.8 pp.1021 - 1024, July 1969.*

47. Discussions. *ICP Information Newsletter, Vol.3, No.8, pp.341, 1978.*

48. Dunken, H., Pforr, G., Mikkeleit, W., and Geller, K., "Fremdenergiezer-staubung in der Flammenphotometrie". *Spectrochimica Acta, Vol.22, pp.1531 - 1542, 1963.*

49. Eckert, H.U., and Danielsson, A., "An equilibrium model for the radial intensity distribution of analyte lines in the ICP discharge". *Spectrochimica Acta, Vol.38B, Nos.1/2, pp.15 - 27, 1983.*

50. Edge, R.A., and Trojak, G.: "An assessment of ICP for the determination of trace elements in common Igneous rocks." *Ann. Geol. Surv. S.A., 15, pp.69 - 77, 1981.*

51. Edmonds, T.E., and Horlick, G.: "Spatial Profiles of Emission from an Inductively Coupled Plasma Source Using a Self- scanning Photodiode Array". *Applied Spectroscopy, Vol.31, No.6, pp.536 - 541, 1977.*

52. Elder, Melanie.L. and Winefordner, J.D. "Temperature Measurements in Flames." A Review. *Prog. analyt. atom. Spectrosc. Vol.6, pp. 293-427, 1983.*

53. Farino, J., and Browner, R.F., "Surface Tension Effects on Aerosol Properties in Atomic Spectrometry". *Anal. Chem., Vol.56, pp.2709 - 2714, 1984.*

54. Fassel, V.A., "Current and potential applications of ICP-AES in the exploration, mining, and processing of materials." *Pure & Appl. Chem., Vol.49, pp.1533 - 1545, 1977.*

55. Fassel, V.A., and Kniseley, R.N., "Inductively Coupled Plasma - Optical Emission Spectroscopy". *Anal. Chem., Vol.46, No.13, pp.1110 -1164, Nov.1974.*

56. Fassel, Velmer.A.: "Analytical ICP spectroscopy - past, present and furure." *Fresenius Z Anal. Chem., Vol. 324, pp. 511-518, 1986.*

57. Freeman, Mark.P. and Katz, S.: "Determination of a Radiance-Coefficient Profile from the Observed Asymmetric Radiance Distribution of an Optically Thin Radiating Medium." *Journal of the Optical Soc. of Am., Vol. 53, No. 10, pp. 1172 - 1179, 1963.*

58. "Fundamentals of Quartz Oscillators":*Hewlett Packard: Application note 200 -2*

59. Furuta, Naoki : "Spatial profile measurement of ionization and excitation temperatures in an inductively coupled plasma." *Spectrochimica Acta, Vol. 40B, No.8, pp. 1013 - 1022, 1985.*

60. Furuta, N., Nojiri, Y. and Fuwa, K. : "Spatial profile measurement of electron number densities and analyte line intensities in an ICP." *Spectrochimica Acta, Vol. 40B, pp. 423 - 434, 1985.*

61. Furuta, N. and Horlick, G. "Spatial characterization of analyte emission and excitation temperature in an ICP plasma." *Spectrochimica Acta Vol 37B, No.1, pp.53, 1982.*

62. Garbarino, J.R., and Taylor, H.E.: "A Babington-type Nebulizer for use in the analysis of Natural Water Samples by ICP spectrometry." *Applied Spectroscopy, Vol.34, No.5, pp.584 - 590, 1980.*

63. Goldfarb, V.M. "Non equilibrium effects in plasma discharges for atomic emmision spectroscopy." *Developments in atomic plasma spectrochemical analysis. Editor. R.M.Barnes, Heyden & Son Ltd, 1981.*

64. Goulden, P.D., and Anthony, D.H.J.: "Modified Ultrasonic Nebulizer for Inductively Coupled Argon Plasma Atomic Emission Spectrometry." *Anal. Chem.,Vol.56, pp.2327 - 2329, 1984.*

65. Greenfield, S., McGeachin, H. McD., and Smith, P.B.: "Plasma Emission Sources in Analytical Spectroscopy - III" *Talanta, Vol.23, pp.1 -14, 1976.*

66. Griem, Hans R. *Plasma Spectroscopy, McGraw Hill Book Company, pp. 297-315, 1964.*

67. Gruetzmacher J., "Piezoelektrischer Kristall mit Ultraschallkonvergenz". *Zeitschrift für Physik, pp.342 - 349, 1935*

68. Gunter, W.H. "'N Ondersoek na Temperatuur en Ionisasie Interferensies in 'n 10 MHz Induktiefgekoppelde Plasmabron." *MSc - Thesis, Universiteit Stellenbosch, 1980.*

69. Gunter, W.H., Visser, K and Zeeman, P.B. "Radial excitation temperatures and electron number densities in a 9, 27 and 50 MHz ICP argon plasma." *Spectrochimica Acta , Vol.38B, No.5/6, pp.949-958.*

70. Gunter, W.H. "Discharge Characteristics of Atmospheric Pressure ICP's operating at 9, 27 and 50 MHz."*PhD-Thesis, University of Stellenbosch, 1984.*

71. Gustavsson, A.: "Some Aspects on Nebulizer characteristics I". *ICP Information Newsletter, Vol.5, No.6, pp.312 - 328, 1979.*

72. "Guidelines for Data Acquisition and Data Quality Evaluation in Environmental Chemistry," *Anal. Chem., Vol. 52, pp. 2242, 1980.*

73. Ham, N.S., and Willis, J.B., "Atomization prboems in atomic absorption spectroscopy IV. Impact devices, spray chambers and interferences". *Spectrochimica Acta, Vol.40B, Nos.10 - 12, pp.1607 - 1629, 1985.*

74. Hieftje, G.M., and Malmstadt, H.V.: "A New Approach to Flame Spectrometric Analysis Utilizing Isolated Droplets of Sample Solution." *Anal. Chem., Vol.41, No.13, pp.1735 - 1744, 1969*

75. Hoare, H.C., Mostyn, R.A., and Newland, B.T.N.: "An ultrasonic atomiser applied to AAS." *Analytica Chem. Acta., Vol.40, pp.181 - 186, 1968.*

76. Horvath, F.J., Bradshaw, J.D., and Winefordner, J.D.: "Comparison of Nebulization-Spray Chamber Arrangements for Atomic Fluorescence and Atomic Emission Flame Spectrometry." *Applied Spectroscopy, Vol.35, No.2, p.149, 1981.*

77. Horvath, J.J., Bradshaw, J.D., Bower, J.N., Epstein, M.S., and Winefordner, J.D.: "Comparison of Nebulizer-Burner Systems for Laser-Excited Atomic Fluorescence Flame Spectrometry." *Anal. Chem.,Vol.53, pp.6 - 9, 1981.*

78. Houk, R., Svec, H.J., and Fassel, V.A., "Mass Spectrometric Evidence for Suprathermal Ionization in an Inductively Coupled Argon Plasma". *Applied Spectroscopy, Vol.35, No.4, pp.380 - 384, 1981.*

79. Houre, H.C., and Mostyn, R.A.: "Emission Spectrometry of Solutions and Powders with a high-frequency Plasma Source." *Anal. Chem., Vol.39, pp.1153 - 1155, 1967.*

80. "International Union of Pure and Applied Chemistry : Nomenclature, symbols, units and their usage in spectrochemical analysis-II. Data Interpretation." *Spectrochimica Acta, Vol. 33, pp.241 - 245, 1978.*

81. Issaq, H.J. and Morgenthaler, L.P.: "Utilization of Ultrasonic Nebulization in AAS A Study of Parameters." *Anal. Chem., Vol.47, No.9, pp.1661 - 1669, Aug 1975.*

82. Issaq, H.J., and Morgenthaler, L.P.: "Utilization of Ultrasonic Nebulization in AAS Trace Metal Analysis in Samples of High Salt Content." *Anal. Chem., Vol.47, No.11, pp.1748 - 1752, Sept. 1975.*

83. Jarosz, Jean., Mermet, Jean Michel. and Robin, Jaques. P. " A spectrometric study of a 40 MHz ICP - III.Temperatures and electron number density." *Spectrochimica Acta, Vol.33B, pp. 55 - 78, 1978.*

84. Kalnicky, D.J., Fassel, V.A. and Kniseley, R.N. " Excitation Temperatures and Electron Number Densities Experienced by Analyte Species in ICP with and without the Presence of an Easily Ionized Element." *Applied Spectroscopy, Vol.31, pp. 137 - 149, 1977.*

85. Kawaguchi, H., Ito, T., Ota, K., and MiZuike, A. "Effects of matrix on spatial profiles of emission from an ICP." *Spectrochimica Acta, Vol.35B, pp.199 - 206, 1980.*

86. Kirkbright, G.F. : "Dry aerosol analyte presentation and excitation mechanisms in the ICP." *Developments in atomic plasma spectroscopy analysis, Editor: Ramon M. Barnes pp. 223-238, 1980.*

87. Kristen, W.J., and Bertilsson, G.O.B.: "Direct Continuous Quantitative Ultrasonic Nebulizer for Flame Photometry and Flame Absorption Speltophotometry". *Anal. Chem., Vol.38, pp.647 - 649, 1966.*

88. La Freniere, K.E., Rice, G.W. and Fassel, V.A.: "Flow injection analysis with ICP-AES: critical comparison of conventional pneumatic, ultrasonic and direct injection nebulization. *Spectrochimica Acta Vol.40B, Nos.10/12, pp.1495 - 1504.*

89. Lang, R.J., *Acoust, J. Soc. Am., Vol.34, p.6, 1962.*

90. Larson, G.F., Fassel, V.A., Winge, R.K., and Kniseley, R.N.: "Ultratrace Analyses by Optical Emission Spectroscopy: The Stray Light problem" *Applied Spectroscopy, Vol.30, No.4, pp.384 - 391, 1976.*

91. Larson, G.F., and Fassel, V.A.: "Comparison of Interelement. Effects in a Microwave Single Electrode Plasma and in a Radiofrequency Inductively Coupled Plasma". *Anal. Chem., Vol.48, No.8, pp.1161 - 1166, July 1976.*

92. Lobdell, D.D.: "Particle Size. Amplitude Relations for the Ultrasonic Atomizer." *Journ. of the Acous. Soc. of Am. Vol.43, No.2, pp.229 - 231, 1968.*

93. Long, Gary L, and Winefordner, J.D.: "Limit of Detection". A closer look at the IUPAC Definition". *Report, pp. 712 - 724, June 1983.*

94. Long, Stephen.E. and Browner, Richard.F.:"Influence of water on the spatial excitation behaviour of selected elements in the ICP."*Spectrochimica Acta Vol. 41B, No.7, pp.639-649, 1986*

95. Maessen, F.J.M.J., Coevert, P., and Balke, J.: "Comparison of Pneumatic Nebulizers in Current Use for ICP-AES". *Anal. Chem., Vol.56, pp. 899 - 903, 1984.*

96. Maessen, F.J.M.J., Kreuning, G. and Balke, J. :"Experimental control of the solvent load of inductively coupled argon plasmas and the effects of the chloroform plasma load on their analytical performance." *Spectrochimica Acta, Vol. 41B, Nos. 1/2, pp. 3 - 25, 1986.*

97. Mandelshtam, S.L. : "Some problems of the emission spectral analysis theory." *Spectrochimica Acta, Vol. 33B, pp. 577-590, 1978.*

98. Magyar, B., Lienemann, P and Vonmont, H.: "Some effects of aerosol drying and oxygen feeding on the analytical performance of an ICP nitrogen-argon plasma. *Spectrochimica Acta, Vol.41, Nos.1/2, pp.27 - 38, 1986.*

99. Mermet, J.M., and Robin, J.P.: "Ultrsonic Nebulizers for Easily Changing Sample Solutions". *Anal. Chem.,Vol.40, No.12, pp.1918 - 1920, Oct.1968.*

100. Mermet, J.M.: "Instrumentation - Sample Introduction and Plasma Torch". *ICP Information Newsletter, Vol.4, No.3, pp.89 - 127, 1978.*

101. Mermet, J.M, quoted in Gunter, W.H "Discharge Characterization of Atmospheric Pressure ICP's operating at 9, 27 and 50 Mhz.", *PhD Thesis, University of Stellenbosch, 1984.*

102. Michaud-Poussel, E and Mermet, J.M.: "Comparison of nebulizers working below 0,81 1/min in ICP-AES." *Spectrochimica Acta, Vol.41B, Nos.1/2, pp.4961, 1968.*

103. Moore, G.L., Humphries-Cuff, P.J., and Watson, A.E.: "Simplex optimization of a nitrogen-cooled argon ICP for multi-element analysis." *Spectrochimica Acta, Vol.39B, No.7, pp.915 - 929, 1984.*

104. Montaser, A., Fassel, V.A.: "Electron Number Density Measurements in Ar and $Ar-N_2$ Inductively Coupled Plasmas". *Applied Spectroscopy, Vol.36, No. 6, pp. 613 - 617, 1982.*

105. Muller, C "Die aanwending van 'n plasmabron vir die ontleding van poeiermonsters." *MSc.Tesis, Universiteit van Stellenbosch, 1985.*

106. Nelder, J.A and Mead, R in Deming, Stanley.N and Morgan, Stephen.L, "Simplex Optimization of Variables in Analytical Chemistry.", *Anal. Chem., Vol. 45, No. 3, pp. 279A - 283A, 1973.*

107. Nicol, R., and Smith, P., "The Simplex method as a laboratory analysis tool". *Laboratory Practice, Vol.34, No.10, pp.102 - 104,* October 1985.

108. Nikdel, S., Massoumi, A., and Winefordner, J.D.: "Detection Limits of Rare Earths by Inductively Coupled Plasma Atomic Emission Spectroscopy". *Microchemical Journal, Vol.24, pp.1 - 7, 1979.*

109. Novak, J.W., (Jr), and Browner, R.F.: "Characterization of Sprays Produced by Pneumatic Nebulizers". *Anal. Chem., Vol.52, pp.792 - 796, 1980.*

110. Novak, J.W., Lillie, D.E., Boom, A.W., and Browner, R.F.: "Fixed crossflow. Nebulizer for use with ICP and flames". *Anal. Chem., Vol.52, pp.576-579, 1980.*

111. Nukiyama, S and Tanasawa, Y. in Stupar, J. and Dawson, J.B, "Theoretical and Experimental Aspects of the Production of Aerosols for use in AAS." *Applied Optics, Vol. 7, No. 7, pp. 1351 - 1358, 1968.*

112. Ohls, K.: "ICP Emission Spectrometry - Nebulizer Considerations". *ICP Information Newsletter, Vol.2, No.12, pp.357 - 365, 1977.*

113. Olson, K.W., Haas, W.J., and Fassel, V.A.: "Multielement Detection Limits and Sample Nebulization Efficiencies of an Improved Ultrasonic Nebulizer and a conventional Pneumatic Nebulizer in ICP - AES". *Anal. Chem., Vol.49, No.4, pp.632 - 637,* April 1977.

114. Olsen, S.D., and Böhmer, R.G.: "The Inductively Coupled Plasma as Spectroscopic Source". *Analytica 1984 as supplement to Chem. S.A.*, *pp. 913, 1984.*

115. Olsen, S.D., and Strasheim, J.X.,: Correlation of the Analytical Signal to the characterized nebulizer spray. *Spectrochimica Acta, Vol.38B, No.516, pp.973-975, 1983.*

116. Prost, Michel M. "Critical mathematical considerations involving the Abel integral equation for converting side-on experimental data in plasma spectroscopy I. A study of basic analytical solutions." *Spectrochimica Acta, Vol. 37B, No.7, pp.541 - 570, 1982.*

117. Robin, J.P.:"ICP-AES at the beginning of the eighties."*Prog. Analyt. Atom. Spectrosc., Vol.5, pp.79-110, 1982*

118. Robin, J.: "Letters to Editor". *ICP Information Newsletter, Vol.3, No.6, pp.249 - 250, 1977.*

119. Robin, J.P.:"ICP-AES at the beginning of the eighties."*Prog. Analyt. Atom. Spectrosc., Vol.5, pp.79-110, 1982*

120. Routh, M.W.: Characterization of ICP nebulizer aerosols using near-forward angle Fraunhofer diffraction. *Spectrochimica Acta, Vol.41B, Nos.1/2, pp.39 - 48, 1986.*

121. Sato, Shoji. "ICP-AES of Rare Earth Elements." *ICP Information Newsletter, Vol. 8, No. 3, p.143, 1982.*

122. Skogerboe, R.K., and Olson, K.W.: "Aerosols, Aerodynamics, and Atomic Analysis". *Applied Spectroscopy, Vol.32, No.2, pp.181 - 186, 1978.*

123. Smith, D.D. and Browner, R.F.: "Measurement of Aerosol Transport Efficiency in Atomic Spectrometry". *Anal. Chem., Vol.54, pp.533 - 537, 1982.*

124. Smith, D.D., and Browner, R.F.: "Influence of Aerosol Drop Size on Signals and Interferences in Flame Atomic Absorption Spectrometry". *Anal. Chem., Vol. 56, No. 14, pp. 2702 - 2708, 1984.*

125. Spendley, W., Hext, G.R., and Himsworth, F.R., "Sequential application of simplex designs in optimization and evolutionary operation. *Technometrics, Vol.4, pp.441 - 461, 1962.*

126. Spitz, J and Uny, G. in Issaq,. Haleem. J and Morgenthaler, Lawrence. P, "Utilization of Ultrsonic Nebulization in Atomic Absorption Spectrometry - A Study of Parameters.", *Anal. Chem., Vol. 47, No. 9 pp. 1661 - 1669, 1975.*

127. Stupar, J., and Dawson, J.B.: "Theoretical and Experimental Aspects of the Production of Aerosols for use in AAS". *Applied Optics, Vol.7, pp.1351, July 1968.*

128. Suddendorf, R.F., Gutzler, D.E., Denton, M.B.: "On the utilization of pulse ultrasonic nebulization for analyzing small volumes of solution by flame emission spectrometry". *Spectrochimica Acta, Vol.31B, pp.281 - 287.*

129. Suddendorf, R.F and Boyer, K.W. "Nebulizer for analysis of high salt content samples with ICP-AES, *Anal. Chem., Vol. 50, pp. 1769 - 1771, 1978.*

130. Suddendorf, Ronald F. and Boyer, Kenneth W. "New approaches to sample introduction with the ICP." *Developments in atomic plasma spectroscopy analysis, Editor: Ramon M. Barnes pp.278 - 286, 1986.*

131. Tang, Y.Q., and Trassy, C.: "ICP: The role of water in axial excitation temperatures. *Spectrochimica Acta, Vol.41B, Nos.1/2, pp.143 - 150, 1986.*

132. Taylor, C.E., and Floyd, T.L.: "Inductively Coupled Plasma - Atomic Emission Spectrometric Analysis of Environmental Samples Using Ultrasonic Nebulization". *Applied Spectroscopy, Vol.35, No.4, p.403, 1981.*

133. Thompson, M and Walsh, J.Nicholas "A handbook of Inductively Coupled Plasma Spectrometry." *Blackie & Son Ltd, 1983.*

134. Tourin, Richard.H. *Spectroscopic Gas Temperature Measurement. Elserivier Publishing Company, Amsterdam-London-New York, pp.41-57, 1966*

135. Uchida, H., and Matsui, H., "Desolvation system with ultrasonic nebulizer for plasma jet emission spectroscopy". *Spectroscopy Letters, Vol.11, No.1, pp.1 - 8, 1978.*

136. Van Rensburg, H.C., and Zeeman, P.B.: *Anal. Chim. Acta, Vol.43, p.173,1968.*

137. Veillon, C., and Margoshes, M.: "An evaluation of the induction-coupled, radio-frequency plasma torch for atomic emission and atomic absorption spectrometry". *Spectrochimica Acta, Vol.23B, pp.503 - 512, 1968.*

138. Venghiattis, A.A.: "A Heated Chamber Burner for AAS". *Applied Optics, Vol.7, pp.1313 - 1316.*

139. Wallace, G.F., "A Comparision of the capabilities of atomic absorption and Inductively coupled Plasma Spectroscopy for the Analysis of Metallurgical Samples". *New Analytical Techniques for Trace Constituents of Metallic and Metal - Bearing Ores, ASTM STP 747, Adelina Javier-Son, Ed., America Society for Testing and Materials, pp.55 - 63, 1981.*

140. Walsh, J.N., Buckley, F., and Barker, J.: "The simultaneous determination of the REE in rocks using ICP". *Chemical Geology, Vol.33, pp.141 - 153, 1981.*

141. Watson, A.E., and Humphries-Cuff, P.:   "The direct analysis of solids materials in the form of sluries by the ICP". *Mintek Publication.*

142. Wendt, R.H. and Fassel, V.A.:   "Induction-Coupled Plasma Spectrometric Excitation Source". *Anal. Chem., Vol.37, No.7, pp.920 - 922, June 1965.*

143. West, C.D., and Hume, D.N.:   "Radio frequency Plasma Emission spectrophotometer". *Anal. Chem., Vol.36, No.2, pp.412 - 415, 1964.*

144. West, C.D.:   "Ultrasonic Sprayer for Atomic Emission and Absorption Spectrochemistry". *Anal. Chem., Vol. 40, No. 1, pp. 253 - 254, 1968.*

145. Winefordner, J.D., and Vickers, T.J.:   "Calculation of the Limit of Detectability in Atomic Emission Flame Spectrometry". *Anal. Chem., Vol. 36, No. 10, September 1964.*

146. Winge, R.K., Peterson, V.J., and Fassel, V.A.: "Inductively Coupled Plasma-Atomic Emission Spectroscopy: Prominent Lines". *Applied Spectroscopy, Vol. 33, No. 3, pp. 206 - 219, 1979.*

147. Willis, J.B.: "Atomization problems in atomic absorption spectroscopy I. A study of the operation of a typical nebulizer, spray chamber and burner system." *Spectrochimica Acta, Vol. 23A, pp. 811 - 830, 1967.*

148. Wohlers, C.C.:   "Comparison of Nebulizers for the Inductively Coupled Plasma". *ICP Information Newsletter, Vol.3, No.2, pp.37 - 50, 1977.*

149. Wolcott, J.F. and Sobel, C.B.:   "Fabrication of a Babington-type Nebulizer for ICP sources". *Applied Spectroscopy, Vol.36, No.6, pp.685 - 686, 1982.*

ACKNOWLEDGEMENTS

I wish to express my sincere gratitude to the following persons and institutions for their assistance and contribution towards this project.

The Council for Mineral Technology for the research bursaries granted to me, without which the project would not have materialized.

The University of Stellenbosch for the opportunity for advanced study granted to me.

Doctor D.H. Cornell, my supervizer, and Professor P.E. Walters, my co-supervizer, for their support and encouragement which played a major part in the progress of this project.

Ulrich Deutschländer, Wolfgang Gauernack, Lawrence Ashworth, Bull Botha and the other personnel of the mechanical workshop who assisted in the electrical and mechanical construction of the apparatus used in this study.

Henri Ruta for his contribution through the writing of computer programmes to execute certain tasks.

Trevor Gordon for his assistance during experimentation and many other tasks.

My wife for typing this thesis and for her encouragement.

APPENDIX 1

1. THE SIMPLEX METHOD

A simplex is a geometric figure that is defined by a number of points one greater than the dimensions of the relevant space. The simplex is a triangle in two dimensions, a tetrahedron in three dimensions, etc. for higher dimensions. A visual display of a higher dimensions is difficult. Figure 1 illustrates a two dimensional simplex on a iso-response contour map. The object of the sequential simplex method is to force the simplex 123 in the optimum direction. The response is experimentally measured at each vertex of the simplex. Once the initial simplex has been established, the following rules and steps apply.
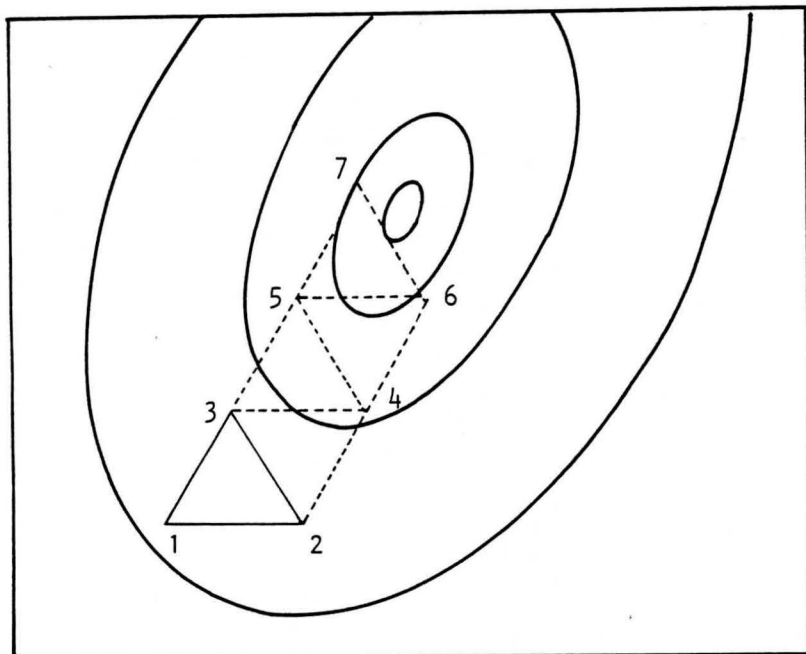

Fig. 1   Progress of two-dimensional simplex towards optimum.

Rule 1:   After each single response measurement, a move is made. The direction of movement is determined as soon as the response is measured.

Rule 2: The simplex moves by rejecting the point of the current simplex that shows the least desirable response. This point is replaced by its mirror image across the hyperface of the remaining points. The movement is illustrated in figure 1

If the vertices of the k-dimensional simplex are represented by the coordinate vectors P_1, P_2, ... P_j, ..., P_{k+1}, where P_j has the worst response, the elimination of the most undesirable response leaves the hyperface P_1, P_2, ... P_{j-1}, P_{j+1}, ... P_{k+1} with centroid C, where

$$P = 1/K \ (P_1 + P_2 + ... P_{j-1} + P_{j+1} + P_k + P_{k+1}) \tag{1}$$

The new simplex is defined by this hyperface, and a new vertex $P_j^\star$ is generated by the reflection of P_j across the hyperface through P:

$$P_j = P + (P - P_j). \tag{2}$$

If the new vertex yields the worst response in the new simplex, the application of Rule 2 would result in an occillation that would become stranded. Hence, Rule 3 is needed.

Rule 3: If the new vertex shows the worst reponse in the new simplex, Rule 2 is ignored and the vertex with the second-worst response is rejected instead. An example of the movement of a simplex on a ridge is illustrated in figure 1.2
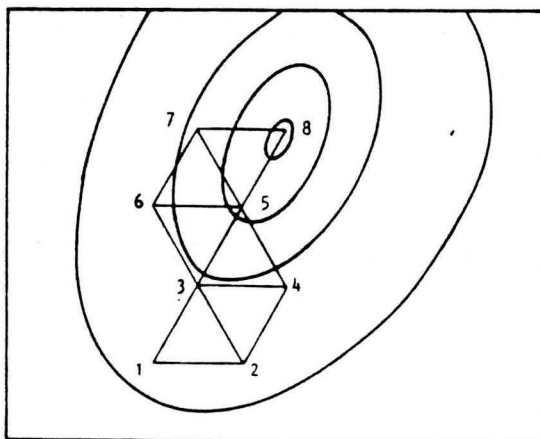

Fig.1.2 Progress of simplex on ridge

In the simplex 356 point 3, instead of point 6, is rejected. To prevent a wrong measurement at one of the vertices and therefore a false high, the next rule is applicable.

Rule 4: If a vertex has not been replaced in k + 1 simplices before applying Rule 2, the response at the persistent vertex must be retested.

Rule 5: If the new vertex lies beyond the boundaries of the variables, the response must not be observed and a very undesirable response must be assigned to that vertex. Application of rules 2 and 3 will then force the simplex back inside its boundaries, and will continue to seek the optimum response. Once an optimum has been found, the rule forces the simplex to circle around the optimum region. (See figure 1.3)
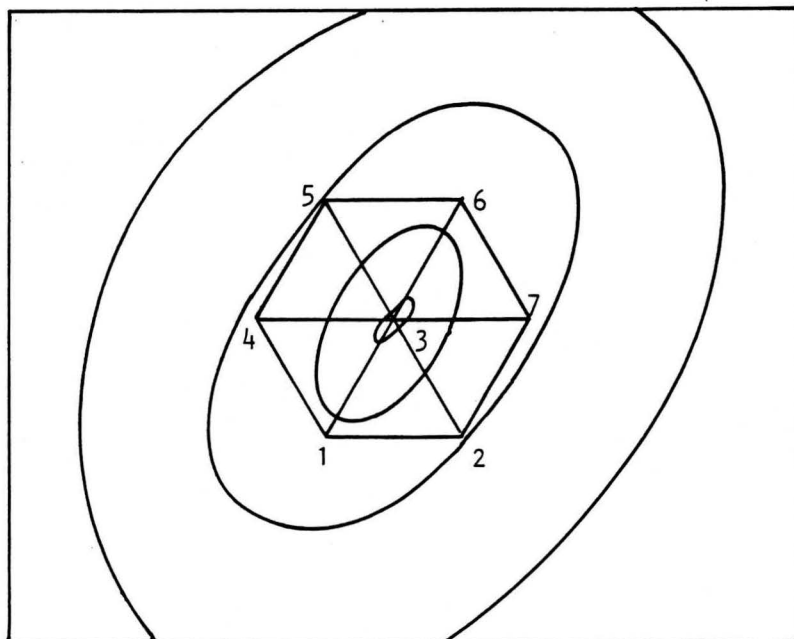
Fig. 1.3 Circling simplex.

1.2 THE MODIFIED SIMPLEX-METHOD

The modified simplex procedure employs the rules for the basic simplex, but allows for the contraction or expansion of the simplex to enable it to travel faster over the response surface and to define the final optimum more precisely. The operations of expansion and contraction are added to the operation of reflection.

Consider the initial simplex BNW in figure 1.4, with B the best vertex, W the worst and N the second-worst vertex. P is the centroid of the hyperface BN and the reflection of W through BN gives vertex R in the new simplex.

$$P_R = P + (P - P_W)$$ (3)
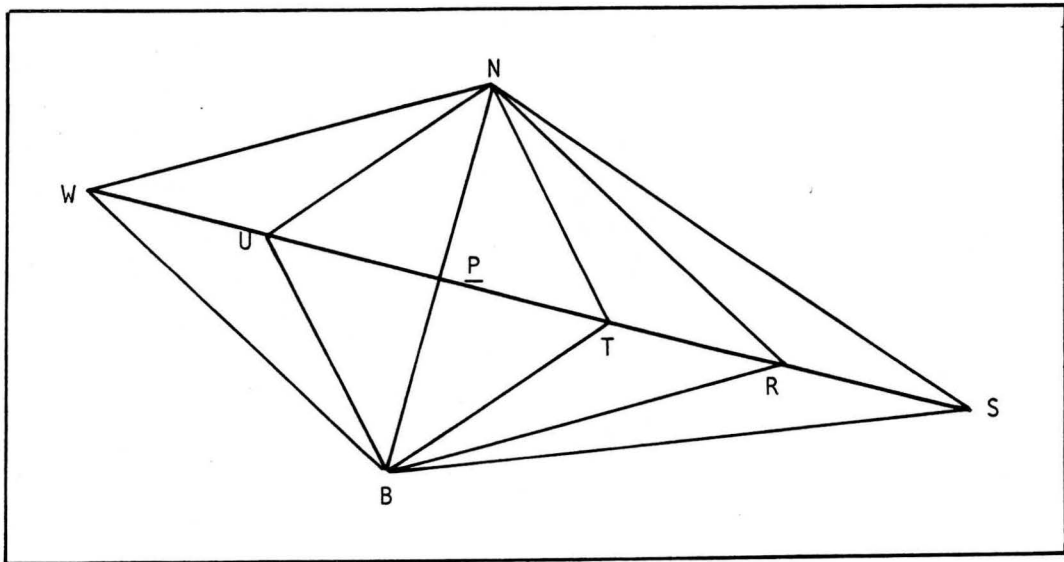
Fig. 1.4 Possible moves in modified simplex method

The response at R can belong to one of any of the following classes.

(a) The response at R is better than the response at B. This is an indication of movement in the proper direction and this justifies further investigation in the same direction. The segment WR is expanded and the response is measured at point S, with

$$P_S = P + \gamma(P - P_W) \tag{4}$$

with $\gamma > 1$ the expansion coefficient. BNS is the new simplex if the response at S is better than R. BNR remains as the new simplex if it is worse than R.

(b) The response at R is neither better than the response at B nor worse at N. The new simplex in this case is BNR.

(c) The response at R is worse than the response at N. This shows that the movement is in the wrong direction and segment WR is contracted. There are now two possibilities. If the response at R is worse than the response at W, then the new contracted simplex should lie at U which is closer to R than to W.

$$P_U = P - \beta(P - P_W) \tag{5}$$

with β the contraction coefficient ($0 < \beta < 1$). If the response at R is worse than the response at N, but better than W, then the new, contracted simplex should lie at T, which is closer to W than to R.

$$P_T = P + \beta(P - P_W) \tag{6}$$

It is clear that the simplex becomes smaller and smaller the closer it approaches the optimum. Once the simplex shrinks to such a size that the indeterminate errors involved in the response measurement mask the true differences between the vertex responses, the simplex will wander erratically near the optimum. The simplex is halted when the step size becomes less than value or when the differences in response approach the value of the indeterminate error.

APPENDIX 2

2.1. THE ABEL TRANSFORMATION METHOD .

2.1.1. The Transformation of the Observed Lateral Radiation Profile to a Radial Radiation Profile.

In the study of fundamental properties of plasmas it is essential to study the radial transform of any lateral function, for the obvious reason that the plasma is not homogeneous. A method is therefore necessary to convert this lateral radiation to radiant volume elements small enough to contain a temperature. Several transformations exist which make use of the Abel integral or its inverted form.[2,13,36,52,57,116] This is applicable to optically thin plasmas with a cylindrical symmetry. This is illustrated by the bottom half of Fig. 2.1.

To be able to describe the non-isothermal plasma in terms of a temperature gradient it is essential to divide the plasma into isothermal zones 1, 2, 3 ... n. Each isothermal ring is described by a single temperature, T_n, which differs slightly from the neighbouring temperature. The lateral measurement, N, for each lateral section through the plasma is executed along the plasma as shown in figure 2.1. The section through zone 1 at temperature T_1 is responsible for the radiation N_1. The second radiation measurement, N_2, is the result of radiation from a section through zone 1 and 2, at temperature T_1 and T_2 respectively. There now exists an unknown temperature T_2 and a measured radiation value, N_2. T_2 can now be determined from a equation for the radiation, N_2. N_2 is similar to N_3, in that the radiation from a section through zones with three different temperatures of which two (T_1 + T_2) are known. For each lateral step one unknown temperature and one measured radiation is added. A temperature profile of the measured radiation, N(x) at a distance x from the yz-plane, is constructed by the above means. The relation of the emission coefficient f(r), that is the radiation for a unit depth at a distance r from the origin, with the spectral radiation of a source with path length $2y_o$ and cross-sectional area of $\Delta x \Delta z$ is given by
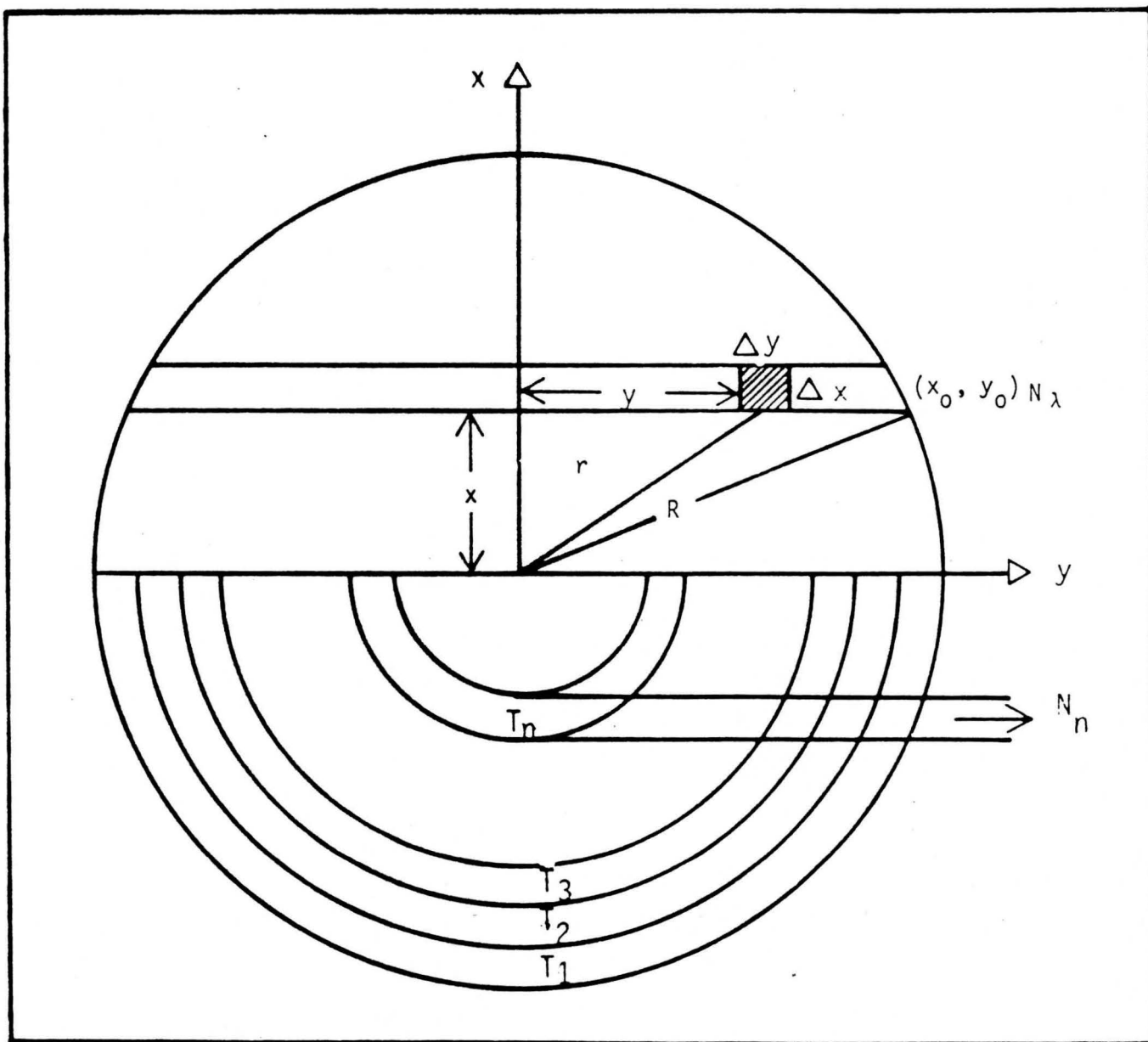
Figure 2.1   Schematic diagram for spatial resolution   of cylindrically
symmetrical sources

$$N_\lambda(x)\Delta x\Delta z = \sum_{-y_o}^{y_o} f_\lambda(r)\Delta x\Delta y\Delta z \qquad (1)$$

For infinitesimal volume elements and with the use of the existing symmetry, we have

$$N_\lambda(x) = 2\int_0^{y_o} f_\lambda(r)dy = 2\int_0^{(R^2-x^2)^{1/2}} f_\lambda(r)dy \qquad (2)$$

Substituting $\quad y = (r^2 - x^2)$

and $\qquad dy = (r^2 - x^2)2rdr \quad$ into the latter equation yields;

$$N_\lambda(x) = 2\int_x^R \frac{f_\lambda(r)rdr}{(r^2-x^2)^{1/2}} \qquad (3)$$

This is the Abel equation. It is possible to obtain the Abel inversion by taking its transform.

$$f_\lambda(r) = -\frac{1}{\Pi}\int_r^R \frac{N'_\lambda(x)dx}{(x^2-r^2)^{1/2}} \qquad (4)$$

where $N'(x)$ = the first derivative of $N(x)$. Equation (4) gives the radial emission coefficients in terms of the measured lateral radiation profile. For a definition of R the reader is refered to figure 2.2. The limit radius, R, of the plasma is defined by the condition $N_\lambda = 0$ where $x > R$. The radius limit, R, and the x-axis are equally divided into n-increments of equal size,Δ , so that $x_k = k\Delta$, $r_k = k\Delta$ and R = kn where k = 0,1,2 .... n - 1. The input data for the inversion is the measured radiations N(x) at lateral positions x = (0, ... (n - 1))Δ with the output data the emission coefficients f(r).
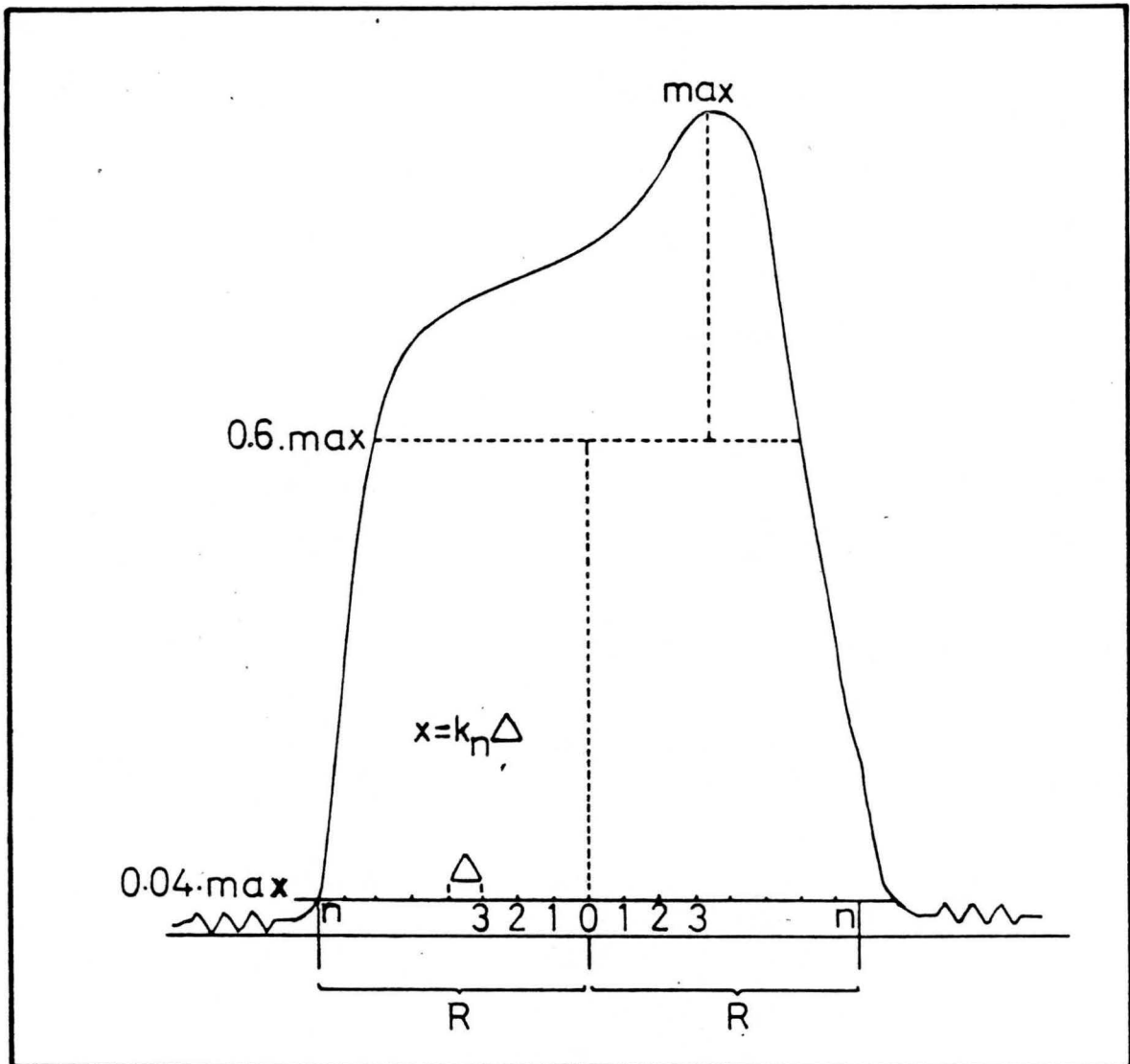
Figure 2.2   The determination of the centre of the lateral data profile

2.2 *The Method of Transformation of the Lateral Radiation Profile to a Radial Radiation Profile*

Because the data usually have considerable experimental scatter, most of the methods did not work satisfactory. A transformation method is needed because $N(x)$ and also its derivative $N'(x)$ is an unknown function. The value $f(r)$ can therefore only be calculated approximately. Various methods have been used: for example the numerical method.[34,93,145] Cremers and Birkebark[36] used a method of division of the data into a number of segments. They then fitted a leastsquares polynomial to each segment so that the inverted Abel integral equation can be integrated exactly to yield the emission coefficient. The method of Freeman and Katz[57] was used in this project. It involves the fitting of a least-square function $F(x)$ by a sixth order polynomial to the entire lateral radiance profile. The process also smoothes the raw data. The next step is to integrate numerically the first derivative of the polynomial expression as in equation (4). The function is given by,

$$F(x) = N_\lambda(x) = \sum_{i=0}^{m} C_i (R^2 - x^2)^i \tag{5}$$

where m = the order of the polynomial (= 6) as a practical limit

C_i = polynomial coefficients

$N(x)$ = lateral radiation measurement

x = lateral position

R = radius of the plasma.

When the first derivative of equation (5) is substituted into equation (4) the following solution is obtained.

$$f(r) = \sum_{i=0}^{m} \lambda_i C_i (R^2 - r^2)^{i-1/2} \tag{6}$$

$$\text{where} \quad \lambda_i = \frac{2^{2i}(i!)^2}{\Pi(2i)!} \tag{7}$$

The values $(R^2 - x^2)$ and $F(x)$, the measured radiation, are fed into a digital computer as x and y-values respectively from which the coefficients C_i (i = 0, ..., 6) of the 6th order polynomial are calculated for the least square fitting. The constant factors, λ, can be calculated from equation (7). It is now possible to calculate the emission coefficient $f(r)$ from equation (6.10). The R-value in equation (5) is the radius of the plasma and x is the lateral position of the measured radiation value. (See Figure 2.2). The centre point of the profile (x = 0) was calculated at 0.6 × maximum value of the lateral radiation profile and the size of R as half the distance between the two points on both sides of the plasma where the net signal disappears into the background. One of the main advantages of this method is that errors occurring near the boundaries of the plasma, because of small signal to background ratios, do not impair the accuracy at the centre of the plasma.

APPENDIX 3

3.1 *DEFINITION FOR DETECTION LIMITS.*

The IUPAC definition, adopted in 1975, states that "the limit of detection, expressed as a concentration, C_L, is derived from the smallest measurement, X_L, of an analyte leading to a signal three times the standard deviation of 20 measurements for a given analytical procedure".[80] The ACS Subcommittee on Environmental Analytical Chemistry (1980) definition stated that "the limit of detection is the lowest concentration of an analyte that an analytical process can reliably detect".[72]. It is of great importance to understand the method of measurement as well as the errors associated with the measurements. The definition given by Boumans [24] goes a step further and he calls it the "limit of determination". This will be discussed later.

3.2 *THEORY OF DETECTION LIMITS.*

Given a completely specified measurement process one must estimate the minimum concentration (C) that may be expected to yield a signal, X, sufficiently large to be detected. This is illustrated in figure 3.1 and figure 3.2. The distribution of the net signal, X, about the value μ is given, i.e. the distribution of the blank signal. The μ value is the mean value of the responses. If a sufficiently large number of measurements is made, plotting the measured responces would produce a curve similar to that shown in figure 3.2. The curve is gaussian symmetrical and extends outwards in units of standard deviation, σ. The area under the curve can be expressed in terms of probability. We can now adopt some critical value, X_L, as the criterion for the decision whether a measured net signal, X, will be considered to be "detected" or "not detected". This critical signal depends on the standard deviation of the distribution. The relationship between the area under the curve and the probability can be measured to estimate the chance that the newly measured X-value, X_L, would be a certain number of standard deviation units away from the mean response, μ. Once X_L is fixed, we have defined the probability, α, of taking a false decision. If X_L is $k\sigma$ away from μ we can say that α is the probability that

$$C_L = \frac{kS_B}{m} \qquad\qquad \ldots\ldots\ldots (5)$$

where $\quad m = \dfrac{X_L - X_B}{C_L}$

This is illustrated in Figure 3.1. The limit of detection is found by relating ks_B to a concentration value by dividing by the slope of the calibration curve line.
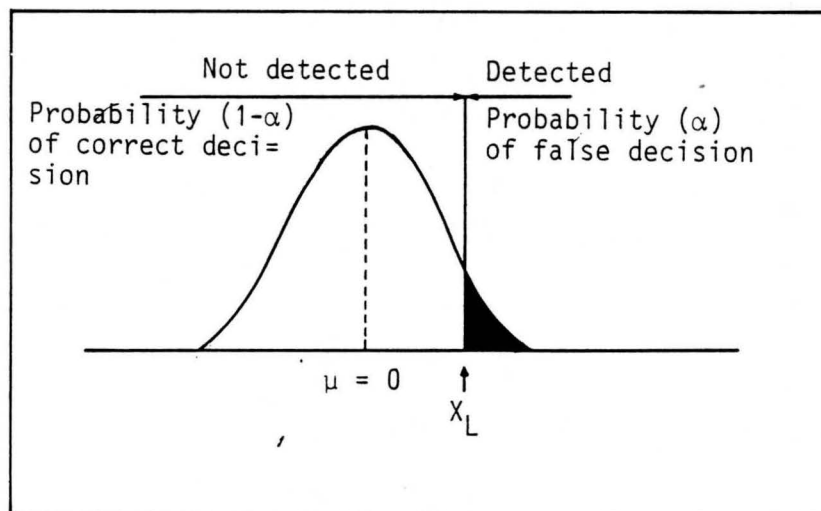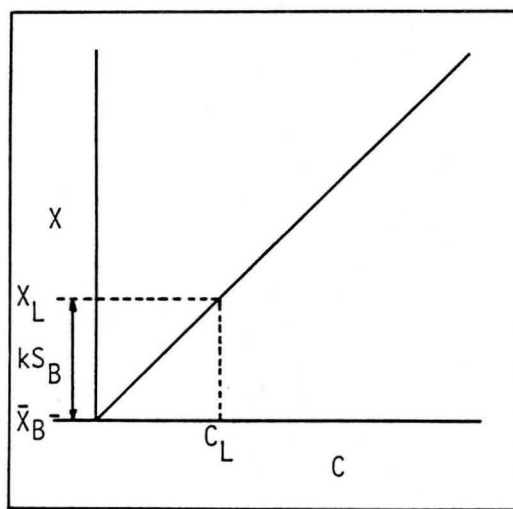

Figure 3.1 The calibration curve of signal, X, vs concentration, C, showing the relationship of kS_B to the limit of detection, C_L.

Figure 3.2 The distribution of the net signal, X, about the value μ, i.e. the distribution of the blank measure.

$X_L \geq (\mu + k\sigma)$. The risk of taking a wrong decision when $\mu = 0$ is called the α error. This error is determined by the choice of X_L, e.g. if we have a normal distribution and fix the critical level at 3σ (k = 3) to the right-hand side of $\mu = 0$, the area under the curve at the right-hand side of X_L is 0,13% of the total area and this is the value of α. We shall therefore run a risk of 0,13% that a random fluctuation of the blank is taken to be a true signal. If we fix the critical level at 2σ (k = 2), the risk will be 2,28% etc.[80]

Blank measurements, X_B, are normally used for the determination of the limit of detection. The mean of the blank, X_B, can be calculated as

$$\bar{X}_B = \frac{\sum\limits_{j=1}^{n_B} X_j}{n_B} \qquad \ldots\ldots\ldots(1)$$

The standard deviation can be calculated as

$$S_B^2 = \frac{\sum\limits_{j=1}^{n_B} (X_{Bj} - \bar{X}_B)^2}{(n_B - 1)} \qquad \ldots\ldots\ldots(2)$$

The value of n_B should be sufficiently large (at least equal to 20) to permit a reliable estimate of σ to be made. In defining C_L, IUPAC states that

$$X_L = X_B + k\,S_B \qquad \ldots\ldots\ldots (3)$$

where k is chosen in accordance with the confidence level desired. The C_L is a function of X_L and therefore within the analytical sensitivity.

$$C_L = \frac{(X_L - \bar{X}_B)}{m} \qquad \ldots\ldots\ldots (4)$$

By substituting equation (3) into equation (4), equation (5) is obtained

Boumans[24] mentioned a well-known but seldom used concept in the calculation of the detection limits, namely the limit of identification, C_I. The β error needs to be defined for this approach. Figure 3.3 represents the distribution of observations associated with a concentration C_I. One can now arbitrarily fix a critical value, X_L, so that the area at the left-hand side of X_L is equal to β, where β is the probability that a true concentration C_I remain undetected. By synthesizing figure 3.2 and figure 3.3, figure 3.4 is obtain. Two distributions no exist: one about $\mu = 0$ (the blank) and one about $\mu = \mu_1$. By adopting a critical value, X_L, α and β can be defined. X_L is defined by fixing α. It is now possible to define β and determine μ_I so that the shaded area of the right-hand distribution is equal to β. There is now a chance α of falsely detecting a signal when nothing is present and simultaneously a chance β of falsely not detecting a concentration C_I. There is therefore a 1-α chance of taking a correct decision when nothing is present and a $1 - \beta$ chance of correctly detecting an analyte with concentration C_I. Boumans used the above explanation to define his "ideal definition of the detection limit". This is done so that both α and β are well balanced. When measurements are made for a sample, the X value obtained should follow a normal distribution around a mean value. If a sample were found to have a mean at the X_L-value, the distribution of these values around X_L would resemble the distribution as shown in Figure 3.4, curve A and B without C. It is clear from curve B that half of the time the measurement would fall below X_L ($\beta=0.5$) and it could therefore not be considered a true signal according to the IUPAC definition. Boumans wanted to avoid this high probability and therefore fixed the critical value at $3S_I$ away from X_L, and a concentration C_I is defined so that it will yield a distribution of measurements about μ_I that makes β equal to α as shown in Figure 3.4. If $S_I = S_B$ then C_I is $3S_B$ away from X_L or $6S_B$ away from $\mu = 0$ (X_B). There is, on the one hand, a small chance that a random fluctuation of the blank will be misread as a true signal, and on the other hand, a small chance that a concentration C_I, when present, will be undetected. By using k = 3, the area of the μ_I distribution curve below X_L, β, is no less than 0,0013. Thus, there is a 0,13% chance that an X value measured at μ_I would fall below the X_L limit and not be considered as a true signal. This "limit of identification" can therefore be summarized as

$$X_I = X_L + 3 S_B \ (S_B = S_I) \qquad \qquad \ldots\ldots\ldots(6)$$
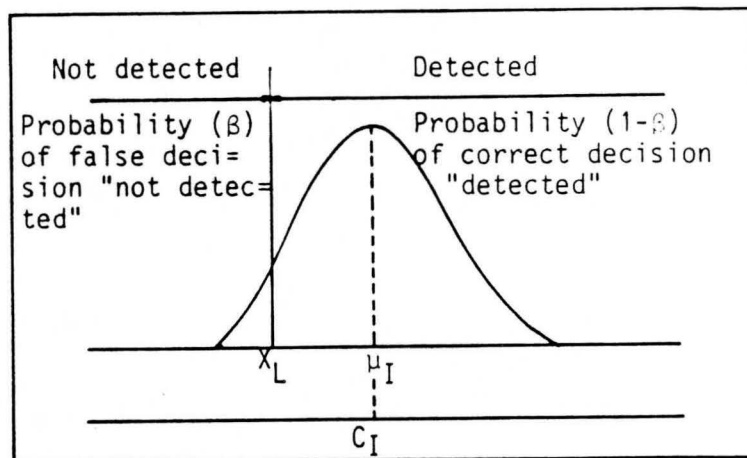
Figure 3.3 The distribution of observations associated
with a concentration C_I
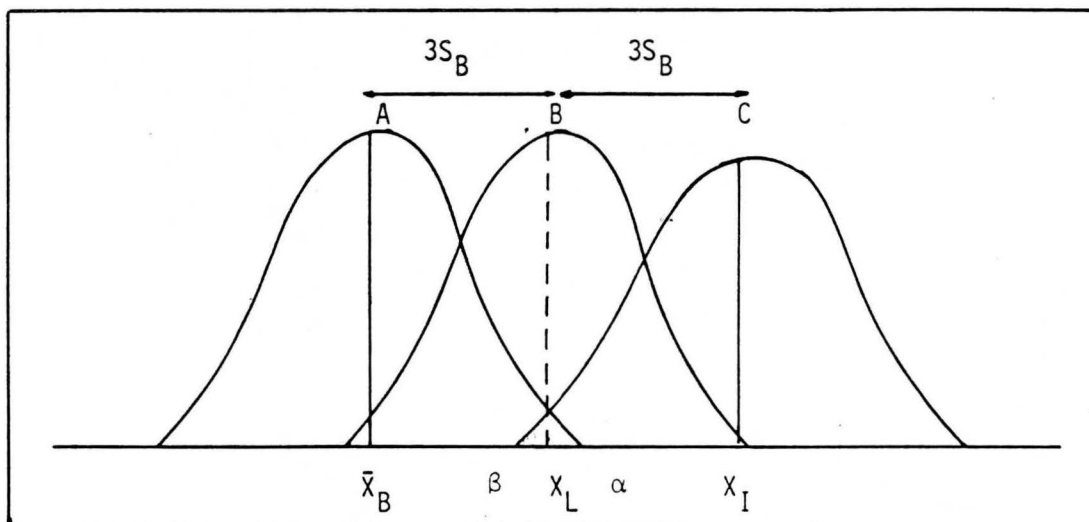
Figure 3.4 Normal distribution curves for the blank observation
X_B, the limit of detection, X_L and the limit of
identification, X_I

Another way of expressing detection limits is found in the article by Winge et al.[146] Under normal operating conditions, with all components in the signal processing system operating properly, the uncertainty or standard deviation in the spectral background usually lies within the range of 0,3 to 1,0% of the background signal level.[146] It was therefore concluded that the standard deviation of the background could be approximated by $0,01X_B$ and the detection limits was estimated from

$$D.L = \frac{3(0.01X_B)\,C}{X_S} = \frac{0.03\,C}{X_S/X_B} \qquad \dots\dots(7)$$

where C is the analyte concentration which yielded X_S/X_B

There is also a theoretical approach to the calculation of detection limits. A theory has been developed for the estimation of the detection limits.[117,145] The general expression for the detection limit with the 3σ criterion is

$$C_L = aL^{-1} (d + bL + c_f L^2)^{1/2} \qquad \dots\dots\dots(8)$$

$$\text{where } a = \frac{5.7 \times 10^{34} g_o \exp(E_u/kT)}{v_o g_u A_{\mu 1} d_{f 1} \gamma}$$

$$b = 2e_c BM \Delta f \, \gamma B_\lambda \Delta\lambda_s$$

$$c_f = \gamma^2 \Delta B_\lambda^2 \Delta\lambda_s^2 \Delta f$$

$$d = 2e_c BM \Delta f_{1d}$$

$$L = (D/f)^2 T_f WH$$

with E_u = excitation energy of state u, J.

g_o = statistical weight of ground state dimention less, d.l.

k = Boltzmann's constant, $J.K^{-1}$

T = excitation source temperature, K.

T_f = transmission factor of optics, d.l.

V_o = frequency at the centre of the line, s^{-1}

g_u = statistical weight of state u, d.l.

$A_{\mu l}$ = transition probability, s^{-1}

d_{fl} = average diameter of the flame region focussed on the entrance slit of the spectral instrument, cm.

γ = photomultiplier sensitivity, AW^{-1}

e_c = electronic charge, C.

B = photomultiplier factor related to gain per stage, d,l. W = slit width, cm

H = slit height, cm

M = amplification factor of the recording syste, d.l.

Δf = frequency response band width, Hz.

B_λ = intensity of excitation source continuum, $W\,cm^{-2}\,ss^{-1}\,nm^{-1}$.

$\Delta\lambda$ = spectral slit width, nm.

D^2 = effective aperture of the spectral instrument, cm^2

The first term aL^{-1} is determined by the emission intensity of a single atom, bL is the level of the shot noise of the excitation source and d is the shot noise due to the thermal electron emission of a photocathode.

Mermet[101] has established an approximate relation between the limits of detection and the properties of the spectral lines of the ionized elements introduced into the plasma. The relation is quoted in the following equation,

$$\text{D.L.} = 2.2 \times 10^{-14}\,(\lambda MQ/gA)\exp|1.9(\epsilon_i + \epsilon_{exc})| \qquad \text{.......(9)}$$

with M = relative atomic mass

λ = wavelenght, nm

A = transition probability, s^{-1}

E_i = ionization energy, eV

E_{ex} = excitation energy, eV

Q = ion partition function

g = statistical weight of the energy level

The theoretical calculation of the detection limits are very much dependent on the availability and accuracy of the different parameters. Prudnikov[117] has used equation (8) for the derivation of an equation for the theoretical calculation of the standard deviation. He has compared his theoretical results with experimental results and has found a very good correlation between the two. He has used the experimental data for the confirmation of the theoretical approach. The theoretical approach to confirm a experimental approach is very helpful in the understanding of problems that might occur.

The signal-to-noise ratio is another important factor to take into consideration in the determination of detection limits. The signal-to-noise ratio in any spectrometric measurement determines two figures of merit;

1. The precision expressed as the relative standard deviations, i.e. $S_B/\bar{X}_B$, where S_B is the standard deviation of the measurement given by the noise, and X_B is the average measure of signal level of the analyte producing S_B ; % relative standard deviation is $100S_B/\bar{X}_B$.

2. The detection limit, $\quad C_L = \dfrac{(S/B)_{lim} \times S_B}{dX/dC_{lim}} = \dfrac{3S_B}{dX/dC_{lim}}$

       with (S/B) = limiting detectable signal-to-noise (or the reciprocal relative standard deviation) and it is taken as 3.

         S_B = blank standard deviation.

    dX/dC = is the sensitivity of the method (slope of analytical curve).

It is important to distinquish between signal noise and additive noise. Additive noise is associated with an extra contribution added to the signal. Signal noise is usually an unwanted signal where additive noise is an unwanted fluctuation in the signal caused by uncontrolled factors. The dark current of a photomultiplier is a perfect example. The whole dark current is normally accepted as a dark noise and subtracted to eliminate the dark current contribution. But if the dark noise is restricted to the fluctuations in the dark current it is seen that by off-setting the mean value makes no difference to the fluctuations it contributes to the signal. It is therefore a problem one cannot get rid off. From a practical point of view it is therefore important to realise that dark currents vary immensely from one tube to the other. It is therefore important to use a tube with a small dark current whenever low signals have to be measured. It is understandable that a signal of 4 is more reliable if it is obtained by subtracting 1 from 5 rather than by subtracting 1001 from 1005. The detection limit is therefore also dependent on the measuring system, and is not a property of the plasma alone. In practice if the background is much larger than the dark current, the change is small.